Dynamic Microfiltration: Critical flux and macromolecular transmission

Beier, Søren; Jonsson, Gunnar Eigil

Publication date:
2008

Document Version
Publisher's PDF, also known as Version of record

Dynamic Microfiltration- Critical Flux and Macromolecular Transmission

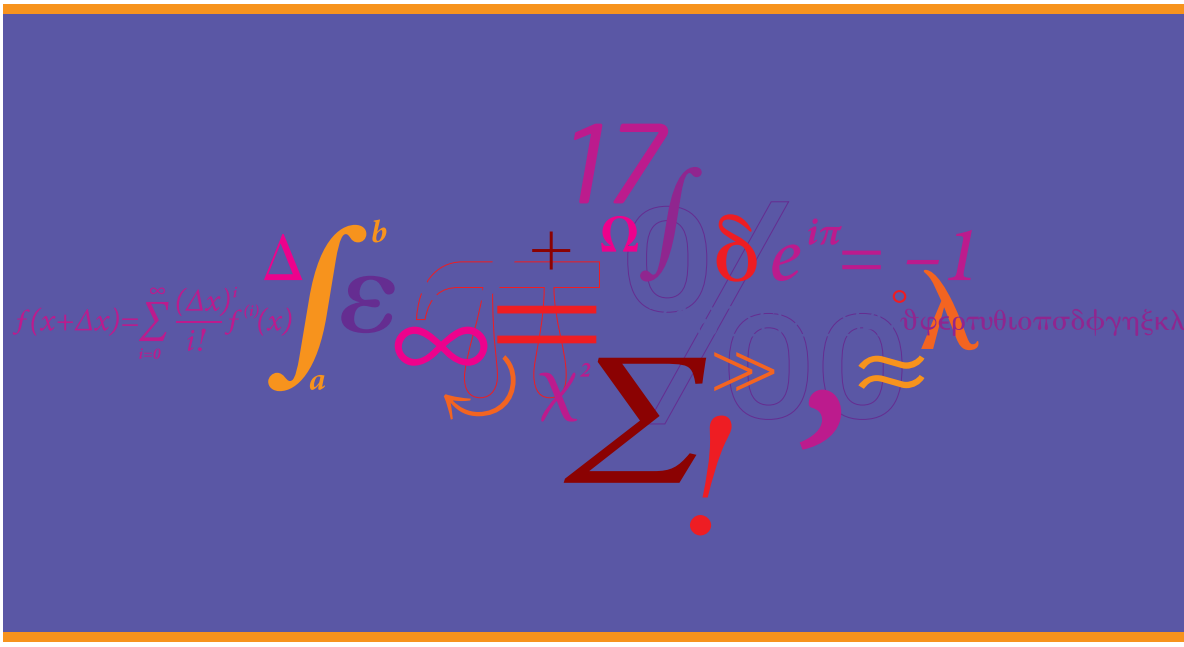

Søren Prip Beier
Ph.D. Thesis
2008

DTU Chemical Engineering
Department of Chemical and Biochemical Engineering

Dynamic Microfiltration Critical Flux and Macromolecular Transmission

Søren Prip Beier
Ph.D. Thesis
2008

DTU Chemical Engineering
Department of Chemical and Biochemical Engineering

Address: Department of Chemical and Biochemical Engineering
Søltofts Plads, Building 229
Technical University of Denmark
DK-2800 Kgs. Lyngby
Denmark

Telephone: +45 4525 2800
Fax: +45 4588 2258
E-mail: kt@kt.dtu.dk
Internet: www.kt.dtu.dk

Print: J&R Frydenberg A/S
København
07-2010

ISBN: 978-87-92481-22-1

Dynamic Microfiltration

Critical Flux and Macromolecular Transmission

Ph.D. Thesis

Søren Prip Beier

Supervisor: Gunnar Jonsson

Department of Chemical and Biochemical Engineering
Technical University of Denmark

Preface

This Ph.D. project was carried out at the CAPEC research center, Department of Chemical Engineering, Technical University of Denmark, from September 2005 until August 2008. I would like to thank my supervisor, Gunnar Jonsson, for excellent guidance and for three wonderful years at DTU. Furthermore, I would like to thank the workshop, especially Henning Koldbech, for realizing my thoughts and ideas about the experimental apparatus. I am very grateful to Peter Stubbe, BiocentrumDTU, for making the software and hardware of the system work. Thanks, also, to the Technical University of Denmark for financing the project. Finally, I would like to thank my wife and children for enduring and bearing with me.

This is the final version of the thesis including all scientific papers in accepted and published versions.

Date:

_____

Søren Prip Beier

English abstract

A dynamic microfiltration system, the *vibrating hollow fiber membrane module*, is presented and described in this Ph.D. thesis. The system is thought to be coupled to the treatment of biological media, e.g. fermentation broth, from which macromolecules eventually continually should be recovered or removed. The advantages of dynamic membrane systems are the possibility of i) minimizing fouling problems, ii) probably lowering operational costs, and iii) enhancing macromolecular transmission.

In the first part of this thesis, a general introduction to pressure driven membrane processes is given, followed by a review of different dynamic membrane filtration systems, reported in the scientific literature, with similarities to our experimental setup. A chapter including some aspects of flux and critical flux modeling is given, as well, from which some of our experimental data is tried to be explained.

The second part of the thesis consists of five publications. Four of the publications cover aspects related to our dynamic microfiltration set-up: Critical flux measurement, determination of average surface shear rate, macromolecular transmission, and operation for extended periods. One paper reports a method to measure macromolecular adsorption on membranes based on the assumption that permeability drop is linearly related to the amount of material adsorbed.

From the adsorption experiments, we have seen that irreversible adsorption strongly influences the hydraulic resistance of the membrane during operation. Furthermore, we have seen that sustainable operation is achievable since a sub-critical flux level is identifiable. One just has to define at “sustainable time period” in which process sustainability is to be evaluated. Sub-critical flux facilitates enhanced and stable macromolecular transmission, and low and stable trans-membrane pressure (TMP). The critical flux is dependent on the degree of module vibrations, but whether the dependency of average surface shear rate is best described by shear-induced diffusivity or a power law correlation is difficult of judge.

Dansk resume

Et dynamisk mikrofiltreringssystem (det vibrerende hollow fiber membranmodul) præsenteres og beskrives i denne Ph.D. afhandling. Systemet er tiltænkt til at virke i forbindelse med behandling af biologiske medier, som f.eks. fermenteringsvæske, fra hvilke, makromolekyler eventuelt kontinuerligt skal fjernes. Fordele ved dynamiske membransystemer er i) at foulingproblemer minimeres, ii) mulighed for sandsynligvis at nedbringer kørselsomkostningerne og iii) at forhøje transmissionen af makromolekyler gennem membranen.

I afhandlingens første del gives en general introduktion til trykdrevne membranprocesser. Derefter følger en oversigt og forskellige dynamiske membranfiltreringssystemer, som er beskrevet i den videnskabelige litteratur, med ligheder til vores eget system. Ligeledes findes et kapitel indeholdende aspekter omkring flux og kritisk flux modellering, hvori nogle af vores eksperimentelle data vil forsøgt at blive forklaret.

Afhandlingens anden del består af fem publikationer. Fire af disse publikationer omhandler vores dynamiske mikrofiltreringsopstilling: Kritisk flux målinger, bestemmelse af gennemsnitlig hastighedsgradient på membranoverfladen, makromolekylær transmission og operationel kørsel gennem forlængede tidsperioder er de emner, som behandles. I en af publikationerne rapporteres en metode til bestemmelse af makromolekylær adsorption på membraner under antagelse af, at permeabilitetsfald er ligefrem proportionalt med mængden af adsorberet materiale.

Ud fra adsorptionseksperimenterne så vi, at irreversibel adsorption i høj grad influerer på den hydrauliske modstand af membraner under kørsel. Vi har yderligere set, at opretholdelig kørsel er mulig, idet et "under-kritisk" fluxniveau var identificerbart. Dog skal man dertil definere en "opretholdelig tidsperiode", i hvilken procesopretholdeligheden skal evalueres. Kørsel under den kritiske flux muliggør forhøjet og stabil transmission af makromolekyler og samtidig et lavt og stabilt transmembrantryk (TMP). Den kritiske flux afhænger at membranmodulets vibreringsgrad, men hvorvidt afhængigheden bedst beskrives vha. forskydningsinduceret diffusivitet eller en potenskorrelation er svært af afgøre.

Table of contents

Introduction / Appetizer

Things only move when they are forced to move! A bicycle only moves when a force is applied in the form of pedaling. A cloud on the sky only moves when a force is applied in the form of a storm or a wind. A soccer ball only flies into the goal net when a force, in the form of a beautiful and precise shot from Bjarne Goldbæk (or another great soccer player), is applied. Thus, all sorts of transport only take place when a force, a *driving force*, is applied.

Transport of mass, energy, momentum, volume, and electricity only takes place when a driving force is applied. Transport can generally be expressed as a flux, J, which is given by the amount of mass, energy, momentum, volume, or charges that is transported pr. area pr. time through a given interface [Mulder, 1996].

$$J = -A \cdot \frac{dX}{dx} \qquad (1)$$

The driving force is expressed as the gradient of X (concentration, temperature, velocity, pressure, or voltage) along the x-axis parallel to the transport direction. The proportionality constant, A, is a phenomenological coefficient which is related to many well known physical terms associated with different kinds of transport.

Table 1: Driving forces, flux equations, SI units for the phenomenological coefficients and flux, and the common names for the "laws" are given for different kinds of transport [Beier, 2006i].

Transport Of	Driving Force	Flux Equation	Phenomenological Coefficient	Flux Unit	Common Name
Mass	Concentration gradient	$J_m = -D \cdot \frac{dc}{dx}$	Diffusion coefficient D [m^2/s]	$\left[\frac{kg}{m^2 \cdot s}\right]$	Fick's law of diffusion
Energy/heat	Temperature gradient	$J_h = -k \cdot \frac{dT}{dx}$	Thermal conductivity k [J/(s·K·m)]	$\left[\frac{J}{m^2 \cdot s}\right]$	Fourier's law of heat conduction
Momentum	Velocity gradient	$J_n = -\mu \cdot \frac{dv}{dx}$	Dynamic viscosity μ [Pa·s]	$\left[\frac{kg \cdot (m/s)}{m^2 \cdot s}\right]$	Newton's law of viscosity
Volume	Pressure gradient	$J_v = -L_p \cdot \frac{dP}{dx}$	Permeability coefficient L_p [m^2/(Pa·s)]	$\left[\frac{m^3}{m^2 \cdot s}\right]$	Darcy's law
Electrical	Voltage gradient	$J_e = -\sigma \cdot \frac{dE}{dx}$	Electrical conductance σ [C^2/(s·J·m)]	$\left[\frac{C}{m^2 \cdot s}\right]$	Ohm's law

As seen in Table 1, many well known physical "laws" are in reality phenomenological equations. In membrane processes, the transport takes place across a barrier, a membrane, and in this case, the phenomenological coefficient is the permeability coefficient of the membrane. In pressure driven membrane processes, the flux is a volumetric flux, J_v, and the applied driving force across the membrane is a pressure difference.

The well know problems concerning concentration polarization and membrane fouling during pressure driven membrane filtration, in practice only makes Darcy's law applicable in determining pure solvent fluxes. In this thesis, we are dealing with pressure driven membrane processes and a new approach, a *dynamic approach*, to reduce the impact of membrane fouling in microfiltration and improve the general performance. The thesis is composed of two parts: Part I) this part of the thesis (chapter 1-3 plus conclusions) is thought as a general introduction into the field of dynamic filtration followed by some modeling aspects related to our data. Part II) is composed of our publications (paper 1 – 5). All experimental details and results are presented in the publication part. The references in the first part of the thesis to our publications will be given as follows: [PAPER 1], [PAPER 2], [PAPER 3], [PAPER 4], and [PAPER 5]. The two parts are not independent, but the conclusions in the first part will be short and very general, whereas specific conclusions to the research work will be given at the end of each paper.

Part I
Chapter 1 gives a general introduction to pressure driven membrane processes, and in chapter 2, some different concepts, all categorized as *dynamic systems*, will be introduced. In this chapter, our own system is briefly introduced. The critical flux is initially reviewed in chapter 3, followed by an introduction of different flux and critical flux models found in the literature. Some of the models will be tried to explain and fit our own critical flux data with references directly to our publications. After chapter 3, conclusions of the whole work will be drawn along with some proposals for future work.

Part II
The first publication, [PAPER 1], is an introduction to our experimental set-up including a few critical flux data. In the second publication, [PAPER 2], the possibility of actually transmitting macromolecules through the microfiltration membranes is presented. The third paper, [PAPER 3], covers a quite different, but still very relevant, area. Here, the influence of adsorption on membrane surfaces is investigated and it is assumed that the permeability drop is linearly related to the amount of adsorbed material. Ultrafiltration, and not microfiltration, membranes were used. However, the paper emphasizes the impact of irreversible macromolecular adsorption on membranes which also can be related to microfiltration. The fourth publication, [PAPER 4], deals with some more technical aspects of critical flux determination procedures and the impact of the chosen operational parameters. In the final paper, [PAPER 5], the transmission of macromolecules is investigated again, but now for extended periods, and the impact of extracellular polymeric substances, EPS, from yeast cells is evaluated.

1 Pressure driven membrane processes

A general introduction to different aspects, related to pressure driven membrane processes, is given in this chapter. Membrane processes find applications in almost all kinds of industries as one or more downstream purification/separation processes:

- Chemical industries
- Biochemical industries
- Pharmaceutical industries
- Food industries
- Dairy industries
- Wastewater treatment
- Etc…

A membrane process is capable of performing a certain separation by use of a membrane. The core in every membrane process is the membrane that allows certain components to pass trough and retain other components. Initially, some of the most important terms used in membrane technology are shown in Figure 1.

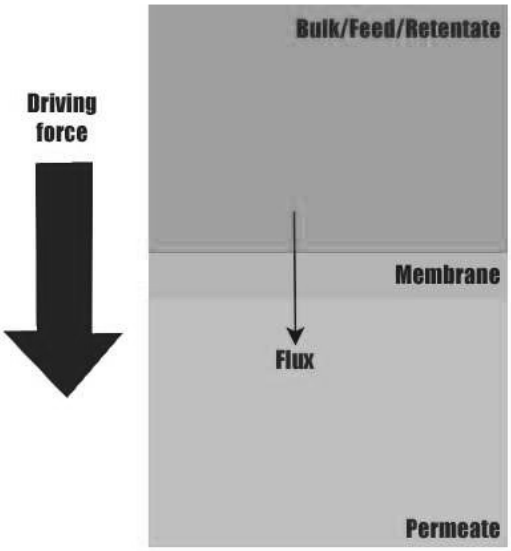

Figure 1: Sketch of a membrane process. The core is the membrane it self, through which a driving force induces a flux from the bulk to the permeate side.

The feed side is often referred to as the *bulk solution*. The bulk solution is also referred to as the *retentate* after it has been in contact with the membrane. When a driving force is

established across the membrane, a *flux* will go through the membrane from the bulk solution to the permeate side. The flux is referred to with the letter *J* and is often given in the units of liter pr. m^2 pr. hour ($L/(m^2 \cdot h)$). The liquid going through the membrane is called *permeate.*

A particular separation is accomplished by use of a membrane with the ability of transporting one component more readily than another. In other words, the membrane is more permeable to certain components than other components because of differences in physical or chemical properties between the membrane and the components that are transported through the membrane.

- *Difference in size*: In many membrane processes (e.g. microfiltration and ultrafiltration), porous membranes with a given pore size distribution are used. Because of the given pore size, some components will be retained by the membrane because of their size, and some components are small enough to pass through the pores of the membrane.

- *Difference in charge:* In some membrane processes (e.g. electrodialysis), differently charged components are separated. This can by done by use of cation and anion exchange membranes which only allows transport of cations and anions, respectively.

As seen in Figure 1, a driving force across the membrane induces a flux of permeate from the bulk solution to the permeate side. Different driving forces are used in different membrane processes, according to Table 2.

Table 2: Different driving forces for different membrane processes [Beier, 2006ii].

Driving force	Membrane process
Pressure difference	Micro-, ultra-, nanofiltration, reverse osmosis
Concentration difference	Gas separation, pervaporation, dialysis
Temperature difference	Membrane distillation, thermo osmosis
Electrical voltage difference	Electrodialysis, membrane electrolysis

When talking about pressure driven membrane processes, the flux through the membrane is induced by a hydrostatic pressure difference between the bulk solution and the permeate side. Pressure driven membrane processes include microfiltration, ultrafiltration, nanofiltration, and reverse osmosis.

Table 3: Approximate pore sizes and applied pressures are given for the different pressure driven membrane processes together with some typical applications [Beier, 2006iii].

	Pore size [µm]	Applied pressure [bar]	Typical applications
Microfiltration	10 – 0.05	0.1 – 2	Separation of colloids and particles
Ultrafiltration	0.05 – 0.002	1 – 10	Separation of macromolecules
Nanofiltration	0.002 – 0.001	5 - 20	Separation of low MW* solutes
Reverse osmosis	< 0.001	10 - 100	Separation of low MW* solutes

* MW = Molecular Weight

In microfiltration and ultrafiltration, porous membranes, with the approximate pore sizes given in Table 3, are used. Membranes for nanofiltration and reverse osmosis can be

considered as an intermediate between porous membranes with very small pores and dense membranes which are used in gas separation, for example. As the membrane pores / structure becomes more open, the necessary applied hydrostatic pressure decreases. Therefore, only relatively small pressure levels are used in microfiltration, whereas relatively high pressures are used in reverse osmosis.

In pressure driven membrane processes, the term *dX/dx* in equation (1) can be replaced by ΔP which is the difference between the hydrostatic pressure of the bulk side and the permeate side. Inserting this in equation (1), one obtains the following expression:

$$J = l_p \cdot \Delta P \qquad (2)$$

The phenomenological coefficient is now replaced by the term l_p which is the permeability coefficient of the membrane. The thickness of the membrane selective layer is incorporated into the permeability coefficient in equation (2) (contradictory to the term "L_p" in Table 1, in which the membrane thickness in not incorporated), and therefore, in order to achieve as high permeability as possible, asymmetric membranes with a very thin selective layer (skin layer) are used, since the permeability coefficient and membrane thickness are inversely proportional. The skin layer is attached onto an open porous support structure, and the membrane is referred to as *asymmetric*. The thickness of skin layers in asymmetric membrane is often in the order of magnitude around 1 μm. The permeability also depends on the dynamic viscosity of the fluid, which is transported through the membrane, and the resistance towards mass transport of the membrane. The permeability of microfiltration membranes are larger than for ultrafiltration membranes, and nanofiltration / reverse osmosis in which the membranes have very low permeabilities compared to microfiltration membranes.

Two fundamentally different ways of running pressure driven membrane processes are possible which is sketched in Figure 2.

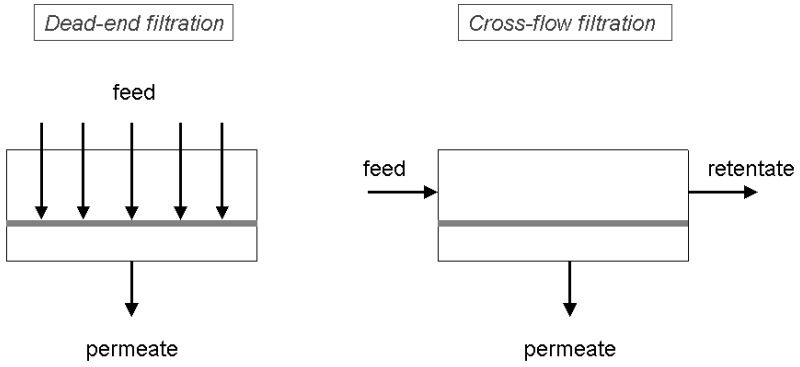

Figure 2: Two different ways of running a pressure driven membrane process [Beier, 2006iii].

In dead-end filtration, the bulk solution is pumped or pressurized through the membrane. That way, the permeate will be forced through the membrane, and the bulk solution will decrease in volume if the feed, for example, is contained in a batch cell. In cross-flow filtration, the bulk solution is pumped tangentially along the membrane surface, and there will be a pressure drop through the membrane module. In Figure 2, the terms *feed* and *retentate* is visualized in the cross-flow case. The feed is introduced in one end of the membrane module, and the retentate is returned at the other end of the module.

If the membrane is semi-permeable, the concentration in the permeate (of the components that are supposed to be retained) is close to zero, and the retention is close to 1 (close to 100%). The retention is, however, often lower than 1 because the concentration increases towards the membrane surface (concentration polarization). The retention can be defined in different ways:

$$\begin{aligned} &\textit{Observed retention}, \quad S = 1 - \frac{c_p}{c_b} \\ &\textit{True retention}, \quad R = 1 - \frac{c_p}{c_m} \end{aligned} \tag{3}$$

The permeate concentration is denoted c_p, the bulk concentration is denoted c_b, and the concentration at the membrane surface is denoted c_m. Because of convective transport of the retained components towards the membrane surface, the concentration at the surface, c_m, is often larger than c_b. This phenomenon is called concentration polarization and will be described later in this chapter. An enhanced surface concentration leads to an increased permeate concentration. Because c_m is larger than c_b, the true retention is often higher than the observed retention. The observed retention, S, "tells" what retention the system, as a whole, is able to perform, whereas the true retention, R, tells what retention the membrane itself is capable of performing. Furthermore, the selectivity, α, of a membrane tells how well a membrane is able to separate between two molecules, A and B, in a solution [Mulder, 1996]:

$$\textit{Selectivity} \ : \ \alpha_{A/B} = \frac{c_{A,permeate} / c_{B,permeate}}{c_{A,bulk} / c_{B,bulk}} \tag{4}$$

From equation (4) it is seen that the selectivity of two components, A and B, is given as the ratio of the permeate concentrations relative to the ratio of bulk concentrations.

1.1 Flux reducing factors

The volumetric flux can, as stated earlier, be determined from Darcy's law, equation (2)), from the membrane permeability and hydrostatic pressure difference, but in practice this equation can only be applied when the pure solvent flux through the membrane is to be determined. In practice, the flux will often decrease dramatically to a level as low as

around 5 % or less, compared to the initial flux, when solutions containing suspended particular material and macromolecules are filtrated [Mulder, 1996]. This can be due to an osmotic pressure difference across the membrane, the build up of a concentration gradient in the laminar film layer, caused by the convective transport of solutes towards the membrane (concentration polarization), formation of a macromolecular gel layer on the membrane surface, and other types of membrane fouling. Therefore, a term concerning the total resistance towards mass transport through the membrane, R_{tot}, has to be incorporated into Darcy's in order to explain the flux-pressure relationship [Mulder, 1996]:

$$J = \frac{\Delta P}{\eta \cdot R_{tot}} \qquad (5)$$

The total resistance increases with time due to different phenomena, leading to a decline in flux, when a constant pressure is applied. The total resistance is the sum of all sub-resistances towards mass transport:

$$R_{tot} = R_m + R_{CP} + R_f \qquad (6)$$

In equation (6), R_m is the membrane resistance, which is a membrane constant, R_{CP} is the resistance caused by concentration polarization, and R_f is the resistance caused by membrane fouling. These different sub-resistances are often functions of one another. Thus, when the feed solution or suspension contains macromolecules or suspended particles or colloids, the flux often decreases very severely due to different phenomena which results in increasing sub-resistances towards mass transport of different kinds. Equation (5) and (6) constitute a so-called *resistance-in-series model* [Mulder, 1996].

1.1.1 Osmotic pressure difference

The osmotic pressure difference between the bulk solution and the permeate is often an important factor to encounter in pressure driven membrane processes. The osmotic pressure difference is established because of the concentration difference between the bulk solution and the permeate. Therefore, when the solute concentrations are different across the membrane, the solvent activity is also different across the membrane. The terms "osmosis" and "osmotic pressure" can be explained in different ways. First we will look at Figure 3.

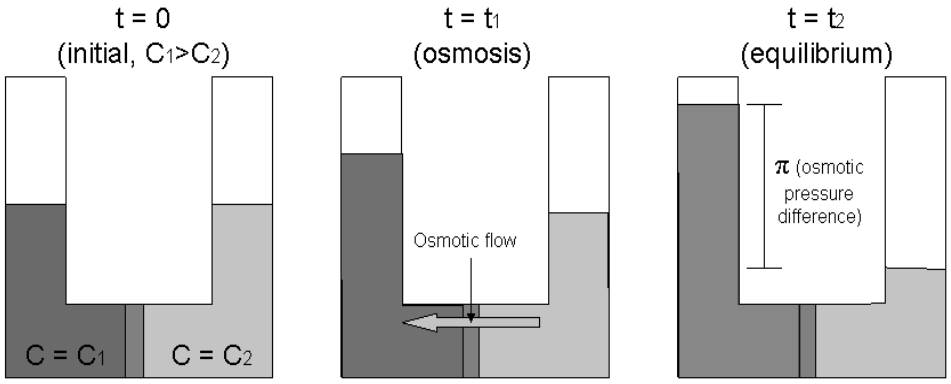

Figure 3: The principle of osmosis and osmotic pressure.

Initially, two solutions at different concentration are separated by a semipermeabel membrane that only allows transport of solvent and not solute. The solute concentration C_1 is larger than the solute concentration C_2. As time passes, solvent will flow through the membrane from the lower solute concentration to the higher solute concentration, as sketched at time t_1. That way, the solvent pursues to dilute the more concentrated solute solution. This solvent flow is called osmosis. Because of the osmosis, the liquid level on the concentrated solute side will increase, yielding a hydrostatic pressure difference build-up. Eventually, the hydrostatic pressure difference (liquid level on the concentrated solute side) reaches a certain level and equilibrium is reached. The hydrostatic pressure difference between the two solutions at equilibrium is called the osmotic pressure. If a hydrostatic pressure, just equal to this osmotic pressure, was initially put on the solution to the left (C_1) at time $t = 0$, the osmotic flow would have been prevented.

The osmotic pressure comes from the phenomenon of osmosis. The phenomenon of osmotic pressure can also be thought of as "osmotic suction". The more concentrated solute solution (C_1) pursues to be more diluted (like the less concentrated solute solution C_2). Thus, the more concentrated solute solution "sucks" solvent through the semipermeabel membrane in order to become more diluted. During the osmotic suction, the liquid level on the concentrated solute side will increase, yielding a hydrostatic pressure difference build-up. The osmotic suction is stopped when the hydrostatic pressure difference (osmotic pressure) between the two solutions has reached a certain level. At this level, equilibrium is reached.

As we have seen now, an osmotic flow of solvent through the semipermeabel membrane is induced from the diluate towards the concentrate. But why does the concentrated solute solution pursues to be more dilute? Why does the diluted solute side pursue to dilute the concentrated solute side? Why does the osmotic flow or osmotic suction exist? And why does the osmotic flow stops at a certain level (at equilibrium)? The answers can be found by looking at the solvent concentrations (or solvent activities), or rather the chemical potentials of the solvent. The chemical potential is denoted μ. The chemical potential of the solvent is defined as follows:

$$\mu_{solvent} = \mu^{0}_{solvent} + R \cdot T \cdot \ln(a_{solvent}) + V_{solvent} \cdot P \qquad (7)$$

The chemical potential, μ, of the solvent is a function of the standard chemical potential μ^0 (at infinite dilution), the temperature T, the solvent activity a, the molar volume V of the solvent, and the pressure P. Again, we look at Figure 3: The *solute* concentration (activity) is higher on the left side ($C_1 > C_2$), and therefore the *solvent* concentration (solvent activity) is higher of the right side. Thus, the initial chemical potential of the solvent is higher of the right side, because of larger solvent activity. Since the system pursues to reach equilibrium (pursues to have equal solvent chemical potential on both sides of the semipermeabel membrane), solvent will flow through the membrane from the "higher" chemical solvent potential towards the "lower" solvent chemical potential. This flow is called osmosis, and the flow is proportional to the solvent chemical potential gradient over the membrane, $-d\mu/dx$. Hence, the osmotic flow increases the solvent activity a and the pressure P on the left side of the membrane (Figure 3), resulting in an increasing solvent chemical potential on the left side. At the same time, the pressure and solvent activity on the right side of the membrane decreases (liquid level drops and solution gets more concentrated). The drop in pressure and solvent activity on the right side decreases the solvent chemical potential. The osmotic flow stops when the chemical potential of the solvent is equal on both sides of the membrane.

In order to obtain a flux through the membrane from the bulk side (with larger solute concentration) to the permeate side (with lower solute concentration), the applied hydrostatic pressure on the bulk side has to be higher than the osmotic pressure difference between the bulk and permeate side. If we again look at Figure 3, this corresponds to applying a hydrostatic pressure on the left side that is larger than the osmotic pressure. An osmotic pressure term has to be added to the resistance-in-series model that was introduced earlier [Mulder, 1996]:

$$J = \frac{\Delta P - \Delta \pi}{\eta \cdot R_{tot}} \qquad (8)$$

Applying a hydrostatic pressure P on the bulk side, the chemical potential of the solvent increases on the bulk side (according to equation (7)). This chemical potential increase induces a gradient in the solvent chemical potential across the membrane, and the system will allow or facilitate a flux of solvent from the bulk to the permeate in order to equalize this solvent chemical potential gradient (to pursue to reach equilibrium). However, as the bulk is often re-circulated, and the permeate is often continually removed in pressure driven membrane processes, equilibrium is never reached, and the flux can therefore be maintained.

The osmotic pressure, π, of a solution can be calculated by use of the van't Hoff equation [Mulder, 1996]:

$$\pi = \frac{R \cdot T}{M_i} \cdot c_i \qquad (9)$$

In this equation, R is the gas constant, T the absolute temperature, M_i the molar mass of component i, and c_i the concentration of component i. When the osmotic pressure is to be calculated for a sodium chloride solution, the concentration of NaCl has to be multiplied with "*2*" because of the dissociation into two ions, a sodium ion and a chloride ion. The proportionality between osmotic pressure and concentration given in equation (9) applies at low concentrations and for low MW molecules. When the osmotic pressure is to be calculated for macromolecular solutions or high concentration solutions, a virial expansion expression can be used [Mulder, 1996]:

$$\pi = \frac{R \cdot T}{M_i} \cdot c_i + B \cdot c_i^{\,2} + C \cdot c_i^{\,3} + \ \ldots \qquad (10)$$

Here, it is seen that the van't Hoffs equation is the first term of the expanded expression. It is also seen that when the concentration is low, almost only the first term contributes to the osmotic pressure. In that way, equation (10) is reduced to van't Hoffs equation (equation (9)). The terms B and C are constants for specific molecules. For macromolecular solutions, a more simple exponential expression can, however, often be used for calculating the osmotic pressure [Mulder, 1996]:

$$\pi = A \cdot c_i^{\,n}, \qquad n > 1 \qquad (11)$$

The term A is a constant for a specific type of macromolecule, and the exponential factor n has a value larger than "1".

1.1.2 Concentration polarization – mass transfer coefficient

During membrane filtration operation, the convective transport of solutes towards the membrane will lead to a concentration increase in the boundary layer at the membrane surface.

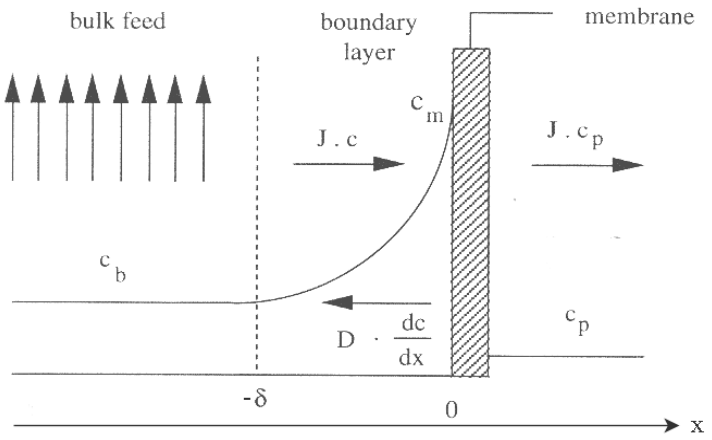

Figure 4: Sketch of the concentration profile in the boundary layer [Mulder, 1996].

In a distance δ from the membrane surface, complete mixing is assumed, resulting in a constant bulk concentration c_b. This is sketched in Figure 4 by the arrows to the left showing the cross-flow along the membrane. In the laminar boundary film layer with the thickness δ, the concentration, c, is increasing due to the convective solute transport in direction x of the flux. This convective transport is balanced, at steady state, by the diffusive transport of solutes back into the bulk solution and the part of the solutes that goes through the membrane to the permeate side. A solute mass balance in the laminar boundary film layer can be set up by these three terms (defined in the direction x according to Figure 4):

- Convective solute transport towards the membrane: $J \times c$
- Diffusive transport back into the bulk: $D \times dc/dx$
- Transport of solutes in the permeate away from the membrane: $J \times c_p$

The diffusion coefficient is denoted D, and dc/dx is the concentration gradient in the laminar boundary film layer. Setting up a mass balance gives the following first order differential equation which describes the concentration polarization in stationary conditions. The boundary conditions (BC) are seen from Figure 4.

$$J \cdot c = D \cdot \frac{dc}{dx} + J \cdot c_p \qquad BC: \begin{cases} x = -\delta \rightarrow c = c_b \\ x = 0 \rightarrow c = c_m \end{cases} \tag{12}$$

The differential equation is solved by integrating over the boundary conditions.

$$\frac{c_m - c_p}{c_b - c_p} = \exp\left(\frac{\delta \cdot J}{D}\right) = \exp\left(\frac{J}{k}\right) \tag{13}$$

This film theory equation describes the connection between the bulk, permeate, membrane surface concentrations, and the flux. The term δ/D can be replaced by $1/k$, where k is the mass transfer coefficient. Thus, it is seen that when the mass transfer coefficient is low, the concentration polarization can be large, resulting in a large surface concentration c_m, compared to the bulk concentration c_b. A high concentration on the membrane surface is often not wanted as it can lead to larger permeate concentrations. It is seen that the ratio between the flux and the mass transfer coefficient, J/k, is a key parameter, and it is often desirable to decrease the thickness of the laminar boundary layer, δ, as it will increase the mass transfer coefficient, k. An increased mass transfer coefficient will, according to the film theory (equation (13)), result in decreased surface concentration and, therefore, a relatively lower permeate concentration. A decrease in the thickness of the laminar boundary layer can be achieved by changing the hydrodynamic conditions on the bulk side. An increased cross-flow velocity along the membrane surface will decrease the laminar boundary layer thickness, but also different inserts and turbulence promoters on the feed side can be used.

The *gel layer model* is often applicable in filtration of macromolecules and typically proteins. When the concentration on the membrane surface, c_m, reaches a certain level, according the model (due to concentration polarization), a gel is formed with a constant gel concentration, c_g. This gel is assumed to be impermeable to the macromolecules, it consists of, and therefore the permeate concentration, c_p, is zero. Inserting this into the film theory model (equation (13)) yields the gel layer model which can be used to determine a limiting flux, J_{lim}, through the membrane.

$$\frac{c_g}{c_b} = \exp\left(\frac{J_{\lim}}{k}\right) \Leftrightarrow J_{\lim} = k \cdot \ln\left(\frac{c_g}{c_b}\right) \qquad (14)$$

The gel layer model can be quite useful although some of its assumptions have been reported in literature not to hold. The gel concentration, for example, should be independent of the bulk concentration which often not seems to be the case. Furthermore, the diffusivity ($D = k \times \delta$) is often not constant, but concentration dependent to some extent. Often deviations from the gel layer model are observed. This can be due to the fact that some macromolecules do not tend to form a gel as easy as other macromolecules. The resistance towards mass transport caused by concentration polarization can be calculated in a sub-resistance, according to equation (6), and when an actual gel layer is formed, the sub-resistance can be referred to as a gel layer resistance, R_g.

As mentioned earlier, the mass transfer coefficient is a very important term to evaluate in a given membrane filtration system. Because of the difference in bulk and surface concentration, due to concentration polarization, a quite large deviation between the observed and true retention (equation (3)) is often observed. A potential high true retention R of a membrane will often not be utilized because of a high surface concentration. This can often be improved by changing the hydrodynamic conditions at the membrane surface. An approximate estimate of the mass transfer coefficient can be determined based on literature correlations including the Reynolds number, Schmidt's

number, and the Sherwood's number which are all dimensionless terms. As seen in the film model and in the gel layer model (equation (13) and (14)), one needs to know the mass transfer coefficient. One way to get a value for the mass transfer coefficient is to use different flow correlations from the literature that combines different dimensionless numbers concerning flow and mass transfer [Mulder, 1996]:

$$\begin{aligned} &\text{Reynolds number}: \mathrm{Re} = \frac{d_h \cdot u}{\nu} \\ &\text{Schmidt number}: \mathrm{Sc} = \frac{\nu}{D} \\ &\text{Sherwood number}: \mathrm{Sh} = \frac{k \cdot d_h}{D} \end{aligned} \qquad (15)$$

The Reynolds number includes the flow velocity u and indicates whether the flow is in the laminar or turbulent region. The Schmidt number is the ratio between the kinematic viscosity ν and the diffusion coefficient D and tells how fast velocity propagates through the fluid compared to how fast mass propagate (diffuses) through the fluid. The Sherwood number is a sort of a dimensionless mass transfer number and includes the mass transfer coefficient, k, the hydraulic diameter, d_h, and the diffusion coefficient, D, and by using correlations combining these three dimensionless number given in equation (15), one can estimate the mass transfer coefficient. Such correlations are shown in Table 4.

Table 4: Different flow correlations for different flow regimes and flow geometries [Mulder, 1996].

	Laminar flow	Turbulent flow
Tube geometry	$\mathrm{Sh} = 1.62 \cdot \left(\mathrm{Re} \cdot \mathrm{Sc} \cdot \mathrm{d_h} / \mathrm{L}\right)^{0.33}$	$\mathrm{Sh} = 0.04 \cdot \mathrm{Re}^{0.75} \cdot \mathrm{Sc}^{0.33}$
Channel geometry	$\mathrm{Sh} = 1.85 \cdot \left(\mathrm{Re} \cdot \mathrm{Sc} \cdot \mathrm{d_h} / \mathrm{L}\right)^{0.33}$	

In the literature, other constants than "1.62", "1.85", "0.33", "0.04", and "0.75" can be found since the given correlations are all empirical and for the given geometries.

1.1.3 Membrane fouling

In stationary conditions, the concentration polarization gives a constant contribution to the total resistance towards mass transport through the membrane. This corresponds to a constant sub-resistance term, R_{CP}, in equation (6). Therefore, the flux should be constant when the applied hydrostatic pressure is constant, but in practice the flux often keeps decreasing during filtration due to membrane fouling. The effects of concentration polarization and membrane fouling on the flux are sketched in Figure 5.

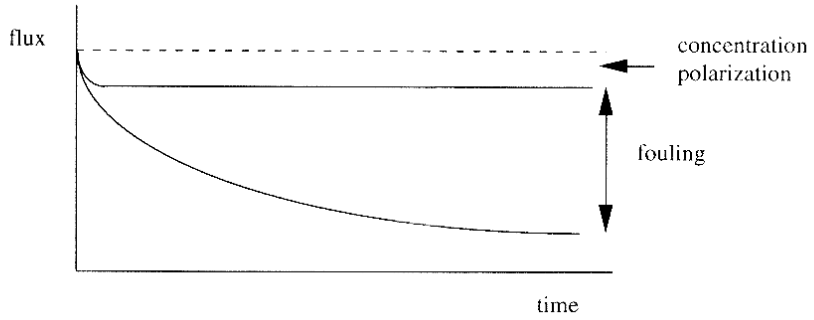

Figure 5: Typical flux decline at constant applied pressure. Concentration polarization contributes with a constant resistance towards mass transport through the membrane, whereas the fouling contribution continually increases resulting in a continually decreasing flux [Mulder, 1996].

Membrane fouling is a complex phenomena affected by many factors such as concentration, temperature, pH, ion strength, hydrophilic/hydrophobic interactions, etc. Membrane fouling can, for example, consist of adsorption of different molecules, colloids or salts on the membrane surface and on the pore walls inside the membrane. In one of our publications, [PAPER 3], we have described the basics of adsorption theory and presented a method to measure the adsorption of macromolecules on membrane surfaces. Adsorption increases the hydraulic resistance of the membrane, and an adsorption sub-resistance, R_a, can be added to the total resistance in the resistance-in-series model (equation (5) and (6)). Membrane fouling also comprises blocking of the pores by different cells, bacteria, particles, or aggregated macromolecules, or it can be the build up of a cake layer on the membrane surface. Membrane fouling can be divided into

- irreversible membrane fouling and
- reversible membrane fouling.

Often, the irreversible membrane fouling is established first. This could be a rather tightly bounded adsorbed mono layer of components on the membrane surface. Such a layer can act a base for further build up of a continually growing fouling layer which is often removable by changing the hydrodynamic conditions. An easily removable outer fouling layer is categorized as reversible membrane fouling. Reversible fouling is often removed when the pressure is released or when the membrane is washed with water, whereas irreversible fouling often has to be removed by cleaning the membrane with certain chemical cleaning agents. Since there in principle is no limit for the growth of a membrane fouling layer, the hydraulic resistance towards mass transport caused by membrane fouling can continually increase, leading to the continually decreasing flux which is sketched in Figure 5. Such behavior is described in our adsorption paper, [PAPER 3], in which we observe the fouling resistance to increase almost linear with the amount of permeate that has been collected during ultrafiltration of an alpha-amylase enzyme concentration experiments in a dead-end batch cell. Thus, the fouling mechanism in that case seemed to be described well by a cake filtration model [PAPER 3], at least at low enzyme concentrations (< 10 g/L). Very detailed literature reviews on membrane

fouling and effects of macromolecules present in the feed stream of a membrane processes can be found in the literature [Marshall et al., 1993; Belfort et al., 1994]. Since it is generally accepted in the literature that proteins play a great role in membrane fouling, simple pH control can reduce protein fouling. Close to the isoelectric point, the proteins are overall uncharged which makes them not repeal each other as much as if the pH is different from the isoelectric point. Kim et al. [Kim et al., 1993] have tested different membrane types, and the pH effect on the BSA fouling in a batch cell and in a cross-flow module. They stated that fouling was less at the pH extremes than at the isoelectric point for all the tested membrane types.

1.2 Membrane materials

Either organic (polymeric), or inorganic (cheramic) membranes can be purchased. The membranes can be fabricated in different shapes such as flat sheet membranes, spiral wound membrane modules, or turbular membranes that further can be divided into i) hollow fibers (diameter < 0.5 mm), ii) capillary membranes (diameter 0.5 – 5 mm), and iii) tubular membranes (diameter > 5 mm) [Mulder, 1996].

1.2.1 Ceramic membranes

In general, cheramic membranes exhibit much higher chemical and thermal stability compared to polymeric membranes. The price is also larger because the preparation process (sintering at very high temperature) requires much more energy [Mulder, 1996]. Different chemical componds can be used for ceramic membraens such as oxides and carabids:

- Al_2O_3 alumina oxide
- ZrO_2 zirkonia oxide
- TiO_2 titanium oxide
- SiC silicon carabid

Especially the silicon carabid (SiC) membranes exhibit very high fluxes because of the relatively high porosity of the material [Cometas.dk, 2008]. In general, ceramic membranes can withstand very high tempeatures (> 1000^0C) and harsh chemical conditions (all pH and solvent) which is due to the covalent nature of the chemical bonds between the atoms in the ceramic. The valence electrons (bond electrons) are very tightly "locked" in the bond orbital which gives a very high bond energy and, therefore, a very high thermal and chemical stability [Hede & Beier, 2007]. The high thermal and chemical stability make the cleaning process very flexible with respect to pH and temperature, and the life time of ceramic membranes is often longer than the life time of polymeric membranes.

1.2.2 Polymeric membranes

Polymeric membranes consist of a skin layer over which the retention and selectitivy is achieved. The skin layer is often very thin (~ 1 μm) which is desired since the membrane resistance, R_m, and the thichness of the skin layer is inversely proportional. The skin layer is suported by a porous layer (support layer) that gives the necessary mechanical strength to the membrane. Membranes can be divided into two main categories:

- Integrated asymetric membranes
- Composite membranes

Integraded asymmetic membranes are characterized by the fact that the skin layer and the support layer are made from the same material. In composite membranes, however, the skin layer and support layer are made from different materials that can be optimized individualle in order to achieve the desired abilities. Membranes can further be chategorized according to their hydrophilicity. Some common membrane polymeric materials are listed in Table 5, according to their hydrophilicity.

Table 5: Common polymeric membrane materials

Hydrophobic polymeric materials	PE, polyethylene
	PP, polypropylene
	PTFE, polytetrafluoroethylene (teflon)
	PVDF, poly(vinylidine fluoride)
	PS, polysulphone
	PES, polyether sulphone
Hydrophilic polymeric materials	CA, cellulose acetate
	CE, cellulose ester
	PC, polycarbonate
	PA, polyamide
	PEEK, polyetheretherketone

The limit between hydrophobic and hydrophilic is not very clear. The transition is fluent and, therefore, the material can be in the boundary region between hydrophobic and hydrophilic. The hydrophilicity can have a great impact on the specific filtration performance. In general, the hydropobic membranes exhibit a larger tendency to foul, especially when proteins are present in the feed stream, than hydrophilic membranes [Jones, 1987; Mulder, 1996]. The hydrophobicity of a surface is related to the surface tension or the surface energy. The surface energy of a substance is the work required to isothermally increase the area of a surface. Therefore, the unit for surface tension is given as “energy pr. area” or “force pr. length”.

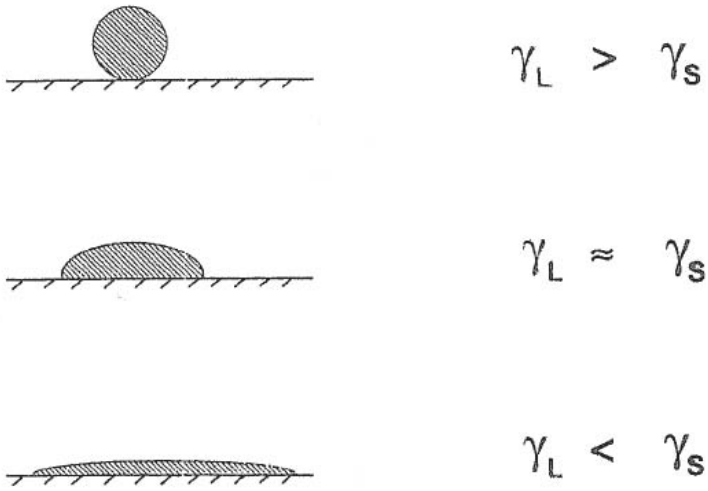

Figure 6: Wetting of a surface depends on the surface tension of the liquid γ_L and of the solid γ_S.

In Figure 6 it is seen that a surface will be wetted when the surface tension of the surface is higher than for the liquid. Therefore, more hydrophilic membranes have higher surface tensions. The surface tension of water is $72 \cdot 10^{-3}$ J/m^2, and therefore surfaces with a higher surface energy than this will be wetted by water droplets.

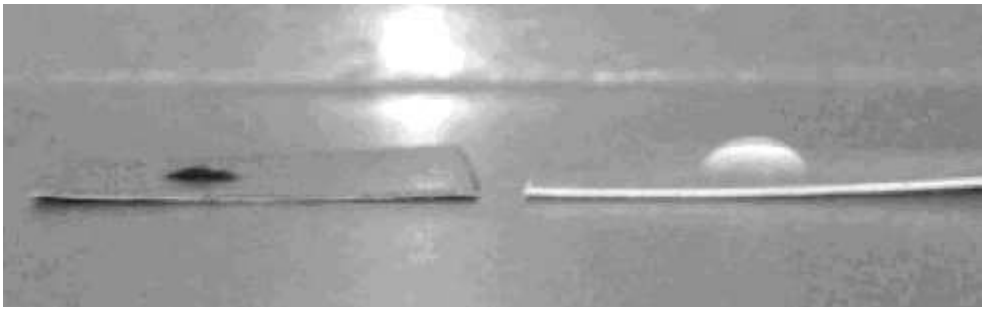

Figure 7: 10 µl droplets of water on a surface-modified poly(vinylidene fluoride) PVDF membrane (to the left) and a polyethersulphone PES membrane (to the right) [PAPER 3].

In Figure 7, water droplets on two different membranes are shown. It is seen that the more hydrophilic surface modified PVDF membrane must have a surface tension larger than the surface tension of water, whereas the surface tension of the PES membrane must be in the same order of magnitude as that of water, when you compare the shape of the droplets with the sketches in Figure 6. This means that more hydrophobic membranes have lower surface energies than more hydrophilic membranes, and the more hydrophobic membranes are more easily fouled by proteins since the large hydrophobic parts of the proteins can interact with the hydrophobic surfaces.

Figure 8: 10 µl droplets of water on a PES/PVP hollow fiber surface.

In Figure 8, a water droplet on one of the hollow fibers, used in the experimental work [PAPER 1, 2, 4, and 5], is seen. Compared to Figure 6, it seems as if the surface tension of the hollow fiber surface and the water is at the same level, judged from the contact angle. The skin layer is located on the outside of the fibers which are made of a polyethersulphone (PES) and polyvinylpyrrolidone (PVP) blend in a 98%/2% ratio. PVP is added in order to make the fibers more hydrophilic. The average water permeability of the clean membrane module has been measured to 7800 L/(m^2·h·bar) with a standard deviation of 1000 L/(m^2·h·bar), corresponding to 13 %, based on 16 measurements [PAPER 4]. The pore sizes of the fibers are around 0.36 – 0.50 µm. In one of our publications [PAPER 2], SEM pictures of the fibers are presented.

1.3 Membrane Cleaning

Almost every membrane process requires some sort of cleaning due to membrane fouling. This is necessary not just in order to regain or maintain the initial flux, but in some cases also to maintain a certain selectivity [Gan et al., 1999]. Different kinds of membrane cleaning can be distinguished [Mulder, 1996]:

- Chemical cleaning
- Hydraulic cleaning
- Mechanical cleaning
- Electric cleaning

These methods are efficient to different extents depending on the feed composition, module configuration, and membrane properties, and a combination of different cleaning methods is often possible which can result in a positive synergy effect on the cleaning procedure [Gan et al., 1999]. In the following sub sections, each cleaning method will be described.

1.3.1 Chemical cleaning

Different chemicals are used to chemical membrane cleaning depending on the type, nature, and composition of the fouling. To draw some general lines, chemicals for chemical membrane cleaning can be divided into the following groups, listed in Table 6, depending on the sort of membrane fouling it is supposed to remove or deal with.

Table 6: Different cleaning agent types [Tragårdh, 1989; Mulder, 1996; Zeman & Zydney, 1996].

Type of chemical	Example	Foulant
Acidic	HCl, HNO_3, H_2SO_4, H_3PO_4, Organic acids	Calcium salts (carbonates, phosphates), metal oxides
Alkali	NaOH, KOH, Na_2CO_3, phosphates	Biological/organic foulants, inorganic colloids, silica foulants
Enzymatic	Proteases, amylases, lipases, cellulases, glucanases	Proteins, starch, fats, oils, cellulose
Surfactant	Nonionic, anionic, cationic	Mostly used in combination with other cleaning agents. Increase wettability.
Chelating agents	EDTA, polyacrylates, hexametaphosphates, citrate, STPP[1], CMC[2]	Mostly used in combination with other cleaning agents.
Disinfectants	H_2O_2, NaOCl, sodium bissulphite	Used after chemical cleaning

[1] Sodium tripolyphosphate (STPP)
[2] Sodium carboxymethylcellulose (CMC)

Before one starts to choose chemicals to clean a membrane system, the chemical stability of the membrane and the whole system has to be considered. In order to ensure that the chemicals work efficiently, the chemicals during the chemical cleaning process have to do the following [Trägårdh, 1989]:

i. Loosen and dissolve the fouling
ii. Keep the foulant in dispersion and solution
iii. Avoid new fouling
iv. Not attack the membrane (and other parts of the system)
v. Disinfect all wetted surfaces

Acidic cleaning agents

Acidic cleaning agents are mostly used to dissolve fouling consisting of inorganic salts or oxide films consisting of metal oxides. For example, inorganic salt calcium carbonate is dissolved and converted into much more soluble calcium chloride by reaction with hydrochloric acid:

$$CaCO_3 + 2HCl \rightarrow CaCl_2 + H_2O + CO_2$$

Calcium chloride is easily removed by the cleaning solution in the membrane system. Metal oxides can also be removed by hydrochloric acid:

$$Fe_2O_3 + 6HCl \rightarrow 2FeCl_3 + 3H_2O$$

In these two cases, hydrochloric acid is used. However, other acids listed in Table 6 can also be used and often phosphorus acid is used since it is less corrosive than strong acids such as hydrochloric, sulfuric, or nitric acid. Furthermore, phosphorus acid provides better pH control because of the buffering capacity [Zeman & Zydney, 1996].

Alkali cleaning agents

Biological/organic foulants, inorganic colloids, and silica foulants are often removed by alkali cleaning agents. Alkali cleaning agents such as potassium and sodium hydroxide solubilize proteins to some extent and saponificate fats:

$$C_3H_5(OOCR)_3 + 3NaOH \rightarrow C_3H_5(OH)_3 + 3NaOOCR$$

The produced soap molecules form micelles in the water and can, therefore, be removed by the cleaning solution. Carbonates usually do not have good cleaning properties, but they are efficient to ensure the pH because of its pH-regulating properties. Phosphates of different kinds (e.g. sodium tripolyphosphate, sodium hexametaphosphate, and trisodium phosphate) are often used as water softeners since they have the ability of forming soluble complexes with calcium and magnesium ions present in the water [Trägårdh, 1989; Zeman & Zydney, 1996]. Actually, these phosphates can be considered as chelating agents which will be describes later.

Enzymatic cleaning agents

Enzymatic cleaning agents can be used when the membrane can not withstand high temperatures and or high or low pH (e.g. cellulose acetate membranes). Enzymatic cleaning agents contain enzymes of different kinds that are able to degrade different types of fouling components. Proteases can break down proteins by cleaving the peptide linkages, and amylases can degrade starch by cleaving the glucose linkages. Fats and oils can be degraded by lipases that hydrolyze the ester bonds in the triglycerides, and cellulose can be degraded by cellulase enzymes [Trägårdh, 1989; Zeman & Zydney, 1996].

Surfactants

Surfactants can be nonionic, anionic, or cationic. Nonionic surfactants can for example be condensates of ethylene oxides (polyethylene oxides), whereas anionic surfactants can be alkyl sulphates or alkyl sulphonates. Cationic surfactants can be quaternary ammonium compounds [Tragårdh, 1989]. Surfactants work by i) displacing foulants from the membrane surface due to their strong surface adsorption, ii) emulsifying oils, and iii) solubulizing hydrophobic foulants by incorporating them into the surfactant micelles [Zeman & Zydney, 1996], according to Figure 9.

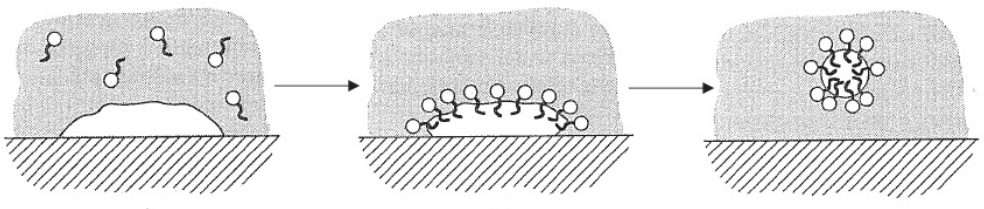

Figure 9: Sketch of a surface fouled by for example an oil droplet. The surfactants solubilize the oil by encapsulating it into a micelle that solubilizes [Zeman & Zydney, 1996].

Surfactants are often used in combination with other types of cleaning agents to i) improve the wettability and rinsability, ii) improve the contact between the cleaning chemicals and the deposits, iii) minimize the amount of water, and iv) minimize the rinsing time [Trägårdh, 1989].

Chelating agents

Chelating agents are sometimes referred to as sequestrants. Chelating agents work in the way that they contain one or more electron donor atoms that can form complexes to for example metal atoms. Thus, coordination compounds are formed and these are soluble in water and can, therefore, be removed with the cleaning solution. Chelating agents are mostly used in combination with other cleaning agents. Often they are added as water softeners that remove calcium and magnesium ions in the same manner as the polyphosphates. Some well know chelating agents can be mentioned such as EDTA (ethylenediamine tetraacetic acid), polyacrylates, hexametaphosphates, citrate, STPP (sodium tripolyphosphate), and CMC (sodium carboxymethylcellulose). [Zeman & Zydney, 1996]. EDTA is the most effective, but because of environmental reasons, it is becoming less popular.

Disinfectants

Disinfectants are often used after the cleaning cycle to destroy all pathogenic microorganisms. When using disinfectants, one has to consider whether the membrane is chemically stable to withstand the disinfectant. H_2O_2, NaOCl, and sodium bissulphite can be mentioned as some well known disinfectants. Disinfectants destroy living pathogens but often not highly resistant bacterial spores that has to be removed by sterilization [Trägårdh, 1989; Zeman & Zydney, 1996].

1.3.2 Hydraulic cleaning

Hydraulic cleaning methods can be introduced or integrated into the membrane process itself. One hydraulic cleaning procedure can be to relief the transmembrane pressure for a while and that way compaction of the fouling layer will be relieved or loosened. Another definition of a hydraulic cleaning procedure could be the induction of the backflushing technique. This technique is mainly applicable to microfiltration and ultrafiltration. When using the backflush procedure, a given volume of permeate is flushed through the membrane from the permeate side to the feed side at given intervals and at given duration. This loosens the deposited fouling layer on the feed side of the membrane, as shown in Figure 10

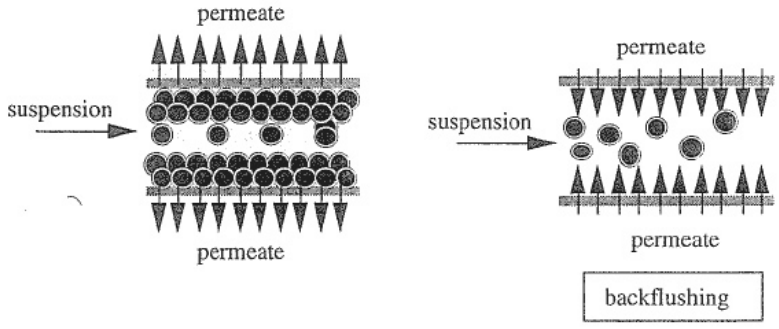

Figure 10: The backflush principle [Mulder, 1996]

When periodically inducing such backflushes, a flux vs. time curve can look as sketched in Figure 11.

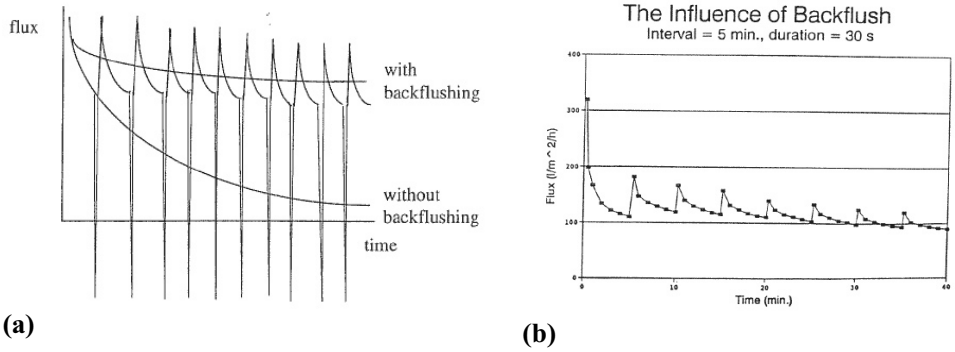

(a) **(b)**

Figure 11: (A) sketch of a typical flux vs. time curve with and without backflushing [Mulder, 1996]. (B) Actual flux vs. time curve for a beer filtration on a microfiltration membrane [Jonsson & Wenten, 1994].

As seen in Figure 11(A), at each backflush an amount of permeate is "lost", but because of the increased flux between the bachflushes, the overall flux can be increased compared to the flux without backflush. The backflush technique has show to be very efficient, but a drawback is that a relatively large amount of permeate is "lost" during the backflushes. To overcome this problem, the backshock technique was introduced by Jonsson and Wenten in 1994 [Jonsson & Wenten, 1994]. Compared to the backflush technique, the backshock durations are much shorter and in the range of 0.1 seconds, and the permeate is here pressurized back through the membrane for a very short time. Therefore, even though the intervals between the backshock are shorter, a much smaller amount of permeate is lost compared to the backflush technique. Actually, Jonsson and Wenten [Jonsson & Wenten, 1994] mention that it is likely that the pressure fluctuations itself (and not the backflushed volume of permeate) is further increasing the performance of this process. The fouling layer on the feed side is continuously destabilized, and therefore a steady-state concentration profile is never reached which will lower the level of compact fouling. When using reverse asymmetric membranes, the fouling can be kept very open and not compact in the support structure, and it is easily controlled by the backshocks if the feed is introduced to the support layer side of the membrane. Jonsson and Wenten [Jonsson & Wenten, 1994] conducted backshock microfiltration of beer and found many advantages: I) Only low cross-flow is necessary which reduces the pumping costs and the surface shear rate thus avoiding protein denaturation, and II) the macromolecular transmission can be close to 100 % which often is very difficult to achieve in microfiltration.

Guerra et al. have also used the backshock technique in the filtration of skim milk with a microfiltration membrane module [Guerra et al., 1997]. They reached the same conclusions as Jonsson and Wenten [Jonsson & Wenten, 1994]: When using reverse asymmetric membranes, the fouling inside the open support structure could be maintained very open and was controlled by the backshocks if the feed is introduced to the support side of the membrane. Thus, even at low cross-flow velocity (low energy

consumption), the flux could be kept very high, the bacteria spore retention was high, and the casein transmission was 100 %.

Another hydraulic approach to reduce fouling is the shear-enhanced filtration techniques which consist of creating a relative motion between the membrane and the feed stream. This is often referred to as *dynamic* filtration. This can be done by vibrations or rotations of the membrane, which makes it possible to decouple high feed cross-flow velocity and high surface shear rate. That way, filtrations can be carried out at low feed cross-flow velocity, low TMP, and with a high surface shear rate that reduces fouling problems. Such dynamic systems will be described in chapter 2 of this thesis.

1.3.3 Mechanical cleaning

Oversized sponge balls can sometimes be used in different tubular membrane systems as a mechanical cleaning method. The sponge balls are flushed through the membrane module on the feed side in order to "hit" and drag away deposited fouling [Mulder, 1996].

Strohwald and Jacobs [Strohwald & Jacobs, 1992] used sponge balls in the mechanical cleaning of a tubular ultrafiltration module for the pretreatment of seawater that later on was to be desalinated by reverse osmosis. They stated that the mechanical cleaning of the tubular seawater ultrafiltration module with the aid of sponge balls and a flow-reversal system proved to be effective in removing substantial amounts of foulant material. The beneficial effect of sponge ball cleaning resulted in a higher seawater flux that could be maintained.

Mechanical cleaning by use of sponge balls can be found in contexts other than membrane cleaning. Pipelines for beer have been reported mechanically cleaned with sponge balls by Müller and Sommer [Müller & Sommer, 2000], and Hanbury et al. [Hanbury et al., 2003] have also tested sponge ball cleaning in a multi-stage flash (MSF) plant for desalination of water.

1.3.4 Electric cleaning

Electric cleaning consists in applying an electric field across a membrane during operation. That way, charged particles will migrate in the direction of the electric field [Mulder, 1996]. Therefore, macromolecules that often are charged can be dragged away from the membrane surface by the electric field and can, thus, not contribute to the fouling of the membrane. It is only charged foulants that will be removed by the electric cleaning.

Enevoldsen et al. have done a substantial amount of work in the area of electro ultrafiltration (EUF) [Enevoldsen et al., 2007] of industrial enzyme solutions. They were

able to increase the flux 3-7 times during electro ultrafiltration with a field strength of 1600 V/m of an industrial charged enzyme compared to conventional ultrafiltration.

2 Dynamic membrane filtration systems

The aim of this chapter is to introduce and describe different membrane filtration systems that all can be put into the category of *dynamic membrane filtration systems*. Generally, these systems all focus on reducing fouling problems by inducing shear at the membrane surface that is decoupled from the feed flow velocity. Surface shear is necessary in order to reduce concentration polarization and reduce fouling phenomena such as deposition, pore blocking, and cake layer formation. By creating a relative motion between the membrane surface and the surrounding fluid, independent of the feed fluid circulation rate, the pressure drop inside the module can be kept low which is beneficial from the point of view of i) pumping costs, ii) having a uniform TMP, and iii) possibility of avoiding compact fouling layer. The latter is advantageous in order to enhance transmission of macromolecules during e.g. microfiltration (MF) separation of macromolecules from larger components like cells, cell debris, or bacteria.

Back in the 1970'ties, one of the first dynamic membrane filtration systems were reported in the scientific literature, and until today, the number of publications in the *dynamic membrane filtration area* has increased, as seen in Figure 12.

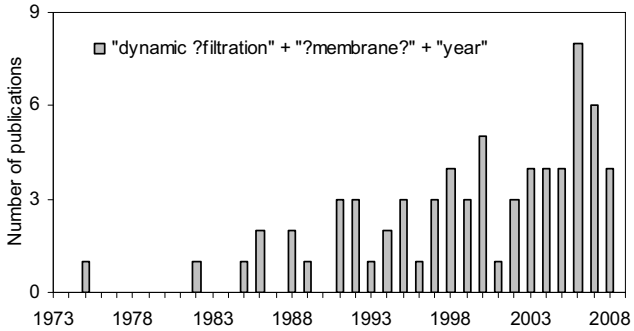

Figure 12: Number of publications found by using the DADS article database at the Technical Knowledge Center, Technical University of Denmark, May 2008, using the search words: "dynamic ?filtration", "?membrane?" and "year".

Even though probably not all dynamic membrane filtration related publications are "caught" by this search, one still gets the impression that the research in this field has increased in the last 20 years. This chapter is not a full review on dynamic filtrations systems but rater an introduction to eight more or less different dynamic membrane filtration concepts. Each concept will be described in a separate sub-sections along with some commercialized approached for some of the systems. At the end of the chapter, a few general trends will be outlined along with a list giving the main features, advantages, and disadvantages of the different concepts.

2.1 Different dynamic concepts

2.1.1 Rotating membrane filter systems (RMF)

The concept of the rotating membrane filter (RMF) was described in the 1970's under the name of a *rotorfermentor* [Margaritis, 1976]. The idea is that a rotating micro porous membrane is enclosed inside a fermentor. If filtering fermentation broth, the living and growing cells are retained by the membrane, and metabolic products (or inhibitors) are continually removed with the filtrate. Rotating membrane filters have been reported mostly in MF contexts [Margaritis, 1976; Tobler, 1982; Kroner & Nissinen, 1988; Rushton & Zhang, 1988; Murase et al., 1991; Park et al., 1994; Choi et al., 1999] but also in UF [Goldinger et al., 1986].

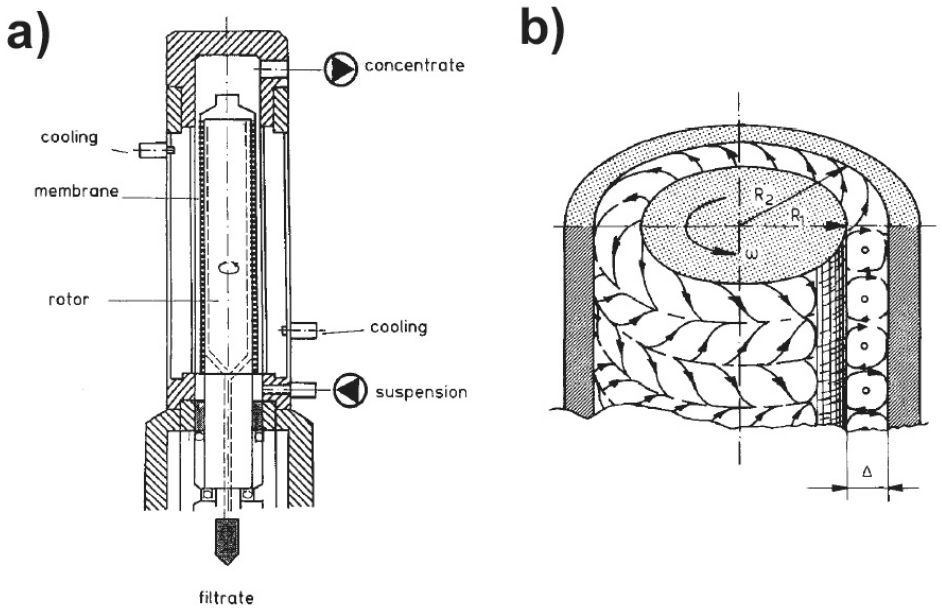

Figure 13: a) Sketch of a rotating membrane filter, b) Schematic drawing of the flow pattern with Taylor vortices in the annular gap between the two cylinders [Kroner & Nissinen, 1988].

The filter unit consists of two coaxial cylinders, as sketched in Figure 13, and the feed (e.g. fermentation broth) is fed in the annular gap between the cylinders. In some configurations, only the inner cylinder wall is used for filtration with a membrane mounted on the outer surface [Kroner & Nissinen, 1988; Murase et al., 1991; Part et al., 1994], whereas in other configurations, membranes are attached to both cylinder walls [Tobler, 1982; Goldinger et al., 1986]. When the inner cylinder is rotating, Taylor vortices are induced between the two cylinders, as sketched in Figure 13b. This creates a flow pattern and a more efficient mean of shear generation, compared to conventional crossflow filtration systems, according to Rushton & Zhang [Rushton & Zhang, 1998],

that reduce fouling and concentration polarization. The shear effect on the cylinder wall is represented by a Taylor number (Ta) [Park et al., 1994].

$$Ta = \frac{\omega_i \cdot r_i \cdot d}{\nu} \cdot \left(\frac{d}{r_i}\right)^{\frac{1}{2}} \quad (16)$$

The angular velocity of the inner cylinder is denoted ω_i, and the outer radius of the inner cylinder is denoted r_i. The width of the gap between the two cylinders is denoted d, and ν is the kinematic viscosity of the feed. As seen in equation (16), the shear effect (Taylor number) is completely decoupled from a feed flow velocity, and therefore, pumping costs to produce shear are avoided. Park et al. [Park et al., 1994] report linear dependency between flux and Taylor number for filtration of silica particle slurries:

$$J = f(Ta) \quad (17)$$

Furthermore, Park et al. [Park et al., 1994] state that Taylor vortices appear if $d/r_i << 1$ and $Ta > 41.3$ which means that the system, rotation speed, and dimensions has to be designed in order to obtain Taylor vortices. The critical Taylor number, Ta_c, at which the Taylor vortices appear, has a tendency to increase with an increase in the d/r_i ratio.

The rotorfermentor is designed to achieve high cell concentrations. Since cell-free filtrate is continually removed, the rotorfermentor could in principle replace ordinary continuous stirred tank fermentors plus cell centrifuges. Furthermore, cell concentration and ethanol productivity were found to be much higher than those for an ordinary continually stirred tank fermentor, according to Margaritis [Margaritis, 1976] who also emphasize the lower operational costs as a clear benefit. Another feature of the RMF system, highlighted by Kroner and Nissinen [Kroner & Nissinen, 1988], is the actual possibility of separating macromolecules from cellular suspension (e.g. fermentation broth). They report a 94 % protease transmission during MF separation from fermentation broth medium with a quite high flux of 70 L/(m^2·h). They state the performance to be three times better compared to conventional crossflow systems [Kroner & Nissinen, 1988], however, without further specification of the reference conventional system. Also, Tobler [Tobler, 1982] mention the lower operational costs and lower washing water requirement in the processing of yellow pigment and the more effective shear generation which is also described by Rushton & Zhang [Rushton & Zhang, 1988] in the concentration of $CaCO_3$ and $CaSiO_3$ slurries using a RMF system. Murase et al. [Murase et al., 1991] describe the relationship between a so-called *dynamic filtration factor* and some operational parameters for design and evaluation purposes of the RMF system, using polymethyl methacrylate (PMMA) particles, and Choi et al. [Choi et al., 1999] proposes an empirical model based on earlier results of Park et al. [Park et al., 1994], using silica particles, for prediction of filtration resistance. The general principles of the system was patented in 1988 [US patent, 1988], and in 1996, Deniega et al. [Deniega et al., 1996] patented the use of a rotating membrane filter in the removal of leukocytes from leukocyte contaminated blood.

In spite of all the different researches, using RMF related systems, no RMF system has been commercialized to our knowledge. This might be due to the relatively complexity of the system and apparatus and the need of actually getting the system to operate submerged directly into the fermentation tank.

2.1.2 Vibratory shear-enhanced processing systems (VSEP)

In 1992, the vibratory shear-enhanced processing system (VSEP) was reported by Culkin and Armando [Culkin & Armando, 1992] as a "new separation system that extends the use of membranes". The advantages were emphasized as the possibility of taking a dilute stream and concentrate it to a very high solid content in a single pass. Furthermore, the system was described as more energy-efficient than conventional crossflow systems.

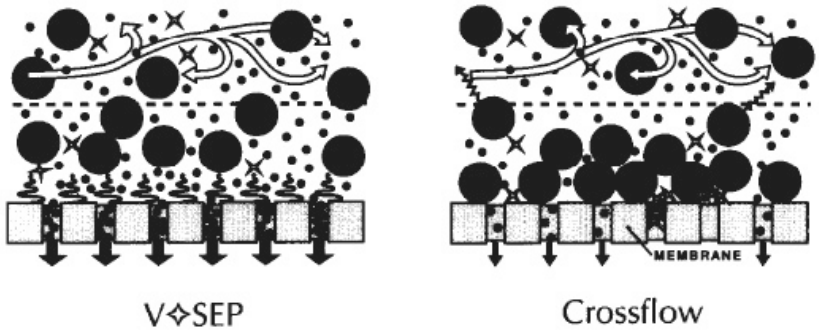

Figure 14: Sketch of the VSEP concept vs. the crossflow concept. Particles are prevented from being deposited on the membrane surface in the VSEP system because of surface oscillation [Culkin & Armando, 1992].

As seen in Figure 14, the principle of the VSEP system is that the membrane is oscillated at high frequency (around 60 Hz) in a parallel motion relative to the membrane surface. Traditional crossflow membranes are easily plugged and fouled because the turbulent flow stream cannot remove the retained particulates within the laminar boundary layer closest to the membrane surface. In the VSEP system, the vibrational energy focuses shear waves directly at the membrane surface repelling solids and foulants while allowing permeate rates up to ten times higher than conventional crossflow systems, according to Culkin and Armando [Culkin & Armando, 1992]. In crossflow designs, it is not economic to create shear forces measuring more than 10,000-15,000 s^{-1}, according to Culkin and Armando [Culkin & Armando, 1992], thus limiting the use of crossflow to low-viscosity fluids. In addition, increased crossflow velocities result in a significant pressure drop from the inlet (high pressure) to the outlet (lower pressure) at the end of the device, which leads to uneven distribution of fouling on the membrane. However, the oscillation of the VSEP system produces a shear at the membrane surface of around 150,000 s^{-1} which is approximately ten times the shear rate of the best conventional crossflow systems. More importantly, the shear in a VSEP system is focused directly at the membrane surface, where it is most useful in preventing fouling, while the bulk fluid between the membrane disks moves very little [Vsep.com, 2008].

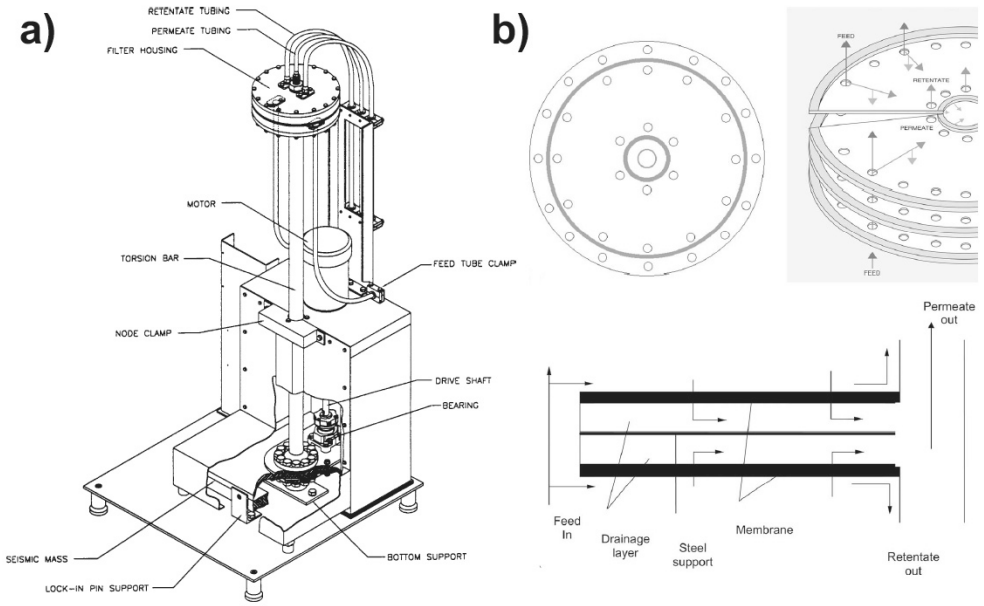

Figure 15: a) Sketch of a VSEP unit. b) Sketch of the membrane stack and internal flow channels inside the membrane stack [Postlethwaite et al., 2004].

VSEP systems in different configurations are reported in the literature. However, the basic principles are the same, and in Figure 15, a sketch of one of the VSEP system is shown. The system uses mechanical energy generated by vibrations to create high and intermittent shear rates at the membrane surface. This allows the shear necessary to prevent membrane fouling to be decoupled from the liquid crossflow velocity, allowing operation at lower trans-module pressure drops and a lowered amount of energy required for pumping. A torsion spring mechanism brings about vibrations of the membrane by causing two equivalent masses (a seismic mass in the bottom end and the filter housing in the top) linked by a torsion bar to vibrate azimuthally 180^0 out of phase.

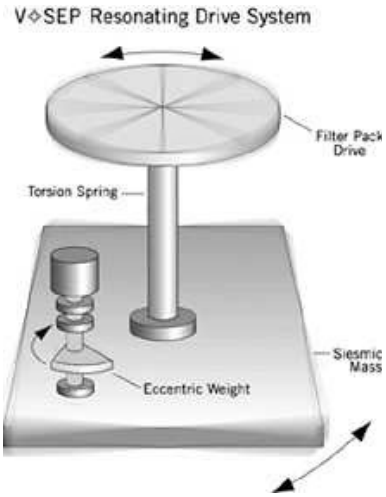

Figure 16: The VSEP vibration principle [Vsep.com, 2008].

Figure 16 shows the principle of the VSEP vibratory system: The eccentric weight is rotating (clockwise in this case and driven by an electromotor) which makes the seismic mass oscillate azimuthally. The azimuthally motion is transferred to the filter pack by the torsion spring, and when the frequency is around the "natural frequency" or a "resonance frequency" of the system, the energy consumption is minimized [Vsep.com, 2008; Pall.com, 2008].

Culkin and Armando [Culkin & Armando, 1992] emphasize the high percentage of the total spent energy that is actually converted to shear forces at the membrane surface. In VSEP systems, nearly 99 % of the total energy is converted at the membrane surface, whereas in crossflow membrane systems only around 10 % of the energy required to run the system is converted to shear forces. Thus, a much more efficient use of the energy is achieved in VSEP systems. However, no further and detailed explanation on these percentages is given. A general advantage of the VSEP system is the very high fluxes and the possibility of achieving very high dry matter contents of the retentate in a single pass.

VSEP systems have been reported in pervaporation [Vane et al., 1999], in NF/RO [Frappart et al., 2008; Zouboulis & Petala, 2008], in UF [Culkin & Armando, 1992; Takata et al., 1998; Akoum et al., 2002i, ii, iii; Jaffrin et al., 2004; Petala & Zouboulis, 2006; Shi & Benjamin, 2008; Zouboulis & Petala, 2008], and in MF [Culkin & Armando, 1992; Akoum et al., 2002i, ii, iii; Jaffrin et al., 2004; Postlethwaite et al., 2004; Petala & Zouboulis, 2006; Zouboulis & Petala, 2008]. A wide variety of applications have been reported in the literature. In the removal of humic substances from river water, a VSEP system was reported superior compared to e.g. conventional sand filter systems and yielded high permeate fluxes and good water quality [Takata et al., 1998]. Separation of macromolecules (BSA) from cellular material (yeast cells) with high macromolecular transmission has also been reported using a VSEP system [Postlethwaite et al., 2004]. Furthermore, treatments of latex polymers, pharmaceuticals, pigment suspensions and wastewater are mentioned as possibilities [Culkin & Armando, 1992]. In MF and

ultrafiltration (UF) of skim milk, Al-Akoum et al. [Al-Akoum et al., 2002i] report high casein rejection and high whey protein transmission, and Zouboulis & Petala [Zouboulis & Petala, 2008] also report high fluxes and enhanced removal of contaminants in nanofiltration (NF) and UF of landfill leaches.

The main factor determining the performance of a VSEP system is the shear rate at the membrane surface. The maximum shear rate at the membrane surface is a function of the oscillation amplitude *amp*, the frequency *F*, and the kinematic viscosity of the feed, ν [Jaffrin et al., 2004]:

$$\gamma_{s,\max} = f\left(amp, F^{3/2}, \nu^{-1/2}\right) \quad (18)$$

Maximum shear rate is present at the periphery of the membrane. Closer to the center of the membrane, the shear rate is lower which means that the inner parts of the membrane is not utilized to the same extent as the outer parts. Often in the literature, empirical correlations between flux and average surface shear rates $\bar{\gamma}_s$ are reported:

$$J = f\left(\bar{\gamma}_s^{\,n}\right) \quad (19)$$

- n = 0.19 – 0.50 in UF/MF of yeast cell suspensions [Jaffrin et al., 2004]
- n = 0.426 for UF/MF of BSA solutions [Al Akoum et al., 2002iii]
- n = 0.2 for BSA solutions containing yeast [Postlethwaite et al., 2004]
- n = 0.215 – 0.567 for UF/MF for skim milk [Al-Akoum et al., 2002ii]
- n = 0.21-0.31 for NF/UF of surface waters [Petala & Zouboulis, 2006]

It is seen that the empirical correlations have powers ranging from around 0.2 to around 0.6 depending on the type of feed. Since the surface shear rate is decoupled from the feed flow velocity, and is only dependent upon the viscosity and the vibration degree of the filter stack, it follows that the flux also is completely decoupled from the inlet velocity of the feed.

A VSEP system has been commercialized by Pall Corporation [Pall.com, 2008], and the Carlsberg Brewery in Fredericia (Denmark) still uses a Pall unit with polymeric teflon-based membranes in the recovery of beer from surplus yeast. The system is by Pall called *VMF*, *V*ibrating *M*embrane *F*ilter. The feed, at Tuborg Brewery, consists of beer with a relatively high content of surplus yeast cells that no longer can be used for fermentation purposes. Therefore, the beer has to be recovered, whereas the surplus yeast has to be concentrated and discarded (e.g. sold at animal feed). The Pall unit operates with a relative low feed inlet velocity of only 2 cm/s, and the system operates for approximately 18-21 hours without cleaning. The retentate after filtration of one tank of surplus yeast contains as high as 21 % dry matter, and the energy consumption during operation is only 11 kW, compared to the 27 kW used during the centrifugation process that was earlier

used to conduct the separation. Furthermore, permeate (beer) quality is much better than if the separation was accomplished by centrifugation [Beier, 2004]. The polymeric membrane-based VSEP solution by Pall is, however, more or less now replaced by a solution (Keraflux) utilizing ceramic membranes in a crossflow mode. This is probably because, still, mechanical problems with the VMF systems occurred. Membrane breakage at Carlsberg often occurred, and in the present system, the whole membrane head then has to be equipped with new membranes since no procedure exists to identify the single membrane(s) with a failure. Thus, it is very costly to actually keep the systems operating since the expenses for reparation are quite large. However, today also New Logic Research Inc. is offering VSEP commercial systems [Vsep.com, 2008].

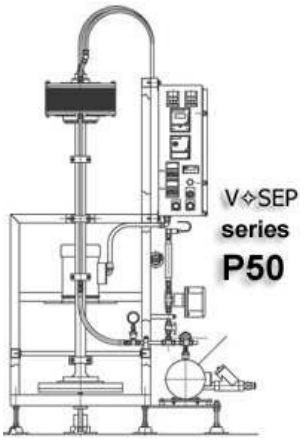

(a)

(b)

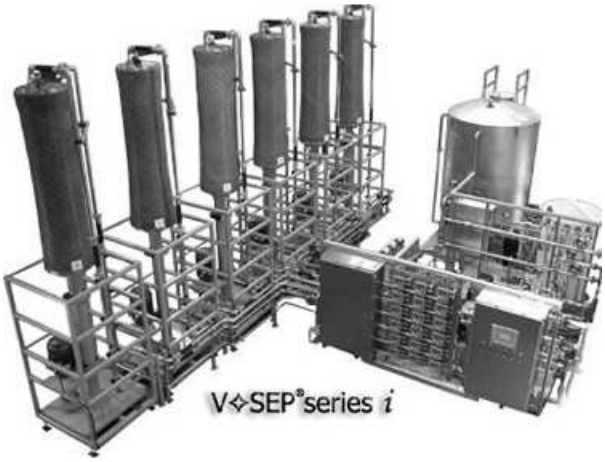

(c)

Figure 17: New Logic Research Inc. commercial VSEP systems. (a) VSEP series P50, (b) VSEP series L/P (Lap/Pilot), (c) VSEP series *i* [Vsep.com, 2008].

Figure 17 shows the three VSEP series offered by New Logic. Many different polymeric membranes are available in the whole spectrum from NF over UF to MF [Vsep.com,

2008]. In MF, however, almost only Teflon-based membranes are used. The *series L/P* (Lap/Pilot) is mainly used for lab and pilot-testing purposes, as indicated by the name. The *series P50* is a larger version of the systems, whereas the *series i* is the "full scale" version.

Table 7: Specifications of the commercial VSEP systems from New Logic [Vsep.com, 2008].

	Membrane area [m^2]	Internal volume [L]	Max. operating pressure [bar]	Max. Flux [L/(m^2·h)]
Series L (lab)	0.16	-	41	-
Series P (pilot)	1.58	3	41	320
Series P50	4.65	12	41	360
Series i	14 (pr. module)	-	38	-

Table 7 summarized the operational specifications of the different versions of the commercial VSEP systems from New Logic. It is seen that rather high flux levels are possible, according to New Logic, and that rather large membrane areas is possible by operating several modules. However, the feed type used to measure the given fluxes is not specified by the manufacturer, and Al Akoum et al. [Al Akoum et al.,2002iii] mention the mechanical complexity and relatively low membrane area pr. module as reasons for the lack of commercial success of VSEP systems.

2.1.3 Rotating disk systems (RD)

A rotating disk system (RD) was reported in 1995 by Lee et al. [Lee et al., 1995] and until today, rotating disk systems have been reported in NF [Bouzerar et al., 2003; Frappart et al., 2006; Mellal et al., 2008], in UF [Ding et al., 2002; Akoum et al., 2006], and in MF [Lee et al., 1995; Frenander & Jönsson, 1996; Bouzerar et al., 2000i; Bouzerar et al., 2000ii].

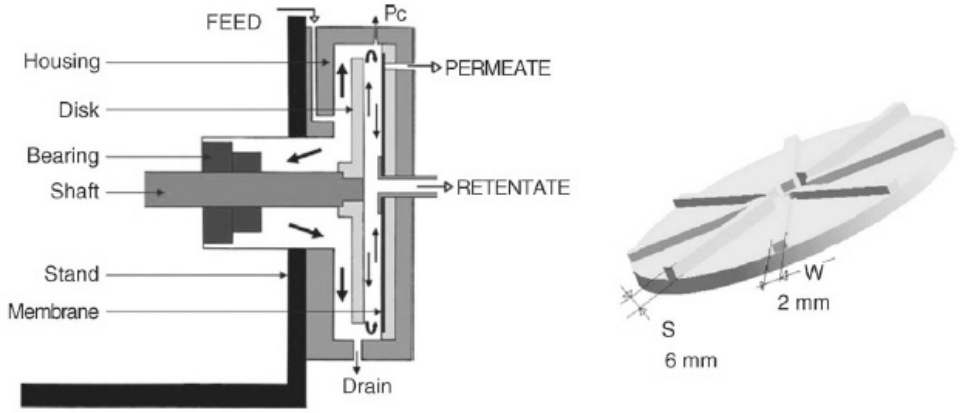

Figure 18: Sketch of a rotating disk system (left) and a disk equipped with vanes (right) [Frappart et al., 2006].

Figure 18 shows a sketch of a rotating disk system. The filtration module contains a disk, rotating around a horizontal axis, driven by an electrical motor with adjustable speed. Pressure is measured at the hosing periphery and at fluid inlet and outlet. Either smooth disks, or disks equipped with vanes have been tested and reported.

Advantages of the RD system are the very high and stable fluxes of 80 L/(m^2·h) (NF), and 370 L/(m^2·h) (UF) measured during filtration of oligosaccharides solutions [Mellal et al., 2008]. Not only is the flux increased by reducing the concentration polarization, but the membrane rejection is also raised by reducing diffusive transport through NF membranes. Additionally, high protein recovery and transmission (around 90 %) from biological feed can be achieved with high fluxes of around 150 L/(m^2·h) [Frenander & Jönsson, 1996] in the filtration of fermentation broth. Lee et al. [Lee et al., 1995] report that in MF of yeast cell, a retentate concentration of 23 g/l is possible when operating with high and stable fluxes of 200 L/(m^2·h) which should be compared to 25 L/(m^2·h) for a conventional filtration system. The maximum shear rate at the membrane surface is a function of the radius of the membrane, R, the product of velocity factor k of the fluid in the gap between disk and membrane and the angular velocity of the disk ω, and the kinematic viscosity of the feed fluid, ν [Bouzerar et al., 2000i].

$$\gamma_{s.\max} = f\left(R^{8/5}, (k \cdot \omega)^{9/5}, \nu^{-4/5}\right) \quad (20)$$

As seen in equation (20), the maximum shear rate is achieved at the periphery of the membrane. Closer to the membrane center, the shear rate is at a lower level. Therefore, the whole membrane area is not utilized to the same extent. As for the VSEP system, empirical correlations between the surface shear rate and the flux is often reported:

$$J = f\left(\bar{\gamma}_{s,\max}{}^{n}\right) \quad (21)$$

- n = 0.7785 for UF of soy milk [Akoum et al., 2006]
- n = 0.1857 – 0.5668 for MF of yeast cells [Jaffrin et al., 2004]

It is seen that the powers, to which the shear rate is raised, is in the same order of magnitude as for the VSEP module.

A commercial version of a rotating disk system, the *DMF filter*, has been offered by Pall Corporation which consists of several disks mounted on the same shaft, each one rotating between two membranes. However, some drawbacks of rotating disk systems, according to Ding et al. [Ding et al., 2006], are the relatively small membrane area, the complexity of the apparatus, and the high production costs of the apparatus. Another disadvantage of the system, compared to the other dynamic systems, is that the shear rate is not induced directly on the membrane surface but rather in the bulk solution. This might result in a less effective utilization of the energy consumed to produce shear compared to other dynamic membrane filtration systems.

2.1.4 Cross-rotational filter systems (CR)

The cross-rotational filter system (CR-filter) is quite similar to the rotating disk system. Huuhilo et al. [Huuhilo et al., 2001] have described a CR system in both lab-scale size and a pilot size model and emphasize the fouling minimization and low internal pressure as clear advantages. Inside the module, a rotor is placed between two membranes which make up one cell, and 10 cells (20 membranes) are stacked in the pilot size module. In the lab-scale module, the recommended rotation frequency of the rotor is 3000 rpm, whereas it is 365 rpm in the pilot module. A sketch of a CR-module is shown in Figure 19.

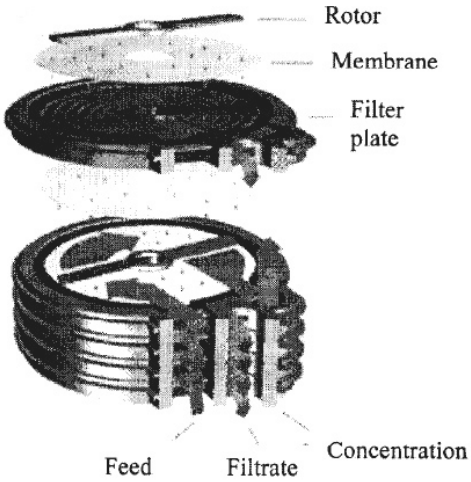

Figure 19: Sketch of the CR-filter system [Huuhilo et al., 2001].

CR-filters have been reported in NF [Mänttäri & Nyström, 2004; Mänttäri et al., 2004], UF [Huuhilo et al., 2001], and in MF [Nuortila-Jokinen, Nyström, 1996; Nuortila-Jokinen et al., 1998]. In UF tests of ground wood mill circulation water from an integrated pulp and paper mill, Huuhilo et al. [Huuhilo et al., 2001] conclude that fouling is minimized at higher rotational frequencies and lower pressures. In NF of dilute paper industrial effluent, Mänttäri et al. [Mänttäri & Nyström, 2004; Mänttäri et al., 2004] reports quite high fluxes (above 100 $L/(m^2 \cdot h)$) and retention (over 80 %) for conductivity and total carbon, using a CR-filter system. Further investigations using CR-filters for paper industry effluents can be found [Nuortila-Jokinen & Nyström, 1996; Nuortila-Jokinen et al., 1998] in which also high fluxes for UF and NF are emphasized in the treatment of paper mill water. However, in none of the publications related to CR-systems, equations for calculating the shear rate at the membrane surface is given. Therefore, no correlations between surface shear rates and fluxes are reported, but Huuhilo et al. [Huuhilo et al., 2001] mention that fouling is minimized as the rotational frequency increases which means, all things being equal, that the fluxes also increase with increasing rotational frequency and thereby with increasing surface shear rate.

Metso Paper [Metsopaper.com, 2008] offers a commercial CR-filter system, which is shown in Figure 20.

Figure 20: Commercial CR-system offered by Metso Paper [Metsopaper.com, 2008].

The system is made specific for industrial water treatment processes for cleaning and recycling process wasters. The CR-system, shown in Figure 20, is of the type *OptiFilter CR* for UF. The stack of membranes is separated by rotors, drainage support plates, and filter cassettes. According to the manufacturer, the benefits of the system are low TMP (very low internal pressure drop), low fouling tendencies, compact module design, possibility of high particle/solute concentrations, and low operational costs [Metsopaper.com, 2008]. Kirkniemi paper mill in Finland uses a CR-filter from Metso Paper to treat their process water (which then can be recycled) and thereby reducing the water requirements of the total process.

2.1.5 Rotary membrane systems (RM)

A rotary membrane system has been reported in the treatment of oil emulsions from metal industry wastewater in 1996 by Lin and Reed, using UF membranes [Lin & Reed, 1996], and by Viadero et al. [Viadero et al., 1997], using MF membranes. In these two publications, the authors actually denote the system as a "centrifugal membrane system (CMS)". However, since another system, also denoted *CMS*, is reported later in this chapter, we refer to the system of this sub-section as a *rotary membrane* system (RM).

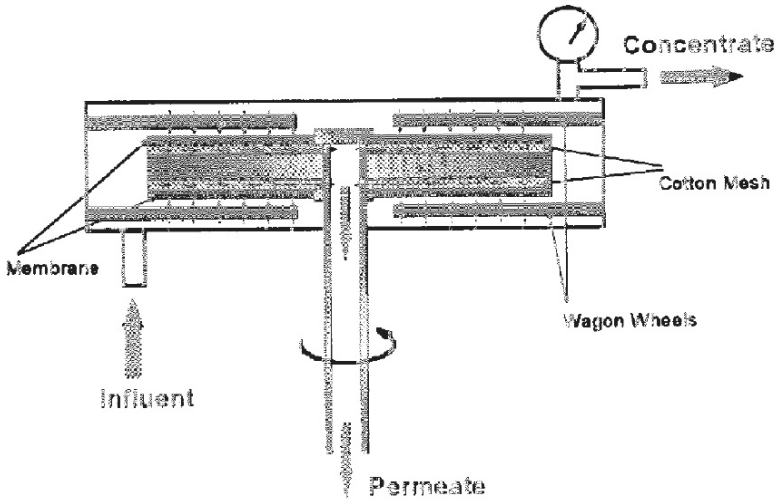

Figure 21: Sketch of a rotary membrane system [Viadero et al., 1997].

Figure 21 shows a sketch of the rotary membrane system. The system consists of a disk-shaped membrane pack with one flat sheet membrane on each side mounted on a hollow rotor inside a cylindrical pressure chamber. Rotation of the disk generates a centrifugal force across the membrane surface, and the rotation rate of the disk can be varied from 150 to 1750 rpm. A centrifugal pump is equipped to provide feed and pressure inside the chamber. Permeate passing through the membrane flows through a cotton mesh underlining the membranes and is collected in the rotor shaft. The concentrate returns to the feed tank. In the UF study by Lin and Reed [Lin & Reed, 1996], polymeric polyvinylidine fluoride membranes are used, whereas Viadero tests the use of ceramic MF membranes composed of TiO_2 and Al_2O_3. Lin and Reed [Lin & Reed, 1996] report that under similar operational conditions and feed concentrations, permeate rates generated from the RM system are 3-4 times larger than those from tubular systems. The centrifugal forces generated by rotations on the membranes provide high shear and turbulence on the surface. Theoretically, higher rotation rates will result in a higher cleaning effect. However, the centrifugal forces generate a back permeate pressure on the membrane which, therefore, decrease the effective transmembrane pressure. Thus, an optimum rotational speed needs to be identified in order to optimize the performance. In none of the publications, equations for calculating the surface shear rate are given. However, Viadero et al. [Viadero et al., 1997] report a power law relationship, in the MF tests of oil-emulsions in metal industry waste water, between flux and rotational speed as given in equation (22):

$$J = f\left(rotation^{n}\right) \qquad \begin{array}{l} \bullet \ n = 0.3 - 0.6 \text{ for laminar flow} \\ \bullet \ n = 0.8 - 1.2 \text{ for turbulent flow} \end{array} \qquad (22)$$

Thus, it is seen that the expression is similar to the correlations between flux and surface shear rate given for the VSEP and the RD systems.

The RM concept has been commercialized by SpinTek who today offers some rotary membrane solutions [SpinTek.com, 2008].

Figure 22: The SpinTek ST-II and ST-II 25 rotary membrane filtration system [SpinTek.com, 2008].

In Figure 22, a picture of the commercial SpinTek rotary membrane system is shown. The membrane area is 14 m^2, and the possible flux levels are in the area of 800 L/(m^2·h), according to the manufacturer [SpinTek.com, 2008]. The high shear allows for concentration and dewatering of solids to in some cases above 40%. It also keeps the membrane surface clean so that permeation of material below the cut off size of the membrane can occur. StinTek reports the ST-II system successfully in the extraction of vanilla extract from bacterial suspensions without color loss. Also, SpinTek reports latex particle recovery up to 50%, hydrated aluminum concentration to 40%, yeast concentration above 35%, biodigester sludge concentration, and blood plasma fractionation. Furthermore, SpinTek mentions that it is typical for traditional crossflow membrane filters to recirculate more than 98% of the feed stream, whereby the SpinTek ST-II requires less than 50% recirculation which then is used for mixing. Due to the high rotor speed, the ST-II is capable of controlling and reducing the boundary layer concentration polarization to effectively cause fractionation, and SpinTek uses the defatting of cheese whey as an example of this [SpinTek.com, 2008]: Conventional static membrane systems build up a layer of solids and fat on the membrane surface which prevents the passage of pure protein through the membrane by up to 65%. The ST-II prevents this material build up on the membrane and allows passage of over 95% of the protein at the same time retaining more than 90% of the fat. Lastly, SpinTek also offers a smaller commercial system, *Speedy*, for UF purposes also based on rotating membranes [SpinTek.com, 2008].

2.1.6 Centrifugal membrane separation systems (CMS)

Centrifugal membrane separation systems (CMS) has been described by Bergen et al. [Bergen et al., 2000; Bergen et al., 2001; Bergen et al., 2003] in reverse osmosis (RO) of

NaCl and $MgSO_4$ solutions, and by Fyles and Lycon [Fyles & Lycon, 2000] in RO and NF of colloidal silica and humic acid solutions.

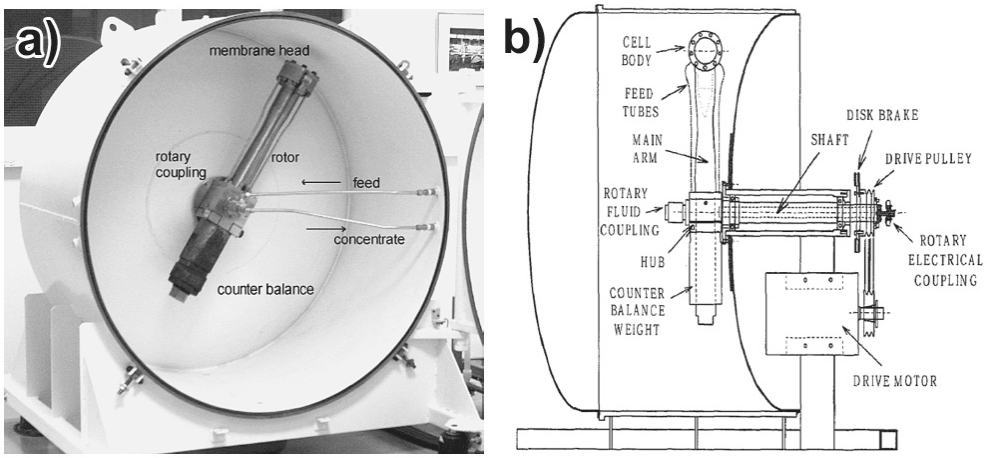

Figure 23: a) Picture of the centrifugal membrane separation system [Bergen et al., 2000]. b) Sketch of the centrifugal membrane separation system [Bergen et al., 2001].

Figure 23 shows a picture and a sketch of the CMS system. The apparatus consists of a membrane head at the end of a rotor arm, containing a plate and frame stack of membranes (Figure 24). Furthermore, the head, rotor arm, and counter weight are placed inside the white housing which has a diameter of 1.5 m. Vacuum inside the housing minimizes the frictional power loss and heating due to windage. The rotor is capable of achieving pressures up to around 82 atm at a rotational speed of 2200 rpm.

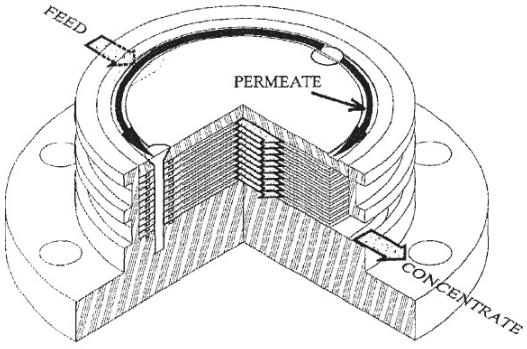

Figure 24: Sketch of the membrane stack [Bergen et al., 2001].

The membrane stack can be orientated in different ways relative to the rotation arm. Part of the CMS investigations was conducted in order to find the most efficient orientation of the membrane stack.

Bergen et al. [Bergen et al., 2000] show that at large salt concentrations (35,000 ppm NaCl or 70,000 ppm $MgSO_4$), the flux improvement, at the optimal orientation direction of the membrane stack, is around 50 % compared to a static filtration situation.

Furthermore, 40-60 % energy saving from similar systems are mentioned by Bergen et al., [Bergen et al., 2000] who explain that the extent of flux enhancement is maximized when the centrifugal force is directed away from, or in the plane of the membrane, and the fluid flow is directed such that the Coriolis force on the bulk flow is directed away from the membrane surface. The flux enhancement is related to a reduction of concentration polarization, due to rotation induced instabilities, which diminish the boundary layer thickness at the membrane surface. Thus, two factors are involved in the flux enhancement: i) The centrifugal force and its action on the solution, and ii) Coriolis force action on the bulk flow. Fyles and Lycon [Fyles & Lycon, 2000] report dramatically reduction in colloidal silica fouling in RO relative to a conventional reference system. Bergen et al. [Bergen et al., 2000] claim that the experimental results confirm earlier conducted computational fluid dynamic (CFD) simulation of similar systems by Pharoah et al. [Pharoah et al., 2000]. Pharoah et al. [Pharoah et al., 2000] calculated velocity vectors across the membrane from parameters such as rotation speed, internal cell geometries, concentrations, and membrane parameters similar to the experimental work of Bergen et al. [Bergen et al., 2000]. The numerical CFD study predicts that surface salt concentration can be kept within only 4 % of the feed concentration, for a rotating membrane, while the surface salt concentration increases up to 28 % for a non-rotating membrane [Pharoah et al., 2000]. Also, in NF of feeds containing proteins, the flux (and the critical flux) is significantly enhanced by CMS processing even though an adsorbed fouling layer is observed at the membrane surface [Fyles & Lycon, 2000].

An advantage of the CMS system is the possibility of achieving very high pressure without using pumps. The pressure in the membrane stack is decoupled for the feed pump and is given as a function of the density of the feed, the angular velocity of the rotor arm, and the radius of the rotation, r [Bergen et al., 2003]:

$$P = f\left(\rho_{feed}, \omega^2, r^2\right) \tag{23}$$

No equation is given for calculating the shear rate at the membrane surface, and therefore no correlations between flux and surface shear rate is available. As seen in this sub-section, the concept of centrifugal membrane separation has been tested on a research level. However, no commercial systems are available to our knowledge. This might be due to the complexity of the apparatus and the precautions that must be taken when operating with such a relatively large and very fast rotating system with forces as large as 3000 times the gravitational force.

2.1.7 Multishaft disk systems (MSD)

The multishaft disk system (MDS) is a rather new concept described in 2006 by Ding et al. [Ding et al., 2006]. A sketch of the MSD system is shown in Figure 25.

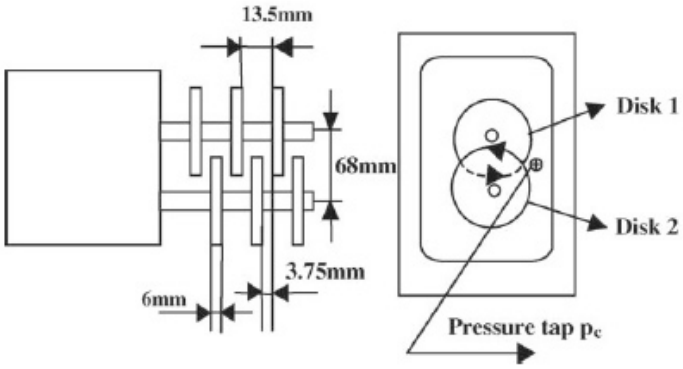

Figure 25: Sketch of the MSD system [Ding et al., 2006].

The MSD tested by Ding et al. [Ding et al., 2006] is a pilot unit built by Aaflowsystems, now a part of Westfalia Separator. The pilot consists of two parallel hollow shafts rotating at the same speed, each on bearing six ceramic membrane disks (only three disks on each shaft are shown in Figure 25). The MF ceramic disks have pore sizes of 0.2 μm and an outer radius of 4.5 cm. The total membrane area is 0.121 m^2. Shafts and disks are enclosed in stainless steel housing, and the disks on each shaft overlap by 15.5 %. Other relevant dimensions of the MSD are given in Figure 25. The permeat is collected inside each disk by 14 flat hollow channels and evacuated through the hollow shafts. It is possible to shut down permeate outlet from one set of disks, if desired, by closing the shaft outlet. The effect of using membranes on both shafts is investigated by Ding et al. [Ding et al., 2006], and He et al. [He et al., 2007] investigate the replacement of one of the shafts with one on which non-permeating rotating disks are mounted. The latter is conducted in order to avoid "over-concentration" in the overlapping zones due to the large fluxes and high feed concentrations. Actually, a similar system was already mentioned by Parkinson [Parkinson, 2001] in 2001 but with only one hollow shaft mounted with 14 ceramic membrane disks enclosed in a housing. That system is actually also similar to the rotary membrane system (RM) described earlier. Parkinson claimed that energy costs can be cut down by 80-90 % in the treatment of waste water compared to conventional crossflow membrane systems since the energy-intensive pumps needed to backwash conventional systems are not needed.

To our knowledge, MSD systems have only been reported in MF contexts using $CaCO_3$ particle slurries at quite high concentrations of 50-280 g/l [Ding et al., 2006; Jaffrin et al., 2006; He et al., 2007]. Generally, very high fluxes are achieved; up to 880 L/(m^2·h) for the configuration with both shafts mounted with permeating disks [Ding et al., 2006], at a rotation speed of 1930 rpm, a pressure of 2 bar, and a feed concentration of 100 g/l $CaCO_3$ slurry. For the configuration with one shaft mounted with non-permeating disks, fluxes up to 1790 L/(m^2·h) were measured for a rotation speed of 1930 rpm, a pressure of 3.1 bar, and a feed concentration of 200 g/l. Furthermore, the energy consumption per m^3 of permeate can be reduced if the non-permeating disks are equipped with vanes at moderate rotation speed which at the same time also yields higher fluxes [He et al., 2007].

As mentioned by He et al. [He et al., 2007], no equation has been derived to calculate the surface shear rate for the MSD system. However, by comparing results done with a rotating disk system (single disk rotating and static membrane), some considerations about the fluid velocity in between the rotating disks are made. From these considerations, He et al. [He et al., 2007] propose the flux to depend on the shear rate raised to a power, *n*:

$$J = f\left(\gamma^{n}\right) \tag{24}$$

The power *n* is then a function of relative ratios between fluxes and surface shear rates obtained with smooth disks, and disk equipped with vanes. The shear rate ratio is adapted from RD experiments and by doing that, He et al. [He et al., 2007] report that the value of the power *n* is at a level around 1. A commercial MSD system is available from Westfalia Separator Filtration GmbH, according to He et al. [He et al., 2007]. However, no information about such a system is available on the website of Westfalia Separator [Westfalia-separator.com, 2008].

2.1.8 Vibrating hollow fiber modules (VHFM)

Vertically vibrating hollow fiber membrane modules have been reported in MF contexts by Genkin et al. [Genkin et al., 2006] and by us [PAPER 1; PAPER 2; PAPER 4: PAPER 5]. Sketches of the two systems are shown in Figure 26.

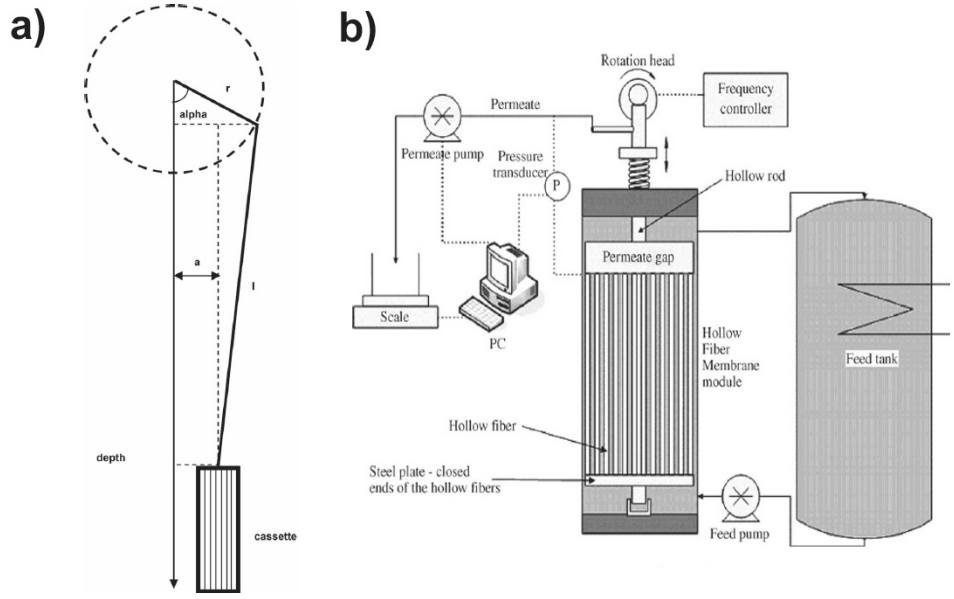

Figure 26: Sketches of vibrating hollow fiber membrane module systems by a) Genkin et al. [Genkin et al., 2006] and by b) Beier et al. [PAPER 1].

In both systems, the membrane modules consist of hollow fiber membranes placed vertically. The skin layer is located on the outside of the fibers which means that when a permeate pump induces a lowered pressure inside the fibers, permeate is sucked through the fibers from outside to the inside. Fouling is minimized as the membrane modules are vibrated in a vertical oscillating motion at frequencies from 0 – 10 Hz in the system of Genkin et al. [Genkin et al., 2006], and 0-30 Hz in our system [PAPER 1; PAPER 2; PAPER 4; PAPER 5]. Whereas the amplitude in the system of Genkin et al. [Genkin et al., 2006] is fixes at 4 cm, the possibility of varying the amplitude in our system [PAPER 1] exists by changing the "rotation heads". Amplitudes of 0.2, 0.7 and 1.2 mm are then possible.

Genkin et al. [Genkin et al., 2006] report that industrially relevant critical fluxes in submerged membranes could be achieved at low frequency vibration of the submerged membranes coupled with addition of a suitable coagulant. Critical fluxes of up to 130 L/(m^2·h) for a 5 g/L bakers yeast suspension are reported. However, the critical fluxes reported by Genkin et al. [Genkin et al., 2006] are determined from flux-step-methods, and they have not been verified against constant operation experiments for extended periods of time. Critical fluxes determined by flux-stepping methods are very dependent on the operational measurement parameters such as flux start level, step length, and step height [PAPER 4] and should therefore always be verified in order to check if the level of the determined critical flux really exists. The critical fluxes measured and reported by us [PAPER 1; PAPER 2; PAPER 4] are in the range of 20-60 L/(m^2·h) for feeds of bakers yeast cells with and without the presence of macromolecules. Relatively high and stable macromolecular transmissions of an alpha-amylase enzyme (above 85 %, [PAPER 2]) and BSA (above 75 %, [PAPER 5]) are observed in the separation from yeast cells at sub-critical flux. Furthermore, our measured critical flux levels [PAPER 1; PAPER 2; PAPER 4] have been verified against long-term constant flux experiments [PAPER 4; PAPER 5]. The VHMF systems are the only dynamic systems reported in the literature that deal with critical fluxes. Determining critical fluxes is beneficial in the point of view of achieving sustainable and long-term operation with low membrane fouling.

For both systems (Figure 26), the surface shear rate is periodically changing due to the oscillating motion of the module. The surface shear rate for both systems is calculated as the derivative of the velocity component along the membrane surface with respect to the length perpendicular to the membrane surface. The maximum surface shear rate is a function of the vibration frequency, F, the amplitude, amp, and the kinematic viscosity, ν [Genkin et al., 2006; PAPER 1].

$$\gamma_{s,\max} = f\left(amp, F^{3/2}, \nu^{-1/2}\right) \quad (25)$$

This function is similar to the shear rate equation for the VSEP system and since they both are probably derived based on the flow behavior close to an oscillating plate described by Bird et al. [Bird et al., 2002]. However, the shear rate of the VHFM system is the same throughout the whole membrane area which is not the case for the RD and VSEP systems where the shear rate increase with increasing distance from the center of

the circular membranes. Therefore, VHMF systems more efficiently use the whole membrane area with the same degree of surface shear rate, and the energy used for vibration is evenly "distributed" as shear over the whole surface. We [PAPER 1: PAPER 2] report power law dependencies between critical flux and average surface shear rate, whereas Genkin et al. [Genkin et al., 2006] report power law dependency between critical flux and vibration frequency.

$J_c = f\left(\bar{\gamma}_s^{\,n}\right)$

- n = 0.26 for MF of yeast cell suspensions [PAPER 1]
- n = 0.38 for MF of alpha-amylase enzyme solutions [PAPER 2]
- n = 0.32 for MF of yeast cell + alpha-amylase enzymes [PAPER 2]

(26)

$J_c = f\left(F^n\right)$

- n = 0.47 for MF of yeast cells 1-5 Hz [Genkin et al., 2006]
- n = 1.42 for MF of yeast cells 5-10 Hz [Genkin et al., 2006]

It is seen in these functions (26) that the same type of power law dependency for flux prediction apparently exists as for the VSEP, RD, RM, and MDS systems. Moreover, the powers n are also at the same levels as reported for the other dynamic systems.

2.2 General trends

As seen in the previous sub-sections, the different dynamic filtration systems all decouple the generation of surface shear rate from the feed flow velocity. Thus, the pumping cost for pumping feed at high velocity into the module can be reduced, and the energy is more efficiently directed to the membrane surface by membrane movement in most cases. The overall achievement is reduced energy consumption and fouling minimization which facilitate e.g. macromolecular MF transmission in separation from particular components. Therefore, the overall idea with these systems is the possibility of performing the separation better and cheaper. The shear rate generation can be divided into two categories: i) Generation of a constant level of shear rate (RMF, RD, CR, RM, CMS, MDS systems), and ii) generation of intermittent shear rate (VSEP and VHFM). Constant levels of shear rate are also generated in conventional crossflow membrane filtration systems, whereas intermittent shear rate generation might be advantageous since the oscillation itself might prevent components in fouling the membrane. Thus, a lower average surface shear rate level of intermittent operation might be more effective than the same shear rate level of a constant operation.

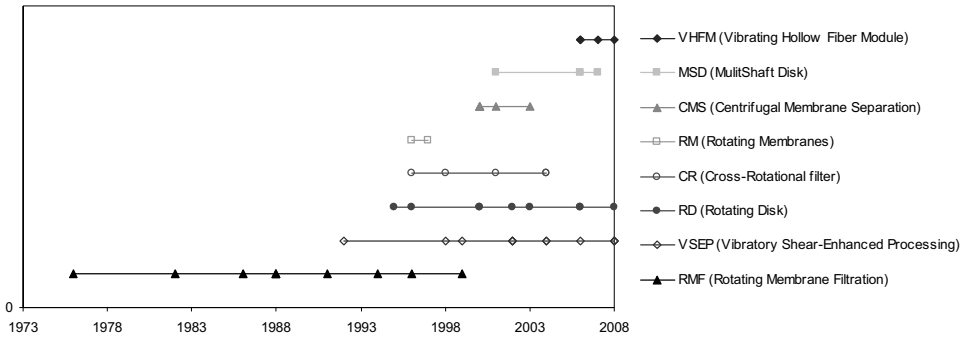

Figure 27: Diagram showing in the years at which papers have been published concerning the different dynamic filtration systems. The dots, triangles, and squares show in which years the papers were brought to publication.

Figure 27 shows a diagram with the year and periods in which scientific papers concerning the different dynamic systems have been published. The rotorfermentor system (RMF) is the oldest concept but there haven't been published any research results related to this system since 1999 to our knowledge. Around 1995-1996 the very similar concepts of RD, CR and RM systems was first reported. The newest reported concepts are the MDS system and our own VHFM system.

Table 8: Overview of different dynamic membrane systems, their advantages, their disadvantages, and some commercial aspects.

	Advantages	Disadvantages	Commercial Systems available
RMF	-Low operational costs (replacement of centrifuges) -Enhanced flux -High macromolecular transmission	-Apparatus complexity (moving parts) -Small membrane area -Lack of commercialization	No
VSEP	-High flux -High macromolecular transmission -High quality permeate -Very high shear rate -Possibility of very high outlet viscosity -99% Energy-to-shear conversion rate (only ~ 10 % for crossflow systems) -Requires small area of production site	-Apparatus complexity (moving parts) -Expensive to change membranes -Low membrane area -Hygiene problems (difficult to keep clean, only up to 70-80°C) -Uneven shear rate distribution on the membrane surface	*PallSep* by Pall Corp. *series i*, *series L/P*, *series P50* by New Logic
RD	-High flux -High protein recovery	-Small membrane area -Apparatus complexity (moving parts) -High costs of apparatus -Uneven shear rate distribution on the membrane surface -Shear not focused at the surface	*DMF filter* by Pall Corp.
CR	-Low operational costs -Low fouling -High flux -Compact module design -High outlet concentrations	-Uneven shear rate distribution on the membrane surface -Shear not focused at the surface	*OptiFilter CR* by Metso Paper
RM	-High flux (3-4 times larger compared to tubular systems under similar conditions) -High transmission -The energy to control fouling is transferred directly to the membrane surface where it is most effective -Boundary layer control (control of selectivity)	-Apparatus complexity (moving parts) -Uneven shear rate distribution on the membrane surface	*ST-II*, *ST-II 25* and *Speedy* by SpinTek
CMS	-Generation of high pressure due to centrifugal forces (RO/NF) -40-60 % energy savings -High fluxes	-Apparatus complexity (moving parts) -Very large forces (dangerous) -Lack of commercialization	No
MSD	-Very high fluxes -Very high feed concentration possible -Chemical resistance of ceramic membranes -80-90 % energy savings	- Uneven shear rate distribution on the membrane surface -Almost only tested with mineral suspensions -Relatively expensive membrane design -Uneven shear rate distribution on the membrane surface	Aaflowsystems / Westfalia Separator
VHFM	-Sub-critical filtration tested -Enhanced macromolecular transmission -Frequency and amplitude can be varied independently -Possibility of large membrane area pr. volume of module -Even shear rate distribution on the whole membrane surface	-Lower fluxes compared to other dynamic systems -Apparatus complexity -Temperature limit for cleaning -Lack of commercialization	No

Table 8 lists some advantages and disadvantages that are reported in the literature, according to the authors. Generally, most of the systems have the apparatus complexity as a clear disadvantage. Moving parts (e.g. rotating or oscillating) are always a source to apparatus break-down compared to static non-moving membranes. It must be mentioned that not many disadvantages of the different dynamic membrane filtration systems are reported by the authors making it quite difficult to identify them. However, the "weight" of the disadvantages and the "weight" of the advantages must somehow be balances in a way explaining the relatively low level of commercialization and industrial use of the dynamic membrane systems. The spread out of the dynamic filtration systems certainly required more work in the area of up-scaling. Energy is probably more efficiently utilized in dynamic filtration systems in terms of shear generation compared to conventional crossflow systems. However, general energy calculations showing the actual benefit of conducting a dynamic filtration process, compared to a conventional static crossflow filtration process, still needs to be worked out in order to really evaluate the energy saved. Only very few such energy calculation are found in the literature for the different dynamic filtration system, making it difficult to verify the postulate of energy savings during operation compared to conventional membrane systems.

3 Critical flux – overview and models

In this chapter, the evolution of the critical flux concept will initially be introduced. After that, different flux prediction models and models explaining the existence of a critical flux will be presented. Some of the data from our publications will in this chapter tried to be explained and fitted to some of the models.

3.1 Critical flux overview

The concept of critical flux, in membrane filtration processes, has in the last 23 years gained more and more interest as a way of controlling fouling and in that way obtain sustainable operation. By operating at sub-critical flux, the need for membrane cleaning will be reduced, and the macromolecular transmission in microfiltration might be improved [PAPER 2; PAPER 5]. In this introduction part of this chapter, an overview of the critical flux concept will be given.

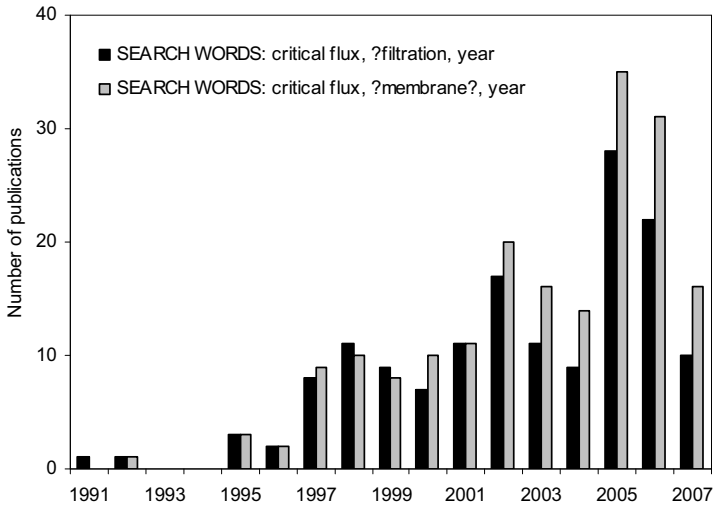

Figure 28: Number of publications found by using different search criteria: "Critical flux", "?filtration" or "?membrane?", and "year". The DADS search function at the Technical Knowledge Center, Technical University of Denmark, February 2008, was used.

In Figure 28 the number of publications since 1991 is seen in topics related to "critical flux" using the search words "?filtration" or "?membrane?"[1]. So, the research related to critical flux in membrane filtration processes has increased.

[1] "?" is a truncation sign.

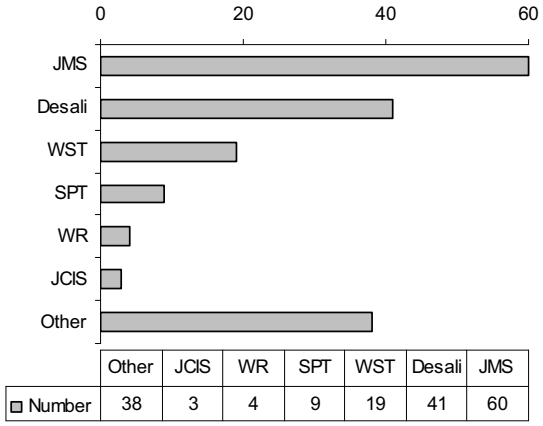

	Other	JCIS	WR	SPT	WST	Desali	JMS
Number	38	3	4	9	19	41	60

Figure 29: Number of publications in different scientific journals concerning critical flux and membrane filtration from 1979 to April 2008. JMS: Journal of Membrane Science, Desali: Desalination / Conferences, WST: Water Science and Technology, SPT: Separation and Purification Technology, WR: Water Research, JCIS: Journal of Colloid and Interface Science, Other: Other scientific journals with no more than two "critical flux" papers.

Figure 29 shows in which scientific journals the research about critical flux and membrane filtration processes has been published. The majority of publications are found in the Journal of Membrane Science, and also a large amount has been published in Desalination as conventional papers or conference contributions. Furthermore, the amount published in other journals, in which no more than two papers can be found, is also relatively large. Thus, overall the research about critical fluxes and membrane processes are spread out over a large spectrum of application areas reflected in the amount of different journals in which the research has been published.

Already in 1986, Cohen and Probstein reported the existence of a "threshold transmembrane velocity" in the investigation of colloidal fouling of reverse osmosis [Cohen & Probstein, 1986]. Below the threshold flux, no flux decline or fouling was observed. They categorized this as an "important experimental finding" and believed that its existence was caused by surface charge and double layer interactions. Therefore, the possibility of operation with no fouling could be increased simply by stabilizing the colloidal solution (maximize the electrostatic repulsive forces) and operate below the threshold flux. Then in 1989, Fordham and Ladva [Fordham & Ladva, 1989] measured a critical limiting flux in the filtration of bentonite clay suspensions through a filter medium with a Darcy permeability of around 10^{-2} μm^2 and a thickness of 8.5 mm [Fordham & Ladva, 1992], corresponding to a water permeability of around 420 $L/(m^2 \cdot h \cdot bar)$ based on a water viscosity of 10^{-3} Pa·s. They reported that if the flow through the filter medium is less than the critical value, no filter cake would be observed. The flux was after an initial phase observed to depend on the surface shear rate with a power law index of around 0.7. Compared to the power law indices from the previous chapter, it is seen that this power is in the same order of magnitude at for many of the dynamic systems. In 1995, the critical flux was modeled by Bacchin et al. [Bacchin et al.,

1995] by an interaction induced migration model able to explain the "colloidal flux anomaly" for back-transport of particles with radii from 10 nm to 10μm. The model balances convection, diffusion, and surface interactions, and since the repulsive surface interactions are accounted for, the predicted critical fluxes are higher than the ones predicted by a classical film theory model based solely on convection and diffusion. That year also, Field et al. [Field et al., 1995] empirically hypothesized about the existence of a critical flux in microfiltration from experimental observations of yeast cell suspensions, yeast cell debris suspensions, and dodecane-water emulsions. Below the critical flux, no fouling should be observed. A strong and a weak definition was given corresponding to a hydraulic filtration resistance equal to the clean water membrane resistance, and a constant filtration resistance below the clean water membrane resistance, respectively. Also in 1995, Howell [Howell, 1995] reviewed some experimental results and confirmed the existence of a critical flux below which no particle deposition occurred. However, the effect of macromolecular fouling was not accounted for by Howell [Howell, 1995].

Until today, the number of publications and interpretations of the critical flux concept has increased. The number of different ways, in which the critical flux is measured and determined, grows very fast making comparisons between different published results very difficult. In 2004, Bacchin proposed a possible theoretical link between the critical and the limiting flux for colloidal ultrafiltration saying that the critical flux equals 2/3 of the limiting flux [Bacchin, 2004] based on considerations about a flux distribution on the membrane. The criteria of the critical flux, being the flux below which no fouling is observed, has been loosened up, and in the later years there seem to be a general agreement that the term "normally sub-critical flux", "sub-critical flux", or "sustainable flux" is a term that can be used as a guideline level for the flux below which only an acceptable TMP increase in a given period of time is observed [Cho & Fane, 2002; Ognier et al., 2004; Hughes & Field, 2006; Guglielmi et al., 2007i; Guglielmi et al., 2007ii]. Sustainable fluxes are often well below the critical level. Wang et al. [Wang et al., 2006] introduced the concept of "proper operational flux" based on long term experiments in a submerged membrane bioreactor, treating municipal wastewater, stating that the level of the proper operational flux is only 56 % of the critical flux value in their case. Furthermore, sub-critical operation is probably only possible in a fixed time interval, and such behavior was experimentally observed by Chuan-yi et al. [Chaun-yi et al., 2007] where the TMP suddenly started to increase dramatically after 24 days of sub-critical flux filtration of wastewater in a MBR system. Similar results have been reviewed and mentioned by Pollice et al. [Pollice et al., 2005]. Guglielmi et al. [Guglielmi et al., 2007i; Guglielmi et al., 2007ii] reported a sustainable time associated with sub-critical operation. This is the time below which the TMP at constant sub-critical flux operation only increases with an acceptable rate. After the sustainable period of time a dramatic TMP increase is observed. The sustainable time is linearly decreasing with the sub-critical flux. The reason for the existence of a sustainable time might be explained by local flux theory accounting for the gradual loss of effective membrane area caused by for example EPS fouling. EPS fouling is mentioned as a serious contributor to membrane fouling [Nagaoka et al., 1998; Cho & Fane, 2002; Cho & Fane, 2003; Fan et al., 2006; PAPER 5; Paul & Hartung, 2008].

In 2006, an in-depth review about critical and sustainable fluxes was published by Bacchin et al. [Bacchin et al., 2006i]. The critical flux concept was clarified both theoretically, and from an experimental point of view. This clarification was indeed needed since the concept of critical flux has been used more or less randomly and in many cases made satisfy a particular point of view of an author. In the review, it is underlined that one has to distinguish between three types of critical fluxes:

$$\begin{aligned} R &= R_m && \text{strong form of critical flux} \\ R &= R_m + R_{ads} && \text{weak form of critical flux} \\ R &= R_m + R_{ads} + R_{rev} && \text{irreversibility form of critical flux} \end{aligned} \quad (27)$$

This means that in order for the critical flux to be of the strong form, the hydraulic resistance, R, should only equal the membrane resistance R_m. When the hydraulic resistance equals the sum of the membrane resistance, and an eventual constant adsorption resistance R_{ads}, the critical flux is of the weak form, and the slope of the pressure-flux curve is less than the slope of the clean water flux curve. Furthermore, since the critical flux is often defined as the onset of irreversible fouling, a third definition is given: The irreversibility form of the critical flux is the flux below which the hydraulic filtration resistance equals the sum of membrane resistance, adsorption resistance, and the resistance caused by reversible fouling, R_{rev}. They underline that i) the strong and weak form critical fluxes must always be evaluated via a check on whether or not the overall resistance has remained invariant, and that ii) the critical flux for irreversibility represents the shift from repulsive interactions (polarized layer) to attractive interactions (deposition). It is the dispersive forces that are the key to the existence of a critical flux. Another review about critical fluxes and ways of determination is available in a Ph.D. thesis by Neal [Neal, 2006] who reviews both experimental and modeling aspects of critical fluxes and the applications related to membrane filtration processes.

By going through the almost 200 “critical flux” publications found by using the search words shown in Figure 28, the distribution among filtration types, operational configurations, types of feed solutions / suspensions, and critical flux determination methods is depicted in Figure 30.

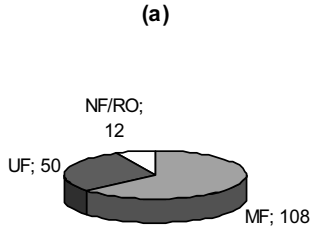

MF: Microfiltration, UF: Ultrafiltration, NF/RO: Nanofiltration / Reverse osmosis.

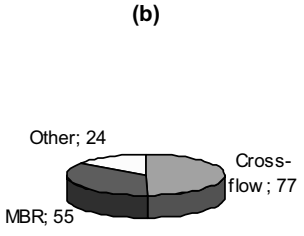

MBR: Membrane Bioreactor related systems, Cross-flow related systems, and other systems.

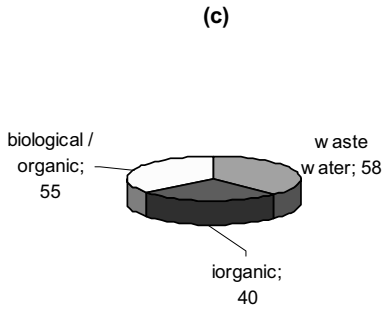

Type of feed solution / suspension.

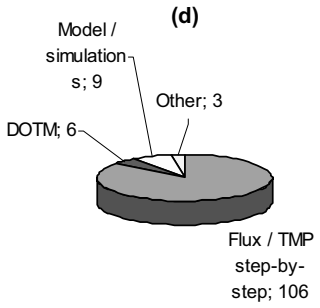

Critical flux determination method (DOTM: Direct Observation Through a Membrane).

Figure 30: Number of publications in different areas: (a) Filtration types, (b) operational configurations, (c) types of feed solutions / suspensions, and (d) critical flux determination methods.

The majority of publications are dealing with microfiltration, followed by ultrafiltration, and a minor fraction with nanofiltration and reverse osmosis. The dominant operational configuration is conventional cross-flow systems. However, in the later years more and more papers in the area of MBR's have been published, so a shift in the forthcoming years into more MBR related critical flux papers might be seen. The types of feed solutions/suspensions are almost divided evenly between different waste water feeds, feeds of biological content or organic content, and inorganic content. The three types of feeds include the following:

- *Waste water feeds*: All kinds of synthetic waste water, synthetic sewage, municipal waste water, real sludge, activated sludge, biologically treated waste water, industrial waste waters like paper mill effluent, organic waste water, olive washing waste water, and agro-industry waste water.
- *Biologically and organic feeds*: Milk, pure whey protein solutions, BSA solutions, other macromolecular solutions, bacterial suspensions, biomass suspensions, yeast cell and yeast cell debris suspensions, and dodecane-water emulsions.

- *Inorganic feeds*: Latex particles, $CaCO_3$ slurry, solutions containing molecular and or colloidal $Fe(OH)_2$, TiO_2, SiO_2, Al_2O_3, colloidal bentonite, kaolin clay suspensions, and gold sol colloidal suspensions.

Different methods for determining the critical flux are reported in the literature. One of them is the DOTM method (Direct Observation Through the Membrane) in which a transparent membrane is applied, and a camera is placed on the permeate side being able to detect the onset of particle deposition which, therefore, will be defined as the critical flux. In 1998, Li et al. [Li et al., 1998] used a DOTM method to detect particle deposition during cross-flow microfiltration. However, they were not able to detect particles smaller than 1 μm, and thus, smaller particles and components could foul the membrane and increase the hydraulic resistance without being detected. The critical flux has also been determined by theoretical models which include different back-transport mechanisms depending on the size of molecules, colloids, or particles being processed. CFD simulations (Computational Fluid Dynamics) have been tried to predict critical fluxes. However, critical fluxes from ultrafiltration simulations of latex particles was found to be four times larger than experimental data from similar conditions by Bacchin et al. [Bacchin et al., 2006ii]. The majority of all critical flux determination methods, however, concern step-by-step method in which the flux, or the TMP, is stepwise increased and the response (either TMP or flux) is monitored. Generally, the point where the TMP starts to increase at a fixed flux, or the point where the flux starts to decrease at a fixed TMP, is taken to be the critical flux. This method is easy to apply which might explain is popularity. A scheme outlining advantages and disadvantages of the different critical flux determination methods is given by Bacchin et al. [Bacchin et al., 2006i], and one of the main disadvantages of the step-by-step technique is that it only measures the critical flux of the dominant fouling species [Cho & Fane, 2002; Fane & Chang, 2002, Fane et al., 2002]. Using step-by-step techniques, the determined critical fluxes can vary quite much depending on the flux start level, step time length, and step height, although not many publications focuses on the influence of these operational parameters on the critical flux determination procedure. Such behavior is investigated and described in one of our publications [PAPER 4].

3.2 Flux and critical flux models

In chapter 2, different dynamic membrane filtration concepts were presented along with different flux values for different feed types. Only the VHFM systems (Vibrating Hollow Fiber Modules) coupled the dynamic filtration concept with the critical flux concept. The latter concept is an important concept in terms of obtaining sustainable operation with boundary layer and fouling control. In this section, different flux predicting models from the literature will be presented. The aim of this chapter is to investigate if one or some of these models can be applied for our own data and contribute to explain the existence and level of the experimentally measured critical fluxes.

From a general point of view, the overall transport, N, of material towards the membrane is the sum of different contributions [Bacchin et al., 2006i]:

$$N = J \cdot C - D \cdot \frac{dc}{dx} + p(\xi) + q(\tau) \qquad (28)$$

The convective flux towards the membrane is given by the term $J \cdot C$, whereas the diffusive back-transport away from the membrane is given by the term $D \cdot dc/dx$. The term $p(\xi)$ represents the migration of solutes/particles due to surface interactions between the membrane and solute/particle. If $p(\xi) > 0$, electrostatic attraction exist between the membrane and the solute/particles (e.g. adsorption), whereas repulsive forces exist if $p(\xi) < 0$. The term $q(\tau)$ represents the effect of the local hydrodynamics which mainly is determined by the shear forces [Bacchin et al., 2006i]. In the study of our dynamic microfiltration system, it is mainly the effect of the shear forces, $q(\tau)$, and the influence on the flux level that is investigated.

In our earlier studies of the vibrating hollow fiber membrane module we have measured critical fluxes in the range from ~ 20 L/(m^2·h) to ~ 60 L/(m^2·h), for yeast cell suspensions with concentrations from 4 to 8 g/L, at vibration degrees corresponding to shear rate levels up to 2000 s^{-1} [PAPER 1; PAPER 4]. These critical fluxes have been empirically correlated to the average value of the surface shear rate by power law expressions [PAPER 1; PAPER 2]. Such empirical power law correlation have been shown to explain the variation of the flux with the surface shear rate quite well for many different dynamic membrane filtration systems, which is evident from chapter 2. As mentioned earlier, our experimentally determined critical fluxes will be tried to be modeled in this chapter using different back-transport mechanisms of some of the models. The outcome of the modeling work will be compared to the earlier proposed empirical power correlations.

In the work of Bacchin et al. [Bacchin et al., 1995], different back-transport mechanisms of solutes, colloids, and particles are mentioned:

- Brownian diffusion
- Interaction induced migration

- Shear-induced diffusion
- Lateral migration (inertial lift)

These models/back-transport mechanisms predict different critical fluxes at different sizes of the species. This is sketched in Figure 31 along with the values of our determined critical fluxes for yeast cells which has particle diameter of approximately 5 μm.

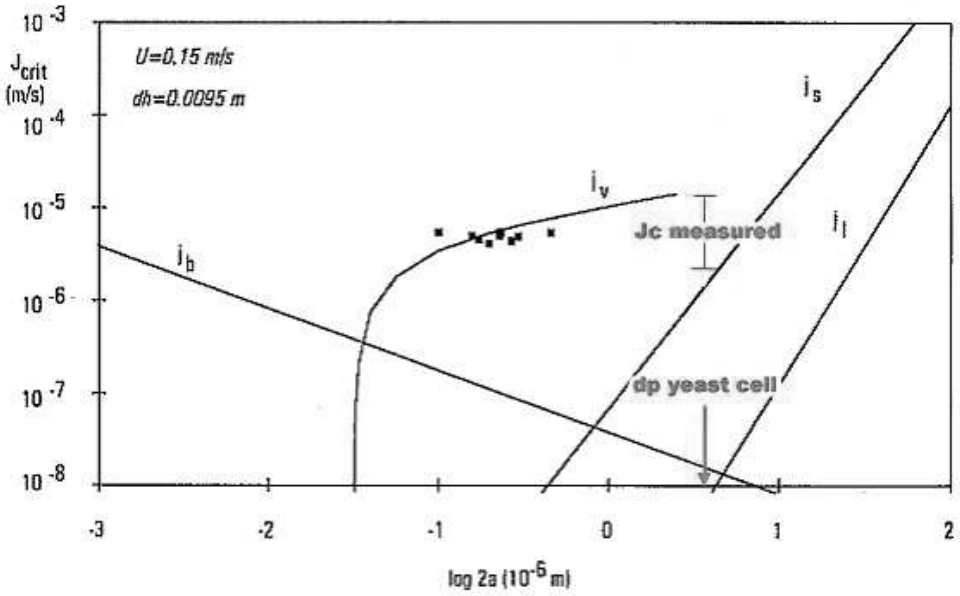

Figure 31: Adapted from Bacchin et al. [Bacchin et al., 1995]. Critical fluxes predicted by different back-transport mechanisms vs. particle-size: Brownian diffusion, j_b, lateral migration, j_l, shear-induced diffusion, j_s, and interaction induced migration, j_v. The values are calculated with a hydraulic diameter of 0.95 cm and a crossflow velocity of 0.15 m/s. Black squares: Critical fluxes during ferric hydroxide RO by Cohen and Probstein [Cohen & Probstein, 1986]. The particle size of a yeast cell (dp = 2a = 5 μm) is pointed out with a red arrow along with our measured critical fluxes for yeast cell suspensions [PAPER 1; PAPER 4].

The critical fluxes depend on particle size but also to a large extent of the hydrodynamic conditions which we saw in chapter 2. The hydraulic diameter (0.95 cm), and the velocity of the feed fluid (0.15 m/s), for the four cases in Figure 31, are more or less at the same level as for our system[2]. From Figure 31 it seems as if the main back-transport mechanisms in our dynamic microfiltration experiments with yeast cells could be the shear-induced diffusion or the interaction induced migration. The Brownian diffusion is the dominant back-transport mechanism for much smaller species below 0.1 - 1 μm, whereas the shear-induced diffusion seems to be the dominating back-transport mechanism for species above 1 μm. From the figure is it also seen that lateral migration apparently mostly affects the back-transport of particles larger than 5 μm. The interaction

[2] The hydraulic diameter in our vibrating microfiltration system is defined as the average distance between the fibers which is 0.3 cm. At a vibration frequency of 20 Hz, and with an amplitude of 1.375, the peak velocity is 0.17 m/s according the expressions in [PAPER 1].

induced migration model mainly explains the back-transport mechanism for components like colloids in the intermediate region between Brownian diffusion back-transport and shear-induced diffusion, where the two latter models clearly underpredicts the critical fluxes, according to Figure 31; a situation often referred to as the *flux anomaly* [Bacchin et al., 1995].

In the following sub-sections, different models predicting (critical) fluxes will be presented and explained. Lastly, some of the relevant models will be applied and fitted to our own experimentally determined critical flux values. Initially, some well known *pore blocking models* will be presented. Then a *hydrodynamic force momentum model*, a *lateral migration model*, and a *shear-induced diffusivity model* will be presented. Finally, an *interaction induced migration model* will be presented. A semi-theoretical and semi-empirical critical flux predicting model for our own critical flux data, including critical flux data from [PAPER 1] and [PAPER 4], will be derived, presented, and compared to the earlier proposed power law critical flux correlation.

3.2.1 Pore blocking models

Because of the complex nature of membrane fouling, no single equation is able to handle the phenomenon all together. Fouling can lead to narrowing of the pores, or complete blocking of the pores. Different fouling mechanisms of porous membranes are sketched in Figure 32.

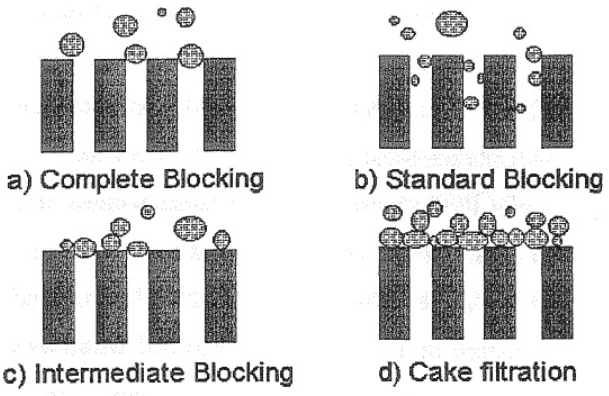

Figure 32: Different fouling mechanisms of porous membranes [Lipnizki, 2003].

In the case of complete blocking (a), each particle reaching the membrane surface is blocking a pore. During standard blocking (b), the pore volume is decreased due to particle deposition on the pore walls inside the membrane structure. Intermediate blocking (c) have similarities to the complete blocking but here the particles may settle on each other. A cake layer (d) can also be built up on the membrane surface. In this case, the cake porosity and other cake properties are often determining the filtration performance rather than the actual membrane properties. When one of the mentioned

fouling mechanisms is dominating, different models have been derived to describe and predict the flux as a function of time for constant pressure operation. When dealing with complete pore blocking, the flux can be described by an exponential decreasing function [Lipnizki, 2003]:

$$J_v(t) = J_{v0} \cdot e^{-\alpha \cdot t} \quad (29)$$

Thus, the flux decreases exponentially with time from the initial volumetric flux level J_{v0}. A system characteristic constant, α, has to be determined. When dealing with standard blocking, intermediate blocking, or cake filtration, another model has been proposed [Lipnizki, 2003]:

$$J_v(t) = \frac{J_{v0}}{(1+\alpha \cdot t)^n}, \quad \begin{cases} n = 2, & \text{standard blocking} \\ n = 1, & \text{intermediate blocking} \\ n = ½, & \text{cake filtration} \end{cases} \quad (30)$$

If the fouling resistance is thought of as a continuous growing cake on the membrane surface, the resistance is dependent on the specific cake resistance which often is constant, and the thickness of the cake which is a function of mass of permeate that passes the membrane [Mulder, 1996]. In this case, the continually increasing cake or fouling resistance can be expressed as follows:

$$R_f = \beta \cdot m_p \quad (31)$$

The "fouling constant", β, depends on the specific cake resistance, the bulk concentration, and the concentration of solutes in the cake. This fouling resistance can be inserted into a resistance-in-series filtration model (like equation (5) and (6)), and if the total resistance is only divided into a membrane resistance and a fouling resistance, the resistance-in-series model can be rewritten into the following expression [Mulder, 1996]:

$$\frac{1}{J_v} = \chi + \frac{\beta}{\Delta P} \cdot m_p \quad (32)$$

Equation (32) is actually a classical filtration model. The constant χ is dependent on the membrane resistance, and the hydrostatic pressure difference. From such a cake-filtration model, it is seen that $1/J_v$ increases linearly with the mass of permeate that passes the membrane. From the slope, the fouling constant, β, can be determined which is dependent on the bulk concentration, the specific resistance of the cake, and the concentration of solutes inside the cake. Such a filtration model, with a continually increasing fouling resistance, has been shown to explain the flux decrease during dead-end ultrafiltration of alpha-amylase macromolecules at constant pressure in our adsorption related paper [PAPER 3]. Furthermore, the almost linear increase in TMP during constant flux filtration of yeast cells, with the vibrating hollow fiber module,

around the critical flux, observed and described in [PAPER 4], might be explained by such a filtration model.

3.2.2 Hydrodynamic force momentum model

A hydrodynamic force momentum model was originally proposed and described by Lu and Ju [Lu & Ju, 1989] for a crossflow microfiltration system during the filtration of calcium carbonate particles in 1989. The model is in this sub-section tried being applied for our own vibrating dynamic MF system in the filtration of yeast cells.

The analysis of the different drag forces and the corresponding overall drag force acting on a particle on the surface of a membrane or a filter cake can be obtained by first solving the equations of continuity and motion in the boundary layer region of the membrane surface in order to know the flow conditions. This is done by Lu and Ju [Lu & Ju, 1989] who, in order to be able to solve the equations, assumed very slow motion in the boundary layer (creeping flow). Intuitively, this might seem unrealistic for our system, but this will be commented and substantiated later in this section. The model originally describes a crossflow filtration system with a filter medium orientated vertically onto which a particle is located. The different hydrodynamic forces acting on the particle are sketched in Figure 33.

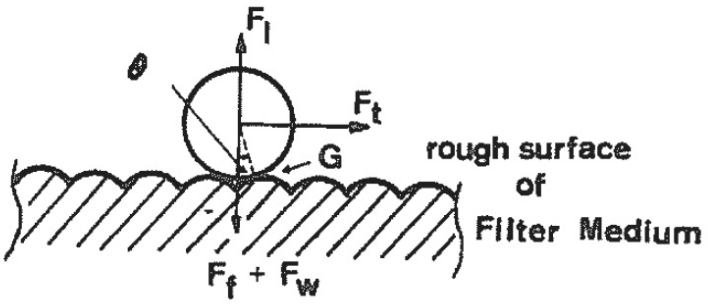

Figure 33: Sketch of the forces acting on a particle on the surface of a filter medium in a crossflow field [Lu & Ju, 1989].

- F_t, tangent drag force due to the crossflow velocity
- F_f, vertical drag force due to the filtration flow
- F_l, vertical lift force due to the gradient of crossflow velocity
- F_w, submerged weight force of the particle

Our vibrating hollow fiber membrane module system is different than the system of Lu and Ju. Thus, in order to apply a similar force momentum model, the different hydrodynamic forces acting on a particle placed on the surface of one of the hollow fibers has to be determined. A description of our experimental apparatus can be found in our

publications [PAPER 1; PAPER 2; PAPER 4; PAPER 5]. The different forces acting in our system during operation are sketched in Figure 34.

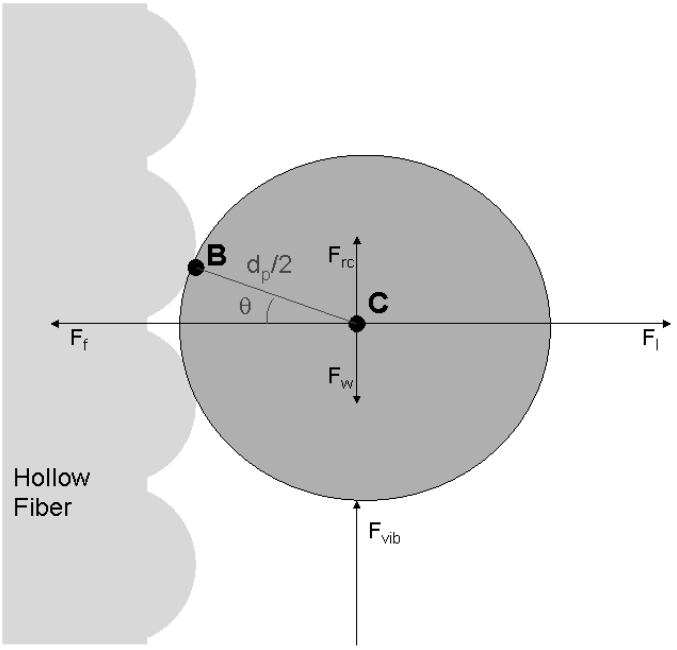

Figure 34: Sketch of the different forces acting on a particle located at the surface of a vertical orientated vibrating hollow fiber in the "down-going" motion.

The porous surface is depicted somehow rough as experienced by the particle. This is done to "simulate" the entrance of a pore. The situation shall be thought of as if the particle is "stuck" at the surface (because of drag forces due to filtration flow) and will, therefore, follow the motion of the vibrating module. The hydrodynamic force momentum model will then help us investigate if this fouling mechanism is valid or not. The "vibration force" exerted on the particle can be thought of as the surrounding fluid exerting a force on the particle. When the fiber is in down-going motion, as in Figure 34, the vibration force is directed upwards, as the fluid will "push" the particle upwards, and when the fiber is in up-going motion, the vibration force is directed downwards. The forces exerted on the particle are listed below:

- F_{rc}, tangent drag force due to the recirculation velocity of the feed fluid in the module cylinder.
- F_{vib}, oscillating drag force acting periodically upwards and downwards on the particle due to fiber vibrations.
- F_f, drag force due to the filtration flow.
- F_l, lift force due to the gradient of the velocity of the oscillating fluid.
- F_w, submerged weight force of the particle.

In the following sub-sections, the different forces acting on the particle located at the surface of the vibrating fiber will be expressed and approximated. Lastly, the sum of all the forces will be calculated into a total force momentum around the contact point ***B*** in order to evaluate whether the particle will stay at the surface or will be swept off during operation.

Tangent drag force due to the recirculation velocity

The force that act on a particle on the surface of a fiber, solely because of the fluid recirculation velocity, is denoted F_{rc}. According to Lu and Ju [Lu & Ju, 1989], the drag force exerted on a single spherical particle touching an impermeable wall, within a simple shear flow field, is given as follows:

$$F_{rc} = 1.7009 \cdot \left(3 \cdot \pi \cdot \mu \cdot d_p \cdot \left(u\Big|_{z=\frac{d_p}{2}} \right) \right) \quad (33)$$

Even though our wall (membrane) is not impermeable, the flux levels are rather low (< 60 L/(m^2·h), and therefore the wall can be assumed impermeable. In equation (33), u is the undisturbed fluid velocity at the position $z = d_p/2$. The direction z is the normal to the membrane surface, and the term "*1.7009*" is the wall correction factor of Stokes' law derived by O'Neill for a fixed sphere in contact with a fixed plane wall when the fluid motion, in the absence of the sphere, is assumed to be a uniform linear shear flow [O'Neill, 1968]. The assumption concerning the wall correction factor may be valid since the flow rate in the module cylinder caused solely by the recirculation is very slow (< 1 cm/s [PAPER 4]). The geometry of the surface is not plane, but the surface "experienced" by a yeast cell (d_p = 5 μm) can be characterized as plane when looking at the surface at the distance $z = d_p/2$ from the surface. This geometry argumentation is also used in one of our publications [PAPER 1] in going from spherical coordinates to Cartesian coordinates near the surface of a cylindrical shaped fiber.

With a recirculation velocity of 1 cm/s, the recirculation drag force will be approximately $F_{rc} = 8.0 \cdot 10^{-10}$ *N*, according to equation (33), for our experimental system when the dynamic viscosity of water is used (10^{-3} Pa·s).

Oscillating drag force due to fiber vibration

In order to determine the drag force that acts on a particle on the surface, due to the vibrations of the membrane module, some rough assumptions are made.

- The drag force can be expressed similar to equation (33) even though the flow field probably hardly can be characterized as "simple".
- The force exerted on the particle is thought of as the surrounding fluid "pushing" the particle periodically upwards and downwards.
- The velocity of the flow field, close to the fibers, is periodically changing due to module vibrations. Thus, the velocity, u, in equation (33) is taken as the maximum or peak velocity of the oscillation.

By solving the Navier-Stokes equation for the fluid surrounding the oscillating fiber, the velocity function at given distances *z* from the fiber, and at a given time, is obtained. This has earlier been calculated for our system [PAPER 1]. The velocity profile at a distance $z = d_p/2$ (radius of yeast cell) from the surface is sketched in Figure 35.

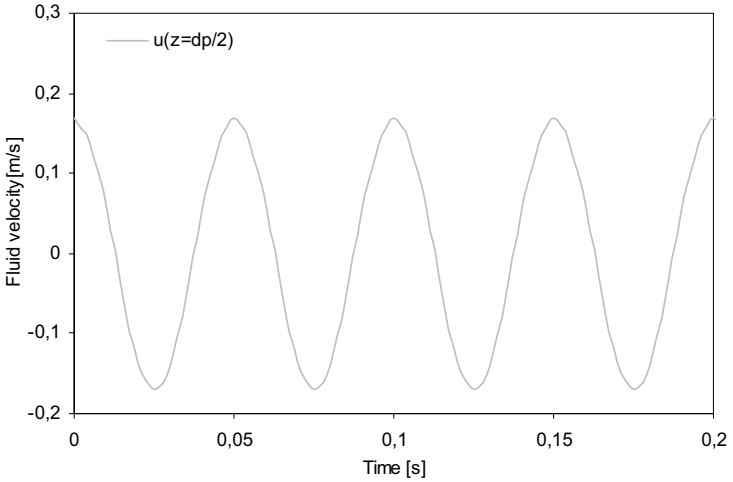

Figure 35: Fluid velocity at a distances $d_p/2$ = 2.5 µm from the surface of a vibrating fiber. Frequency: 20 Hz, amplitude: 1.375 mm. Kinematic viscosity: $10^{-6}m^2/s$.

The oscillating drag force will have a maximum at the maximum fluid velocity which at a frequency of 20 Hz and amplitude of 1.375 mm is ~ 0.17 m/s, according to Figure 35. Thus, from this peak velocity, $u_{vib,max}$, the peak oscillating drag force can be approximated. According to our previous work [PAPER 1], the peak velocity of an oscillating fiber can be expressed as $\omega \cdot amp$ where the angular velocity, ω, is equal to $2 \cdot \pi \cdot freq$, and *amp* is the amplitude of the oscillation [PAPER 1]. Inserting this into equation (33), one obtains the following expression:

$$F_{vib} = 1.7009 \cdot \left(3 \cdot \pi \cdot \mu \cdot d_p \cdot u_{vib,\max}\right) = 1.7009 \cdot \left(3 \cdot \pi \cdot \mu \cdot d_p \cdot \omega \cdot amp\right) \quad (34)$$

The crossflow velocities, used by Lu and Ju [Lu & Ju, 1989], is in the range from 0.57 to 1.14 m/s, and they used the equations from creeping flow in the boundary layer to obtain the equation for the overall drag force based on the work of O'Neill [O'Neill, 1968]. Even though our flow pattern is probably very different, the peak velocity of the vibrating membrane module is even lower than the lowest velocity in the analysis of Lu and Ju. Therefore, it is assumed that for our analysis, we can use the same assumptions in the boundary layer near the fibers. With a maximum velocity of the vibrating module of 0.17 m/s, the vibration force is approximately $F_{vib} = 1.4 \cdot 10^{-8}$ *N* which is around 17 times ($F_{vib}/F_{rc} \sim 17$) larger than the recirculation force F_{rc} acting in the same direction. Thus, in the further analysis of the force momentum model, the recirculation force, F_{rc}, is neglected for reasons of simplification.

Drag force due to filtration flow

The drag force due to filtration flow is denoted F_f and can be expressed as follows [Lu & Ju, 1989]:

$$F_f = \phi \cdot 3 \cdot \pi \cdot \mu \cdot d_p \cdot q \quad (35)$$

The flow through the membrane is denoted q, and the factor ϕ it the wall correction factor of Stokes' law. The value of the wall correction factor depends on the membrane resistance, R_m, and the particle diameter, d_p. Based on the numerical and dimensional analysis of Goren [Goren, 1979], an empirical expression for wall correction factor, applicable in the whole range of $R_m \cdot d_p$ from 0 to $2 \cdot 10^5$, was derived:

$$\phi = \sqrt{\frac{R_m \cdot d_p}{3} + (1.072)^2} \quad (36)$$

Since for our system, $R_m \cdot d_p \sim 2.3 \cdot 10^5$, equation (36) is assumed to be nearly predictable for the wall correction factor in our case[3], even though, as pointed out by Goren, for values of $R_m \cdot d_p$ greater than $2 \cdot 10^5$ the correction factor *1.072* might not be totally applicable.

Lift force due to the gradient of fluid velocity

The lift force due the gradient of the fluid velocity is denoted F_l. According to Lu and Ju [Lu & Ju, 1989], the lift force can be expressed similar to the drag force due to the filtration flow, F_f, just by replacing the filtration flow rate, q, with a lift velocity, u_l. These two terms are oppositely directed, as sketched in Figure 34. The lift velocity which is caused by the gradient of vibration velocity (oscillating shear field) is a function of particle diameter, boundary layer thickness, kinematic viscosity, and bulk fluid velocity, u_m. For the case of particle migration in shear flow for a neutrally buoyant particle that is not allowed to rotate (since it is considered to be "fixed" on the surface, according to Figure 34), u_l is given by Vasseur and Cox as follows [Vasseur & Cox, 1976]:

$$u_l = \frac{61}{576 \cdot \nu} \cdot \left(\frac{u_m}{\delta}\right)^2 \cdot \left(\frac{d_p}{2}\right)^3 \quad (37)$$

Inserting equation (37) into equation (35) with replacement of q with u_l, one obtains an expression for the lift force, F_l:

$$F_l = \phi \cdot 3 \cdot \pi \cdot \mu \cdot d_p \cdot u_l = \phi \cdot 3 \cdot \pi \cdot \mu \cdot d_p \cdot \left(\frac{61}{576 \cdot \nu} \cdot \left(\frac{u_m}{\delta}\right)^2 \cdot \left(\frac{d_p}{2}\right)^3 \right) \quad (38)$$

[3] The permeability l_p of our membrane module is ~7800 L/(m^2·h·bar) [PAPER 4]. With the dynamic viscosity, μ, of water (10^{-3} Pa·s), the membrane resistance, R_m, is then $4.6 \cdot 10^{10}$ m^{-1}. Therefore, with a particle diameter, d_p, of $5 \cdot 10^{-6}$ m, $R_m \cdot d_p \sim 2.3 \cdot 10^5$.

Here, u_m, according to Lu and Ju [Lu & Ju, 1989], can be expressed from a friction velocity at the wall, u^*, by the following expression: $u_m = \frac{\delta \cdot (u^*)^2}{\nu}$, which further is defined from the average velocity of the suspension, u_s, and the fanning friction factor, f [Lu & Ju, 1989]: $u^* = u_s \cdot \sqrt{\frac{f}{2}} \rightarrow u_m = \frac{\delta \cdot \left(u_s \cdot \sqrt{\frac{f}{2}} \right)^2}{\nu} = \frac{\delta \cdot {u_s}^2 \cdot f}{2 \cdot \nu}$

Furthermore, the fanning friction factor is correlated to the Reynolds number in either a turbulent or laminar flow regime:

- Turbulent regime: $f = 0.073 \cdot \mathrm{Re}^{-1/4}$, $6 \cdot 10^3 < \mathrm{Re} < 6 \cdot 10^5$
- Laminar regime: $f = \frac{24}{\mathrm{Re}}$, $\mathrm{Re} < 6 \cdot 10^3$

The Reynolds number, therefore, has to be determined: $\mathrm{Re} = \frac{d_h \cdot u_s}{\nu}$. The hydraulic diameter, d_h, is in our system taken as the average distance between the fibers ($d_h = 3 \cdot 10^{-3}$ m). The average velocity of the fluid, u_s, is in our system very difficult to estimate. However, it is taken as the peak velocity of the vibrating module, $u_s = amp \cdot \omega$. Thus, the friction factors can be rewritten:

- Turbulent regime: $f = 0.073 \cdot \left(\frac{d_h \cdot u_s}{\nu} \right)^{-1/4}$, $6 \cdot 10^3 < \frac{d_h \cdot u_s}{\nu} < 6 \cdot 10^5$
- Laminar regime: $f = \frac{24 \cdot \nu}{d_h \cdot u_s}$, $\frac{d_h \cdot u_s}{\nu} < 6 \cdot 10^3$

Equation (38), hence, can be rewritten into:

$$F_l = \phi \cdot 3 \cdot \pi \cdot \mu \cdot d_p \cdot \left(\frac{61}{576 \cdot \nu} \cdot \left(\frac{\delta \cdot {u_s}^2}{2 \cdot \nu \cdot \delta} 0.073 \cdot \left(\frac{d_h \cdot u_s}{\nu} \right)^{-1/4} \right)^2 \cdot \left(\frac{d_p}{2} \right)^3 \right)$$

$$= \phi \cdot 3 \cdot \pi \cdot \mu \cdot \frac{1.76 \cdot 10^{-5}}{\nu^{5/2} \cdot {d_h}^{1/2}} \cdot {d_p}^4 \cdot {u_s}^{7/2} \quad \text{(turbulent)}$$

&

$$F_l = \phi \cdot 3 \cdot \pi \cdot \mu \cdot d_p \cdot \left(\frac{61}{576 \cdot \nu} \cdot \left(\frac{{u_s}^2}{2 \cdot \nu} \cdot \frac{24 \cdot \nu}{d_h \cdot u_s} \right)^2 \cdot \left(\frac{d_p}{2} \right)^3 \right)$$

$$= \phi \cdot 3 \cdot \pi \cdot \mu \cdot \frac{61}{32 \cdot \nu \cdot {d_h}^2} {d_p}^4 \cdot {u_s}^2 \quad \text{(laminar)}$$

(39)

Submerged weight force of the particle

The submerged weight force of the particle is denoted F_w and can be expressed by the following equation [Lu & Ju, 1989]:

$$F_w = \frac{\pi}{6} \cdot \left(\rho_p - \rho_s \right) \cdot g \cdot {d_p}^3 \qquad (40)$$

Thus, the submerged weight force is a function of the difference in density between the particle and the solvent (ρ_p - ρ_s). Since yeast cells are very "self-buoyant" and only very slowly settle in a suspension, the difference in density of solvent and density of suspended yeast cells is assumed to be very small. The dry weight of a yeast cell is approximately 1.5×10^{-11} g [Sullivan et al., 2006]. The density of a dry yeast cell with a diameter of 5 μm is therefore

$$\rho_p = \frac{m_{cell}}{V_{cell}} = \frac{m_{cell}}{\left(\frac{4}{3} \cdot \pi \cdot \left(\frac{d_p}{2} \right)^3 \right)} = \frac{1.5 \cdot 10^{-14} kg}{\left(\frac{4}{3} \cdot \pi \cdot \left(\frac{5 \cdot 10^{-6} m}{2} \right)^3 \right)} = 230 \frac{kg}{m^3}$$

which is even less than the density of water. Thus, dry yeast cells will flow on top on a liquid surface and wet yeast cells are very slow to precipitate. Even though the density of wet yeast cells is larger than the density of water (otherwise they will not settle), the weight force is neglected since it is assumed to be much smaller than the drag force caused by vibrations, F_{vib}. Furthermore, F_w and F_{rc} are directed oppositely which also compensate for neglecting both F_w and F_{rc}.

Force momentum balance

Now that all the forces acting on a "fixed" particle on the fiber surface are expressed, through equation (33) to (40), it can be investigated whether the particle will stay fixed at the surface or it will be swept off. In order to answer this question, the sign of the force momentum, M, around the contact point ***B*** has to be determined. In order to establish the

force momentum balance, Figure 36 sketches the projection directions perpendicular to the forces. The force momentum vector, *M*, is pointing outwards as indicated in Figure 36. If $M > 0$, the possible rotation/movement direction of the particle will be counter clockwise which mean that the particle will be swept of the surface. If $M < 0$, the rotation/movement direction of the particle will be clock wise which is impossible since it will be stopped (or is stopped) by the surface. Thus, the particle in this case will stay at the surface. The forces F_l and F_f are both expressed to "act" on the center, *C*, of the particle, whereas the vibration force F_{vib} is expressed to act on the "lower" point of the particle surface in the down-going motion (Figure 36) or at the "upper" point of the particle surface in the up-going motion.

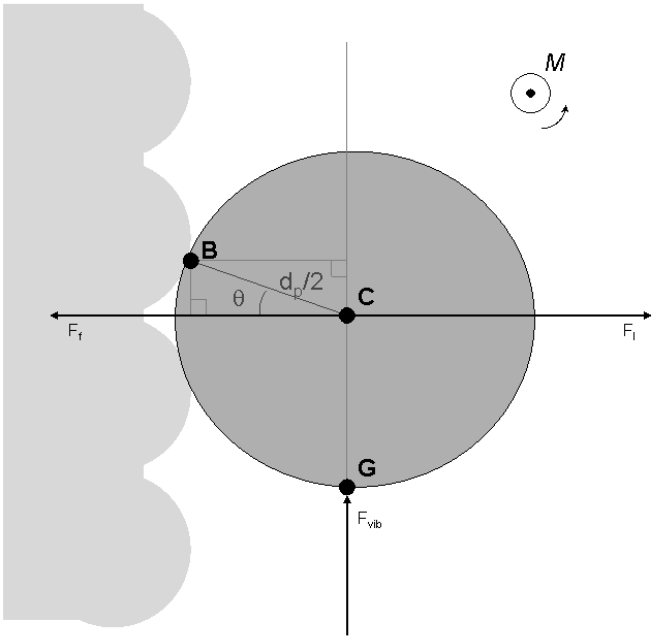

Figure 36: Projection directions perpendicular to the forces F_l, F_f, and F_{vib}. The force momentum vector, *M*, is pointing out of the paper in the normal direction. F_w and F_{rc} are both neglected and not shown.

The force momentum, *M*, is expressed below, according to the procedure described by Christiansen et al. [Christiansen et al., 2000], as the sum of all the force momentum contributions:

$$M = -F_f \cdot \frac{d_p}{2} \cdot \sin\theta + F_l \cdot \frac{d_p}{2} \cdot \sin\theta + F_{vib} \cdot \frac{d_p}{2} \cdot \cos\theta$$
$$= \frac{d_p}{2} \cdot \left(\left(F_l - F_f \right) \cdot \sin\theta + F_{vib} \cdot \cos\theta \right) \quad (41)$$

From a mechanical point of view, it doesn't matter whether the force F_{vib} is sketched towards point **G**, **C** or drawn with **C** as starting point. The perpendicular distance from the contact point **B** to the direction of force F_{vib} is still equal to $\cos\theta \cdot d_p/2$, as sketched in Figure 36. When M equals zero, the force momentum contributions acting on the particle are just balanced and equation (41) can be rewritten:

$$F_{vib} = \left(F_f - F_l \right) \cdot \tan\theta \quad (42)$$

The forces F_f, F_l, and F_{vib} from equation (34), (35) and (39) are inserted into equation (42), and the particle diameter then becomes a critical particle diameter d_{pc} since it will be the larges possible particle diameter that is able to stay on the surface at the given average feed suspension velocity, u_s (vibration degree of the module), and at the given permeate flow rate, q:

$$\left(\frac{1.7009}{\phi \cdot \tan\theta} \right) \cdot u_s + \left(\frac{1.76 \cdot 10^{-5}}{\nu^{5/2} \cdot d_h^{1/2}} \right) \cdot {d_{pc}}^3 \cdot {u_s}^{7/2} = q \quad \text{(turbulent)}$$
$$\left(\frac{1.7009}{\phi \cdot \tan\theta} \right) \cdot u_s + \left(\frac{61}{32 \cdot \nu \cdot {d_h}^2} \right) {d_{pc}}^3 \cdot {u_s}^2 = q \quad \text{(laminar)} \quad (43)$$

These expressions can be used to depict the permeate flow, q, at different *critical particle diameter*, d_{pc}.

The value of the angle of response, θ, (see Figure 36) between the particle and the surface of the membrane is difficult to determine from an isolated experiment. Its actual physical sense is not only an angle of response but also a quantitative parameter of all the combined effects of interfacial forces between the particle and the membrane surface. Lu and Ju determined $\tan\theta$ from data of different permeate flow rates and their corresponding critical particle diameters [Lu & Ju, 1989]. Since we only have data of yeast cell suspensions, a single particle diameter, we are not able to determine $\tan\theta$. Thus, in order to get a value, we use the value of Lu and Ju [Lu & Ju, 1989] $\tan\theta = 0.11$ even though the conditions and suspensions are not the same. As a value for the membrane resistance, we use the value from yeast filtrations obtained from the slope of flux vs. pressure at stepwise flux increasing yeast filtration below a critical flux value. The average slops of these filtrations corresponds to a permeability of $390\ L/(m^2 \cdot h \cdot bar)$ [from PAPER 4] which gives a membrane resistance of $R_m \sim 9 \cdot 10^{11}\ m^{-1}$. In Figure 37, the predictions of the force momentum model for our system are depicted.

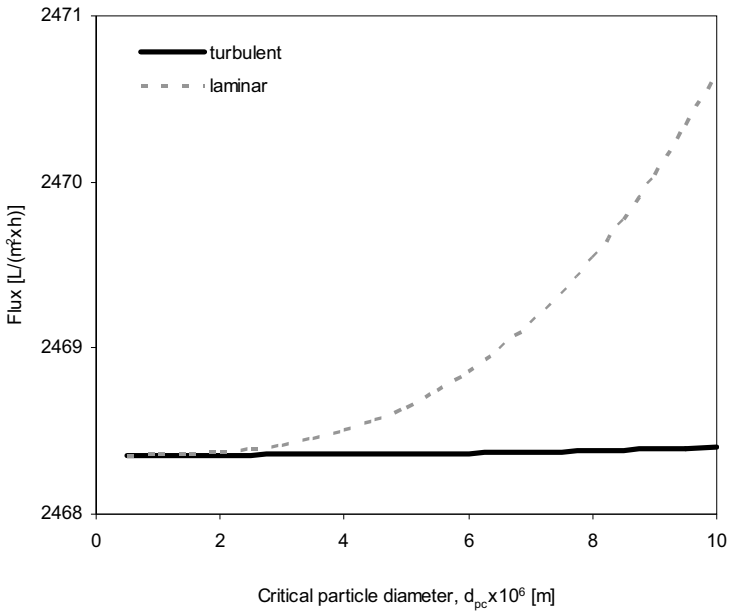

Figure 37: Force momentum model applied for our system. Fluxes at different critical particle diameter at average feed suspension velocity u_s = 0.17 m/s.

It is seen that at the given critical particle diameters, the "necessary" fluxes in order to make the particles stay at the surface are very large (around two orders of magnitudes larger) compared to the measured critical fluxes for this feed suspension at the given operational conditions [PAPER 1; PAPER 4]. Even though much uncertainty is related to using such a force momentum model (uncertainties are discussed at the end of the model chapter), it might give an idea of the fouling mechanism leading to the critical flux level. (However, we have not accounted for eventually interaction forces between the particles and the membrane surface). From Figure 37, it is seen that it is very unlikely that the fouling mechanism, causing a critical flux level to be reached, is pore blocking of whole particles at the pore entrances sticking to the surface without moving (force momentum $M < 0$). Such a fouling mechanism would namely "require" fluxes above ~ 2400-2500 L/(m^2·h) in order to make a whole yeast cell (particle diameter of 5μm) stay on the surface, according to a force momentum model. Therefore, other fouling mechanisms or other components than whole yeast cells must be responsible for the existence of a critical flux in our experiments.

This conclusion is, without working through such a force momentum model, not surprising, since by intuition it would be hard to imagine a relatively large particle, yeast cell, being able to stick to the surface of a fast oscillating membrane surface, and at low transmembrane pressure (< 80 mbar). The result of the force momentum model seems to confirm this intuition.

3.2.3 Lateral migration (inertial lift) model

Lateral migration is the sum of inertial lift forces away from the membrane surface and permeation drag forces due to convection into the porous wall [Altena & Belfort, 1984; Li et al., 2000]. The lift force is similar to the lift force described in the force momentum model. The critical flux, J_c, is reached or exceeded when the convective transport towards the membrane surface is equal to or larger than the lift velocity, u_l, away from the membrane:

$$J_c = u_l \tag{44}$$

The lift velocity, used in force momentum balance, was expressed by Vasseur and Cox [Vasseur & Cox, 1976] for creeping flow. For larger Reynolds numbers (*Re >> 1*), but still for laminar shear flow, Drew et al. presented an expression to determine the lift velocity based not on the fluid velocity but rater on the gradient (shear rate) [Drew et al., 1991] for flow in a membrane duct. Inserting this expression into equation (44), one obtains model based on inertial lift force back-transport:

$$J_c = 0.577 \cdot \frac{\rho \cdot d_p{}^3 \cdot \gamma_s{}^2}{128 \cdot \eta} \tag{45}$$

The number "0.577" comes from analysis of the dimensionless lift velocity as a function of the dimensionless distance from the surface. The maximum dimensionless lift velocity is 0.577 from the analysis of Drew et al. [Drew et al., 1991]. Overall, a rather strong dependency of shear rate, and particle diameter on the critical flux is predicted by this model.

3.2.4 Shear-induced diffusivity model

Shear-induced diffusivity models are based on a self-diffusion coefficient for particles that are retained by the membrane. Shear-induced diffusion of particles away from the membrane surface is assumed to be caused by particle-particle interactions near the membrane wall [Li et al., 2000]. In order to establish a flux predicting model based on shear-induced diffusivity, Zydney and Colton [Zydney & Colton, 1986] used the following approximated expression for the self-diffusivity:

$$D = 0.0075 \cdot d_p{}^2 \cdot \gamma_s \tag{46}$$

As pointed out by Schwinge et al. [Schwinge et al., 2002], such a diffusion mechanism is an adaptation of Brownian diffusion that replaces the Stokes-Einstein diffusivity with on based on back-diffusion caused by the random movement of particles, as they interact in a shear flow. It is seen that the self-diffusion coefficient is proportional to the average shear rate at the membrane surface, and to the square to the particle diameter. For

relatively high feed concentrations (bulk volume fractions ϕ_b from 0.2 to 0.5), the following semi-empirical expression for determining a length averaged flux, with incorporation of equation (46), was obtained from the work of Li et al. [Li et al., 2000]:

$$J = 0.031 \cdot \left(\frac{d_p^{\,4}}{L} \right)^{1/3} \cdot \gamma_s \cdot \ln\left(\frac{\phi_w}{\phi_b} \right) \qquad (47)$$

The length of the membrane feed channels is denoted L, and ϕ is the volume fractions at the wall, and in the bulk suspension, respectively. Li et al. [Li et al., 2000] points out that for more dilute suspensions ($0 < \phi < 0.2$), the shear-induced diffusion is smaller since the impact of particle-particle interactions is less. Thus, they further presented a modified shear-induced diffusivity model with a wall volume fraction dependent diffusion coefficient:

$$D = 0.025 \cdot d_p^{\,2} \cdot \gamma_s \cdot \phi_w \qquad (48)$$

The effect of the particle volume fraction at the surface on the self-diffusivity is accounted for without influence of the bulk concentration. However, determination of the volume fraction at the surface, ϕ_w, is not straightforward and in the case with our own dynamic microfiltration system it is very difficult. Using DOTM in crossflow filtration of yeast cell suspensions, and latex particle suspension, Li et al. [Li et al., 2000] determined the wall volume fraction as $\phi_w = 2/3 \cdot \xi$, where ξ is the fraction of membrane covered by particles slightly above the critical flux. In most of the cases with yeast cell filtrations, the yeast cells coverage was around 0.3, corresponding to a wall volume fraction of $\phi_w = 0.2$. With this value of the wall volume fraction, the experimentally determined critical fluxes for yeast cell suspensions (0.15 – 2.4 g/l), with crossflow velocities from 0.1 – 1 m/s, was quite well predicted by Li et al. [Li et al., 2000]. Inserting this value *($\phi_w = 0.2$)* at the critical flux into equation (48), and then incorporation into a shear-induced diffusivity model, one obtains the following modified shear-induced diffusivity model [Li et al., 2000]:

$$J = 0.024 \cdot \left(\frac{d_p^{\,4}}{L} \right)^{1/3} \cdot \gamma_s \cdot \ln\left(\frac{\phi_w}{\phi_b} \right) \qquad (49)$$

It is seen that the modification (equation (49)) just lowers the predicted fluxes by ~ 23 % ((0.031-0.024)/0.031) compared to the first shear-induced diffusivity model (equation (47)) when assuming a surface volume fraction of particles of 0.2. Because of the relatively large uncertainty associated with determining ϕ_w from the coverage, Li et al. tested the model with very large value for the particle coverage at the surface ($\xi = 0.9$), and this only yielded an increase of less than 20 % in the predicted fluxes. Thus, Li et al. [Li et al., 2000] concluded that the predicted fluxes are not very sensitive to the assumed value of the wall volume fraction. Therefore, it could be argued why one should include the effect of surface coverage in the diffusivity expression when it is very difficult to

determine this coverage, and when the coverage after all does not affect the predicted fluxes that much!

As pointed out earlier, the shear-induced diffusivity is mainly caused by particle-particle interactions. Thus, the diffusivity is concentration dependent and increases with increasing particle concentration, according to equation (48). Moreover, the shear-induced diffusivities depend on the shear rate. Davis and Sherwood [Davis & Sherwood, 1990] used an empirical correlation to determine the diffusion coefficient from the bulk volume fraction (and not the wall volume fraction) rather than using the expressions for the diffusivities in equation (46) or (48):

$$D = 0.0825 \cdot {d_p}^2 \cdot \gamma_s \cdot {\phi_b}^2 \cdot \left(1 + 0.5 \cdot e^{8.8 \cdot \phi_b}\right) \quad (50)$$

According to Li et al. [Li et al., 2000], using this diffusivity, and assuming that no particles stick on the membrane, Davis and Sherwood [Davis & Sherwood, 1990] used the following expression for the length averaged flux:

$$J = 0.024 \cdot \gamma_s \cdot \left(\frac{{d_p}^4}{\phi_b \cdot L}\right)^{1/3} \quad (51)$$

Li et al. [Li et al., 2000] refer to this model as the “shear-induced hydrodynamic model”. Overall, three more or less identical shear-induced diffusivity models have been presented in this sub-section (equation (47), (49), and (51)). They are all equal in terms of dependency on surface shear rate (linear dependency). The difference lies in how the self-diffusivities are expressed and how they depend on particle diameter and concentration at the membrane surface or in the bulk.

3.2.5 Interaction induced migration model

In 1995, Bacchin et al. [Bacchin et al., 1995] presented a model for colloidal membrane fouling. Their definition of colloids covers species smaller than 5 μm, stable in suspensions, or charged macrosolutes such as proteins. It is a theoretically proposed model, referred to as an *interaction induced migration model*, describing colloids deposition on membrane surfaces accounting for surface interactions, hydrodynamic conditions, and the physicochemical properties of the feed suspension. The model predicts critical fluxes for reverse osmosis, ultrafiltration, and microfiltration of large size colloids [Bacchin et al., 1995]:

$$J_c = \frac{D}{\delta} \cdot \ln\left(\frac{V_B}{\delta}\right) \quad (52)$$

The critical flux is denoted J_c, and D and V_B are the physicochemical properties of the suspension (diffusion coefficient, D, and a potential barrier or interaction energy between

a particle and the membrane surface, V_B). The hydrodynamics of the system is accounted for as the boundary layer thickness (δ) is included. As pointed out by Kwon et al. [Kwon et al., 2000], the critical flux according to this model is strongly dependent upon the particle size since it affects both the diffusion properties, D, and the potential barrier, V_B. For particles around 0.1 μm, back-diffusion is important, and the critical flux depends mainly on the surface charge of the particles. For particles larger than 1 μm, shear-induced diffusion, which lifts particles away from the membrane surface, is most important. In this case, the surface charge effect becomes less significant. Bacchin et al. [Bacchin et al., 1995] claim that this model explains trends observed when processing protein solutions, and that the "flux anomaly"[4] is also explained. According to Figure 31, the model should explain the dominant back-transport mechanism for particles and colloids from ~ 0.3 μm to ~ 3 μm, and from Figure 31 the explanation of the flux anomaly is obviously explained, at least for the RO data of Cohen and Probstein [Cohen & Probstein, 1986]. Contradictory to the other models (lateral migration and shear-induced diffusivity), this model predicts the changes observed in filtration with the physicochemical properties of the suspension (pH and ionic strength) since these terms influence the potential barrier.

In the development of the model, the mass flux (Sherwood number, Sh) is expressed as a function of the hydrodynamic conditions (Peclet number, Pe, and the boundary layer thickness, δ), and the physicochemical properties, V_B, which represents the potential barrier induced by the surface interactions. The potential barrier is linearly related to the stability ration of the suspension, W_d, with respect to deposition on a surface in cross-flow conditions. If $V_B < 0$, the interactions are attractive, and during filtration the attractive interaction case can only be a transient one as the membrane is soon covered with particles. In this case, the model (equation (52)) is invalid. However, it is often the case in filtration that the interactions are repulsive, $V_B > 0$ (interactions between suspended particles and particles deposited on the surface). Thus, in order to apply equation (52) for a colloidal system, one has to have values of the stability ratio or the potential barrier as well as the boundary layer thickness. Bacchin et al. [Bacchin et al., 1995] give such values[5] along with diffusion coefficients for i) Bentonite clay particles (particle diameter ~ 0.7 μm), and ii) BSA macromolecules (molecular diameter ~ 7 nm). Thus, with these values, critical fluxes can be predicted in a filtration case using equation (52) [Bacchin et al., 1995]:

Bentonite particle suspension:

$$J_c = \frac{D}{\delta} \cdot \ln\left(\frac{V_B}{\delta}\right) = \frac{6.3 \cdot 10^{-13} \frac{m^2}{s}}{10^{-6} m} \cdot \ln\left(\frac{10^{10} m}{10^{-6} m}\right) = 84 \frac{L}{m^2 \cdot h}$$

[4] The "flux anomaly" is that conventional stationary state film theory models tend to underestimate fluxes in case of processing suspension with particle sizes between 10 nm and 1 μm [Bacchin et al., 1995].

[5] Using flow field correlations including Reynolds number (Re = 800), Schmidt's number (Sc = 10^{-6} Pa·s·m^3/kg × D), and the Sherwood number (Sh) based on a hydraulic diameter of $5 \cdot 10^{-4}$ m and a membrane length of 0.3 m.

BSA macromolecular solution:

$$J_c = \frac{D}{\delta} \cdot \ln\left(\frac{V_B}{\delta}\right) = \frac{6 \cdot 10^{-11} \frac{m^2}{s}}{4.3 \cdot 10^{-6} m} \cdot \ln\left(\frac{10^{-4} m}{4.3 \cdot 10^{-6} m}\right) = 158 \frac{L}{m^2 \cdot h}$$

For a yeast cell filtration case, the model is difficult to apply since we have no values for the stability ratio and the potential barrier, and neither is the boundary layer thickness known due to the complicated flow field surrounding the vibrating fibers. However, the values of critical fluxes above are not so far from our experimentally determined critical fluxes, even though they are calculated for a different system, with different flow conditions, and geometries. We have actually earlier determined at critical flux with our vibrating membrane module of around 200 L/(m^2·h) for a 1 g/l BSA solution using a *step-up* critical flux determination procedure.

However, guessing a value of the boundary layer thickness, in our system, at a given vibration frequency and amplitude, along with guessing a certain diffusivity of the yeast cells and potential barrier would be associated with quite much uncertainty. Thus, this model will not be applied for our own data.

3.2.6 Comparison of models with our experimental data

In this sub-section we will try to see whether our own critical flux data from PAPER 1 and PAPER 4 can be explained by one of the different models. A combined theoretical and empirical model, predicting critical fluxes for our own system, will then be proposed. In order to apply the shear-induced diffusivity models, the bulk volume fraction, ϕ_b, has to be determined. With a dry yeast cell content of 5 g/l and 8 g/l, respectively, in a 3 liter feed tank (m_{cells} = 15 g and 24 g), d_p of 5μm, and a yeast cell weight of $1.5 \cdot 10^{-11}$ g/cell [Sullivan et al., 2006], the bulk volume fractions can be calculated:

$$\phi_b(5\ g/l) = \frac{V_{cells}}{V_{total}} \cdot \frac{V_{cell} \cdot n_{cells}}{V_{total}} = \frac{\left(\frac{4}{3} \cdot \pi \cdot \left(\frac{d_p}{2}\right)^3\right) \cdot \frac{m_{cells}}{m_{cell}}}{V_{total}} = \frac{\left(\frac{4}{3} \cdot \pi \cdot \left(\frac{5 \cdot 10^{-6} m}{2}\right)^3\right) \cdot \frac{15g}{1.5 \cdot 10^{-11} g}}{3 \cdot 10^{-3} m^3}$$

$$= 0.022$$

$$\phi_b(8\ g/l) = \frac{V_{cells}}{V_{total}} \cdot \frac{V_{cell} \cdot n_{cells}}{V_{total}} = \frac{\left(\frac{4}{3} \cdot \pi \cdot \left(\frac{d_p}{2}\right)^3\right) \cdot \frac{m_{cells}}{m_{cell}}}{V_{total}} = \frac{\left(\frac{4}{3} \cdot \pi \cdot \left(\frac{5 \cdot 10^{-6} m}{2}\right)^3\right) \cdot \frac{24g}{1.5 \cdot 10^{-11} g}}{3 \cdot 10^{-3} m^3}$$

$$= 0.035$$

The length, L, of the membrane fibers in our system is 12 cm. The average surface shear rate of the vibrating membrane module has been determined as function of the vibration frequency and amplitude in our first publication [PAPER 1]. The predicted fluxes by the presented models as function of the average surface shear rate are depicted in Figure 38 along with some of our experimental values.

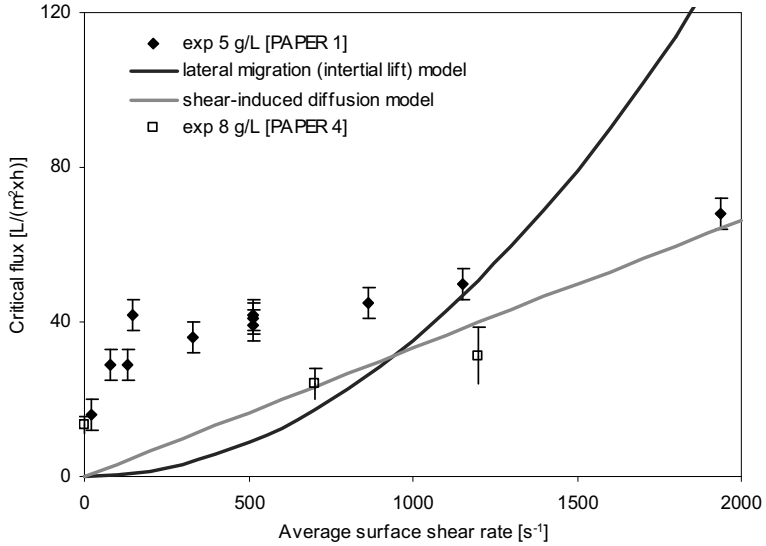

Figure 38: Critical flux vs. average surface shear rate for bakers yeast filtration for i) experimental data 5 g/l [PAPER 1] and 8 g/l [PAPER 4] dry weight, ii) lateral migration (inertial lift) model, equation (45), and iii) modified shear-induced diffusivity model, equation (49).

Contradictory to the force momentum model, the lateral migration model and the shear-induced diffusivity models predict critical fluxes in the same order of magnitude as our experimental results. In the force momentum model, the "critical flux criteria" was whether a whole particle could stick to the surface without moving or not. Obviously, no whole yeast cell was able to stick to the vibrating membrane module with negative force momentum. In the other models depicted in Figure 38, it is not necessarily assumed as a criteria for reaching the critical flux that the particles has to stick to the surface without moving. These models are based on the rate of back-transport, and thus, these surface particles could in principle very well be rotating or moving (force momentum $M > 0$). This means that the "criteria" for reaching the critical flux for the latter three models are much more "loose" than for the force momentum model, and therefore, much lower critical fluxes are predicted by these models.

The main mechanism for the back-transport in the lateral migration model is the inertial lift on the particles induced by the velocity gradient (shear rate). A square dependency between flux and shear rate is predicted which is responsible for the relatively fast increase in predicted fluxes around shear rates of ~ 700 s^{-1} (see Figure 38). However, by looking at the experimentally determined critical fluxes, the dependency between critical flux and shear rate (at least above 250 s^{-1}) seems to be more or less linear. Therefore, the

mechanism responsible for the back-transport in the shear-induced diffusivity models (self-diffusion due to particle-particle interactions) might more correctly be the mechanism responsible for the back-transport in our experiments.

Over the entire range of experimentally tested shear rate levels, we have earlier proposed an empirical power dependency between average surface shear rate and critical flux for a 5 g/l dry weight yeast cell suspension ($J_c = 8.22 \cdot \gamma_s^{0.26}$) [PAPER 1]. However, linear relationship might be more correct at least above a shear rate level of ~ 100 s^{-1} (as seen in Figure 38) and theoretically in agreement with a shear-induced particle-particle interaction back-transport mechanism. The difference between fitting a power law dependency or a linear dependency is not large. A power law dependency explains ~ 88 % of the variation in the data [PAPER 1], whereas a linear regression can explain ~ 83 % of the variation in the same data ($R^2 = 0.88$ for power law fit, and $R^2 = 0.83$ for linear fit). Furthermore, these R^2 values are 0.90 (linear fit), and 0.78 (power law fit) if the lowest critical flux value at a shear rate of 22 s^{-1} is neglected. Therefore, by evaluating these R^2 values, it is very hard to judge which model/correlation is best at describing the variation in the data.

Flux predicting model for the vibrating microfiltration system

Compared to the lateral migration model, the shear-induced diffusivity models include concentration factors (volume fractions of particles) for the flux prediction. As stated earlier, the fundamental reason for this is according to Li et al. [Li et al., 2000] that shear-induced diffusion of particles away from the membrane surface is assumed to be due to particle-particle interactions near the membrane wall. Since a clear dependency on the concentration is seen from the experimental data, the bulk volume fraction is very likely necessary in a critical flux predicting model. For larger concentrations, the fluxes are lower, probably because of larger hydrodynamic resistance near the membrane surface, and probably also because of increase in viscosity near the surface.

A general trend, seen in Figure 38, is that critical fluxes experimentally determined at zero vibration degree are not zero as predicted by the models. Actually, critical fluxes of ~ 24 L/(m^2·h) and ~ 14 L/(m^2·h) were measured a zero vibration with 5 and 8 g/l dry weight yeast cell suspensions. Thus, in deriving a critical flux predicting model for our system, the critical flux at zero vibration degree shall be added, and then the shear-induced diffusivity back-transport mechanism is used to explain the further variation in critical fluxes at varied average surface shear rate. Therefore, the important factors influencing the critical flux level are:

- Critical flux at zero vibration degree, J_{c0}
- Bulk volume fraction of yeast cells, ϕ_b
- Average surface shear rate, γ_s
- Particle diameter, d_p (which for our experiments have not been varied)

In setting up a critical flux predicting model for our system, the critical flux a zero vibration degree will be added to the flux predicting part of the model. The shear-induced diffusivity back-transport mechanism is chosen to explain the shear rate variation on the critical flux because the linear dependency apparently is close to the experimental

observations. According the shear-induced diffusivity model, the follow relationships are assumed:

- $J_c \propto \gamma_s$
- $J_c \propto \ln\left(\frac{1}{\phi_b}\right)$ (from eq.(49), shear-induced diffusivity model). The dependency given by equation (51) could be chosen as well.
- $J_c \propto d_p^{4/3}$

The shear-induced diffusivity models will thus attain the following form:

$$J_c = J_{c0}\big|_{zero\ vibration} + \alpha \cdot \gamma_s \cdot d_p^{4/3} \cdot \ln\left(\frac{1}{\phi_b}\right) \quad (53)$$

The α term is a constant that has to be fitted to the 5 and 8 g/l experimental data.

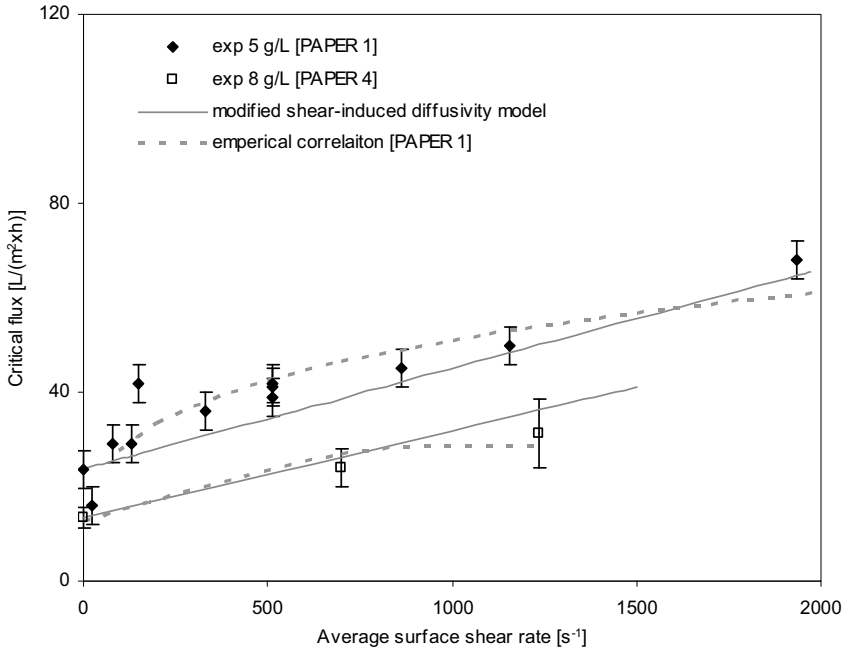

Figure 39: Experimental data [PAPER 1; PAPER 4] and modified shear-induced diffusivity critical flux predicting models along with the earlier proposed power law correlation [PAPER 1].

In Figure 39, the proposed shear-induced diffusivity model for our systems is plotted along with the power law correlation of our first publication [PAPER 1]. The power law plot for the 5 g/l data is taken from our earlier paper [PAPER 1], whereas the power law plot for the 8 g/l data is obtained by fitting a similar power law correlation to the three

measured critical flux values. It is hard to judge whether the fitted shear-induced diffusivity model or our earlier proposed power law correlation is best at describing the variation in the critical fluxes at different levels of average surface shear rate. Both models are more or less within the standard deviation of the measured critical fluxes. The shear-induced diffusivity model has not been tested for particles with other particle diameters, and therefore, the dependency $J_c = f(d_p^{4/3})$ have not been verified. However, the particle size dependency is included in the model to show that particle size has an impact on the critical flux level as described for all the different models in this chapter.

3.2.7 Uncertainties in the modeling work

When applying the different models (force momentum model, lateral migration (inertial lift) model, and shear-induced diffusivity models) to our system a number of assumptions are made.

- Yeast cells are in the force momentum model considered as "hard" spheres. In reality yeast cells are quite soft and can be "squeezed".
- Flow field can hardly be characterized at simple linear shear flow. However, since the peak velocity of the vibrating membrane module at 20 Hz and 1.375 mm amplitude is "only" 0.17 m/s, the models are adapted to our system.
- Even though the peak velocity of the vibration module is "only" 0.17 m/s, at 20 Hz and 1.375 mm amplitude, it is constantly changing which probably induces a whole other flow field. Thus, one has to be cautious in interpreting the results of the models.
- We use the same value for $\tan\theta$ in the force momentum model as Lu and Ju [Lu & Ju, 1989] that was obtained at fluxes from 1800 – 3600 L/(m^2·h) which is around 2 orders of magnitude larger that our flux levels during filtrations. However, since we have no data with different particle diameters and their critical fluxes, we adapted the value for the angle of response from Lu and Ju [Lu & Ju, 1989].
- In the calculation of the bulk volume fraction of yeast cells, the dry weight of the cells were used because the suspended weight of the yeast cells were not available.

More questionable assumptions might be listed. However, overall, and since the proposed critical flux predicting model for yeast cell filtrations for our system (equation (53)) is semi-empirical and semi-theoretical and includes a parameter that is fitted to experimental data, we find the model relevant since it by a well known and well described back-transport mechanism explains the variation in the measured critical fluxes.

4 Conclusions and future work

Dynamic membrane filtration facilitates the possibility of reducing fouling problems without necessarily having to increase the crossflow velocity on the feed side in the membrane module. Since the feed flow velocity and surface shear rate are decoupled, the TMP can be kept low and uniform. This is advantageous in terms of i) minimizing fouling problems, ii) possibility of lowering operational costs, and iii) enhancing macromolecular transmission in microfiltration.

Our dynamic microfiltration system, the *vibrating hollow fiber membrane module*, is thought to be coupled to treatment of biological media, e.g. fermentation broth. The system is somewhat different from other dynamic systems reported in the literature: The generated shear rate is evenly distributed throughout the whole membrane surface, and therefore, the membrane area is more effectively utilized. Furthermore, the vibration amplitude and frequency can be varied independently. The effects of vibrating the module have been reported in our publications: The critical flux increases with increasing vibration degree. Whether the dependency between the critical flux and the average surface shear rate is best described by shear-induced diffusivity back-transport or by a power law correlation is difficult to judge. The value of critical flux is very dependent on how it is actually determined, using step-by-step determination procedures. Moreover, the critical flux determination has to be verified with constant operation experiments for extended periods. However, when this is done, and when a sub-critical region has been identified, the possibility of sustaibable operation emerges with enhanced and stable macromolecular transmission as a clear benefit. However, one should bear in mind that a "critical time period" always should be defined when talking about process sustainability. Through the work, different fouling aspects have been further investigated. The impact of EPS fouling as well as macromolecular adsorption has been evaluated, and we have concluded that irreversible fouling can not be prevented in our dynamic system. Therefore, it is the reversible parts of the fouling that is strongly reduced at vibrational mode. The ultrafiltration adsorption results are based on the assumption that amount of adsorbed material is linearly dependent on the permeability drop.

Altogether, our experimental system findings are interesting contributions to the field of dynamic membrane filtration. However, more aspects, certainly, have to be further investigated. A general postulate in many of the "dynamic papers", found in the literature, is the possibility of strongly reduce the operational costs. In spite of that, a seriously lack of energy calculations proving such postulates seems to exist, also in our case. This should be investigated. Furthermore, we are dealing much with the critical flux determination. From that point of view, it could be interesting to further investigate the real impact of individually varying the step height, and the flux start level. The aspects covering the possibility of sustainability for extended periods, also, need further investigation especially in terms of macromolecular transmission. Lastly, an interesting idea could be to implements a control strategy so that the flux level could be adjusted online in order to maintain process sustainability as the feed composition, e.g. fermentation broth, might change during operation.

References

[Al-Akoum et al., 2002i] Al-Akoum, O.; Ding, L.; Chotard-Ghodsnia, R.; Jaffrin, M.Y.; Gésan-Guiziou, G. Casein micelles separation from skimmed milk using a VSEP dynamic filtration module, Desalination 144 (2002) 325-330.

[Al-Akoum et al., 2002ii] Al-Akoum, O.; Ding, L.H.; Jaffrin, M.Y. Microfiltration and ultrafiltration of UHT skim milk with a vibrating membrane module, Separation and Purification Technology 28 (2002) 219-234.

[Al Akoum et al., 2002iii] Al Akoum, O.; Jaffrin, M.Y.; Ding, L.; Paullier, P.; Vanhoutte, C. An hydrodynamic investigation of microfiltration and ultrafiltration in a vibrating membrane module, Journal of Membrane Science 197 (2002) 37-52.

[Akoum et al., 2006] Akoum, O.; Richfield, D.; Jaffrin, M.Y.; Ding, L.H.; Swart, P. Recovery of trypsin inhibitor and soy milk protein concentration by dynamic filtration, Journal of Membrane Science 279 (2006) 291-300.

[Altena & Belfort, 1984] Altena, F.W.; Belfort, G. Lateral migration of spherical particles in porous flow channels: Application to membrane filtration, Chemical Engineering Science 39(2) (1984) 343-355.

[Bacchin et al., 1995] Bacchin, P.; Aimar, P.; Sanchez, V. Model for colloidal fouling of membranes, AIChE Journal 41(2) (1995) 368-376.

[Bacchin, 2004] Bacchin, P. A possible link between critical and limiting flux for colloidal systems: consideration of critical deposition formation along a membrane, J. Membr. Sci. 228 (2004) 237-241.

[Bacchin et al., 2006i] Bacchin, P; Aimar, P.; Field, R.W. Review critical and sustainable fluxes: Theory, experiments and applications, J. Membr. Sci. 281 (2006) 42-69.

[Bacchin et al., 2006ii] Bacchin, P.; Espinasse, B.; Bessiere, Y.; Fletcher, D.F.; Aimar, P. Numerical simulation of colloidal dispersion filtration: description of critical flux and comparison with experimental results, Desalination 192 (2006) 74-81.

[Beier, 2004] Beier, S.P. Treatment of surplus yeast, Company project at Carlsberg Brewery and BioCentrum DTU, Technical University of Denmark, 2004.

[Beier, 2006i] Beier, S.P. Transport phenomena, 1st edition, Ventus Publishing, Copenhagen, Denmark, 2006.

[Beier, 2006ii] Beier, S.P. Electrically driven membrane processes, 1st edition, Ventus Publishing, Copenhagen, Denmark, 2006.

[Beier, 2006iii] Beier, S.P. Pressure driven membrane processes, 1st edition, Ventus Publishing, Copenhagen, Denmark, 2006.

[Belfort et al., 1994] Belfort, G.; Davis, R.H.; Zydney, A.L. Review The behavior of suspensions and macromolecular solutions in crossflow microfiltration, Journal of Membrane Science 96 (1994) 1-58.

[Bergen et al., 2000] Bergen, A.; Fyles, T.M.; Lycon, D.S.; Vickers, G.W.; Wild, P. Flux enhancement in reverse osmosis using centrifugal membrane separation, Journal of Membrane Science 176 (2000) 257-266.

[Bergen et al., 2001] Bergen, A.; Wild, P.M.; Djilali, N.; Vickers, G.W. Fundamental aspects of centrifugal membrane separation, Proc. Instn. Mech. Engrs. 215(4) (2001) 355-365.

[Bergen et al., 2003] Bergen, A.; Djilali, N.; Fyles, T.M.; Vickers, G.W.; Wild, P.M. An experimental assessment of centrifugal membrane separation using spiral wound RO membrane elements, Desalination 154(3) (2003) 225-232.

[Bird et al., 2002] Bird, R.B.; Stewart, W.E.; Lightfoot, E.N. Transport Phenomena, 2nd edition, John Wiley & Sons Inc., 2002.

[Bouzerar et al., 2000i] Bouzerar, R.; Jaffrin, M.Y.; Ding, L.; Paullier, P. Influence of geometry and angular velocity on performance of a rotating disk filter, AIChE Journal 46(2) (2000) 257-265.

[Bouzerar et al., 2000ii] Bouzerar, R.; Ding, L.; Jaffrin, M.Y. Local permeate flux-shear-pressure relationships in a rotating disk microfiltration module: Implications for global performance, Journal of Membrane Science 170 (2000) 127-141.

[Bouzerar et al., 2003] Bouzerar, R.; Paullier, P.; Jaffrin, M.Y. Concentration of mineral suspensions and industrial effluents using a rotating disk dynamic filtration module, Desalination 158 (2003) 79-85.

[Chaun-yi et al., 2007] Chaun-yi, Z.; Yi, D.; Li-mei, Y.; Yan-qiu, Z.; Dan-li, X. Characteristics of Membrane Fouling in an anarobic-(Anoxic/Oxic)^n-MBR Process, Journal of China University of Mining & Technology 17(3) (2007) 0387-0392.

[Cho & Fane, 2002] Cho, B.D.; Fane, A.G. Fouling transients in nominally sub-critical flux operation of a membrane bioreactor, J. Membr. Sci. 209 (2002) 391-403.

[Cho & Fane, 2003] Cho, B.D.; Fane, A.G. Fouling phenomena in MBR: transmembrane pressure transients and the role of EPS (extracellular polymeric substances), Water Science and Technology 3(5-6) (2003) 261-266.

[Choi et al., 1999] Choi, C.K.; Park, J.Y.; Park, W.C.; Kim, J.J. A study on dynamic separation of silica slurry using a rotating membrane filter: 2. Modelling of cake formation, Journal of Membrane Science 157 (1999) 177-187.

[Christiansen et al., 2000] Christiansen, G.; Both, E.; Sørensen, P.Ø., Mekanik, Institut for Fysik, Danmarks Tekniske Universitet, Stougaard Jensen/Albertslund (2000).

[Cohen & Probstein, 1986] Cohen, R.D.; Probstein, R.F. Colloidal fouling of reverse osmosis membranes, Journal of Colloid and Interface Science 114(1) (1986) 194-207.

[Cometas.dk, 2008] website of Copenhagen Membrane Technology A/S visited June 2008: www.cometas.dk

[Culkin & Armando, 1992] Culkin, B.; Armando, A.D. New separation system extends the use of membranes, Filtration & Separation, September/October (1992) 376-378.

[Davis & Sherwood, 1990] Davis, R.H.; Sherwood, J.D. A similarity solution for steady-state crossflow microfiltration, Chemical Engineering Science 45(11) (1990) 3203-3209.

[Deniega et al., 1996] Deniega, J.C.; Duf, D.H.; Schoendorfer, D.W.; Miller, W.R.; Apparatus and methods for generating leukocyte free platelet concentrate, Transfus. Science 17(1) (1996) 1, patent no: 5403272.

[Ding et al., 2002] Ding, L.; Al-Akoum, O.; Abraham, A.; Jaffrin, M.Y. Milk protein concentration by ultrafiltration with rotating disk modules, Desalination 144 (2002) 307-311.

[Ding et al., 2006] Ding, L.H.; Jaffrin, M.Y.; Mellal, M.; He, G. Investigation of performances of a multishaft disk (MSD) system with overlapping ceramic membranes in microfiltration of mineral suspensions, Journal of Membrane Science 276 (2006) 232-240.

[Drew et al., 1991] Drew, D.A.; Schonberg, J.A.; Belfort, G. Lateral intertial migration of a small sphere in fast laminar flow through a membrane duct, Chemical Engineering Science 46(12) (1991) 3219-3224.

[Enevoldsen et al., 2007] Enevoldsen, A.D.; Hansen, E.B.; Jonsson, G. Electro-ultrafiltration of industrial enzyme solutions, Journal of Membrane Science 299 (2007) 28-37.

[Fan et al., 2006] Fan, F.; Zhou, H.; Husain, H. Identification of wastewater sludge characteristics to predict critical flux for membrane bioreactor processes, Water Research 40 (2006) 205-212.

[Fane & Chang, 2002] Fane, A.; Chang, S. Membrane bioreactors: Design & Operational options, Filtration and Separation 39(5) (2002) 26-29.

[Fane et al., 2002] Fane, A.G.; Chang, S.; Chardon, E. Submerged hollow fibre membrane module – design options and operational considerations, Desalination 146 (2002) 231-236.

[Field et al., 1995] Field, R.W.; Wu, D.; Howell, J.A.; Gupta, B.B. Critical flux concept for microfiltration fouling, J. Membr. Sci. 100 (1995) 259-272.

[Fordham & Ladva, 1989] Fordham, E.J.; Ladva, H.K.J. Cross-flow filtration of bentonite suspensions, Physicochemical Hydrodynamics 11(4) (1989) 411-439.

[Fordham & Ladva, 1992] Fordham, E.J.; Ladva, H.K.J. Cross-flow filtration of bentonite suspensions II, Journal of Colloid and Interface Science 148(1) (1992) 29-34.

[Frappart et al., 2006] Frappart, M.; Akoum, O.; Ding, L.H.; Jaffrin, M.Y. Treatment of dairy process waters modeled by diluted milk using dynamic nanofiltration with a rotating disk module, Journal of Membrane Science 282 (2006) 465-472.

[Frappart et al., 2008] Frappart, M.; Jaffrin, M.; Ding, L.H. Reverse osmosis of diluted skim milk: Comparison of results obtained from vibratory and rotating disk modules, Separation and purification Technology 60 (2008) 321-329.

[Frenander & Jönsson, 1996] Frenander, U.; Jönsson, A.S. Cell harvesting by cross-flow microfiltration using a shear-enhanced module, Biotechnology and Bioengineering 52 (1996) 397-403.

[Fyles & Lycon, 2000] Fyles, T.M.; Lycon, D.S. Fouling reduction using centrifugal membrane separation, Journal of Membrane Science 176 (2000) 267-276.

[Gan et al., 1999] Gan, Q.; Howell, J.A.; Field, R.W.; England, R.; Bird, M.R.; McKechinie, M.T. Synergetic cleaning procedure for a ceramic membrane fouled by beer microfiltration, Journal of Membrane Science 155 (1999) 277-289.

[Genkin et al., 2006] Genkin, G.; Waite, T.D.; Fane, A.G.; Chang, S. The effect of vibration and coagulant addition on the filtration performance of submerged hollow fibre membranes, Journal of Membrane Science 281 (2006) 726-734.

[Goldinger et al., 1986] Goldinger, W.; Rebsamen, E.; Brändli, E.; Ziegler, H. Dynamische Mikro- und Utrafiltration in der Biotechnologie, Technische Rundschau Sultzer 3 (1986) 10-12.

[Goren, 1979] Goren, S.L. The hydrodynamic force resisting the approach of a sphere to a plane permeable wall, Journal of Colloid and Interface Science 69(1) (1979) 78-85.

[Guerra et al., 1997] Guerra, A; Jonsson, G.; Rasmussen, A.; Nielsen, E.W.; Edelsten, D. Low Cross-flow velocity Microfiltration of Skim Milk for Removal of Bacterial Spores, Int. Dairy Journal 7 (1997) 849-861.

[Guglielmi et al., 2007i] Guglielmi, G.; Chiarani, D.; Judd, S.J.; Andreottola, G. Flux criticality and sustainability in a hollow fibre submerged membrane bioreactor for municipal wastewater treatment, J. Membr. Sci. 289 (2007) 241-248.

[Guglielmi et al., 2007ii] Guglielmi, G.; Saroj, D.P.; Chiarani, D.; Andreottola, G. Sub-critical fouling in membrane bioreactor for municipal wastewater treatment: Experimental investigation and mathematical modeling, Water Research 41 (2007) 3903-3914.

[Hanbury et al., 2003] Hanbury, W.T.; Hodgkiess, T.; Al-Omari, K. Aspects of acid-cleaning operatons in MSF plants, Desalination 158 (2003) 1.

[He et al., 2007] He, G.; Ding, L.H.; Paullier, P.; Jaffrin, M.Y. Experimental study of a dynamic filtration system with overlapping ceramic membranes and non-permeating disks rotating at independent speeds, Journal of Membrane Science 300 (2007) 63-70.

[Hede & Beier, 2007] Hede, P.D.; Beier, S.P. Inorganic and applied chemistry, Ventus Publishing, Copenhagen, Denmark, 2007.

[Howell, 1995] Howell, J.A. Sub-critical flux operation of microfiltration, J. Membr. Sci. 107 (1995) 165-171.

[Hughes & Field, 2006] Hughes, D.; Field, R.W. Crossflow filtration of washed and unwashed yeast suspensions at constant shear under nominally sub-critical conditions, J. Membr. Sci. 280 (2006) 89-98.

[Huuhilo et al., 2001] Huuhilo, T.; Väisänen, P.; Nuortila-Jokinen, J.; Nyström, M. Influence of shear on flux in membrane filtration of integrated pulp and paper mill circulation water, Desalination 141 (2001) 245-258.

[Jaffrin et al., 2004] Jaffrin, M.Y.; Ding, L.H.; Akoum, O.; Brou, A. A hydrodynamic comparison between rotating disk and vibratory dynamic filtration systems, Journal of Membrane Science 242 (2004) 155-167.

[Jaffrin et al., 2006] Jaffrin, M.Y.; He, G.; Ding, L.H.; Paullier, P. Effect of membrane overlapping on performance of multishaft rotating ceramic disk membranes, Desalination (2006) 269-271.

[Jones, 1987] Jones, A.J. Membrane and Separation Technology, Australian Government Publishing Service, 1987.

[Jonsson & Wenten, 1994] Jonsson, G.; Wenten, I.G. Control of concentration polarization, fouling and protein transmission of microfiltration processes within the agro-based industry, proceedings of the ASEAN-EC workshop on membrane technology in agro-based industry, July 26-29 (1994) Kuala-Lumpur, Malaysia. pp. 157-166.

[Kim et al., 1993] Kim, K.J.; Sun, P.; Chen, V.; Wiley, D.E.; Fane, A.G. The cleaning of ultrafiltration membranes fouled by protein, Journal of Membrane Science 80 (1993) 241-249.

[Kroner & Nissinen, 1988] Kroner, K.H.; Nissinen, V. Dynamic filtration of microbial suspensions using an axially rotating filter, Journal of Membrane Science 36 (1988) 85-100.

[Kwon et al., 2000] Kwon, D.Y.; Vigneswaran, S.; Fane, A.G.; Ben Aim, R. Experimental determination of critical flux in cross-flow microfiltration, Separation and Purification Technology 19 (2000) 169-181.

[Lee et al., 1995] Lee, S.S.; Burt, A.; Russotti, G.; Buckland, B. Microfiltration of recombinant yeast cells using a rotating disk dynamic filtration system, Biotechnology and Bioengineering 48(4) (1995) 386-400.

[Li et al., 1998] Li, H.; Fane, A.G.; Coster, H.G.L.; Vigneswaran, S. Direct observation of particle deposition on the membrane surface during crossflow microfiltration, J. Membr. Sci. 149 (1998) 83-97.

[Li et al., 2000] Li, H.; Fane, A.G.; Coster, H.G.L.; Vigneswaran, S. An assessment of depolarization models of crossflow microfiltration by direct observations through the membrane, Journal of Membrane Science 172 (2000) 135-147.

[Lin & Reed, 1996] Lin, W.; Reed, B.E. Comparison of cross flow ultrafiltration and centrifugal membrane technology in treating an oil/grease wastewater, Industrial and hazardous waste (Mid-Atlantic Conference) (1996) 278-285.

[Lipnizki, 2003] Lipnizki, J. Fouling and scaling in membrane processes: Mechanisms and how to control these phenomena, Ph.D. Thesis, Department of Chemical Engineering, Technical University of Denmark, 2003.

[Lu & Ju, 1989] Lu, W.M.; Ju, S.C. Selective particle deposition in crossflow filtration, Separation science and technology 24(7-8) (1989) 517-540.

[Mänttäri et al., 2004] Mänttäri, M.; Pekuri, T.; Nyström, M. NF270, a new membrane having promising characteristics and being suitable for treatment of dilute effluents from the paper industry, Journal of Membrane Science 242 (2004) 107-116.

[Mänttäri & Nyström, 2004] Mänttäri, M.; Nyström, M. Ultrafiltration and nanofiltration in the pulp and paper industry using cross-rotational (CR) filters, Water Science and Technology 50(3) (2004) 229-238.

[Margaritis, 1976] Margaritis, A. A study of the rotorfermentor and the kinetic of ethanol fermentation, Dissertation Abstracts International B 37(1) (1976) 358.

[Marshall et al, 1993] Marshall, A.D.; Munro, P.A. Trägårdh, G. The effect of protein fouling in microfiltration and ultrafiltration on the permeate flux, protein retention and selectivity: A literature review, Desalination 91 (1993) 65-108.

[Mellal et al., 2008] Mellal, M.; Jaffrin, M.Y.; Ding. L.H.; Delattre, C.; Michaud, P.; Coutoris, J. Separation of oligoglucoronans of low degrees of polymerization by using a high shear rotating disk filtration module, Separation and Purification Technology 60 (2008) 22-29.

[Metsopaper.com, 2008] website visited June 2008: www.metsopaper.com

[Mulder, 1996] Mulder, M. Basic principles of membrane technology, 2nd edition, Kluwer Academic Publishers, 1996.

[Müller & Sommer, 2000] Müller, U.; Sommer, K. Neue Erkenntnisse zur Hygiene an Getränkeschankanlagen (New information on hygiene in beverage dispensing equipment), Brauwelt 140(41) (2000) 1648-1654.

[Murase et al., 1991] Murase, T.; Pradistsuwana, C.; Iritani, E.; Kano, K. Dynamic microfiltration of dilute slurries with a rotating ceramic membrane, Journal of Membrane Science 62 (1991) 187-199.

[Nagaoka et al., 1998] Nagaoka, H.; Yamanishi, S.; Miya, A. Modeling of biofouling by extracellular polymers in a membrane separation activated sludge system, Water Science and Technology 38(4-5) (1998) 497-504.

[Neal, 2006] Neal, P.R. An examination of the nature of critical flux and membrane fouling by direct observation, Ph.D. thesis, School of Chemical Science and Engineering, The University of New South Wales, 2006.

[Nuortila-Jokinen & Nyström, 1996] Nuortila-Jokinen, J.; Nyström, M. Comparison of membrane separation processes in the internal purification of paper mill water, Journal of Membrane Science 119 (1996) 99-115.

[Nuortila-Jokinen et al., 1998] Nuortila-Jokinen, J.; Kuparinen, A.; Nyström, M. Tailoring an economical membrane process for internal purification in the paper industry, Desalination 119 (1998) 11-19.

[Ognier et al., 2004] Ognier, S.; Wisniewski, C.; Grasmick, A. Membrane bioreactor fouling in sub-critical filtration conditions: a local critical flux concept, J. Membr. Sci. 229 (2004) 171-177.

[O'Neill, 1968] O'Neill, M.E. A sphere in contact with a plane wall in a slow linear shear flow, Chemical Engineering Science 23 (1968) 1293-1298.

[Pall.com, 2008] website visited June 2008: www.pall.com

[Park et al., 1994] Park, J.Y.; Choi, C.K.; Kim, J.J. A study on dynamic separation of silica slurry using a rotating membrane filter 1. Experiments and filtrate fluxes, Journal of Membrane Science 97 (1994) 263-273.

[Parkinson, 2001] Parkinson, G. Chementator, Chemical engineering 108(7) (2001) 19.

[Paul & Hartung, 2008] Paul, P.; Hartung, C. Modeling of biological fouling propensity by interference in a side stream membrane bioreactor, Desalination 224 (2008) 154-159.

[Petala & Zouboulis, 2006] Petala, M.D.; Zouboulis, A.I. Vibratory shear enhanced processing membrane filtration applied for the removal of natural organic matter from surface waters, Journal of Membrane Science 269 (2006) 1-14.

[Pharoah et al., 2000] Pharoah, J.G.; Djilali, N.; Vickers, G.W. Fluid michanics and mass transport in centrifugal membrane separation, Journal of Membrane Science 176 (2000) 277-289.

[Pollice et al., 2005] Pollice, A.; Brooks, A.; Jefferson, B.; Judd, S. Sub-critical fouling in membrane bioreactors – a review of the recent literature, Desalination 174 (2005) 221-230.

[Postlethwaite et al., 2004] Postlethwaite, J.; Lamping, S.R.; Leach, G.C.; Hurwitz, M.F.; Lye, G.J. Flux and transmission characteristics of a vibrating microfiltration system operated at high biomass loading, Journal of Membrane Science 228 (2004) 89-101.

[Rushton & Zhang, 1988] Rushton, A.; Zhang, G.S. Rotary microporous filtration, Desalination 70 (1988) 379-394.

[Schwinge et al., 2002] Schwinge, J; Neal, P.R.; Wiley, D.E.; Fane, A.G. Estimation of foulant deposition across the leaf of a spiral-wound module, Desalination 146 (2002) 203-208.

[Shi & Benjamin, 2008] Shi, W.; Benjamin, M.M. Membrane interactions with NOM and an adsorbent in a vibratory shear enhanced filtration process (VSEP) system, Journal of Membrane Science 312 (2008) 23-33.

[SpinTek.com, 2008] website visited June 2008: www.spintek.com

[Strohwald & Jacobs, 1992] Strohwald, N.K.H.; Jacobs, E.P. An investigation into UF systems in the pretreatment of seawater for RO desalination, Waster Science Technology 25(10) (1992) 69-78.

[Sullivan et al., 2006] Sullivan, D.P.; Ohvo-Rekilä, H.; Baumann, N.A.; Beh, C.T.; Menon, A.K. Sterol trafficking between the endoplasmic reticulum and plasma membrane in yeast, Biochem. Soc. Trans. 34 (2006) 356-358.

[Takata et al., 1998] Takata, K.; Yamamoto, K.; Bian, R.; Watanabe, Y. Removal of humic substances with vibratory shear enhanced processing membrane filtration, Desalination 117 (1998) 273-282.

[Tobler, 1982] Tobler, W. Dynamic filtration: Principle and applicaton of shear filtration in an annular gap, Filtration & Separation July/August (1982) 329-332.

[Trägårdh, 1989] Tragårdh, G. Membrane cleaning, Desalination 71 (1989) 325-335.

[US patent, 1988] US Patent 4790942, Filtration method and apparatus, 1988.

[Vane et al., 1999] Vane, L.M.; Alvarez, F.R.; Giroux, E.L. Reduction of concentration polarization in pervaporation using vibrating membrane module, Journal of Membrane Science 153 (1999) 233-241.

[Vasseur & Cox, 1976] Vasseur, P.; Cox, R.G. The lateral migration of spherical particle in two-dimensional shear flows, J. Fluid Mech. 78(2) (1976) 358-413.

[Viadero et al., 1997] Viadero, R.C.; Reed, B.E., Lin, W. The effects of membrane rotation on the operational performance of a centrifugal ultrafiltration separaton system, Steelmaking conference Proceedings 29 (1997), 614-621.

[Vsep.com, 2008] website visited June 2008: www.vsep.com

[Wang et al., 2006] Wang, Z.; Wu, Z.; Yu, G.; Liu, J.; Zhou, Z. Relationship between sludge characteristics and membrane flux determination in submerged membrane bioreactors, J. Membr. Sci. 284 (2006) 87-94.

[Westfalia-separator.com, 2008] website visited June 2008: www.westfalia-separator.com

[Zeman & Zydney, 1996] Zeman, L.J.; Zydney, A.L. Microfiltration and ultraltration – principles and applications, Marcel Dekker, Inc., 1996.

[Zouboulis & Petala, 2008] Zouboulis, A.I.; Petala, M.D. Performance of VSEP vibratory membrane filtration system during the treatment of landfill leachates, Desalination 222 (2008) 165-175.

[Zydney & Colton, 1986] Zydney, A.L.; Colton, C.K. A concentration polarization model for the filtrate flux in crossflow microfiltration of particulate suspensions, Chem.. Eng. Commun. 47 (1986) 1-21.

Publications

Each paper is followed by its own reference list. As explained in the introduction, the references in the thesis are given as [PAPER 1], [PAPER 2], [PAPER 3], [PAPER 4], and [PAPER 5]. In the following pages the publications are given in the original published format.

[PAPER 1] Beier, S.P.; Guerra, M.; Garde, A.; Jonsson, G. Dynamic microfiltration with a vibrating hollow fiber membrane module: Filtration of yeast suspensions, Journal of Membrane Science 281 (2006) 281-287.

[PAPER 2] Beier, S.P.; Jonsson, G. Separation of enzymes and yeast cells with a vibrating hollow fiber membrane module, Separation and Purification Technology 53 (2007) 111-118.

[PAPER 3] Beier, S.P.; Enevoldsen, A.D.; Kontogeorgis, G.M.; Hansen, E.B.; Jonsson, G. Adsorption of amylase enzyme on ultrafiltration membranes, Langmuir 23 (2007) 9341-9351.

[PAPER 4] Beier, S.P.; Jonsson, G. Critical flux determination by flux-stepping, AIChE Journal 56(7) (2010) 1739-1747.

[PAPER 5] Beier, S.P.; Jonsson, G. A vibrating membrane bioreactor (VMBR): Macromolecular transmission – influence of extracellular polymeric substances, Chemical Engineering Science 64 (2009) 1436-1444.

Available online at www.sciencedirect.com
ScienceDirect
Journal of Membrane Science 281 (2006) 281–287
journal of MEMBRANE SCIENCE
www.elsevier.com/locate/memsci

Dynamic microfiltration with a vibrating hollow fiber membrane module: Filtration of yeast suspensions

Søren Prip Beier, Maria Guerra, Arvid Garde, Gunnar Jonsson *

CAPEC, Department of Chemical Engineering, Technical University of Denmark, DK-2800 Kgs. Lyngby, Denmark

Received 9 December 2005; received in revised form 28 March 2006; accepted 31 March 2006
Available online 18 April 2006

Abstract

A novel dynamic microfiltration system consisting of a vibrating hollow fiber membrane module is presented. The vibrations induce the shear rate at the membrane surface which makes it possible to filtrate at low feed cross-flow velocity and thus at a low transmembrane pressure. Results from test filtrations of bakers yeast suspensions are presented and the critical flux concept is used to evaluate the filtration data. The critical flux at the maximum degree of vibration is improved 325% compared to the critical flux at the minimum degree of vibration. An equation to calculate the membrane surface shear rate from the vibration frequency and amplitude is presented. The correlation between the critical flux and average surface shear rate is $J_{p,crit} = 8.22(\bar{\gamma}_s)^{0.26}$. It is further shown that when operating below the critical flux in a 4.5 h test filtration the permeability is kept constant. Above the critical flux, the transmembrane pressure increases resulting in a decrease in membrane permeability.

Keywords: Vibrating dynamic microfiltration; Shear-enhanced filtration; Critical flux; Surface shear rate; Hollow fibers

1. Introduction

In microfiltration of colloids and macromolecules, the flux often drops to a level much below the level of the clean water flux due to severe membrane fouling. The fouling layer can be reduced by increasing the shear rate at the membrane surface so that deposition of colloids and macromolecules is reduced or avoided. Enhancing the surface shear rate can be done in different ways. One possibility is to let the feed stream pass along the surface at high cross-flow velocity which results in a high surface shear rate. By doing this, the permeate also has to pass along the membrane in the same direction and at the same velocity as the feed stream on the other side of the membrane. This is necessary to keep the transmembrane pressure (TMP) low, because a high TMP results in a faster and more compact fouling layer [1]. Guerra et al. [2] have shown that above a TMP value of around 0.3×10^5 Pa (0.3 bar) the flux decreased as the TMP was increased in the microfiltration of skim milk. This emphasizes the importance of keeping the TMP low. The high cross-flow velocity technique is used by Alfa-Laval to remove bacterial spores from skim milk [3], but one problem with this method is that the overall pumping costs become very high.

High membrane shear rate can also be achieved by creating a relative motion between the membrane and the feed stream. This can be done by vibrations or rotations of the membrane, which makes it possible to decouple high feed cross-flow velocity and high surface shear rate. Thus, filtrations can be carried out at low feed cross-flow velocity (and thus low TMP) and with a high surface shear rate. Pall Corporation has developed a vibrating membrane filter (VMF) based on this technique. The membrane stack is vibrated by a torsion bar, and such a system is installed at Tuborg Brewery in Fredericia (Denmark) to remove surplus yeast from beer. Postlethwaite et al. [4] have tested a commercial Pall VMF system for the removal of proteins from a feed of high biomass loading, and Jaffrin et al. [5] have worked with a similar system called the vibrating shear-enhanced processing (VSEP) system for filtration of bakers yeast suspensions.

Another way of decoupling high feed flow velocity and high surface shear rate is to let an object rotate at high speed close to the membrane surface. The rotations then induce high surface shear rate. Bouzerar et al. [6] have concentrated industrial effluents on a rotating disk system, and Jaffrin et al. [5] have filtrated bakers yeast suspensions also with a rotating disk system.

* Corresponding author. Tel.: +45 4525 2946; fax: +45 4588 2258.
E-mail address: gj@kt.dtu.dk (G. Jonsson).

0376-7388/$ – see front matter © 2006 Elsevier B.V. All rights reserved.
doi:10.1016/j.memsci.2006.03.051

High frequency back flushing [7] is another way to avoid severe membrane fouling. Here, the shear at the membrane surface itself is not so high but due to the destabilization of the fouling layer a steady-state concentration profile is never reached. A similar phenomenon might be observed for the vibrating membrane systems.

In general dynamic microfiltration systems seem efficient in the recovery of macromolecules from fermentation broths [6].

In this work, a novel dynamic microfiltration system is presented. The membrane, which consists of hollow fibers placed parallel in a module, is vibrated up and down at variable frequency and amplitude, which creates the shear rate at the membrane surface. Thus, it is possible to filtrate at very low feed cross-flow velocity and with a very low TMP. Results from test filtrations of bakers yeast suspensions are presented, and the critical flux concept formulated by Field et al. [1] is used to evaluate the results. The results are compared to results from filtration tests conducted with a similar system described by Genkin et al. [8]. The test fluid is selected because it is reproducible and has been extensively reported in the literature. The average shear rate on the membrane surface is calculated, and it is investigated how the critical flux varies with the average membrane surface shear rate. The permeability of the membrane below and above the critical flux is also evaluated and discussed in a long-term operation condition.

2. Theory

2.1. Calculation of surface shear rate

The membrane module consists of hollow fibers placed parallel vertically in a plastic cylinder. The feed stream is led to the vibrating module on the outside of the membrane fibers. The shear rate at the surfaces of the fibers is defined as the derivative of the velocity component along the membrane surface with respect to the length perpendicular to the membrane surface:

$$\gamma_s = \frac{dv_z}{dy} \tag{1}$$

The coordinate system is orientated so that the z-axis is in the same direction as the feed flow along the fibers and the y-axis is perpendicular to the membrane surface with $y = 0$ at the surface. The x-axis is a tangent to the surface perpendicular to the z- and y-axis. Very close to the surface, the surface is almost plane and therefore it makes sense to use Cartesian coordinates, which will simplify the equations. The velocity component in the z-direction therefore corresponds to the velocity at an oscillating plate, which is given by Bird et al. [9]:

$$v_z(y,t) = v_0\, e^{-\sqrt{(\omega/2\nu)}y} \cos\left(\omega t - \sqrt{\frac{\omega}{2\nu}}y\right) \tag{2}$$

The angular frequency ω (equals $2 \times \pi \times f$) is proportional to the vibration frequency, and the velocity amplitude v_0 (equals amp $\times\ \omega$) is the product of the vibration amplitude and the angular frequency. Using this equation for the velocity in the direction along the fibers at a given time and distance from the fiber one has to assume, that the velocity in the z-direction is zero at infinite y-distance from the fibers according to the boundary conditions given by Bird et al. [9]. This implies that the motion of one fiber does not influence the velocity of the fluid surrounding the neighboring fiber. At first this could seem unrealistic since the distance between the fibers is in the range of 1 mm, but by looking at the velocity profile calculated using Eq. (2) (in Fig. 1) one can see that at a distance of just 0.5 mm from the surface, the velocity is decreased to a level where it is a good approximation to state, that the motion of the fibers does not influence the flow pattern of the neighboring fiber. This tendency will be even more pronounced at higher vibration frequencies and amplitudes.

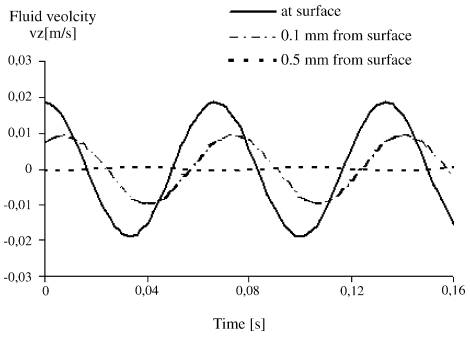

Fig. 1. Fluid velocities at different distances from the membrane surface at low frequency (10 Hz) and small amplitude (0.2 mm) calculated by using Eq. (2).

With the velocity component in the z-direction, the shear rate can be found as the derivative of the velocity with respect to the distance y as stated in Eq. (1):

$$\gamma = \frac{dv_z}{dy} = v_0\sqrt{\frac{\omega}{2\nu}}\, e^{-\sqrt{(\omega/2\nu)}y} \times \left[\sin\left(\omega t - \sqrt{\frac{\omega}{2\nu}}y\right) - \cos\left(\omega t - \sqrt{\frac{\omega}{2\nu}}y\right)\right] \tag{3}$$

The shear rate at the membrane surface is found by setting $y = 0$:

$$\gamma_s = v_0\sqrt{\frac{\omega}{2\nu}}[\sin(\omega t) - \cos(\omega t)] \tag{4}$$

This is the expression for the shear rate at the membrane surface as a function of time (t), angular frequency ($\omega = 2 \times \pi \times f$) and velocity amplitude ($v_0 = \text{amp} \times \omega$). A time mean average of the numerical value of the oscillating shear rate is used as a value for the surface shear rate for a given combination of vibration frequency and amplitude:

$$\overline{\gamma}_s = \frac{\sum_{i=0}^{1000} |\gamma_s(t = i/1000)|}{1000} \tag{5}$$

In this equation, the numerical value of the shear rate (from Eq. (4)) at times from $t = 0$ to 1 s at intervals of 1/1000 s are summarized and divided by 1000 to get a time mean average of the shear rate.

2.2. Critical flux concept

The critical flux concept was used to evaluate the filtration performance. The critical flux hypothesis for microfiltration is that on start-up there exists a flux below which a decline of flux with time does not occur; above it fouling is observed. This flux is the critical flux and its value depends on the hydrodynamics and probably other variables [1]. This critical flux concept implies that it is possible to maintain a constant flux and constant TMP as long as the constant flux is kept below the critical flux because no severe membrane fouling at this stage occurs. The critical flux is determined experimentally at different levels of vibration frequency and amplitude as described in Section 3.

3. Material and methods

3.1. Experimental apparatus

A sketch of the experimental apparatus is shown in Fig. 2.

The membrane module with a total membrane area of 256 cm^2 is composed of 12 cm long hollow fibers, fixed in parallel between a steel plate in the bottom of the module and a permeate gap in the top. The fibers are closed in the bottom ends with silicon glue and are open in the top into the permeate gap. To prevent breakage caused by the vibrations a flexible sealing consisting of silicone tubes where placed as a transition between the fiber ends and the steel plate in the bottom and the entrance into the permeate gap in the top. The hollow fibers supplied by X-Flow were made of polyethersulfone (PES) with the skin layer on the outer surface and a nominal pore size of 0.45 μm. The steel plate in the bottom and the permeate gap were fixed to a hollow steel rod, which was extended through the top of the cylindrical acrylic module vessel to connect with a "rotation head" fixed to an electro motor. Rotation of the rotation head hereby induced perpendicular movement of the membrane module, which was kept in contact with the rotation head by a strong spring. Three different rotation heads were used which corresponded to three levels of vibration amplitudes; 0.2, 0.7 and 1.175 mm (the peak-to-peak amplitude is twice as big). By changing the rotation speed of the rotation head, the frequency of the vibrations could be adjusted between 0 and 30 Hz. A cavity for positioning the steel rod was placed in the bottom of the module vessel to direct the vibrations of the module in the vertical direction. The upper ends of the fibers were open into a permeate gap connected through the hollow rod to a progressing cavity pump (Seepex M120-0, Seeberger, Germany). This permeate pump sucked permeate through the hollow fibers via the permeate gap and the hollow rod to the beaker placed on the electronic scale. Transmembrane pressure was measured as the differences between permeate and module headspace pressure using a pressure transducer (RS 286-692, RS-components, USA) linked to the PC. With this pressure transducer it was possible to detect variation in the transmembrane pressure in the order of a few $\times 10^5$ mPa (mbars). Mass flow of permeate was measured and collected on a scale (Mettler PJ3000, Switzerland) connected to the PC. Feed solution was circulated from the feed tank via a gear pump (Micropump F5734, USA) to the intake at the bottom of the module vessel and then returned to the feed tank from the top of the module vessel.

3.2. Yeast suspensions

Bakers yeast suspensions were used as filtration fluids. The motive for choosing this media is the widespread use of bak-

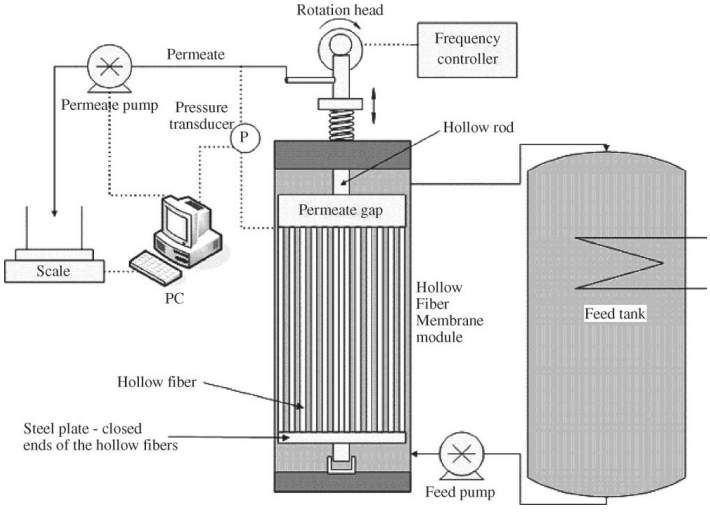

Fig. 2. Schematic drawing of the experimental apparatus.

Table 1
Critical fluxes obtained for different amplitudes and frequencies

Experiment number	Freq. (Hz)	Amp. (mm)	Critical flux (L/(m^2 × h))	Flux improvement (%)	Time mean avg. surface shear rate (1/s) using Eq. (5)
Y1	5	0.2	16	0	22
Y2	30	0.2	36	125	330
Y3	5	1.175	29	81	132
Y4	30	1.175	68	325	1936
Y5	5	0.7	29	81	78
Y6	30	0.7	50	213	1154
Y7	17.5	0.2	42	163	147
Y8	17.5	1.175	45	181	863
Y9	17.5	0.7	39	144	514
Y10	17.5	0.7	42	163	514
Y11	17.5	0.7	41	156	514

Experiment Y9 is repeated in experiment Y10 and Y11. Corresponding avg. surface shear rate in the last column.

ers yeast in the biotechnology industry, its easy availability and the large amount of studies done with the microfiltration of this media. Yeast cell suspensions with dry weight 5 g/L were prepared by using commercially available wet cake bakers yeast (Malteserkors Gær, Danisco, Denmark) suspended in 1 mM phosphate buffer and 1 g/L of bacteriological peptone. The average dry weight content of the wet yeast is 27% with small variations (±1%).

3.3. Experimental procedure

The vibration frequency and amplitude determines the average surface shear rate. These two parameters were investigated at three levels each. The experimental plan consisted of 11 filtrations with different combinations of amplitude (three levels) and frequencies (three levels) in random order according to Table 1. Between each filtration the clean water flux was 100% recovered by cleaning the membrane with a base solution of 1% (Divos 124 from Scan Diversey) and a 0.1% solution of hydrogen peroxide.

In order to find the critical flux the permeate flux was controlled in steps according to a computer program. The step height is approximately 4 L/(h × m^2) and the step length is 3 min. The flux is increased two steps for 3 min and then reduced one step for 3 min, which is sketched in Fig. 3.

The step height and step length is easily changed in the software program code. This procedure was repeated throughout the filtration. The transmembrane pressure and permeate flux was logged every 0.5 s. The critical flux ($J_{p,crit}$) was identified as the maximum permeate flux where $\Delta P/\Delta t$ was less than 2×10^5 mPa/step (2 mbar/step) and TMP was recovered when returning to the last tested permeate flux (one step back). This procedure is similar to a procedure, described by Espinasse et al. [10], to determine critical fluxes in ultrafiltration except that Espinasse keeps the pressure constant and measures the corresponding flux.

A 4.5 h test filtration was also conducted to test the long-term performance of the system when operating below the critical flux. The test filtration was conducted with another membrane module consisting of 54 hollow fibers with a total membrane area of 488 cm^2. The fibers were made of PES with a minimum and maximum pore size of 0.36 and 0.5 μm. The frequency and amplitude was set to 25 Hz and 0.7 mm, and the feed cross-flow velocity was adjusted to 0.91 cm/s. In all experiments, the fluid level in the feed tank was kept constant by continually filling up with water.

4. Results and discussion

As described earlier, 11 filtrations were carried out at different degrees of vibration frequency and amplitude. In each experiment, the flux was increased stepwise as sketched in Fig. 3. In Fig. 4, the flux and TMP as a function of time is shown for experiment Y4 at 30 Hz and 1.175 mm amplitude. It was not possible to go beyond 30 Hz and 1.175 mm amplitude because

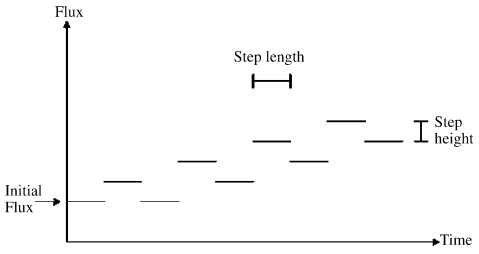

Fig. 3. Sketch of the computer controlled flux as a function of time.

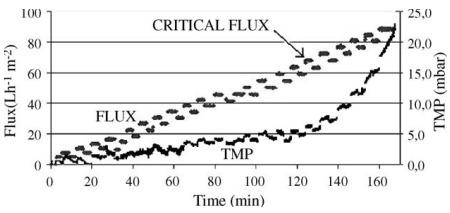

Fig. 4. The stepwise flux increase and corresponding TMP as a function of time for experiment Y4. Frequency = 30 Hz and amplitude = 1.175 mm. Yeast concentration = 5 g/L.

of the mechanical limitations of the system. Increased degree of vibration would have broken the apparatus.

The critical flux is identified as the maximum permeate flux where $\Delta P/\Delta t$ is less than 2×10^5 mPa/step (2 mbar/step) and TMP is recovered when returning to the last tested permeate flux (one step back). For experiment Y4, the critical flux is 68 L/(m^2 × h). As seen in Fig. 4, the TMP is very low. The step height used in these experiments is approximately 4 L/(m^2 × h), which of course yield an uncertainty in the determined critical fluxes. The critical flux will never be estimated too high, but there is a possibility of under predicting the critical flux by 4 L/(m^2 × h). These uncertainties can be reduced by lowering the step height in future experiments.

The kinematic viscosity used to calculate the shear rate is set to 10^{-6} m^2/s, which equals the kinematic viscosity of pure water at 25 °C. The calculated average surface shear rate Eq. (5) for each filtration is shown in Table 1 together with the measured critical flux values.

In Fig. 5, the critical fluxes are depicted as a function of the average surface shear rate in a log–log graph. The effect of the shear rate is clearly seen as the critical flux is increased 325% when going from the minimum frequency and amplitude to the maximum (see Table 1). Each point in Fig. 5 is associated with an error bar of +4 L/(m^2 × h) to indicate the possibility of under predicting the critical fluxes (these error bars are hardly seen at the larger values because of the logarithmic scale). In comparison data from filtrations of 5 g/L bakers yeast suspensions done with a similar system [8] is show as well. A power function is chosen to describe the critical flux as a function of the average surface shear rate. This is done because such a function describes most of the variation in the measured critical fluxes. The r^2-value is around 0.88 which means, that the expression

$$J_{p,crit} = 8.22(\bar{\gamma}_s)^{0.26} \quad (6)$$

explains 88% of the variation in the measured critical fluxes. It has to be noted, that the parameters 8.22 and 0.26 are associated with uncertainties because of the used step height as discussed earlier, and that the standard deviation of the correlation is 5.2 L/(m^2 × h). The standard deviation is calculated as the square root of the mean square error based on the 11 measured critical fluxes [11]. This relatively high standard deviation is due to the earlier mentioned uncertainties in determining the critical flux because of the relatively high step height, and because of the relatively few data points. Another explanation for some of the uncertainties is that even though the membrane module is directed in the vertical direction by the cavity in the bottom of the module cylinder, small movements of the fibers in the *y*-direction perpendicular to the fiber direction was observed. These small oscillations in the *y*-direction are neglected in the calculation of the surface shear rate as they would complicate the derivation of the equation for the velocity field in the *z*-direction Eq. (2). The oscillation in the *y*-direction might influence the value of the surface shear rate and thus the parameters in Eq. (6) and the standard deviation.

Other researchers have reported similar correlations as Eq. (6) between flux and surface shear rate for other dynamic filtration systems [4,5,12,13,14], although these systems are operated in fundamentally different ways. In those systems, the pressure is kept constant and the corresponding flux is measured. Their operation pressures are typically one order of magnitude higher and the surface shear rate is typically two orders of magnitude higher than for this apparatus. In Fig. 5 results from similar experiments with another vibration hollow fiber module [8] is show as well. These results are in the same order of magnitude as our results. At low shear rate values the critical fluxes are a bit smaller which could be due to the fact that the pore size of the hollow fiber membranes is only 0.2 μm. At the larger values of the shear rate Genkin et al. [8] have measured critical fluxes of all most the same values as our results. The fact that Genkin et al. [8] operates at much smaller frequencies (0–10 Hz) and a much larger peak-to-peak amplitude (40 mm) shows that the shear rate (combination of frequency and amplitude) rater than the individual terms determines the critical flux according to Eqs. (4) and (5).

In Figs. 6 and 7, the critical fluxes are depicted versus the frequency and amplitude, respectively.

The general trend is that both increasing frequency and amplitude increases the critical flux. This is also expected as these variables both increase the surface shear rate as seen in Eq. (4), but Figs. 6 and 7 also shows the earlier mentioned uncertainties

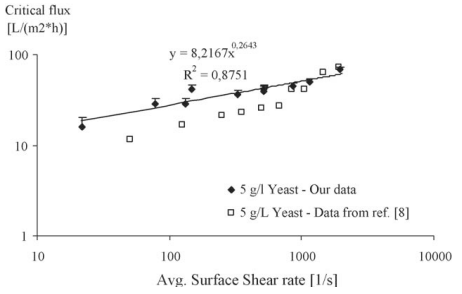

Fig. 5. Log–log plot of the critical flux as a function of the time mean average surface shear rate. Error bars of +4 L/(m^2 × h) are associated with each point. Data from reference [8] is show as well.

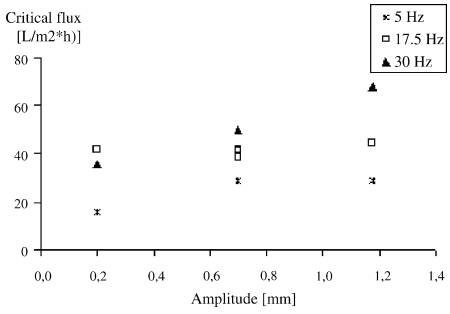

Fig. 6. Critical flux as a function of the amplitude for the three levels of vibration frequency.

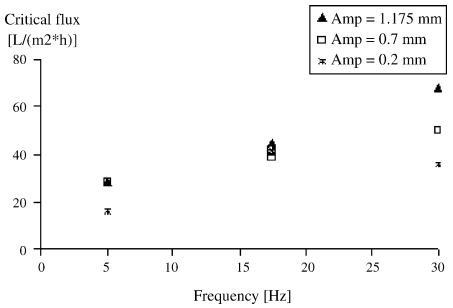

Fig. 7. Critical flux as a function of the frequency for the three levels of vibration amplitude.

in critical fluxes. This is seen as the "17.5 Hz curve" in Fig. 6 and the "0.2 mm curve" in Fig. 7 seems not to fit well with Eq. (6). The shear rate is proportional to the frequency raised to the power of 3/2 and to the amplitude raised to the power of 1 ($\gamma_s \propto f^{3/2}$amp), which is seen in Eq. (4). This means that by increasing the frequency by a factor of 6 (30 Hz/5 Hz = 6) the shear rate increases more than when the amplitude is increased by a factor of 6 (1.175 mm/0.2 mm ∼ 6). Thus, the critical flux should increase more when the frequency is raised by a factor of 6, than when the amplitude is increased by a factor of 6. That actually seems to be the case as the average distance between the "5 Hz curve" and "30 Hz curve" in Fig. 6 seems to be larger than the average distance between the "0.2 mm curve" and the "1.175 mm curve in Fig. 7 (also when the earlier discussed uncertainties are taken into account).

The effect of the enhanced shear rate is visualized in Fig. 8. After ended filtration, the module is clearly heavily fouled at the low degree of vibration whereas the module seems to be kept free of fouling when the filtration have been carried out at a high degree of vibration.

A 4.5 h test filtration was conducted in order to show that the system is capable of operating with a constant flux and TMP below the critical flux. The flux and TMP data vs. time is show in Fig. 9.

The test filtration was conducted with another membrane module consisting of 54 hollow PES fibers and a total membrane area of 488 cm^2. The frequency and amplitude was adjusted to 25 Hz and 0.7 mm, and the filtration fluid yeast concentration was 4 g/L dry weight. The feed cross-flow velocity in the module was adjusted to 0.91 cm/s. Initially, the critical flux at these conditions was measured to 15 L/(m^2 × h) according to the earlier described method. This relatively small value (compared to the earlier presented data) shows that this module has

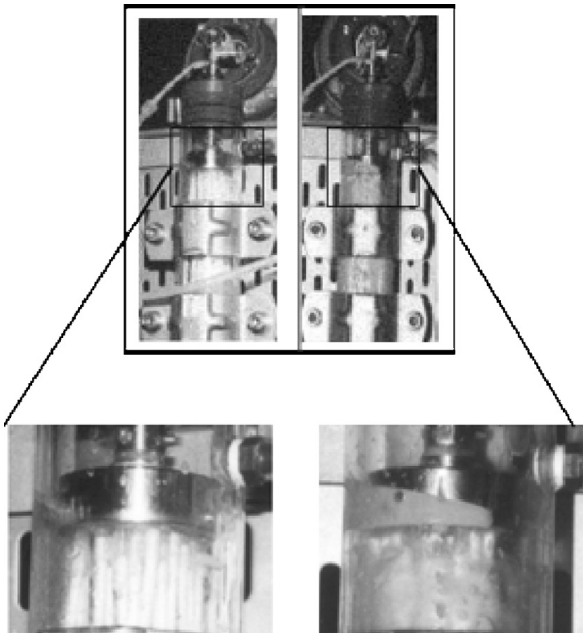

Fig. 8. Photography of the membrane module after filtration. On the left with a vibration of 30 Hz and 1.175 mm amplitude and on the right with a vibration of 5 Hz and 0.2 mm amplitude.

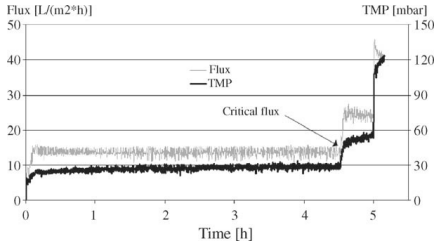

Fig. 9. TMP and Flux vs. time in a long-term test filtration of a bakers yeast suspension (4 g/L dry weight). Frequency = 25 Hz and amplitude = 0.7 mm. Module feed cross-flow velocity = 0.91 cm/s. The critical flux (15 L/(m^2 × h)) is marked with an arrow.

a smaller permeability than the module used to collect the data in Table 1. In Fig. 9, it is seen that when the flux is kept below the critical flux it is possible to filtrate for a long time (here 4.5 h) with a very low cross-flow velocity (0.91 cm/s) and with a very low constant transmembrane pressure (∼30 × 10^5 mPa (∼30 mbar)). The constant values of flux and TMP result in a constant membrane permeability. After 4.5 h, the flux was raised above the critical flux to 25 L/(m^2 × h) and the TMP started to continually increase, resulting in a continually permeability decrease. After 5 h, the flux was further raised to 45 L/(m^2 × h) resulting in both a continually flux decrease and a TMP increase.

5. Conclusion

A novel dynamic microfiltration system has been presented. Filtration tests of bakers yeast suspensions showed that it is possible to filtrate with a very low transmembrane pressure. An equation for calculating the membrane surface shear rate is presented which makes it possible to calculate the average surface shear rate at the different degrees of vibration frequency and amplitude at which the critical fluxes are measured. When filtration at maximum vibration frequency and amplitude the critical flux is improved 325% compared to the critical flux measured at minimum frequency and amplitude. From the corresponding values of the critical fluxes and average surface shear rates it is suggested that the critical flux increases as a power function with respect to the average membrane surface shear rate. This type of function is able to explain 88% of the variation in the measured critical fluxes. It is also shown that the system is capable of operating for a long time below the critical flux with a very low and constant TMP and at a very low module feed cross-flow velocity.

To summarize the work, it is advantageous to operate at enhanced surface shear rate to get the highest possible critical flux, which is achieved at high vibration frequency and amplitude. By operating below the critical flux, the fouling problems are strongly reduced. At this stage, the permeability of the membrane is kept constant whereas the permeability continually decreases when the flux raised above the critical flux.

Nomenclature

amp	vibration amplitude (mm)
f	vibration frequency (Hz) = (1/s)
$J_{p,crit}$	critical flux of permeate (L/(m^2 × h))
t	time (s)
v_j	velocity component in one of the directions $j = x$, y, z (m/s)
v_0	amplitude of velocity (v_0 = amp × ω) (m/s)
x, y, z	directions/distances in a Cartesian coordinate system (m)

Greek letters

γ	shear rate (1/s)
γ_s	membrane surface shear rate (1/s)
$\bar{\gamma}_s$	time mean average surface shear rate (1/s)
ν	kinematic viscosity (m^2/s)
ω	angular frequency ($\omega = 2 \times \pi \times f$) (1/s)

References

[1] R.W. Field, D. Wu, J.A. Howell, B.B. Gupta, Critical flux concept for microfiltration fouling, J. Membr. Sci. 100 (1995) 259–272.
[2] A. Guerra, G. Jonsson, A. Rasmussen, E.W. Nielsen, D. Edelsten, Low cross-flow velocity microfiltration of skim milk for removal of bacterial spores, Int. Dairy J. 7 (1997) 849–861.
[3] S. Holm, R. Malmberg, K. Svensson, Method and plant producing milk with low bacterial content, World Patent WO 86/01687, 1986.
[4] J. Postlethwaite, S.R. Lamping, G.C. Leach, M.F. Hurwitz, G.J. Lye, Flux and transmission characteristics of a vibration microfiltration system operated at high biomass loading, J. Membr. Sci. 228 (2004) 89–101.
[5] M.Y. Jaffrin, L. Ding, O. Akoum, A. Brou, A hydrodynamic comparison between rotating disk and vibratory dynamic filtration systems, J. Membr. Sci. 242 (2004) 155–167.
[6] R. Bouzerar, P. Paullier, M.Y. Jaffrin, Concentration of mineral suspensions and industrial effluents using a rotating disk dynamic filtration module, Desalination 158 (2003) 79–85.
[7] G. Jonsson, I.G. Wenten, Control of concentration polarization, fouling and protein transmission of microfiltration processes within the agro-based industry, in: Proceedings of the ASEAN-EC Workshop on Membrane Technology in Agro-Based Industry, Kuala-Lumpur, Malaysia, July 26–29, 1994, pp. 157–166.
[8] G. Genkin, T.D. Waite, T.G. Fane, S. Chang, The effect of axial vibrations on the filtration performance of submerged hollow fibre membranes, vol. 1, Extended abstracts of ICOM 2005, Seoul, pp. 281–282.
[9] R.B. Bird, W.E. Stewart, E.N. Lightfoot, Transport Phenomena, second ed., John Wiley & Sons Inc., 2002, pp. 120–121.
[10] B. Espinasse, P. Bacchin, P. Aimar, On an experimental method to measure critical flux in ultrafiltration, Desalination 146 (2002) 91–96.
[11] J.D. Petruccelli, B. Nandram, M. Chen, Applied Statistics for Engineers and Scientists, Prentice-Hall Inc., 1999.
[12] O.A. Akoum, M.Y. Jaffrin, L. Ding, P. Paullier, C. Vanhoutte, An hydrodynamic investigation of microfiltration and ultrafiltration in a vibrating membrane module, J. Membr. Sci. 197 (2002) 37–52.
[13] O.A. Akoum, L.H. Ding, M.Y. Jaffrin, Microfiltration and ultrafiltration of UHT skim milk with a vibration membrane module, Sep. Purif. Technol. 28 (2002) 219–234.
[14] O.A. Akoum, L. Ding, R. Chotard-Ghodsnia, M.Y. Jaffrin, G. Gésan-Guiziou, Casein micelles separation from skimmed milk using a VSEP dynamic filtration module, Desalination 144 (2002) 325–330.

Available online at www.sciencedirect.com
ScienceDirect
Separation and Purification Technology 53 (2007) 111–118
Separation and Purification Technology
www.elsevier.com/locate/seppur

Separation of enzymes and yeast cells with a vibrating hollow fiber membrane module

Søren Prip Beier, Gunnar Jonsson *

CAPEC, Department of Chemical Engineering, Technical University of Denmark, DK-2800 Kgs. Lyngby, Denmark

Received 6 April 2006; received in revised form 28 June 2006; accepted 29 June 2006

Abstract

In this work it is shown that the vibrating microfiltration hollow fiber membrane module is able to separate macromolecules (the enzyme Fungamyl produced by Novozymes A/S) from bakers yeast suspensions at a very low transmembrane pressure, at a very low cross-flow velocity and with a high enzyme transmission. The critical flux is determined at different degrees of module vibration. The critical flux increases as the vibration frequency and amplitude is increased. The correlations between the critical flux and the average membrane surface shear rate are found. For a pure 1% Fungamyl solution the correlation is $J_{crit} = 2.10(\bar{\gamma}_s)^{0.38}$, and for a 1% Fungamyl solution with 5 g/l suspended bakers yeast the correlation is $J_{crit} = 1.79(\bar{\gamma}_s)^{0.32}$. These correlations are compared to the correlation $J_{crit} = 8.22(\bar{\gamma}_s)^{0.26}$ from filtrations of 19 g/l bakers yeast suspensions from an earlier study with the same apparatus. The powers to which the shear rate is raised are all around the same value (around 1/3) and describe the degree of dependency between the critical flux and the average surface shear rate. The term multiplied to the shear rate depends on the feed fluid composition. Below the critical flux high enzyme transmission is observed whereas above the critical flux the transmission decreases dramatically as the fouling resistance increases.

Keywords: Shear-enhanced filtration; Critical flux; Surface shear rate; Enzyme transmission; Vibrating microfiltration

1. Introduction

Severe membrane fouling often decreases the flux dramatically compared to the clean water flux in membrane separation of macromolecules from cellular suspensions. In microfiltration of protein solutions the membrane fouling mostly consists of: (i) a monolayer of macromolecules adsorbed to the pore walls and to the membrane surface and (ii) deposition of macromolecules and other feed stream components on the adsorbed monolayer. Denaturated and aggregated macromolecules may also stick to the membrane and act as sites for further fouling buildup [1]. The buildup of such a fouling layer may lead to the formation of a protein gel-layer on the membrane surface which turns the membrane into an ultrafiltration membrane with a much lower permeability [2]. High frequency back flushing [3] is a way to avoid severe membrane fouling. The destabilization of the fouling layer causes a steady state concentration profile never to be reached which makes the method useful in reducing membrane fouling. Another way to reduce the extent to which the fouling layer is established is to increasing the shear rate on the membrane surface. In conventional cross-flow microfiltration this is done by passing the feed fluid and the permeate along the membrane at both sides at a high cross-flow velocity. In this way the shear rate at the membrane surface is high and the transmembrane pressure (TMP) is kept low and uniform. The disadvantage of this procedure is the high pumping costs due to the high pressure drops at both sides of the membrane. The idea in dynamic microfiltration is to decouple the connection between high cross-flow velocity and high surface shear rate. By creating a relative motion between the membrane and the feed fluid the surface shear rate can be enhanced, and the cross-flow velocity can be kept low. The low cross-flow velocity keeps the TMP at a low level, which is important in order to avoid a fast establishing and compact fouling layer. Guerra et al. [4] have shown that above a certain TMP the flux decreases due to the formation of a fouling layer in microfiltration of skim milk. This emphasized the importance of maintaining a low TMP. Different dynamic microfiltration systems, some efficient in the recovery of macromolecules from fermentation broths, have been reported in the literature. The rotation disk system

* Corresponding author. Tel.: +45 4525 2946; fax: +45 4588 2258.
E-mail address: gj@kt.dtu.dk (G. Jonsson).

1383-5866/$ – see front matter © 2006 Elsevier B.V. All rights reserved.
doi:10.1016/j.seppur.2006.06.019

Nomenclature

a	constant
amp	vibration amplitude (mm)
f	vibration frequency (Hz) = (s^{-1})
J	permeate flux (l/m^2 h)
J_{crit}	critical flux of permeate (l/m^2 h)
n	constant
P	pressure, ΔP = TMP (mbar)
R_f	fouling resistance (m^{-1})
R_m	membrane resistance (m^{-1})
t	time (s)
TMP	transmembrane pressure (mbar)
v_z	velocity in the z-direction (m/s)
v_0	amplitude of velocity ($v_0 = \text{amp}\,\omega$) (m/s)
x, y, z	directions/distances in a Cartesian coordinate system (m)

Greek symbols

γ_s	membrane surface shear rate (s^{-1})
$\bar{\gamma}_s$	average surface shear rate (s^{-1})
η	dynamic viscosity (Pa s)
ν	kinematic viscosity (m^2/s)
ω	angular frequency ($\omega = 2\pi f$) (s^{-1})

consists of a disk rotating close to the membrane surface. The rotations create the necessary surface shear rate in order to reduce fouling problems [5,6]. Vibrations of the membrane can also induce the necessary surface shear rate in order to operate at a low cross-flow velocity. Vibrating membrane systems have been described and tested by different authors [6–10]. The vibrating hollow fiber membrane module is a novel dynamic microfiltration system described by Beier et al. [11]. The vertical oscillating motion of the membrane module induces the necessary surface shear rate, making it possible to filtrate at a very low cross-flow velocity, with a very low TMP and with a high enzyme transmission.

In this work the vibrating hollow fiber membrane module is tested in separation of a commercially available enzyme (Fungamyl from Novozymes A/S) from bakers yeast suspensions. A similar system is tested and described by Genkin et al. [12]. It has earlier been shown [11] that the system is efficient in the filtration of bakers yeast suspensions in a long term operational mode, but in this study also transmission of enzymes through the membrane is investigated. The purpose of this work is to show that the system is also capable of handling content of macromolecules in the feed stream and still be able to operate at a low TMP and with a high enzyme transmission. The filtration results are evaluated by using the critical flux concept formulated by Field et al. [13]. It is investigated how the critical flux depends on the average surface shear rate and the feed stream composition. The resistance to mass transport through the membrane caused by membrane fouling and the enzyme transmission is also evaluated and discussed.

2. Theory

2.1. Calculation of surface shear rate

The membrane module consists of hollow fibers placed parallel vertically in a plastic cylinder. The feed stream is led to the vibrating module on the outside of the membrane fibers. The vibration frequency and amplitude can be varied independently. The shear rate at the surfaces of the fibers is defined as the derivative of the velocity component along the membrane surface with respect to the length perpendicular to the membrane surface:

$$\gamma_s = \frac{dv_z}{dy} \tag{1}$$

The coordinate system is orientated so that the z-axis is orientated in the same direction as the flow along the fibers and the y-axis is orientated perpendicular to the membrane surface with $y = 0$ at the surface. The x-axis is a tangent to the surface perpendicular to the z- and y-axis. Very close to the surface the membrane is almost plane which makes the use of Cartesian coordinates acceptable. This simplifies the calculations and equations. The velocity component in the z-direction for laminar flow is found by solving the Navier–Stokes equation of motion, and the surface shear rate is calculated according to Eq. (1). This has been done by Beier et al. [11] and the equation for the periodic oscillating surface shear rate is given below:

$$\gamma_s = v_0\sqrt{\frac{\omega}{2\nu}}[\sin(\omega t) - \cos(\omega t)] \tag{2}$$

The angular frequency is denoted ω ($\omega = 2\pi f$), and the vibration frequency is denoted f. The velocity amplitude is denoted v_0 ($v_0 = \text{amp}\,\omega$), and the amplitude is denoted amp. A time mean average of the numerical value of the oscillating shear rate is used as a value for the surface shear rate [11]:

$$\bar{\gamma}_s = \frac{\sum_{i=0}^{1000}|\gamma_s(t = i/1000)|}{1000} \tag{3}$$

In this equation the numerical value of the shear rate (from Eq. (2)) at times from $t = 0$ to 1 s at intervals of 1/1000 s are summarized and divided by 1000 to get a time mean average of the shear rate.

2.2. Calculation of fouling resistance

The total resistance towards mass transport through the membrane can be divided into sub-resistances. One sub-resistance is the membrane resistance (R_m) and all other contributions to the total resistance can be gathered as the fouling resistance (R_f). The membrane resistance is determined from water flux experiments whereas the fouling resistance can be calculated from flux and TMP data according to the following equation [14]:

$$J = \frac{\Delta P}{\eta(R_m + R_f)} \tag{4}$$

2.3. Critical flux concept

The critical flux concept is used to evaluate the filtration performance. The critical flux hypothesis for microfiltration is that on start-up there exists a flux below which a decline of flux with time does not occur; above it fouling is observed. This flux is the critical flux and its value depends on the hydrodynamics and probably other variables [13]. The critical flux concept implies that it is possible to maintain a constant flux and constant TMP as long as the constant flux is kept below the critical flux because no severe membrane fouling at this stage occurs. The critical flux is determined experimentally at different levels of vibration frequency and amplitude.

3. Materials and methods

3.1. Experimental apparatus

The experimental apparatus have been described in details earlier [11]. A sketch of the experimental apparatus is shown in Fig. 1.

The membrane module with a total membrane area of 488 cm^2 is composed of 54 hollow fibers with a length of 12.5 cm and a diameter of 2.3 mm fixed in parallel between a steel plate in the bottom of the module and a permeate gap in the top. An earlier study of the system was done with another membrane module with an area of only 256 cm^2 [11]. The fibers are closed in the bottom ends with silicone glue and are open in the top into the permeate gap. To prevent breakage caused by the vibrations a flexible sealing consisting of silicone tubes where placed as a transition between the fiber ends and the steel plate in the bottom and the entrance into the permeate gap in the top. The hollow fibers supplied by X-flow are made of polyethersulfone (PES) with the skin layer on the outer surface and a minimum and maximum pore size of 0.36 and 0.5 μm, respectively. The clean water permeability of these membrane fibers at 25 °C were measured to 2150 l/m^2 h bar. A scanning electron microscopy (SEM) picture of the membrane surface and of a cross-sectional cut is seen in Fig. 2. On the right side the compact skin layer on the outside is visually easily distinguished from the much more open support structure inside the fiber.

The steel plate in the bottom and the permeate gap are fixed to a hollow steel rod, which was extended through the top of the cylindrical acrylic module vessel to connect with a "rotation head" fixed to an electro motor. Rotations of the rotation head hereby induced perpendicular movement of the membrane module, which was kept in contact with the rotation head by a strong spring. Three different rotation heads were used which corresponds to three levels of vibration amplitudes: 0.2, 0.7 and 1.175 mm (the peak to peak amplitude is twice as big). By changing the rotation speed of the rotation head, the frequency of the vibrations was adjusted between 5 and 25 Hz. A cavity for positioning the steel rod was placed in the bottom of the module vessel to direct the vibrations of the module in the vertical direction. The upper ends of the fibers were open into a permeate gap connected through the hollow rod to a progressive

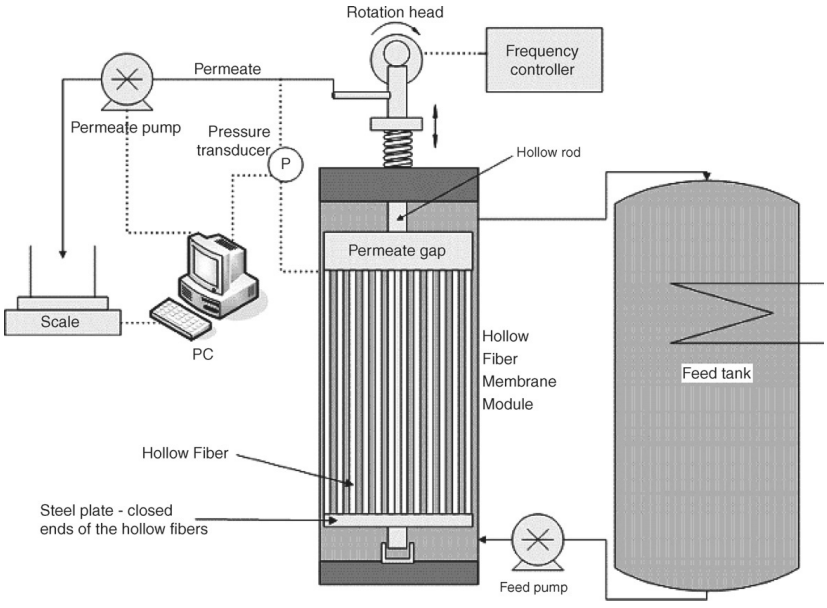

Fig. 1. Schematic drawing of the experimental apparatus.

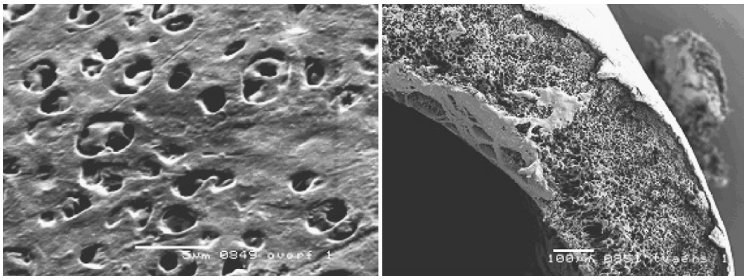

Fig. 2. SEM pictures of the PES hollow fiber membrane with the skin layer outside. On the left a close-up of the surface is seen. On the right a cross-sectional cut is seen.

cavity pump (Seepex M120-0, Seeberger, Germany). This permeate pump sucked permeate through the hollow fibers via the permeate gap and the hollow rod to the beaker placed on the electronic scale. Transmembrane pressure (TMP) was measured as the difference between permeate and module headspace pressure using a pressure transducer (RS 286-692, RS-components, USA) linked to the PC. With this pressure transducer it was possible to detect variation in the transmembrane pressure in the order of a few mbar. Mass flow of permeate was measured and collected on a scale (Mettler PJ3000, Switzerland) connected to the PC before it manually was returned to the thermostatic feed tank. Feed solution was circulated from the feed tank via a gear pump (Micropump F5734, USA) to the intake at the bottom of the module vessel and then returned to the feed tank from the top of the module vessel.

3.2. Feed fluids

Two types of feed fluids were used as filtration fluids. The first type of filtration fluid consisted of a pure aqueous solution of the enzyme Fungamyl (produced by Novozymes A/S). The α-amylase Fungamyl is for example used in the baking industry as an oxidation agent. The enzyme concentration was in most cases 1%, but experiments with 0.5% and 2% solutions were also carried out. The second type of filtration fluid consisted of both Fungamyl and suspended wet cake bakers yeast (Malteserkors Gær, Danisco, Denmark). The average dry weight content of the wet yeast is 27% with small variations (±1%). Most experiments were done with 5 g/l of wet bakers yeast. Experiments with 2.5 and 10 g/l of wet bakers yeast were also carried out. Table 1 gives an overview of the different feed fluids.

3.3. Experimental procedure

For feed fluids containing 1% Fungamyl with and without suspended yeast (5 g/l) the critical flux was determined at different levels of vibration frequency and amplitude. The frequency and amplitude were adjusted between 5 and 25 Hz and 0.2, 0.7 and 1.175 mm, respectively. Because of mechanical limitations it was not possible to raise the frequency further. For these experiments the Fungamyl concentration in the bulk solution and in the permeate was determined by UV spectroscopy of small samples. This was done in order to determine the Fungamyl transmission, which was calculated as the ratio between the concentration in the permeate and in the bulk. Additional filtrations at a fixed frequency of 25 Hz and an amplitude of 0.7 mm were also carried out with enzyme concentrations of 0.5% and 2% and with yeast contents of 2.5 and 10 g/l. In all these filtrations a very low feed cross-flow velocity of 0.91 cm/s was used. The last filtration was done with a cross-flow velocity of 1.83 cm/s (∼100% increase) for a 1% enzymes and 5 g/l yeast feed fluid at 25 Hz and 0.7 mm amplitude. In Table 1 an overview of the different filtrations is given.

As described in details elsewhere [11] the flux was stepwise increased (two steps forward and one step backward) by a progressive pump controlled by a PC. The duration of each step (step length) was in these experiments adjusted to 4 min, and the step height was adjusted to 3 l/m^2 h which of course gives raise to uncertainties in the measured critical fluxes in that order of magnitude. The critical flux (J_{crit}) is identified as the maximum permeate flux where $\Delta P/\Delta t$ is less than 2 mbar/step (2 mbar over 4 min) and TMP is recovered when returning to the last tested permeate flux (one step back). This method is similar to

Table 1
Overview of the experimental work

Feed composition	Varied parameters	Fixed parameters	Transmission measured
1% Fungamyl	Frequency [5, 15, 25] Hz; amplitude [0.2, 0.7, 1.175] mm	Cross-flow velocity	+
1% Fungamyl + 5 g/l yeast			+
1% Fungamyl + yeast	Yeast content [2.5, 5, 10] g/l	Frequency 25 Hz; amplitude 0.7 mm	–
Fungamyl + 5 g/l yeast	Fungamyl concentration [0.5, 1, 2]%		–
1% Fungamyl + 5 g/l yeast	Cross-flow velocity [0.91, 1.83] cm/s		–

the method used to determine the critical flux in ultrafiltration described by Espinasse et al. [15]. Some of the filtrations were continued until a maximum flux was reached. This was done in order to investigate the fouling resistance and enzyme transmission above the critical flux. Between each filtration the clean water flux was 100% recovered by cleaning the membrane system with a 0.5% solution of P3-ultrasil 67.

4. Results and discussion

In the first experimental run 1% solutions of Fungamyl were filtrated with and without suspended bakers yeast (5 g/l) at different levels of vibration frequency and amplitude.

In Fig. 3 data for one of the filtrations is shown. The stepwise increased flux as well as the very low level of the TMP is seen. The critical flux (J_{crit}) is identified as the maximum permeate flux where $\Delta P/\Delta t$ is less than 2 mbar/step and TMP is recovered when returning to the last tested permeate flux (one step back). For the filtration shown in Fig. 3 the critical flux is 16 l/m^2 h, and it is seen that the filtration was continued way above the critical flux in order to investigate the system in this condition.

In an earlier study of the vibrating hollow fiber membrane module [11] filtrations of bakers yeast suspensions (yeast dry weigh of 5 g/l corresponding to wet cake bakers yeast content of 19 g/l) were filtrated at the same levels of amplitude and at frequencies between 5 and 30 Hz. Results from that study together with the critical flux results from this study are depicted in a log–log plot in Fig. 4.

The intention of using a log–log coordinate system is to show that the experimental data suits an expression of the following kind:

$$J_{crit} = a(\bar{\gamma}_s)^n \quad (5)$$

Similar correlations between flux and surface shear rate for other dynamic microfiltration systems have been reported in the literature [6–10]. As seen in Fig. 4 the three series of filtrations fits a power function (as Eq. (5)) well. The standard deviation, calculated as the square root of the mean square error [16], for the yeast suspension experiments is 5.2 l/m^2 h whereas the standard

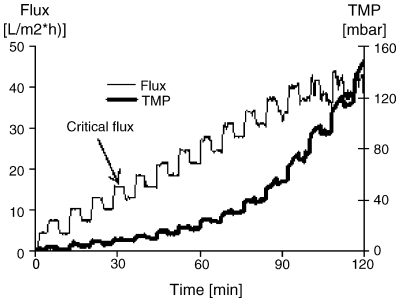

Fig. 3. Flux and TMP vs. time. Filtration of 1% Fungamyl solution with suspended yeast 5 g/l. Vibration frequency = 25 Hz. Vibration amplitude = 0.7 mm.

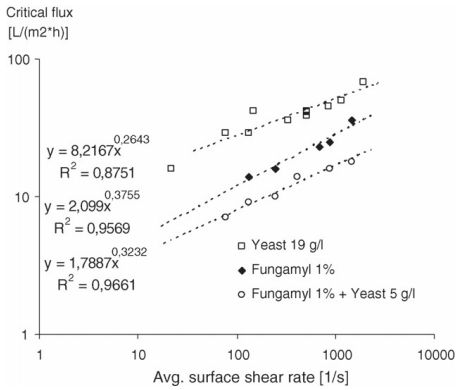

Fig. 4. Critical flux vs. average surface shear rate for: (i) 19 g/l yeast suspensions [11], (ii) 1% Fungamyl solutions and (iii) 1% Fungamyl solutions with 5 g/l yeast.

deviation for the pure Fungamyl experiments and the Fungamyl and yeast experiments is 2.5 and 1.0 l/m^2 h, respectively. The smaller standard deviation for the Fungamyl containing experiments is properly due to smaller step height (3 l/m^2 h) compared to the step height of 4 l/m^2 h [11] used in the pure yeast experiments. Power functions of the kind in Eq. (5) are able to explain most of the variation in the measured critical fluxes compared to other kind of functions. It is further seen that the constant n in Eq. (5) is nearly the same (around 1/3) for the three filtration series, which indicates that the constant n is independent of the feed composition and only describes the average surface shear rate dependency on the critical flux.

The factor of 1/3 is actually the same as theoretically derived by Belfort et al. [17] for cross-flow microfiltration, where the feed is composed of non-adhesive spherical particles which form a cake layer on the membrane surface. The reason that our "n-value" is close to the theoretical value from Belfort et al. [17] might be, that the theoretical value is derived from laminar flow theory. This is consistent with the low flow velocity in the module cylinder. The transport mechanism described by Belfort et al. is Brownian diffusion where the cake layer dominates the total resistance towards mass transport. It should be noted that the Brownian diffusion correlation derived by Belfort et al., underpredicts the actual fluxes by an order of magnitude or more, and therefore the correlations derived by Belfort et al. will not be used further in this study.

The constant a in Eq. (5) is different in the three filtration series. This constant depends on the feed fluid composition. It is seen that macromolecular content and suspended yeast in the feed decrease the critical flux. The fact that the highest critical fluxes are measured for the feed without macromolecules but with high yeast content indicates that the macromolecular content influences the critical flux to a larger extent than the yeast content. It is generally accepted that macromolecular content has severe impact on microfiltration performance [1,2,17]. This was further investigated by evaluating the fouling resistance towards

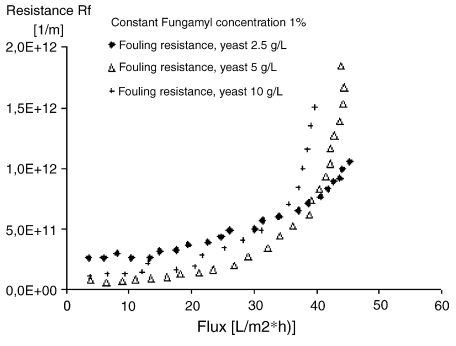

Fig. 5. Fouling resistance vs. flux for constant Fungamyl concentration (1%) and varying yeast content. Vibration frequency = 25 Hz. Vibration amplitude = 0.7 mm.

mass transport through the membrane as a function of the stepwise increased flux.

In Figs. 5 and 6 the fouling resistances (calculated according to Eq. (4)) are depicted as functions of the stepwise increased flux. In all cases the fouling resistance at low fluxes is almost constant and at a low level showing that at this stage the critical flux is not exceeded. The difference in fouling resistance seen in Figs. 5 and 6 at these low values is properly due to uncertainties in the very small values of the measured TMP. In the initial stage the membrane fouling is probably only composed of a monolayer of adsorbed Fungamyl molecules on the membrane surface and on the pore walls. Such a strong bounded adsorbed monolayer, which is very often seen in microfiltration of macromolecules, only results in a very small decrease in permeability and thus a small increase of resistance [1,17]. When the fouling resistance starts to increase the critical flux has been exceeded. In Fig. 5 it is seen that the varying yeast content (four times increase; from 2.5 to 10 g/l) does not influence the fouling resistance curves as much at the varying Fungamyl content (also four times increase; from 0.5% to 2%) depicted in Fig. 6. This might indicate that the Fungamyl content influences the critical flux more than the yeast cell content. This could be due to the fact that the yeast cells are not able to enter the membrane pores because of the size, whereas the macromolecules can enter the membrane and adsorb to the pore walls as well as the membrane surface. Furthermore the larger particles on the surface occupy a larger volume in the region of high shear rate than the smaller macromolecules. Thus, the larger particles on the surface are exposed to a larger lift force away from the membrane surface, which hinder them more in staying close to the surface than the macromolecules. Therefore, high yeast content does not influence the critical flux and fouling resistance as much as high macromolecular content.

All filtrations were done with a very low cross-flow velocity of 0.91 cm/s. In the derivation of Eq. (2) [11] it was assumed that the surface shear rate was only influenced by the module vibrations and not by the cross-flow velocity. This assumption was investigated in two similar filtrations with different cross-flow velocities. In both cases the feed fluid consisted of 1% Fungamyl and 5 g/l suspended yeast at 25 Hz and 0.7 mm amplitude. At the two different cross-flow velocities (0.91 and 1.83 cm/s) a critical flux of 16 l/m^2 h was measured in both cases. This shows that the cross-flow velocity (at these low values) does not influence the value of the critical flux meaning that the assumption in the derivation of Eq. (2) is acceptable.

For some of the filtrations the transmission of Fungamyl through the membrane was measured during the filtration (see Table 1) by UV spectroscopy of small samples of bulk and permeate solutions. For these experiments the procedure of increasing the flux stepwise was continued above the critical flux until a maximum flux was reached and a bit further. This was done in order to investigate the fouling resistance and transmission of enzymes through the membrane at these conditions. In Figs. 7 and 8 results from these experiments are shown.

In Figs. 7 and 8 the fouling resistance and enzyme transmission are depicted versus the stepwise increased flux, which in these experiments was increased until a certain maximum flux was reached and a bit further. Only every second flux step is shown. A maximum flux was reached in all cases, and even though the pump setting was still increased after the maximum flux was reached, the flux dropped. This is the reason that the

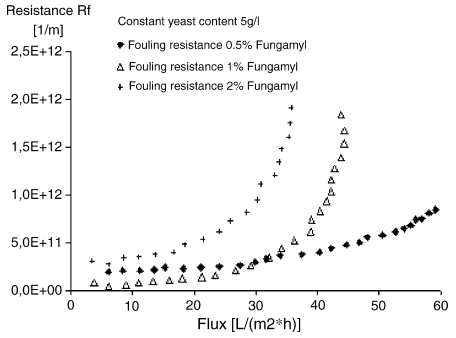

Fig. 6. Fouling resistance vs. flux for constant yeast content (5 g/l) and varying Fungamyl concentration. Vibration frequency = 25 Hz. Vibration amplitude = 0.7 mm.

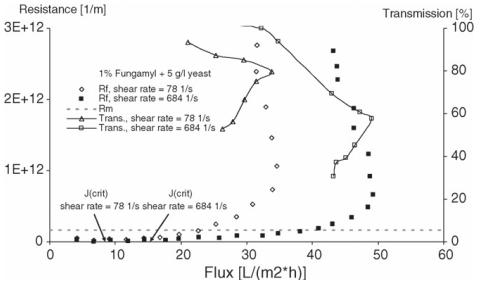

Fig. 7. Fouling resistance R_f and Fungamyl transmission vs. flux. The constant membrane resistance R_m is show as well. Filtration of 1% Fungamyl solution with 5 g/l suspended yeast at two different levels of surface shear rate.

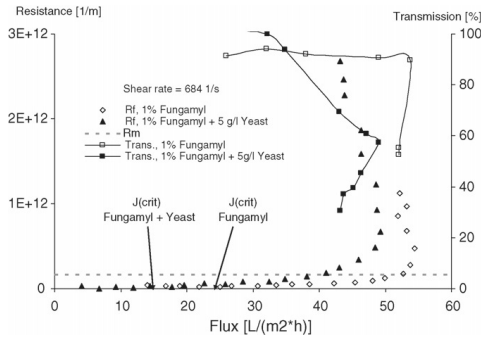

Fig. 8. Fouling resistance R_f and Fungamyl transmission vs. flux. The constant membrane resistance R_m is shown as well. Filtration of 1% Fungamyl solution with and without 5 g/l suspended yeast at a surface shear rate of 684 s^{-1}.

curves "go back". In Fig. 7 the Fungamyl transmission and the fouling resistance are depicted as functions of the flux for two filtrations with 1% Fungamyl and 5 g/l suspended yeast at two different levels of surface shear rate. The membrane resistance, which has been determined to 1.67×10^{11} m^{-1} from water flux experiments and Eq. (4) (with $R_f = 0$), is shown as well. In Fig. 8 the fouling resistance and the Fungamyl transmission are depicted as functions of the flux for filtrations of 1% Fungamyl solutions with and without suspended yeast at a fixed level of surface shear rate (684 s^{-1}). In all filtrations the fouling resistance is initially very low and constant showing that the critical flux is not exceeded. High Fungamyl transmission (>90%) is observed at this stage. In both Figs. 7 and 8 it is seen, that above the critical flux the fouling resistance initially increases very slowly and when approaching the maximum flux the increase is very severe. The point at which the fouling resistance increases strongly is very dependent on the surface shear rate (which can be seen as the large distance between the R_f-curves in Fig. 7) and less dependent on the presence of yeast cells (which can be seen as the smaller distance between the R_f-curves in Fig. 8). An explanation could be that when the surface shear rate is high the yeast cells on the surface is exposed to a large lift force away from the surface because of the velocity gradient, preventing them from contributing to the buildup of membrane fouling. Therefore, the presence of yeast cells does not have a large impact on when and how fast the fouling resistance increases and therefore does not influence the maximum flux much. The lift force on the macromolecules is much lower because of the much lower molecule volume compared to the yeast cell volume. Increasing surface shear rate increases the lift force away from the surface, which is seen in Fig. 7 where the fouling resistance at the largest shear rate increases severely much later than at the lower shear rate. So from Figs. 7 and 8 it is seen that the maximum flux is much more dependent on the surface shear rate than on the presence of yeast cells. An initial high transmission was generally observed in all filtrations. At the stage of high transmission a low fouling resistance was observed. This shows that below the critical flux the fouling resistance is kept low and a high enzyme transmission is achieved. Actually high enzyme transmission is observed above the critical flux and in some cases almost until the maximum flux is reached. In all cases the Fungamyl transmission decreases dramatically when the fouling resistance increases. An explanation to this phenomenon could be that when the fouling resistance increases a Fungamyl gel-layer is established on the surface. This layer, which eventually turns the membrane into an ultrafiltration membrane, is impermeable of Fungamyl resulting in a large decrease in transmission. The established fouling layer actually in some cases decreased the flux as the TMP (pump setting) was increased, which make the fouling resistance and transmission curves "go back" (seen in Figs. 7 and 8). Similar behavior is described by Guerra et al. [4] in microfiltration of skim milk.

A mechanism for the buildup of a gel-layer is proposed by Jonsson et al. [2] for microfiltration of BSA solutions. At a certain point the local shear rate at the pore entrances reaches a level resulting in denaturation of the BSA molecules. This leads to aggregation of the macromolecule content and the formation of a gel-layer on the membrane surface. This gel-layer turns the membrane into an ultrafiltration membrane with much larger resistance towards mass transport and very low enzyme transmission. This means that at a certain flux denaturation of Fungamyl and gel-layer buildup is unavoidable due to the high shear rate at the pore entrances. Thus, at every level of surface shear rate a maximum flux exists. The flux at which the fouling layer is established is increased by increasing the average surface shear rate because the increased lift force away from the surface delay the denaturated macromolecules in establishing a fouling layer. The membrane fouling is delayed by increased average surface shear rate but not avoided.

5. Conclusion

In this work it has been shown that the vibrating hollow fiber membrane module is able to operate at a very low cross-flow velocity, with a very low TMP and with a high enzyme transmission in the separation of the enzyme Fungamyl from bakers yeast suspensions. The critical flux was determined for different series of filtrations at different degrees of module vibration. The critical flux increased as the vibration frequency and amplitude was increased. For all series of filtrations the correlation between the critical flux and the average surface shear rate showed to be a power function. The power to which the shear rate is raised, describes to which degree the critical flux depends on the average surface shear rate. This power is independent of the feed fluid composition, whereas the constant term multiplied to the shear rate describes the dependency on the feed fluid composition. By evaluating the fouling resistance towards mass transport through the membrane, the content of macromolecules rather than the yeast content in feed fluid seems to determine how fast and to which degree the membrane fibers are fouled. Below the critical flux the fouling resistance is low and high enzyme transmission is observed. Above the critical flux the fouling resistance initially increased slowly but when approaching the maximum flux the increase was very severe resulting in a large decrease of the enzyme transmission. The point, at which the Fungamyl

transmission decreases, is very dependent on the average surface shear rate and less dependent on the presence of yeast cells.

To summarize the work, it is advantageous to operate at enhanced surface shear rate to get the highest possible critical flux when macromolecules are to be separated from cellular material. By operating below the critical flux with a very low feed cross-flow velocity and with a very low TMP the fouling problems are strongly reduced and high enzyme transmission is achieved.

References

[1] A.D. Marshall, P.A. Munro, G. Trägårdh, The effect of protein fouling in microfiltration and ultrafiltration on the permeate flux, protein retention and selectivity: a literature review, Desalination 91 (1993) 65–108.

[2] G. Jonsson, P. Johansen, W. Li, Influence of membrane fouling on ultrafiltration and microfiltration processes, in: Proceedings of the Processes of the CEE-Brazil Workshop on Membrane Separation Processes, Rio de Janeiro, Brazil, May 3–8, 1992, pp. 265–276.

[3] G. Jonsson, I.G. Wenten, Control of concentration polarization, fouling and protein transmission of microfiltration processes within the agro-based industry, in: Proceedings of the ASEAN-EC Workshop on Membrane Technology in Agro-Based Industry, Kuala-Lumpur, Malaysia, July 26–29, 1994, pp. 157–166.

[4] A. Guerra, G. Jonsson, A. Rasmussen, E.W. Nielsen, D. Edelsten, Low cross-flow velocity microfiltration of skim milk for removal of bacterial spores, Int. Dairy J. 7 (1997) 849–861.

[5] R. Bouzerar, P. Paullier, M.Y. Jaffrin, Concentration of mineral suspensions and industrial effluents using a rotating disk dynamic filtration module, Desalination 158 (2003) 79–85.

[6] M.Y. Jaffrin, L. Ding, O. Akoum, A. Brou, A hydrodynamic comparison between rotating disk and vibratory dynamic filtration systems, J. Membr. Sci. 242 (2004) 155–167.

[7] O.A. Akoum, M.Y. Jaffrin, L. Ding, P. Paullier, C. Vanhoutte, An hydrodynamic investigation of microfiltration and ultrafiltration in a vibrating membrane module, J. Membr. Sci. 197 (2002) 37–52.

[8] O.A. Akoum, L.H. Ding, M.Y. Jaffrin, Microfiltration and ultrafiltration of UHT skim milk with a vibration membrane module, Sep. Purif. Technol. 28 (2002) 219–234.

[9] O.A. Akoum, L. Ding, R. Chotard-Ghodsnia, M.Y. Jaffrin, G. Gésan-Guiziou, Casein micelles separation from skimmed milk using a VSEP dynamic filtration module, Desalination 144 (2002) 325–330.

[10] J. Postlethwaite, S.R. Lamping, G.C. Leach, M.F. Hurwitz, G.J. Lye, Flux and transmission characteristics of a vibration microfiltration system operated at high biomass loading, J. Membr. Sci. 228 (2004) 89–101.

[11] S.P. Beier, M. Guerra, A. Garde, G. Jonsson, Dynamic microfiltration with a vibrating hollow fiber membrane module: filtration of yeast suspensions, J. Membr. Sci. 281 (2006) 281–287.

[12] G. Genkin, T.D. Waite, T.G. Fane, S. Chang, The effect of axial vibrations on the filtration performance of submerged hollow fibre membranes, in: Proceedings of the Extended Abstracts of ICOM 2005, vol. 1, Seoul, 2005, pp. 281–282.

[13] R.W. Field, D. Wu, J.A. Howell, B.B. Gupta, Critical flux concept for microfiltration fouling, J. Membr. Sci. 100 (1995) 259–272.

[14] M. Mulder, Basic Principles of Membrane Technology, 2nd ed., Kluwer Academic Publishers, 1996.

[15] B. Espinasse, P. Bacchin, P. Aimar, On an experimental method to measure critical flux in ultrafiltration, Desalination 146 (2002) 91–96.

[16] J.D. Petruccelli, B. Nandram, M. Chen, Applied Statistics for Engineers and Scientists, Prentice-Hall Inc., 1999.

[17] G. Belfort, R.H. Davis, A.L. Zydney, Review: the behavior of suspensions and macromolecular solutions in crossflow microfiltration, J. Membr. Sci. 96 (1994) 1–58.

Adsorption of Amylase Enzyme on Ultrafiltration Membranes

Søren Prip Beier,[†] Ann Dorrit Enevoldsen,[†] Georgios M. Kontogeorgis,[‡] Ernst B. Hansen,[§] and Gunnar Jonsson*,[†]

CAPEC, Department of Chemical Engineering, Technical University of Denmark, DK-2800 Kgs. Lyngby, Denmark, IVC-SEP, Department of Chemical Engineering, Technical University of Denmark, DK-2800 Kgs. Lyngby, Denmark, and Recovery Development, Novozymes A/S, Smørmosevej 9, 3AM, DK-2880 Bagsværd, Denmark

Received May 29, 2007. In Final Form: June 26, 2007

A method to measure the static adsorption on membrane surfaces has been developed and described. The static adsorption of amylase-F has been measured on two different ultrafiltration membranes, both with a cutoff value of 10 kDa (a PES membrane and the ETNA10PP membrane, which is a surface-modified PVDF membrane). The adsorption follows the Langmuir adsorption theory. Thus, the static adsorption consists of monolayer coverage and is expressed both as a permeability drop and an adsorption resistance. From the adsorption isotherms, the maximum static permeability drops and the maximum static adsorption resistances are determined. The maximum static permeability drop for the hydrophobic PES membrane is 75%, and the maximum static adsorption resistance is 0.014 $m^2 \cdot h \cdot bar/L$. The maximum static permeability drop for the hydrophilic surface-modified PVDF membrane (ETNA10PP) is 23%, and the maximum static adsorption resistance is 0.0046 $m^2 \cdot h \cdot bar/L$. The difference in maximum static adsorption, by a factor of around 3, affects the performance during the filtration of a 5 g/L amylase-F solution at 2 bar. The two membranes behave very similarly during filtration with almost equal fluxes and retentions even though the initial water permeability of the PES membrane is around 3 times larger than the initial water permeability of the ETNA10PP membrane. This is mainly attributed to the larger maximum static adsorption of the PES membrane. The permeability drop during filtration exceeds the maximum static permeability drop, indicating that the buildup layer on the membranes during filtration exceeds monolayer coverage, which is also seen by the increase in fouling resistance during filtration. The accumulated layer on the membrane surface can be described as a continually increasing cake-layer thickness, which is independent of the membrane type. At higher concentrations of enzyme, concentration polarization effects cannot be neglected. Therefore, stagnant film theory and the osmotic pressure model can describe the relationship between flux and bulk concentration.

1. Introduction

During ultrafiltration (UF) and microfiltration (MF) of macromolecular solutions, a severe flux decline is often observed after a short period of time. The decline is caused by concentration polarization and fouling on the membrane surface. In the literature, it is generally accepted that macromolecular content such as proteins, enzymes, and so forth in the feed solution highly contributes to the buildup of membrane fouling and thus has a great impact on the flux decline.[1,2] Ultrafiltration membranes are mainly fouled by macromolecules on the membrane surface, whereas microfiltration membranes are also fouled inside the porous structure. In general, membrane fouling consists of the following:

(i) A monolayer of macromolecules is adsorbed to the membrane surface (both UF and MF membranes) and to the pore walls inside the membrane (MF membranes).

(ii) Macromolecules and other feed stream components are deposited on the adsorbed monolayer. Denaturated and aggregated macromolecules may also stick to the membrane and act as sites for further fouling buildup.[1]

The adsorbed monolayer is often tightly bounded to the membrane and cannot be removed by rinsing with water but requires chemical cleaning to be removed. Therefore, such a monolayer is often referred to as being an irreversible adsorbed monolayer (chemical adsorption). The further deposition of macromolecules on the monolayer is often more loosely attached, which in some cases makes it possible to remove by cleaning with water. This layer is therefore referred to as being a reversible fouling layer (physical adsorption).[3]

Different investigations of the adsorption of proteins and biomolecules on different surfaces have been published.

The adsorption of proteins on membrane surfaces can be studied by various methods. The amount of protein adsorbed on membranes can be determined, for example, by streaming potential measurements,[4] radioactive measurements of isotopically labeled proteins,[5] contact angle determinations,[6] SEM pictures of the membrane surface,[7] or simply soaking the membrane in a protein solution and following the development of concentration.[1,2,8−10] In general, the adsorption in the above cases can be described by a Langmuir isotherm regardless of whether it is measured under static or dynamic conditions.

* Corresponding author. E-mail: gj@kt.dtu.dk. Tel: (+45) 4525 2946. Fax: (+45) 4588 2258.

† CAPEC, Department of Chemical Engineering, Technical University of Denmark.

‡ IVC-SEP, Department of Chemical Engineering, Technical University of Denmark.

§ Novozymes A/S.

(1) Marshall, A. D.; Munro, P. A.; Trägårdh, G. *Desalination* **1993**, *91*, 65−108.

(2) Belfort, G.; Davis, R. H.; Zydney, A. L. *J. Membr. Sci.* **1994**, *96*, 1−58.

(3) Shaw, D. J. *Introduction to Colloid and Surface Chemistry*, 4th ed.; Butterworth-Heinemann: Boston, 1992.

(4) Kontturi, K.; Vuoristo, M. *Desalination* **1996**, *104*, 99−105.

(5) Wei, J.; Helm, G. S.; Corner-Walker, N.; Hou, X. *Desalination* **2006**, *192*, 252−261.

(6) Bayramoğlu, G.; Yalçin, E.; Arica, M. Y. *Biochem. Eng. J.* **2005**, *26*, 12−21.

(7) Li, X.; Zhang, Y.; Fu, X. *Sep. Purif. Technol.* **2004**, *37*, 187−198.

(8) Cattoli, F.; Boi, C.; Sorci, M.; Sarti, G. C. *J. Membr. Sci.* **2006**, *273*, 2−11.

(9) Cattoli, F.; Sarti, G. C. *Desalination* **2002**, *149*, 465−470.

(10) Khokhlova, T. D.; Mchedlishvili, B. V. *Colloid J.* **1996**, *58*, 793−795.

10.1021/la701524x CCC: $37.00
Published on Web 08/04/2007

The adsorption of proteins can be a slow process especially if the experiment is carried out under static conditions. Bayramoğlu and co-workers have measured the adsorption of five different proteins on surface-modified track membranes.[6] The amount of adsorbed protein changes with time. Lysozyme, cytochrome, and γ-globulin adsorb to the membrane surface, and after approximately 2 days, the maximum adsorption level is reached. γ-Globulin has the highest adsorption level, followed by cytochrome and lysozyme. BSA and ferritin do not adsorb to the membrane surface at all.[6] However, adsorption is not always a slow process. Li and co-workers have measured the static adsorption of glutamicum onto a polysulphone ultrafiltration membrane at different ionic strengths and pH values.[7] In their work, the maximum adsorption is reached after just 1 h in all cases. Furthermore, they found a large influence of ionic strength and pH on adsorption. Generally, the highest amount of protein is adsorbed at a pH equal to the proteins' isoelectric point (pI), where the electrostatic repulsions between membrane−protein and protein−protein are at a minimum. If the protein has a net surface charge, then the amount of adsorbed protein depends on the charge of the membrane surface. Bayramoğlu and co-workers and Li and co-workers[6,7] both found that proteins with opposite surface charge compared to that of the membrane had the strongest adsorption.

The influence of hydrophilicity on surface adsorption was studied by Wei and co-workers.[5] They have shown that membranes made of hydrophobic materials such as polysulphone and polyethersulphone caused severe fouling during the filtration of BSA compared to UF membranes (ETNA01PP and ETNA10PP) made of more hydrophilic surfaces (e.g., surface-modified poly(vinylidene fluoride)). However, there are other considerations to take into account when choosing the proper membrane for a filtration process. When comparing a 10 kDa polysulphone membrane with a ETNA10PP membrane, the water permeability of the ETNA10PP membrane is easily restored just by rinsing with water after filtration with BSA. In contrast, the polysulphone membrane requires chemical cleaning before water permeability is restored. However, the filtration rate is higher using the polysulphone membrane than using the ETNA10PP membrane, probably because of the higher initial water permeability.[5] The retention (selectivity), lifetime, and cleaning needs are also important parameters to consider when choosing a membrane for a specific filtration purpose.

Thom et al. investigated how protein adsorption on membrane surfaces influences the biocompatibility of these surfaces. They also found that the amount of protein adsorption decreased with increasing hydrophilicity. However, the state of the adsorbed protein seemed to depend on the amphiphilic character of the surface, showing the lowest degree of protein denaturation when there was a large difference between the advancing and receding contact angles.[11]

The scope of this work is to investigate the adsorption of macromolecules (an amylase enzyme, 55 kDa) on two different UF membranes under static and pressure-forced conditions. One of the objectives is to show whether chemical (static) adsorption can be described by the well-known Langmuir adsorption theory. A method to measure the static adsorption is described. The relative adsorption is measured both as a membrane permeability drop based on the permeabilities before and after static adsorption and as an adsorption resistance. The effect of static adsorption is also investigated during the filtration (pressure-forced condition) of the amylase solution.

(11) Thom, V. H.; Altankov, G.; Groth, Th.; Jankova, K.; Jonsson, G.; Ulbricht, M. *Langmuir* **2000**, *16*, 2756−2765.

2. Theory

The adsorption of various components on different surfaces can be described by the Gibbs adsorption isotherm. The Gibbs adsorption isotherm is given below:

$$\Gamma_i = -\frac{C_i}{RT}\frac{\mathrm{d}\gamma}{\mathrm{d}C_i} \tag{1}$$

The adsorption of species i is denoted by Γ_i and is typically given in dimensions of mol/area. The concentration of species i in solution, from which the molecules are adsorbed, is denoted C_i. Equation 1 shows that, in order to determine the adsorption, knowledge of the surface tension γ as a function of concentration C_i is required. R is the gas constant, and T is the absolute temperature. The Gibbs equation has several applications:

- The surface concentration can be determined from the relationship between the surface tension and the concentration.
- The area occupied by each adsorbed molecule can be estimated.
- The molecular weight of the adsorbed macromolecules (proteins, enzymes, etc.) can be estimated, under the assumption that they form ideal films at low surface pressure.

The surface tension and adsorption phenomenon are linked, and at constant temperature, the adsorption can in many cases also be described by the Langmuir adsorption isotherm:

$$\Gamma_i = \frac{\Gamma_{i,\max} k C_i}{1 + kC_i} \tag{2}$$

The maximum adsorption of component i is denoted $\Gamma_{i,\max}$, and k is the adsorption equilibrium constant, which is related to the Gibbs adsorption energy. The Langmuir equation is often used in a linear form:

$$\frac{C_i}{\Gamma_i} = \frac{C_i}{\Gamma_{i,\max}} + \frac{1}{k\Gamma_{i,\max}} \tag{3}$$

Maximum adsorption corresponds to the surface being covered by a monolayer. In many cases, the adsorption of large molecules on solid surfaces follows Langmuir theory. The Langmuir adsorption equation is based on the following assumptions:

- The surface is homogeneous.
- Adsorption cannot occur beyond monolayer coverage.
- All adsorption sites are equivalent.
- There are no interactions between the adsorbed molecules and the molecules in the solution and no interactions between the solvent and the surface.

According to the last assumption, the Langmuir adsorption equation is only valid for dilute solutions. Although the last assumption can, in some contexts, seem unrealistic, the equation is still quite useful. The theory also assumes that the adsorption rate is proportional to the concentration in solution and the fraction of the free non-covered area of the adsorbent. Furthermore, the desorption rate is assumed to be proportional to the fraction of surface covered by adsorbed molecules. At equilibrium, the adsorption and desorption rates are equal. By plotting the adsorption and the concentration (eq 3), $\Gamma_{i,\max}$ can be determined. This value corresponds to the concentration at which the whole surface is covered by a monolayer of adsorbed molecules.

Adsorption is affected by many different parameters. The salt concentration in the solution can influence the geometric structure of the macromolecules, which in turn can influence the adsorption. Increased ionic strength decreases the thickness of the diffuse double layer around the macromolecule, and the electrostatic

Table 1. Membrane Data

name	producer	cutoff value	material	water permeability
ETNA10PP	Alfa Laval	10 kDa	PVDF (surface-modified poly(vinylidene fluoride))	63 ± 6 L/(m²·h·bar)
PES	Pall	10 kDa	PES (polyethersulfone)	207 ± 18 L/(m²·h·bar)

interactions between the proteins thus decrease. If the membrane and protein have opposite surface charge, then a higher ionic strength will, in general, decrease the adsorption due to weaker electrostatic interactions. A higher adsorption can, however, be achieved by increasing the ionic strength in the solution if the membrane and protein have the same surface charge because the repelling forces are reduced.[6,7]

The pH of the solution can also influence the adsorption because the charge of a macromolecule is highly dependent on the pH value. Equally charged molecules repeal each other, thus adsorption is assumed to be highest when the molecules have a low charge (close to the isoelectric point) or are uncharged.

The hydrophilic/hydrophobic nature of the surface also influences the adsorption. Hydrophobic surfaces tend to attract hydrophobic molecules more than hydrophilic molecules, and hydrophilic surfaces tend to attract hydrophilic molecules more than hydrophobic molecules. This is also the case for membrane surfaces. The membrane material and structure have an effect on the degree of adsorption and fouling, but the membrane material is not always crucial; its influence also depends on the filtration system. If cake buildup at the membrane surface is observed, then the filtration process will mostly depend on the cake properties.[1] The morphology and structure of the membrane also have an effect on fouling. Membranes with straight-through pores are more sensitive to fouling than isotropic membranes, where the membranes make up a network structure in which the fluid can pass the blocked pores.[12,13]

The chain length also influences the adsorption of, for example, hydrocarbons because of their hydrophobic nature. The temperature is also important because the surface tension depends on the temperature.[3]

Thus, the adsorption is affected by many parameters, which affects the maximum adsorption. In some cases, it is reached in a few hours, whereas in other cases, it takes several days before the maximum adsorption is reached.

In the evaluation of the adsorption, the permeabilities (l_p) of the membranes are determined. The permeability can be calculated according to Darcy's law from flux and pressure data.[14]

$$J_v = l_p \Delta P \tag{4}$$

The volumetric flux through the membrane is denoted J_v, and ΔP is the applied hydrostatic pressure across the membrane. In further analysis, the permeabilities can be interpreted as different subresistances. Thus, eq 4 can be rewritten into the following resistance-in-series model:[15]

$$J_v = \frac{1}{R_{tot}} \Delta P = \left(\frac{1}{R_m + R_a + R_f} \right) \Delta P \tag{5}$$

The total resistance toward transport through the membrane (R_{tot}) can be divided into different subresistances such as the membrane resistance (R_m), the adsorption resistance (R_a), and the fouling resistance (R_f). The membrane resistance is a membrane constant, whereas the adsorption resistance is a term that is used in the evaluation of the static adsorption. The fouling resistance is used in the evaluation of the pressure-forced adsorption. The fouling resistance can in some cases be thought of as a continuous growing cake on the membrane surface, similar to conventional filtration theory. In that case, the first layer of the cake corresponds to the adsorbed monolayer, and thus the adsorption resistance and the fouling resistance can be looked upon as one term. The resistance of such a cake is dependent on the specific cake resistance, which is a constant, and the thickness of the cake, which is a function of the mass of permeate, that passes the membrane.[15] In this case, the continually increasing cake layer (or fouling resistance) can be expressed as follows:

$$R_f = \alpha m_p \tag{6}$$

The fouling constant (α) depends on the specific cake resistance, the bulk concentration, and the concentration of solutes in the cake layer.[15] The mass of permeate is denoted m_p.

The fouling resistance is inserted into the resistance-in-series filtration model:

$$J_v = \left(\frac{1}{R_m + R_a + \alpha m_p} \right) \Delta P \tag{7}$$

This model can be rewritten as[15]

$$\frac{1}{J_v} = \left(\frac{R_m + R_a}{\Delta P} \right) + \frac{\alpha}{\Delta P} \cdot m_p \tag{8}$$

Thus, if the fouling on the membrane surface forms or can be described as a continually growing cake, one should get a straight line when plotting $1/J_v$ versus m_p because R_m, R_a, ΔP, and α are all constants.

At high macromolecular concentrations, the osmotic pressure difference across the membrane also has to be taken into account.[16] Because of concentration polarization on the feed side of the membrane, the concentration at the membrane surface will be larger than in the bulk solution. The enhanced concentration results in a lower solvent chemical potential on the feed of the membrane surface compared to the solvent chemical potential on the permeate side. This gives an osmotic "back suck effect" of solvent that has to be taken into account at high macromolecular concentrations on the feed side. This gradient of solvent chemical potential across the membrane can be expressed as an osmotic pressure difference ($\Delta\pi$) across the membrane. When the osmotic pressure difference is taken into account, eq 5 can be extended to an osmotic pressure model:

$$J_v = \frac{1}{R_{tot}} (\Delta P - \Delta \pi) \tag{9}$$

The flux in eq 9 is therefore determined by different subresistances in series (R_{tot}) and from an osmotic pressure difference that arises from concentration polarization on the feed side of the membrane. When the concentration polarization phenomenon is the domi-

(12) Ho, C.; Zydney, A. L. *J. Membr. Sci.* **1999**, *155*, 261−275.
(13) Ho, C.; Zydney, A. L. *Ind. Eng. Chem. Res.* **2001**, *40*, 1412−1421.
(14) Beier, S. P. *Pressure Driven Membrane Processes*; Ventus Publishing: Copenhagen, 2006.
(15) Mulder, M. *Basic Principles of Membrane Technology*, 2nd ed.; Kluwer Academic: Boston, 1996.
(16) Jonsson, G. *Desalination* **1984**, *51*, 61−77.

nating factor affecting the flux, stagnant film theory can be used to describe the flux dependency on the bulk concentration:[17]

$$J_v = K\left(\frac{C_m - C_p}{C_b - C_p}\right) \quad (10)$$

The mass transfer coefficient (K) is therefore a very important factor describing the level of back diffusion from the boundary layer on the feed side of the membrane. The concentration on the membrane surface (C_m) will be larger than the bulk concentration (C_b) due to concentration polarization. The permeate concentration (C_p) can be neglected if the retention of the membrane is close to 100%. The mass transfer coefficient can be determined from literature correlations. For a stirred cell (in the laminar region), the following correlation can be used:[18]

$$Sh = 0.285(Re)^{0.55}(Sc)^{0.33} \quad (11)$$

The Sherwood number is a dimensionless mass transfer coefficient ($Sh = Kr/D$), which is given by the mass transfer coefficient (K), cell radius (r), and diffusion coefficient of the solute/macromolecule in the solvent (D). The Reynolds number (Re) is calculated as $\omega r^2/\nu$, where ω is the stirring speed and ν is the kinematic viscosity. The Schmidt number is defined as the ratio between the kinematic viscosity and the diffusivity ($Sc = \nu/D$).

The initial and final water permeabilities of the membranes (before and after adsorption) are also used in the evaluation of the adsorption. The permeability drop is defined as follows:

$$\text{permeability drop} = \frac{(\overline{l_{p,initial}} - l_{p,final})}{\overline{l_{p,initial}}} \times 100\% \quad (12)$$

As a value of the initial water permeability, an average value is used that is given for the two investigated membranes in Table 1. The final permeability is measured (after adsorption) after rinsing the membrane with only water.

3. Material and Methods

In this section, the apparatus, solutions, and procedures used for the experimental work are described.

3.1. Apparatus, Materials, and Solutions. *3.1.1. Experimental Apparatus.* A dead-end batch cell is used for the adsorption experiments. The circular membrane area is 44 cm^2, and the pressure in the cell can be established by connecting the cell to a nitrogen gas flask. Permeate is collected in a beaker placed on a balance. A sketch of the system is given in Figure 1.

Pressure in the cell is established only when the water permeability of the membranes is measured, when the membrane before each adsorption experiment is chemically cleaned, and during the pressure-forced adsorption experiments. During the static adsorption experiments, no pressure is established in the cell, and the batch cell is stored in the refrigerator. Stirring in the cell is turned on only during the water flux measurements and during the pressure-forced experiments.

3.1.2. Membranes. Two commercial ultrafiltration membranes with different hydrophilicity have been tested. Relevant data for the two membranes are given in Table 1.

The PES membrane is more hydrophobic than the ETNA10PP. The difference in contact angles is visualized in Figure 2.

(17) Zeman, L. J.; Zydney, A. L. *Microfiltration and Ultrafiltration*; Marcel Dekker: New York, 1996.

(18) Blatt, W. F.; Dravid, A.; Michaels, A. S.; Nelson, L. Solute Polarization and Cake Formation in Membrane Ultrafiltration: Causes, Consequeneces, and Control Techniques; *Membrane Science and Technology - Industrial, Biological, and Waste Treatment Processes*, Columbus Laboratories of the Battelle Memorial Institute in Columbus, Ohio, Oct 21−22, 1969; pp 47−97.

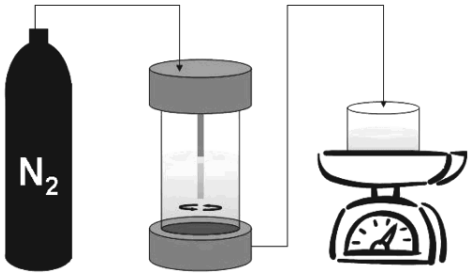

Figure 1. Sketch of the experimental apparatus.

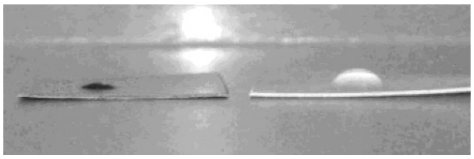

Figure 2. Two dry pieces of the membranes, ETNA10PP to the left and PES to the right. A 10 μL water droplet has been placed on each membrane.

In Figure 2, it is seen that the PES membrane is more hydrophobic than the ETNA10PP membrane because the contact angle is larger. The contact angle of the ETNA10PP membrane is around 40° whereas the contact angle of the PES membrane is around 85−90°. The contact angle of a polysulphone film that is very similar to the PES membrane surface had earlier been measured to be around 90°.[11] The ETNA10PP membrane is made hydrophilic by introducing a surface modification consisting of grafting a thin layer of hydrophilic polymer onto the PVDF surface. Because of the grafting, covalent bonds are formed between the PVDF membrane and the hydrophilic polymer layer. This ensures the stability of the surface-modified membrane.[5] The water permeability of the PES membrane is around 3 times higher than the water permeability of the ETNA10PP membrane. The water permeabilities of the two membranes are determined as an average from 10 and 7 measurements of the PES and the ETNA10PP membranes, respectively. The standard deviations of the water permeability measurements are also given in Table 1.

3.1.3. Membrane Water Permeability. The water permeability (l_p) is determined by measuring the water flux (J_v) at different pressures between 0 and 2 bar according to eq 4. The water permeability is measured in each experiment before and after the exposure to enzyme solution. The final water permeability is measured after the batch cell is emptied, and the rest of the enzyme solution is removed by rinsing with water.

3.1.4. Amylase Enzyme Solutions. Solutions of an amylase enzyme called amylase-F have been used. The concentrated enzyme solution is produced by Novozymes A/S. The molecular weight is 55 kDa, and the isoelectric point is around 3.5. The solutions were supplied by Novozymes A/S and were diafiltrated with demineralized water to remove salts and other minor components until the conductivity in the permeate is below 0.5 mS/cm. Beside the amylase enzymes, other compounds might be present (e.g., amino acids produced during fermentation or flocculation chemicals such as calcium chloride). However, a vast majority of these compounds are removed by diafiltration. A detailed description can be found elsewhere.[19] Adsorption has been measured in the concentration range from 0.1 to 100 g/L. The solubility of the amylase is above 200 g/L. The pH of the aqueous enzyme solutions is 5.5, which means that the enzymes are negatively charged. Concentration measurements are conducted by the Bradford reagent method.[20]

(19) Enevoldsen, A. D; Hansen, E. B.; Jonsson, G. *J. Membr. Sci.* **2007**, *299*, 28−37.

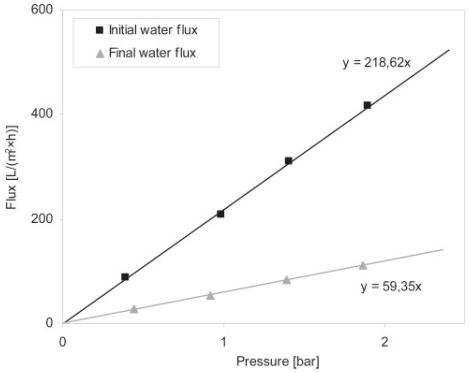

Figure 3. Water flux vs pressure for the PES membrane before and after static adsorption for 144 h at 5 °C. Amylase-F concentration = 50 g/L.

3.2. Adsorption Experiments. Two types of adsorption experiments were conducted: the static adsorption experiments and the pressure-forced adsorption experiments, which are defined as follows:

•Static adsorption is the adsorption of components from a solution that is in contact with a membrane under atmospheric pressure with no volumetric flux through the membrane.

•Pressure-forced adsorption is the adsorption of components that occurs during a membrane filtration experiment with volumetric flux through the membrane.

Both types of experiments are conducted in a batch cell. During static adsorption, the batch cell ensures that the adsorption takes place only on the skin layer of the membrane and not onto (and into) the support structure on the back side of the membrane. This would not have been the case if a piece of membrane was just immersed in the enzyme solution. However, some adsorption might take place on the pore walls inside the membrane, especially if the membrane has a broad pore size distribution, which seems to be the case for the ETNA10PP membrane (Figure 9).

3.2.1. Static Adsorption Experiments. In the static adsorption experiments, the batch cell is used only as a container. The membrane is placed in the bottom, and the solution is contained above the membrane. The permeate outlet of the cell is closed so that no volumetric flux occurs. No pressure above the membrane and no stirring are established. The batch cell with the membrane and the enzyme solution is kept in the refrigerator (to avoid decomposition of the enzymes) for 6 days. This rather long period of time is chosen to ensure that adsorption equilibrium is reached because adsorption can be a time-consuming process, as described earlier. Adsorption experiments have been carried out with different concentrations of the enzyme solution. The experimental procedure is the following:

•A virgin membrane is placed in the stirred cell.

•Cleaning is carried out with 300 mL of a 0.125% NaOH solution at 0.5 bar. Approximately 160−200 mL of permeate is collected. The cleaning temperature is 20 °C, and the cleaning time is ∼1 h.

•The membrane is rinsed with water. The remaining cleaning solution is removed as the cell is opened and separated. The different parts, including the membrane, are cleaned with demineralized water under a running tap.

•Initial water permeability is measured. Water (300 mL) is placed in the cell, and the flux is measured at approximately 0.5, 1.0, 1.5, and 2.0 bar. The temperature is 20 °C.

•Adsorption in the refrigerator is carried out for 144 h (6 days) at different enzyme concentrations between 0.1 and 100 g/L. The volume of enzyme solution is 30 mL with no stirring, and the temperature is 5 °C.

•Removal of enzyme solution followed by gently rinsing the membrane with water for 3 to 4 s under a running tap. The different parts of the batch cell are held under the running tap as well.

•The final water permeability is measured in a similar way as the initial water permeability.

From the initial and final water permeabilities, the permeability drop can be calculated according to eq 12. Furthermore, the adsorption resistance is calculated according to eq 5. The activity of a reference enzyme solution has been measured at Novozymes' laboratories before and after it has been placed in the refrigerator for 6 days. This is done to detect any loss in enzyme activity during the adsorption experiment.

3.2.2. Pressure-Forced Adsorption Experiments. In this case, the adsorption is conducted during concentration of the enzyme solution under a pressure of 2 bar. The flux is measured by collecting permeate in a beaker placed on the balance. The experimental procedure is as follows:

•Virgin membrane is placed in the batch cell.

•Cleaning is carried out with 300 mL of a 0.125% NaOH solution at 0.5 bar. Approximately 160−200 mL of permeate is collected. The cleaning temperature is 20 °C, and the cleaning time is ∼1 h.

•The membrane is rinsed with water. The remaining cleaning solution is removed, and the cell is opened and separated. The different parts, including the membrane, are cleaned with demineralized water under a running tap.

•Initial water permeability is measured. Water (300 mL) is placed in the cell, and the flux is measured at approximately 0.5, 1.0, 1.5, and 2.0 bar. The temperature is 20 °C.

•Enzyme solution (300 mL) is placed in the stirred cell (300 rpm), and the pressure is set to 2 bar. Filtration is continued until 150 g of permeate was collected. The enzyme concentrations are 5 and 50 g/L, and the filtration temperature is 20 °C.

•Removal of remaining enzyme solution followed by gently rinsing the membrane with water for 3 to 4 s under a running tap. The different parts of the batch cell are held under the running tap as well.

•The final water permeability is measured in a similar way as the initial water permeability.

In the pressure-forced adsorption experiments, the permeability drop is again calculated according to eq 12. From the static adsorption experiments, the adsorption resistance is known. Because the membrane resistance is also known, from the initial permeabilities given in Table 1, the fouling resistance can be calculated according to eq 5.

3.3. SEM Picture Analysis. Scanning electron microscopy (SEM) pictures have been made in the back-scattering mode of the two membrane types under different conditions:

•with clean surfaces (cleaned with 0.125% NaOH solution);

•with surfaces at which enzymes have been adsorbed for 144 h from a 100 g/L solution in the refrigerator (static adsorption); and

•with surfaces at which enzymes have been adsorbed during the concentration of enzyme solution from 50 to 100 g/L at 2 bar (pressure-forced adsorption).

These pictures have been taken as a supplement to the permeability data. The pictures are present in Figure 9.

3.4. Overview of Experimental Work. An overview of the different experiments and analysis is given in Table 2.

4. Results and Discussion

4.1. Permeability Drop and Adsorption Resistance. In Figure 3, the initial and final water permeabilities are depicted for one of the static adsorption experiments.

The membrane water permeability (l_p) corresponds to the slope of the fitted line according to Darcy's law.[14] In Figure 3, it is seen that for this amylase-F concentration the final water permeability is ∼59 L/(m²·h·bar). In this case, the initial water permeability is ∼219 L/(m²·h·bar), and according to Table 1, the average value of the PES membrane water permeability is 207 L/(m²·h·bar). According to eq 12, this gives a permeability

(20) Bradford, M. M. *Anal. Biochem.* **1976**, *72*, 248−254.

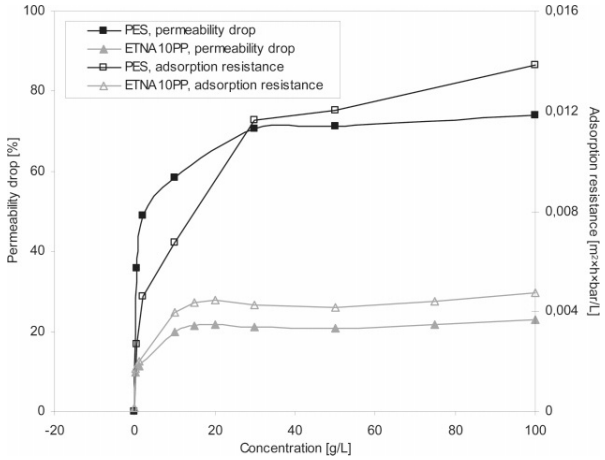

Figure 4. Adsorption isotherms. Permeability drop and adsorption resistance vs concentration for static adsorption experiments on the two membrane types at constant temperature (5 °C).

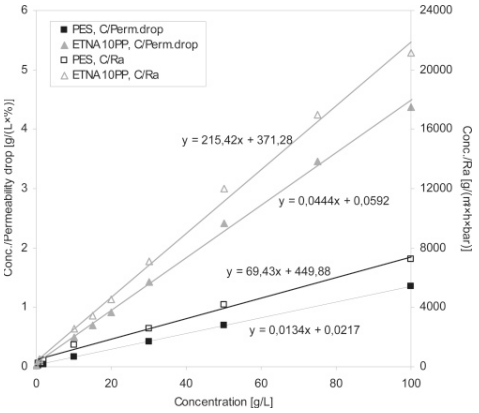

Figure 5. Linear plot of the static adsorption according to the Langmuir equation (eq 3). Concentration divided by permeability drop (Conc./Perm.drop) vs concentration and concentration divided by adsorption resistance (Conc./R_a) vs concentration at constant temperature (5 °C).

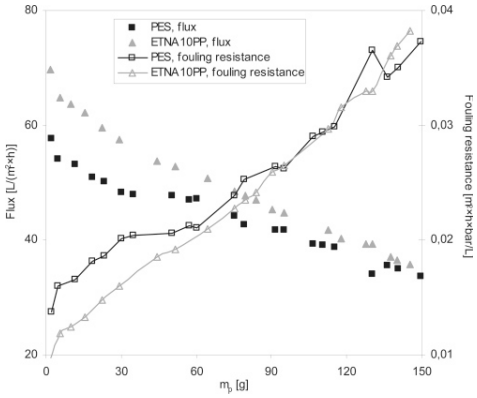

Figure 6. Flux and fouling resistance vs collected mass of permeate (m_p) during the pressure-forced adsorption experiments on the two different membranes at low enzyme concentration (5−10 g/L). Temperature = 20 °C, P = 2 bar.

drop of 71%. The permeability drop for all experiments listed in Table 2 are calculated according to eq 12.

Beside the permeability drop, the adsorption resistance (R_a) toward mass transport through the membrane can be determined by using eq 5. This adsorption resistance is also used to express the degree of adsorption. From the initial water permeability, the membrane resistance (R_m) is determined because at this stage the adsorption resistance and the fouling resistance (R_f) are both zero. The membrane resistance is calculated on the basis of the average water permeability value given in Table 1. The total resistance (R_{tot}) toward transport is determined on the basis of the final water permeability. In the static adsorption experiments, the fouling resistance is assumed to be zero. Thus, the adsorption resistance can be calculated as the difference between the total resistance and the membrane resistance. This has been done for all concentrations listed in Table 2 for both membrane types.

4.2. Static Adsorption. The permeability drop and the adsorption resistance can, as mentioned, be translated into a relative measurement of the adsorption. To determine if the static adsorption follows the Langmuir theory, these terms are plotted in Figure 4 at different concentrations.

The adsorption isotherms have the shape of a Langmuir isotherm. However, there is a clear difference in the level of permeability drop and adsorption resistance between the PES and the ETNA10PP membrane. The maximum permeability drop and adsorption resistance are around 3 times larger for the PES membrane compared to those for the ETNA10PP membrane. The adsorption for the PES membrane increases from around 40 to 60% when the concentration increases from 0.5 to 10 g/L. The curve levels out at a concentration of 30 g/L, where the permeability has dropped to around 70% from its initial value and the adsorption resistance has reached a value of ∼0.013 m^2·h·bar/L. The permeability drop and adsorption resistance for

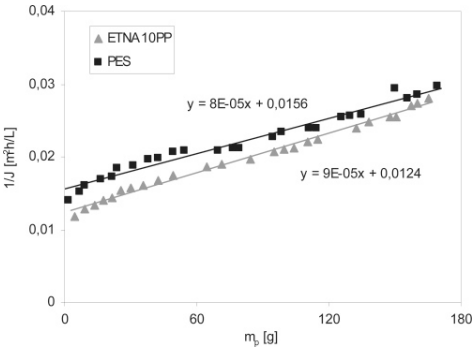

Figure 7. $1/J_v$ versus m_p during the pressure-forced adsorption experiments on the two different membranes at low enzyme concentration (5−10 g/L). Temperature = 20 °C, P = 2 bar.

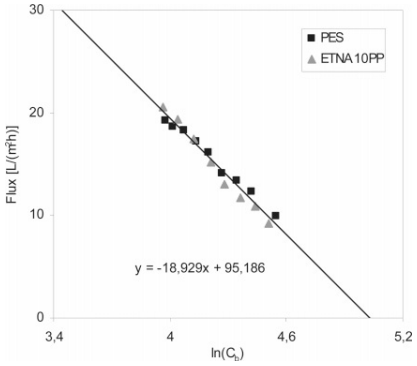

Figure 8. Flux vs $\ln(C_b)$ according to the stagnant film theory for the high-concentration pressure-forced experiments. Enzyme concentration = 50−100 g/L, P = 2 bar.

the ETNA10PP membrane are much smaller. At a concentration of 10 g/L, the permeability has dropped around 20% from the initial value, which is around the value of the maximum permeability drop. The adsorption resistance for the ETNA10PP membrane is also much smaller than for the PES membrane with a maximum value of around 0.004 m^2·h·bar/L.

The activity analysis of the enzyme solution showed no change in activity during the 6 days in the refrigerator. Thus, the enzymes are not degraded during the adsorption experiments at 5 °C.

To determine whether the Langmuir theory (eq 2) actually describes the adsorption, the data in Figure 4 are plotted according to the linear form of the Langmuir adsorption theory (eq 3). In Figure 5, the concentrations divided by the permeability drop and the adsorption resistance are plotted as a function of the concentrations, respectively.

In Figure 5, it is seen that the linear form of the Langmuir isotherm fits the data for both membranes, regardless of whether the plots are based on the permeability drop or the adsorption resistance. This means that the Langmuir theory can indeed describe the adsorption over the entire concentration range, even though the membrane surfaces are not totally homogeneous as assumed in the derivation of the theory. Because the Langmuir theory describes the adsorption data well, we conclude that the static adsorption of amylase-F on the two different UF membranes consists of monolayer coverage. From the linear plots, the maximum static adsorption Γ_{max} (maximum static permeability drop or maximum static adsorption resistance) and the adsorption equilibrium constant k can be determined from eq 3. These terms are determined from the slopes and the intercepts of the linear plots in Figure 5, respectively. The results are given in Table 3.

The maximum static adsorption is around 3 times larger for the PES membrane compared to that for the ETNA10PP membrane. This shows that the degree of adsorption is significantly smaller on the ETNA10PP membrane than on the PES membrane, probably because of a more hydrophilic surface. This is in agreement with the results found by Wei and coworkers.[5] Because of the large adsorption on the PES membrane, the amylase-F molecules must be more closely packed on the PES surface than on the ETNA10PP surface. The adsorption equilibrium constants are determined from the intercepts with the y axis (Figure 5). The equilibrium constants, based on both the permeability drop and the adsorption resistance, have approximately the same value for the two different membranes except for one estimation, which is smaller. The Gibbs adsorption energy is related to the adsorption equilibrium constant;[3] therefore, the amylase-F must be attached to the adsorption sites on the PES membrane and on the ETNA10PP membrane, respectively, at approximately equal strength if the adsorption equilibrium constants are assumed to be at the same level. Thus, the number of adsorption sites on the ETNA10PP membrane seems to be less than on the PES membrane because the maximum static adsorption is 3 time larger for the PES membrane. This also supports the statement of the amylase-F molecules being more closely packed on the PES surface.

4.3. Pressure-Forced Adsorption. Pressure-forced adsorption experiments have been conducted for both membrane types during the collection of 150 g of permeate from an initial bulk volume of 300 mL, as seen in Table 2. The experiments are conducted at 20 °C. The permeability of the membranes is measured before and after each experiment similar to the static adsorption experiments, as described earlier. The permeability drop for the low concentration pressure-forced adsorption experiments is shown in Table 4.

It is seen in Table 4 that during filtration the maximum static adsorption is exceeded for both membranes, even at low enzyme concentrations. The static adsorption is measured at 5 °C, and the pressure-forced adsorption is measured at 20 °C. However, according to the Gibbs adsorption equation (eq 1), a higher temperature would result in a lower adsorption if the change in surface tension with concentration ($d\gamma/dC$) is assumed to be more or less constant at the two temperatures. Thus, the higher adsorption (permeability drop) for the pressure-forced adsorption measured at the higher temperature emphasizes that the maximum static adsorption is actually exceeded at the pressure-forced conditions. The higher permeability drop in the pressure-forced condition is likely due to a higher concentration on the membrane surface during filtration (concentration polarization), which leads to coverage of the surface beyond a monolayer. In this case, the Langmuir adsorption theory can no longer be applied, and permeability drops above the maximum static adsorption can be observed. The number of adsorbed macromolecules on membranes can be determined in many different ways, as extensively discussed in the literature.[4−10,21] The adsorption in these cases could be described by the Langmuir adsorption theory regardless of whether it is measured under static or dynamic conditions. In our case, this is in agreement only in the static case. The Langmuir

(21) Bowen, W. R.; Hughes, D. T. *J. Membr. Sci.* **1990**, *51*, 189−200.

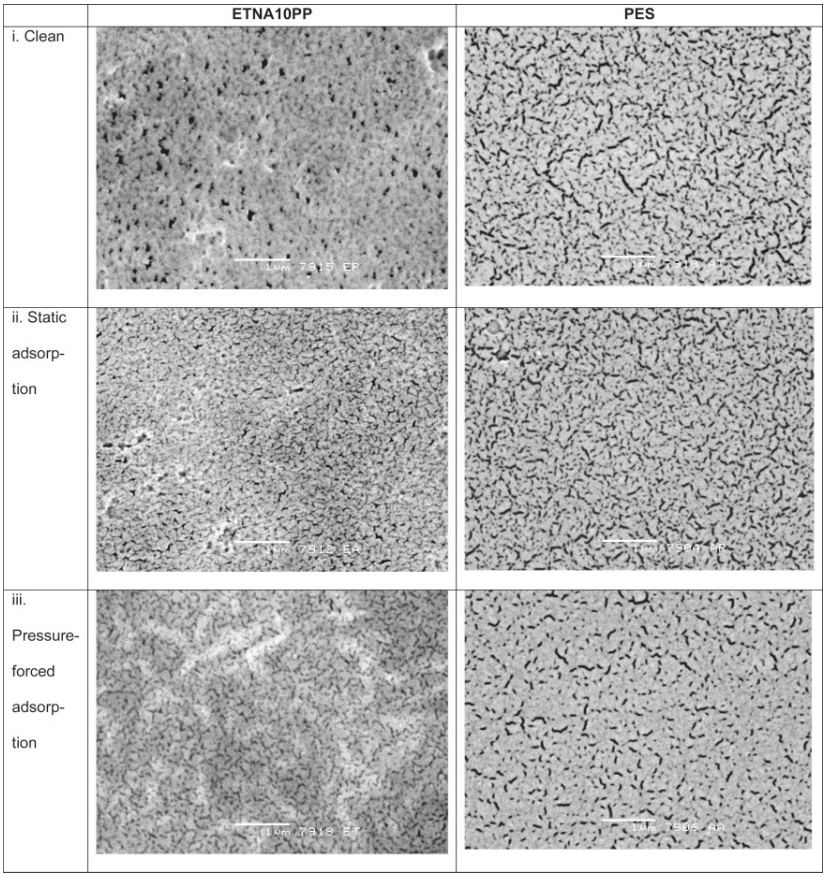

Figure 9. SEM pictures (backscattered mode) of the ETNA10PP and PES membranes. Magnification on the actual pictures is 20 000×. (i) Clean membrane surface, (ii) static adsorbed membrane surface (100 g/L enzyme solution at 5 °C for 144 h), and (iii) pressure-forced adsorbed membrane surface (50 g/L enzyme solution concentrated to 100 g/L at 20 °C). White lines corresponding to 1 μm are present at each SEM picture.

Table 2. Overview of Conducted Experiments and Analysis

membrane	static adsorption	pressure-forced adsorption	SEM pictures
ETNA10PP	enzyme concentration: 0, 0.1, 1, 10, 15, 20, 30, 50, 75, 100 g/L temperature: 5 °C pressure: atmospheric	enzyme concentration: 5, 50 g/L temperature: 20 °C pressure: 2 bar	clean static adsorbed pressure-forced adsorbed
PES	enzyme concentration: 0, 0.5, 2, 10, 30, 50, 100 g/L temperature: 5 °C pressure: atmospheric	enzyme concentration: 5, 50 g/L temperature: 20 °C pressure: 2 bar	clean static adsorbed pressure-forced adsorbed

adsorption theory is not able to describe the permeability drop during the pressure-forced experiments, in which a volumetric flux through the membrane exists.

It is interesting that because of the adsorption/fouling the two membranes behave similarly during filtration even though the initial water permeability of the PES membrane is around 3 times larger than for the ETNA10PP membrane even at low enzyme concentrations. The flux is depicted in Figure 6 at low enzyme concentration (concentration from 5 to 10 g/L) as a function of the collected mass of permeate for two of the pressure-forced experiments. The fouling resistance is depicted as well. The fouling resistance is calculated according to eq 5 in which the adsorption resistances (the maximum static adsorption resistance) and the membrane resistances are known from the static adsorption experiments. Thus, the level of maximum static adsorption resistance is assumed to be the same in the pressure-forced case, and thus the fouling resistance can be calculated according to eq 5.

Table 3. Results from Static Adsorption Experiments at Constant Temperature (5 °C), Maximum Static Adsorption (Maximum Static Permeability Drop or Maximum Static Adsorption Resistance), and Adsorption Equilibrium Constant

	membrane			
	ETNA10PP (perm. drop)	ETNA10PP (R_a)	PES (perm. drop)	PES (R_a)
maximum static adsorption $\Gamma_{max,}$ (1/slope)	23%	0.0046 m²·h·bar/L	75%	0.014 m²·h·bar/L
adsorption equilibrium constant k (1/(intercept·Γ_{max}))	0.75 L/g	0.58 L/g	0.62 L/g	0.15 L/g

Table 4. Permeability Drop during Pressure-Forced Adsorption and Maximum Static Permeability Drop during Static Adsorption for the ETNA10PP and the PES Membranes[a]

membrane	permeability drop (%) (pressure-forced adsorption)	maximum static permeability drop (%) (static adsorption)[b]
ETNA10PP	63	23
PES	89	75

[a] Concentration from 5 to 10 g/L. [b] From Table 3.

It is seen in Figure 6 that even though the PES membrane has a high initial water permeability (Table 1), in practice this has no effect. Actually, the ETNA10PP membrane has a slightly larger flux. However, the flux during the amylase-F filtration is approximately the same for the two membranes at the end of the experiment, in spite of the initial difference in water permeability. It is also interesting that the fouling resistances during the experiments are almost the same for the two membranes. From the static adsorption experiments, we saw that the maximum static adsorption resistance is around 3 times larger for the PES membrane, which is attributed to a more dense adsorbed monolayer on the PES membrane. However, because the fouling resistance level and rate of increase are almost the same for the two membranes, the fouling layer on the adsorbed monolayer yields the same resistance whether it is on the PES or the ETNA10PP membrane. Because the increase in fouling resistances is almost identical for the two membranes, the fouling mechanisms on the adsorbed monolayer must be equal and independent of the membrane type. The fouling resistances versus mass of permeate increase more or less linearly, which is in agreement with the increasing resistance of a growing cake layer according to eq 6. This indicates that the fouling appears as cake-layer formation at the low enzyme concentration. This is further investigated in Figure 7, which shows a plot of $1/J_v$ versus m_p according to eq 8.

In Figure 7, it is seen that for both membranes almost straight lines with nearly equal slopes are obtained. Therefore, fouling during the pressure-forced experiments actually occur as or can be described by cake-layer formation. This is emphasized by the almost equal slopes, which shows that fouling parameter α is equal for both membranes and therefore independent of the membrane type. Thus, the increase in fouling resistance depends on the volume of permeate and is independent of the membrane itself. At these rather low enzyme concentrations (5−10 g/L), the osmotic pressure is neglected because it is assumed to be very low compared to the hydrostatic pressure. According to eq 8, the y-axis intercepts are related to the sum of the membrane resistance and the maximum static adsorption resistances. The two intercepts are almost equal, which is in agreement with results from the static adsorption experiments.

It has been shown that at low enzyme concentration the flux can be described by a resistance-in-series model (eq 7) with increasing fouling resistance that is dependent on the mass of permeate that passes the membrane. However, the osmotic pressure difference has to be taken into account at higher macromolecular concentrations at which the concentration polarization can play the role expressed as an osmotic pressure difference that has to be subtracted from the hydrostatic pressure difference (eq 9).[16] Therefore, when concentration polarization is the main factor determining the flux (when the osmotic pressure of the macromolecular solutions cannot be neglected), it can be shown that the flux is mainly determined by the bulk concentration. This can be shown for the pressure-forced experiments conducted with an initial bulk concentration of 50 g/L. Data for those high-concentration pressure-forced experiments are plotted according to stagnant film theory (eq 10).

Because straight lines for both membrane types are obtained (Figure 8) and because they are almost completely overlapping, it can be concluded that at these rather high enzyme concentrations, concentration polarization and thus the osmotic pressure difference determine the flux. Furthermore, the concentration polarization is independent of the membrane type. From the slope, the mass transfer coefficient is ∼19 L/(m²·h). With a stirring speed in the cell of 300 rpm, the flow in the cell is laminar, and from the flow and mass transfer literature correlation (eq 11), a mass transfer coefficient of ∼11 L/(m²·h) is obtained. This is rather close to the experimentally determined mass transfer coefficient, which emphasizes that at these concentrations the osmotic pressure difference caused by concentration polarization is the main term determining the flux. Using the osmotic pressure model combined with the stagnant film theory (eqs 9 and 10) and inserting $J_v = 0$, the concentration at which the osmotic pressure equals the hydrostatic pressure can be found.[16] From Figure 8, it can be seen that an enzyme concentration of around 150 g/L ($C = \exp(95/19)$) gives an osmotic pressure of 2 bar, which equals the hydrostatic pressure difference and thus gives zero flux.

Overall, it has been shown that when the immediate adsorbed monolayer has been established, a growing fouling layer is formed. The formation of this fouling layer can be described as a cake-layer formation. This cake-layer gives a subresistance that when added to the membrane resistance, and the adsorption resistance gives the total resistance toward transport through the membrane. Furthermore, it has been shown that at higher enzyme concentrations the concentration polarization results in osmotic pressure differences that cannot be neglected. Under these conditions, the flux is mainly determined by the bulk concentration and thus the concentration polarization. Cake-layer formation and concentration polarization are independent of the membrane type. The effect of static adsorption also affects cross-flow systems. Jonsson et al.[22] have reported flux decreases due to BSA adsorption in cross-flow ultrafiltration under both static and pressure-forced conditions.

The retention of amylase-F is also measured at the end of the pressure-forced experiments. For both membranes, the retention at the end is very close to 100%. This means that the two membranes act almost equally with the same retention and the

(22) Jonsson, G.; Johansen, P.; Li, W. Proceedings of The CEE-Brazil Workshop on Membrane Separation Processes, Rio de Janeiro, Brazil, May 3−8, 1992; pp 265−276.

same flux and indicates that the membrane properties of the two investigated UF membranes in our experiments are mainly determined by the (adsorbed) monolayer formed on the membrane surface (often referred to as a secondary membrane) rather than by the virgin membrane properties. It should be noted that the initial retention for the ETNA10PP membrane was measured to be approximately 97% whereas the initial retention for the PES membrane is measured to be close to 100%. The initial retentions were measured after 5 min of filtration (concentration 5−10 g/L), and after 20 min of filtration (concentration 5−10 g/L), the retention of the ETNA10PP membrane was close to 100%. The retentions are determined on the basis of enzyme concentration measurements of bulk and permeate samples, as described earlier. Thus, the retention of the ETNA10PP membrane increases relatively quickly to approximately 100% during filtration, resulting in a membrane with very similar properties compared to those of the PES membrane. This was also concluded by Wei and co-workers, who measured very similar BSA fluxes for the two UF membranes during filtration at 2 bar and a BSA concentration of 0.1 wt %, even though the initial water flux of the PES membrane is much larger than for the ETNA10PP membrane.[5]

Wei and co-workers[5] have described anti-fouling behavior during filtration for the ETNA10PP membrane. This is also seen in our data in Figure 6, where the fluxes are at the same level even though the initial water flux at 2 bar is around 3 times larger for the PES membrane. Thus, the maximum static adsorption (permeability drop and adsorption resistance), shown in Figure 4 and Table 3, gives an idea as to what extent the flux decreases during filtration from its initial water flux. The maximum static permeability drop of 23% and maximum static adsorption resistance of 0.0046 $m^2 \cdot h \cdot bar/L$ for the ETNA10PP membrane result in a relatively smaller flux decrease from the initial water flux during filtration (Figure 6) compared to that for the PES membrane with a maximum static permeability drop of 75% and a maximum static adsorption resistance of 0.014 $m^2 \cdot h \cdot bar/L$.

4.4. SEM Picture Analysis. SEM pictures have been taken for both membranes after they have been exposed to either static or pressure-forced adsorption. A picture of a chemically cleaned membrane was also taken. The pictures are shown in Figure 9.

The surfaces of the ETNA10PP and PES membranes are very different. The pictures of the clean surfaces show that the PES membrane has a more open structure compared to that of the ETNA10PP membrane. The pores are distributed more evenly on the clean PES membrane. The ETNA10PP membrane has a denser surface, which is consistent with the lower water permeability measured for that membrane compared to that for the PES membrane. The water permeability of the PES membrane is around 3 times larger than that of the ETNA10PP membrane, according to Table 1. Furthermore, the pores are not as evenly distributed for the ETNA10PP membrane. Some areas appear to be denser than others, and some large pores are present, which could be the reason for the lower initial retention (97%) measured for this membrane compared to the retention of almost 100% measured for both membranes after 20 min of the pressure-forced experiments. Also, the fact that the ETNA10PP membrane relatively quickly reached a retention of around 100% is in agreement with Jonsson et al.,[22] who reported relatively large pores to be blocked by protein adsorption, which therefore changed the retention of the membrane.

After static adsorption, the surface of the PES membrane appears to be denser than the clean membrane. The difference is clearer for the ETNA10PP membrane, where the surface has a denser appearance and the pore size has apparently decreased, which can explain the increase in retention after pressure-forced adsorption. The static adsorption gives monolayer coverage of the membrane surfaces. Whether the monolayer packing of molecules on the PES surface is denser than on the ETNA10PP surface is difficult to conclude from the SEM pictures. It shall be noted that denaturation is likely to occur for the vacuum under which the samples are prepared and coated with gold. Thus, the actual SEM pictures can be "disturbed" by this.

For both membranes, a change in the surface structure has taken place after pressure-forced adsorption. The membranes have a denser surface, and a large number of the pores have been blocked or narrowed by enzymes. The change in the surface structure is more pronounced for the ETNA10PP membrane than for the PES membrane after pressure-forced adsorption. There is a resemblance to the surface structure of the PES membrane regardless of whether it has been exposed to static or pressure-forced adsorption. There is a clear difference in the surface structure of the ETNA10PP membrane. The surface exposed to static adsorption has a granulated surface, whereas the pores have an oblong shape in the surface exposed to pressure-forced adsorption. The permeability drop after the pressure-forced experiments exceeds the maximum static permeability drop during static adsorption. This can be explained by the addition of a fouling resistance, which is seen in Figure 6. Therefore, it can be concluded that the adsorption (or rather fouling) during the pressure-forced experiments goes beyond monolayer coverage and the flux and mass of permeate data are in agreement with a cake filtration model. The SEM pictures seem to support this statement because the surfaces of the pressure-forced membranes seem to be denser and different in appearance than the surfaces of the static-adsorbed membranes. In particular, exceeding the monolayer coverage under the pressure-forced condition for the ETNA10PP membrane is visualized by the white "spaghetti areas", but the surface of the pressure-forced PES surface also seems to be much denser than under the static condition.

5. Conclusions

Static adsorption experiments were conducted with two different ultrafiltration membranes. The following can be stated:

- An easy method to measure static adsorption on a membrane surface in terms of a permeability drop or an adsorption resistance has been developed. The method ensures that the adsorption is facilitated only from the skin-layer side of the membrane and not from the support-layer side.
- It has been shown that the static adsorption of a 55 kDa amylase-F enzyme onto two different polymeric ultrafiltration membranes follows the Langmuir adsorption theory. Thus, static adsorption consists of monolayer coverage on the surface.
- From the adsorption isotherms, the maximum static adsorption (permeability drop and adsorption resistance) is determined. The maximum static adsorption is more than 3 times larger on the more hydrophobic surface (the PES membrane) compared to that on the more hydrophilic surface (the ETNA10PP membrane). On the basis of the maximum static permeability drops, the value is around 3 (75%/23%), and on the basis of the maximum static adsorption resistance, the value is also around 3 (0.014 $m^2 \cdot h \cdot bar/L$/0.0046 $m^2 \cdot h \cdot bar/L$). The amylase-F molecules must therefore be more closely arranged and packed in the monolayer on the PES surface than on the ETNA10PP surface.

In addition, some filtration experiments have been conducted to investigate the so-called pressure-forced adsorption. On the basis of these experiments, the following can be stated:

- The permeability drop during filtration exceeds the maximum static permeability drop, even at low enzyme concentration. Thus,

the surfaces are covered beyond a monolayer, which is also seen by the increasing fouling resistance during filtration. The fouling resistances are at the same level for the two membranes during filtration. Fouling onto the absorbed monolayer can be described as a cake-layer formation with a resistance that increases with the amount of permeate that passes the membrane. The exceeding of the monolayer coverage and cake/fouling formation are supported by SEM.

- The two membranes show almost equal properties during filtration, even at low enzyme concentration. Thus, the very high initial water flux for the PES membrane has no effect in practice because the flux during filtration and the final flux are almost equal to the flux of the ETNA10PP membrane that has a much lower initial permeability. This is attributed to the difference in static adsorption for the two membranes.
- At higher enzyme concentrations, concentration polarization has to be taken into account. High enzyme concentrations yield significant osmotic pressures; therefore, the flux can be described from stagnant film theory and the osmotic pressure model.

Overall, the static adsorption on the membrane contributes to the total resistance to transport through the membrane. The static adsorption is highly dependent on the membrane surface chemistry, but other factors such as cake-layer buildup and concentration polarization also have to be taken into account when the performance of a certain membrane is to be evaluated. The latter two phenomena are independent of the type and surface chemistry of the membrane.

List of Symbols

C	concentration (g/L)
D	diffusion coefficient (m^2/s)
J_v	volumetric flux ($L/(m^2 \cdot h)$)
k	adsorption equilibrium constant (L/g)
K	mass transfer coefficient ($L/(m^2 \cdot h)$)
l_p	membrane permeability ($L/(m^2 \cdot h \cdot bar)$)
m_p	mass of permeate (g)
P	pressure (bar)
r	cell radius (m)
R	gas constant ($J/(kg \cdot K)$)
$R_{m,a,f,tot}$	resistance ($m^2 \cdot h \cdot bar/L$)
T	absolute temperature (K)

Greek Symbols

α	fouling constant ($m^2 \cdot h \cdot bar/(L \cdot g)$)
Γ	adsorption (permeability drop) (%)
Γ_{max}	maximum static permeability drop (%)
Γ_{max}	maximum static adsorption resistance ($m^2 \cdot h \cdot bar/L$)
γ	surface tension (J/m^2)
ν	kinematic viscosity (m^2/s)
π	osmotic pressure (bar)
ω	stirring speed (rad/s)

LA701524X

AIChE

Critical Flux Determination by Flux-Stepping

Søren Prip Beier and Gunnar Jonsson
CAPEC, Dept. of Chemical and Biochemical Engineering, Technical University of Denmark, DK-2800 Kgs. Lyngby, Denmark

DOI 10.1002/aic.12099
Published online November 2, 2009 in Wiley InterScience (www.interscience.wiley.com).

In membrane filtration related scientific literature, often step-by-step determined critical fluxes are reported. Using a dynamic microfiltration device, it is shown that critical fluxes determined from two different flux-stepping methods are dependent upon operational parameters such as step length, step height, and flux start level. Filtrating 8 kg/m^3 yeast cell suspensions by a vibrating 0.45 $\times$ 10^{-6} m pore size microfiltration hollow fiber module, critical fluxes from 5.6 $\times$ 10^{-6} to 1.2 $\times$ 10^{-5} m/s have been measured using various step lengths from 300 to 1200 seconds. Thus, such values are more or less useless in itself as critical flux predictors, and constant flux verification experiments have to be conducted to check if the determined critical fluxes can predict sustainable flux regimes. However, it is shown that using the step-by-step predicted critical fluxes as start guesses, in our case, in constant flux verification experiments for 5 and 1/2 hours, a sustainable flux was identifiable. © 2009 American Institute of Chemical Engineers *AIChE J*, 56: 1739–1747, 2010
Keywords: critical flux, dynamic microfiltration, yeast cells, step length, flux-stepping, bioseparation, membrane separations

Introduction

The concept of critical flux in membrane filtration processes has in the last 15 years gained more and more interest as a way of controlling fouling to achieve sustainable operation. When talking about critical fluxes, sustainable flux regimes are defined as sub-critical flux regions that are sustainable from a constant flux and TMP point of view. By operating at sub-critical flux, the need for membrane cleaning, necessary due to enhanced hydraulic resistance will be reduced. In that way, for example macromolecular transmission in microfiltration can be improved.[1] In 2006, an in-depth review about critical and sustainable fluxes was published by Bacchin et al.[2] In this review it is underlined that three different forms of the critical flux should be distinguished according to the level of hydraulic resistance: The *strong form*, the *weak form*, and the *irreversible form*. The strong and weak forms of the critical flux are well known and described in the literature. In the irreversible form of the critical flux, however, the hydraulic resistance "just" has to be kept below the sum of a membrane resistance, an eventual adsorption resistance, and a reversible fouling resistance not to be exceeded. When using the search words "critical flux," "membrane," or "?filtration," almost 200 papers appear, published since 1979 (using the DADS database, Technical Knowledge Center, Technical University of Denmark, February 2008).

The majority of all critical flux determinations reported in the literature are conducted using step-by-step methods, in which either the transmembrane pressure (TMP) or the flux is stepwise increased, and the response (either flux or TMP) is monitored. This method is easy to apply, which might explain its popularity, and out of the almost 200 mentioned "critical flux papers", the step-by-step method is applied in more than 100 of these papers to determine critical fluxes. However, a main disadvantage of the step-by-step technique is that it only measures the critical flux of the dominant fouling species.[3–5] Furthermore, when using this method, the determined critical fluxes can vary quite much depending on the flux start level J_0, step length sl, and step height sh although, only very few publications actually focus on this. The step height was reported by Le Clech et al.[6] to be the

Correspondence concerning this article should be addressed to G. Jonsson at gj@kt.dtu.dk.

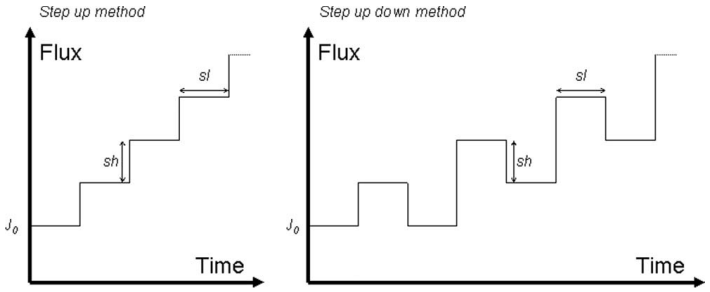

Figure 1. Sketch of two different approaches for critical flux determination.

Step up method and *step up down* method. J_0: Initial flux level, sh: step height, sl: step length.

main parameter impacting the fouling rate (dP/dt), using an MBR system processing sewage, whereas the step length has been reported by Kwon and Vigneswaran[7] not to influence the determined critical fluxes for crossflow microfiltration of latex particles with step lengths of 1200 and 2400 seconds. Neither did Guo et al.[8] detect a difference in the determined critical fluxes in crossflow microfiltration of synthetic wastewater when using step lengths of either 2400 or 7200 seconds. Also, Le Clech et al.[6] only detected minor differences in the determined critical fluxes for step lengths of 300, 600, 900, and 1800 seconds in MBR filtration of synthetic sewage. Only when the step length was increased to 7200 seconds, a significant change in the critical flux could be detected, whereas Choi and Dempsey[9] observed the determined critical fluxes to decrease when the step length was increased from 600 over 1200 to 1800 seconds, using a low pressure membrane system processing raw water.

The aims of this article are (i) to show that one cannot be sure to use a critical flux value based on one single step-by-step measurement to actually determine a critical flux, (ii) to show that a step-by-step determined critical flux has to be verified against constant flux experiments, and (iii) to emphasize that when talking about critical fluxes and sustainable flux regimes, a time period for sustainability has to be assessed. Two different flux-stepping critical flux determination methods are tested using our dynamic microfiltration system. It must be emphasized that we use the term "critical flux" as the outcome of the flux-stepping experiments, although it is later shown that many of these determined values actually are not real critical fluxes able to predict long term behavior. A step up method and a step up down method are tested using different values of the step length to evaluate the response in the determined critical fluxes. Furthermore, the onset of irreversible fouling will be tried to be determined using the step up down method. The experimentally determined critical fluxes are verified against constant flux experiments at, above and below, the average critical fluxes to check if one actually can predict sustainable behavior for an extended period, which in this case is 5 and 1/2 hours. Suspensions of bakers yeast cells are being processed. This medium is chosen to use some sort of a model fluid to simulate fermentation broth or other biological media as we in our earlier work also have added macromolecules to such suspensions.[1] Furthermore, our later results[10] are also obtained using yeast cell suspensions containing different macromolecules. Our system is in many contexts thought to be coupled to treatment of such media.

Flux-stepping concept

When the critical flux is determined by a step-by-step method, the flux is often controlled, and the corresponding TMP is monitored. The flux is increased in steps and at a point, at which the TMP increase exceeds some defined threshold limit, the critical flux is said to be exceeded. However, as pointed out by Bacchin et al.,[2] it would be more correct to talk about this level as a sustainable flux beause the transition detected by this method is often the transition from "slow fouling" to "rapid fouling." Still, we will use the term "critical flux" to emphasize that this is the flux one has to stay below to achieve sustainable filtration. Two different flux-step approaches are sketched in Figure 1.

These two methods are chosen, as they are both well known and often reported in the literature. Important parameters in both methods are the initial flux level (J_0), the step height (sh), and the step length (sl). Le Clech et al.[6] introduced three key TMP related parameters, useful to determine the onset of fouling, for a step up method. In this work, these parameters have also been applied for a step up down method. In Figure 2, the concept is sketched for both methods.

The average of the TMP values for a flux step is denoted P_{avg}, whereas dP/dt is the slope of the linear regression line covering the TMP data of a flux step. The latter parameter is often referred to as the "fouling rate". The sudden increase in TMP in the transition from one flux step to another is denoted ΔP_0 and can be determined as the distance between the linear regression lines for the two particular flux steps at the time of transition. The critical flux is determined from plots of P_{avg}, dP/dt, and ΔP_0 vs. the flux as the point where the curves "break". The advantage of the step up down method is that, in theory, fouling irreversibility can be recognized at a certain flux level as each flux level is "touched" two times. Thus, the onset of irreversible fouling, irreversibility form of critical flux can be identified by plotting the difference in P_{avg}, J, and dP/dt, $(P_{avg,n,ii} - P_{avg,n,i})$, $(dP/dt_{n,ii} - dP/dt_{n,i})$, and $(J_{n,i} - J_{n,ii})$, as function of the flux. This method, distinguishing the reversible fouling and the irreversible fouling, is earlier described by Espinasse et al.[11]

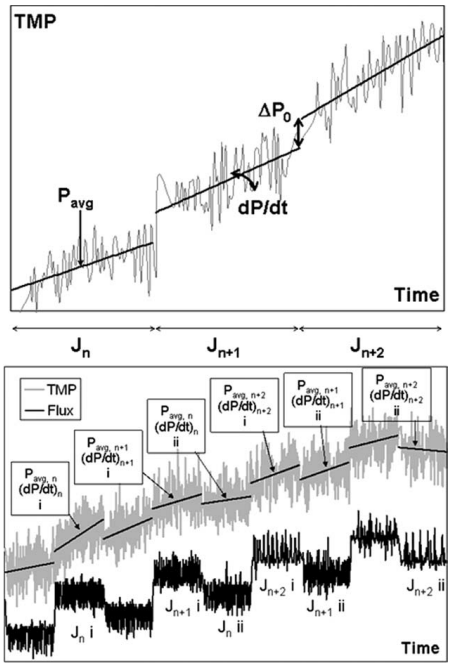

Figure 2. TMP related key parameters.

Upper plot: *Step up* method. P_{avg}, dP/dt, and ΔP_0^6. Lower plot: *Step up down* method. P_{avg} and dP/dt. n: number of the flux step J_n.

Materials and Methods

Apparatus and feed suspensions

The vibrating microfiltration system, often referred to as a dynamic microfiltration system, used in this work consists of a module with 9 hollow fibers placed vertically in a bundle. The system is sketched in Figure 3.

The hollow fibers are all closed in the bottom ends by a steel plate. The top ends of the fibers are, via a permeate gap and the permeate pipe, connected to a suction pump (permeate pump) that sucks permeate through the fibers at a constant rate. Permeate is collected in a beaker on an electronic scale connected to a PC. Permeate is manually poured back to the feed tank when the volume in the permeate beaker is around 100 ml. The permeate pump is controlled by a PC, and the corresponding TMP is monitored and logged by the PC by use of a pressure transducer. The module is placed in a plastic cylinder connected to a feed tank. The feed fluid (3 liters in total) is circulated between the feed tank and module cylinder by a feed pump at very low pumping rate, corresponding to a velocity in the module cylinder below 1×10^{-2} m/s. The temperature is monitored during the experiment by a thermometer in the feed tank, and the temperature is kept constant by a thermostatic regulation on the feed side. The membrane module can be vibrated in the module cylinder at variable frequency and amplitude by a "rotation head," and the frequency and amplitude can be varied independently. Suspensions of bakers yeast cells are filtrated. Solutions contained 8 kg/m^3 dry weight bakers yeast. The suspensions were all buffered to a pH of 6.3 by adding 100 ml of 30 mM phosphate buffer ($KH_2PO_4/Na_2HPO_4 \cdot 7H_2O$), which yield a feed buffer concentration of 1 mM. Relevant membrane parameters are listed in Table 1 together with the module hydrodynamic parameters used in this work.

The skin layer is located on the outside of the fibers, which are made of a polyethersulphone (PES) and polyvinylpyrrolidone (PVP) blend in a 98/2% ratio. PVP is added to make the fibers more hydrophilic as hydrophilic membranes tend to foul less. The average water permeability of the clean membrane module was measured to 2.2×10^{-8} m/(s $\times$ Pa) with a standard deviation of 13% based on 16 measurements. Neither an increasing nor a decreasing tendency of the water permeability was observed during the experimental work. Between each experiment, the membrane module was chemically cleaned with a 2% alkaline solution (P3 Ultrasil-141) for 30 minutes at 50°C.

Improvements of the system have been made compared with the system used and described earlier.[1,12] The number of fibers has been decreased from 54 to 9. The membrane area/module volume ratio has, therefore, been decreased, but the modified configuration makes it much easier to do reparation in case of a single fiber breakage. The liquid level above the module has also been increased from 1×10^{-2} m to 15×10^{-2} m. In the old system, with a liquid level above the module of only 1×10^{-2} m, air bubbles were induced and spread out in the whole module cylinder because of the fast vibrating module. The air bubbles might have disturbed the picture so that the effect of the pure vibrations was not clear. In the new system, with a liquid level of 15×10^{-2} m above the module, no air bubbles are induced at the liquid

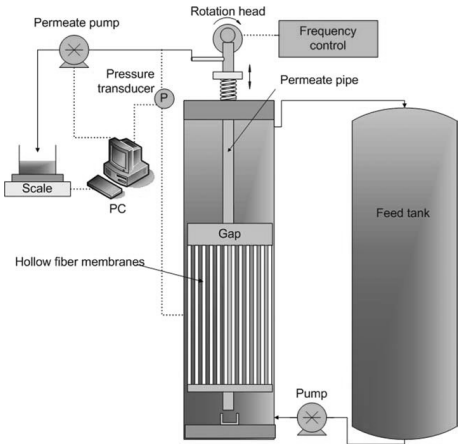

Figure 3. Sketch of the experimental apparatus.

[Color figure can be viewed in the online issue, which is available at www.interscience.wiley.com.]

Table 1. Characteristics of the Membrane Module and Hydrodynamic Conditions During the Experimental Runs

Membrane Material	Number of Fibers	Length of Fibers (m)	Total Membrane Area (m^2)	Pore Size (m)	Permeability of Module [m/(s × Pa)]
PES/PVP (98/2%)	9	0.125	0.084	$0.36 \times 10^{-6} - 0.50 \times 10^{-6}$	$2.2 \times 10^{-8} \pm 13\%$
Feed flow velocity (m/s)	**Vibration frequency (s^{-1})**	**Vibration amplitude (m)**	**Average surface shear rate (s^{-1})**	**Temperature (°C)**	**Bakers yeast concentration (kg/m^3)**
9×10^{-3}	20	1.375×10^{-3}	1235	29	8

surface. Though air bubbles are often reported to reduce fouling in MBR systems, we focus on investigating effects of pure vibrations with our system so the elimination of air bubbles is an advantage from that point of view.

Experimental Procedures

All experiments were conducted at the same hydrodynamic and physical conditions as listed in Table 1. The vibration frequency and amplitude of 20 s^{-1} and 1.375×10^{-3} m, respectively, can be calculated into an average surface shear rate of 1235 s^{-1} according to the fluid dynamical equation of our previous work.[12] The mass flow of permeate and TMP were logged every 4th second in all experiments, and the feed recirculation velocity was kept very low, below 9×10^{-3} m/s in the module cylinder between the module and the feed tank. The operational parameters for the critical flux determination experiments are listed in Table 2. Each experimental run was repeated three times. As a limit for acceptable fouling rate (dP/dt), we use a value of 1.1 Pa/s (40 mbar/h), which we have defined and used in a previous study, in which critical fluxes were determined using a step up down method, for the same type of feed suspension.[12] This limit indicates the shift from slow fouling to rapid fouling.

The values of the flux start level, step length, and step height were chosen at the same level as for many earlier reported critical flux studies. Constant suction experiments for 5 and 1/2 hours were also conducted to verify the experimentally determined critical fluxes. Each constant suction experiment was conducted three times. Experiments were conducted at, above and below, the average experimentally determined critical flux:

- Sub-critical flux: $\sim 2.8 \times 10^{-6}$ m/s below the average determined critical flux (Cho and Fane[13] state that extended operation at a fixed "sustainable" flux should be possible as long as the flux is substantially below the nominal critical flux of the dominant foulant).
- At the average determined critical flux.
- Supra-critical flux: $\sim 2.8 \times 10^{-6}$ m/s above the average determined critical flux.

Each experiment was initiated by slowly step-wise increasing the flux until the fixed flux level was reached. Step length of 120 seconds and step heights of 5.6×10^{-7} m/s were used to reach the fixed flux level not to over-foul the membrane by imposing the given flux level immediately. The importance of a slow start-up procedure is underlined by Le Clech et al,[6] who proposed a small initial step height. Also, Chen et al.,[14] working with microfiltration and ultrafiltration of silica particles, stated that slow incrementation of the flux to a given value can result in a significantly lower TMP than the direct application of that flux.

Results and Discussion

Critical flux determination

The critical fluxes were determined in different ways using a step up and a step up down method. The TMP curves were analyzed as sketched in Figure 2. At a certain flux level, for both methods, the increase of pumping rate was not able to increase the flux further, and the limiting flux was reached (around 1.25×10^{-5} m/s). After that, the flux actually decreases when the pumping rate is increased. This is probably because after the critical flux has been reached, cavities are induced in the permeate pump because of deposition, fouling, and probably pore blocking of the membrane which lead to a large increase in hydraulic resistance. The pump is, therefore, not able to maintain the flux. Bacchin[15] has proposed a theoretical link, stating that the critical flux equals 2/3 of the limiting flux, which then will give a critical flux of around 8.3×10^{-6} m/s.

In Figure 4, it is seen how the critical flux is determined based on the dP/dt parameter, fouling rate, when plotted vs. the flux for both methods for a random choice of operational parameters. The uncertainty in the fouling rates is seen as the standard deviation, especially above the critical flux, is very high whereas below this level the fouling rate is relatively constant. The convective forces dragging the main foulant species toward the membrane must exceed the drag forces away from the membrane surface around the critical flux, making the fouling rate curve "break". However, the fouling rate is not zero below the critical flux, which indicates a slow, progressive fouling build-up below the critical flux. Therefore, in our case the critical flux indicates a change in the type of fouling and not the onset of fouling.

Using the method of Le Clech et al.,[6] the critical flux was further determined from plots of the flux vs. the average pressure P_{avg} (TMP), which is shown in Figure 5 for a random choice of operational parameters. The deviation from linearity can be identified as a critical flux. It is, furthermore, seen that the critical flux is of the weak form, according to the definition of the work of Field et al.,[16] as the slope is smaller than the slope of the water flux curve. This, probably, indicates adsorption that changes the permeability of

Table 2. Operational Parameters for the Critical Flux Determination Experiments

	Step Up Method	*Step Up Down* Method
J_0, flux start level (m/s)	1.9×10^{-6}; 4.4×10^{-6}	1.9×10^{-6}
sl, step length (s)	300; 600; 1200	300; 600
sh, step height (m/s)	5.8×10^{-7}; 1.3×10^{-6}	5.8×10^{-7}

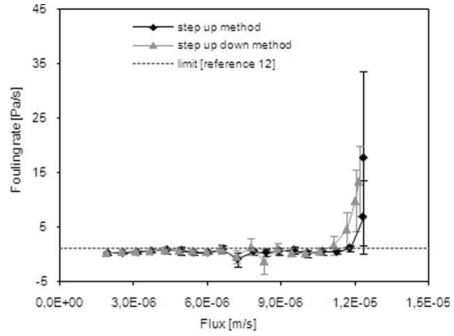

Figure 4. Fouling rate (*dP/dt*) vs. flux for one of the *step up* experiment (step length: 1200 s, step height: 5.8×10^{-7} m/s, flux start level J_0: 1.9×10^{-6} m/s) and for one of the *step up down* experiments (step length: 600 s, step height: 5.8×10^{-7} m/s, flux start level: 1.9×10^{-6} m/s).

Standard deviation for the three identical experiments is shown with error bars. The fouling rate threshold limit of 1.1 Pa/s is adapted from our previous work[12].

[Color figure can be viewed in the online issue, which is available at www.interscience.wiley.com.]

the membrane. We have earlier determined such irreversible adsorption resistances caused by macromolecular adsorption on ultrafiltration membranes.[17] The decreasing behavior of the flux is probably caused by cavitations in the pump at the largest flux levels.

The critical flux based on the parameter ΔP_0 (Figure 6) is identified at the point where the value (or the standard deviation) undergo a dramatic change. In Figure 6, three step lengths for the step up method are shown. It is seen that using this parameter for identification of the critical flux, with our experimental system, is very uncertain. For a step length of 1200 s, a relatively large deviation in the curve is observed slightly above 1.1×10^{-5} m/s, but the deviation could also be assessed just slightly above 5.6×10^{-6} m/s if the fluctuation in the curve at that point is defined as being too large. For the step length of 600 and 300 s, the critical flux has to be identified as the levels where the standard deviation of the curves starts to increase, since the value itself fluctuate, which is around 8.3×10^{-6} m/s and 6.1×10^{-6} m/s, respectively. Le Clech et al.[6] have observed a significant increase in ΔP_0 for the longer step length (7200 s), using a MBR system processing sludge and sewage, but at lower step lengths, the effect on ΔP_0 is less pronounced, which also seems to be the case with our system. Altogether, as seen in Figure 6 for our system, the critical flux determination using this parameter is very uncertain.

As seen in Figure 7, the experimentally determined critical fluxes are mostly sensitive to the used step length when the step up method is used, but also to some extent for the step up down method. For the step up method, the average critical flux value is 8.3×10^{-6} m/s $\pm$ 30%, whereas the value is 9.7×10^{-6} m/s $\pm$ 11% for the step up down method. Therefore, the results of the two methods cannot be characterized as being different within the experimental error. It should be noted that the prediction of the critical flux as 2/3 of the limiting flux, reported by Bacchin,[15] seems to be reasonable in our case although one should not really conclude much based on data with such large error. However, the "2/3" theoretical link between critical and limiting flux is based on the assumption that a flux distribution and a boundary layer thickness distribution exist along the membrane surface. Bacchin states, "the critical flux is reached when irreversible fouling occurs locally on the membrane, whereas

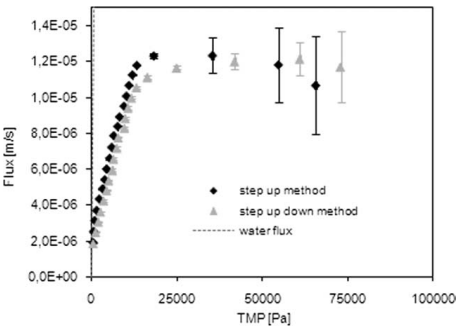

Figure 5. Flux vs. TMP for one of the *step up* experiment (step length: 1200 s, step height: 5.8×10^{-7} m/s, flux start level J_0: 1.9×10^{-6} m/s) and for one of the *step up down* experiment (step length: 600 s, step height: 5.8×10^{-7} m/s, flux start level: 1.9×10^{-6} m/s).

Standard deviation for the three identical experiments is shown with error bars and the water flux curve is shown as well.

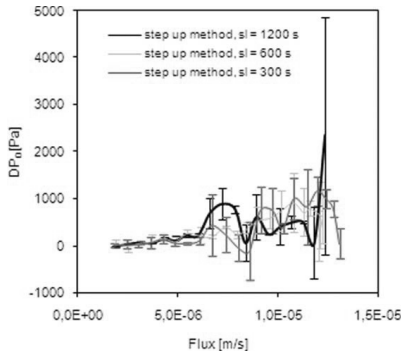

Figure 6. ΔP_0 vs. flux for the *step up* experiments. Step length: 1200, 600, and 300 s, step height: 5.8×10^{-7} m/s, flux start level J_0: 1.9×10^{-6} m/s.

Standard deviation is shown with error bars.

[Color figure can be viewed in the online issue, which is available at www.interscience.wiley.com.]

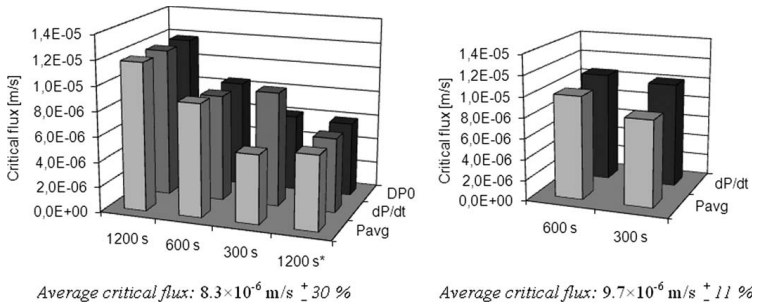

Figure 7. Critical fluxes for *step up* method (left) using step lengths of 300, 600, and 1200 s and based on different pressure related parameters (P_{avg}, dP/dt, and ΔP_0), and for the *step up down* method (right) using step lengths of 300 and 600 s using the P_{avg} and dP/dt parameters.

Step height = 5.8×10^{-7} m/s and flux start level = 1.9×10^{-6} m/s. NB: 1200 s*; experiment conducted with a step length of 1200 s, a flux start level of 4.4×10^{-6} m/s, and a step height of 1.3×10^{-6} m/s.

the limiting flux is reached when the whole membrane surface operates above the critical flux."[15] This could be the same case for our system.

Generally, the determined critical fluxes increase with increasing step length. This is opposite to the observations reported by Le Clech et al.,[6] and Choi and Dempsey[9] who reported decreasing critical fluxes with increasing step length, which might be due to the possibility for fouling to build-up during a longer step length period, causing a decreased critical flux. However, other effects must be dominant during operation of our system. Kwon and Vigneswaran,[7] and Guo et al.[8] reported no effect of different step lengths on the determined critical fluxes, which is also contradictory to our observations. Even though one has to remember that these systems are different from our system, as well as the nature of the feed solutions/suspensions are not the same, the reason and mechanism behind our observed tendency of increasing critical flux with increasing step length is not known, but part of the variation in the data might be ascribed to experimental error. Furthermore, when using step length of 1200 s, a higher flux start level of 4.4×10^{-6} m/s, and a larger step height of 1.3×10^{-6} m/s, the determined critical flux is around half the value as that with the lower flux start level and step height. However, it is surprising that less fouling is observed at longer filtration step lengths when the step height and flux start level are fixed.

Overall, it must be concluded that experimentally determined critical fluxes, in our case, are very sensitive to choice of operational parameters. Altogether, it must be stated in our case that these critical flux measurements are useless in itself as critical flux predictors. However, as will be shown later, the data will be used as starting points for verification experiments.

Fouling irreversibility

The advantage of the step up down method is, in theory, the possibility of determining the onset of irreversible fouling which by Bacchin et al.[2] is referred to as the irreversibility critical flux form. This can be done by depicting the difference in flux, TMP, and fouling rate for "same level steps," which is similar to the SWB method described by Espinasse et al.[11]

Figure 8 shows the difference in flux, TMP, and fouling rate between the same level steps, *n*. When fouling is reversible, the flux, TMP, and fouling rate difference should be zero as the pump operates at the same rate at that certain step and, therefore, an eventual polarized layer should decrease when the suction pressure is released back to a previous level. When fouling starts to get irreversible, the TMP will not be restored when moving from step *n,i* to step *n,ii* because in-between the flux has passed a higher flux step. According to Espinasse et al.,[11] a transition from a dispersed to a condensed phase occur at the membrane surface when the permeate flux is high enough to overcome the dispersive repulsive forces between the suspended components, and between the surface and the suspended components. At this stage, pore blocking or constriction is probably likely to occur. The point, where the differences in flux, TMP, and

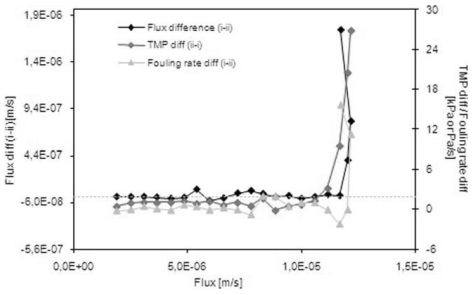

Figure 8. *Step up down* method.

Flux, TMP, and fouling rate difference between same level steps. Indication of fouling irreversibility. Step length: 600 s, step height: 5.8×10^{-7} m/s, flux start level: 1.9×10^{-6} m/s. [Color figure can be viewed in the online issue, which is available at www.interscience.wiley.com.]

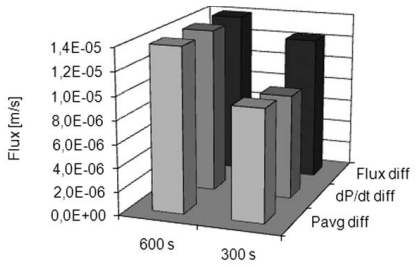

Average critical flux of the irreversible form: 1.1×10⁻⁵m/s±13%

Figure 9. The flux level at the onset of irreversible fouling based on flux, *dP/dt*, and P_{avg} difference. *Step up down* method.

Step length: 300 and 600 s, step height: 5.8×10^{-7} m/s, and flux start level 1.9×10^{-6} m/s.

fouling rate are no longer zero, is taken as the irreversible critical flux form. Actually, when looking at Figure 8, it is seen that the TMP difference curve, before the break, is throughout most of the flux interval slightly above zero (0.8 kPa ± 0.4 kPa), which indicate slow build-up of irreversible fouling during the whole experiment. Therefore, it might be more correct to refer to a "sustainability of fouling irreversibility" even though 0.8 kPa ± 0.4 kPa is a very low and almost undetectable pressure difference. The flux and fouling rate difference, before the curves break, is 5.8×10^{-8} m/s ± 150% and 0.22 Pa/s ± 410%, respectively, which shows that within the standard deviation, these values are not significantly different from zero. The fluxes, at which irreversible fouling is observed (irreversible critical flux form), by using the step up down method is depicted in Figure 9.

It can be seen that the flux level, at which irreversible fouling is observed, is dependent upon the used step length as well as the method, by which the flux level is determined (flux, *dP*/*dt*, or P_{avg} difference). The main tendency, similar to the step up method, is that increased step length leads to increase in critical irreversibility flux. The average flux level for irreversible fouling is 1.1×10^{-5} m/s ± 13% which is slightly higher compared with the critical fluxes for the step up method (8.3×10^{-6} m/s ± 30%) and for the step up down method (9.7×10^{-6} m/s ± 11%). This was also expected, according to the definitions of the different types of critical fluxes given in the appendix A of Bacchin et al.,[2] as the difference between weak form of critical flux and irreversible form of critical flux is that the total hydraulic filtration resistance is the sum of membrane and adsorption resistance (weak form critical flux) and membrane, adsorption and reversible resistance (irreversible form critical flux), respectively. However, regarding the large variation in the determined critical fluxes and in the irreversible form critical fluxes, one should be very cautious in differentiating between weak form critical flux and irreversible form critical flux from our measurements as the values are all within the experimental error (standard deviation). Therefore, one cannot conclude a difference in the different determined critical flux forms.

Critical fluxes tested against constant suction experiments

As seen in the previous section, the determined critical fluxes vary quite much from 5.6×10^{-6} m/s to 1.2×10^{-5} m/s and are very dependent upon the used step length and also the combination of step height and the flux start level as well as the determination method. Therefore, the data should be verified against constant suction experiments. Three 5 and 1/2 hours constant suction experiments were conducted, each repeated three times. The three flux levels were chosen based on the average values of the determined critical fluxes from the flux-stepping experiments:

- $J_0 = 5.6 \times 10^{-6}$ m/s. This flux level was chosen in order to be below the average critical flux value.
- $J_0 = 8.3 \times 10^{-6}$ m/s. This flux level was chosen in order to seek to be around the critical flux.
- $J_0 = 1.1 \times 10^{-5}$ m/s. This flux level was chosen in order to seek to be in the supra-critical flux regime around the onset of irreversible fouling.

In Figure 10 and Figure 11 the flux and TMP versus time for the constant suction experiments are shown.

The 1.1×10^{-5}m/s experiments clearly show that this flux level is supra-critical and not sustainable. The flux in the supra-critical regime is not sustainable and decreases relatively fast in the first 4 and 1/2 hours (16,200 s), probably because of cavitations in the pump. The TMP curve at supra-critical flux increases linearly in the first 1 and 1/2 hour with a slope, fouling rate, of 14.5 Pa/s which is more than one order of magnitude larger than the acceptable fouling rate limit of 1.1 Pa/s. After around 2 hours (7200 s), the permeate pump probably started to cavitate, explaining the flux decrease and the leveling out of the TMP curve. It is seen that in the experiment at 8.3×10^{-6}m/s, the flux level might be at some critical or intermediate level with a TMP

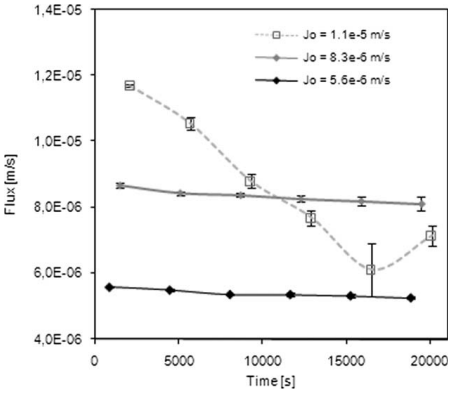

Figure 10. Flux vs. time for the constant suction experiments with flux start levels J_0 of 1.1×10^{-5}m/s, 8.3×10^{-6}m/s, and 5.6×10^{-6}m/s.

Error bars show the standard deviation between the three repetitions of each experiment.

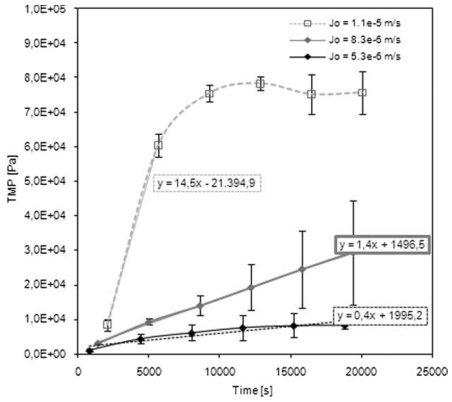

Figure 11. TMP vs. time for the constant suction experiments with flux start levels J_0 of of 1.1×10^{-5}m/s, 8.3×10^{-6}m/s, and 5.6×10^{-6}m/s.

Linear regression lines are shown for each of the curves. For the $J_0 = 1.1 \times 10^{-5}$m/s experiment, the linear regression line is only fitted to the first part of the curve until $\sim 1\frac{1}{2}$ h (5400 s). Error bars show the standard deviation between the three repetitions of each experiment.

increasing almost linearly with a slope, fouling rate, of 1.4 Pa/s. This fouling rate is slightly above the earlier defined limit. Only the experiments conducted at 5.6×10^{-6} m/s, seems to be in a sub-critical and sustainable flux regime with a fouling rate below the accepted limit (0.4 Pa/s). The difference in the TMP curves probably indicate differences in the mode of fouling at the different flux levels or at least the degree of fouling is significantly different. Where pore blocking is probably likely to have occurred at the highest flux level, only minor depositions and pore constrictions might have occurred at the lowest flux level. However, as seen in Figure 10, the fluxes also decrease slightly in the experiments, $J_0 = 5.6 \times 10^{-6}$ m/s and 8.3×10^{-6} m/s, which indicate slowly, but progressively, fouling build-up on the membrane.

As mentioned earlier, step-by-step methods only determine critical fluxes for the dominant fouling species, which in our case probably corresponds to whole yeast cell, or maybe larger yeast cell debris, but still, extracellular polymeric substances (EPS) from the yeast cells can cause severe fouling and is likely also to cause part of the permeability drop. The influence of EPS on membrane fouling and on macromolecular transmission has been investigated and described in other parts of our research.[10]

Altogether, the step-by-step experiments generated critical flux values with very large standard deviation. Thus, in itself these values are useless to predict critical fluxes. However, when using these values as start guesses in constant flux verification experiments, a sub-critical and sustainable flux was actually identifiable. The duration of the verification experiment was 5 and 1/2 hours, and therefore the sustainable time period is 5 and 1/2 hours.

Conclusions

The aims of this article are

(i) to show that one cannot be sure to use a critical flux value based on one single step-by-step measurement to actually determine a critical flux.

This has been proved, as two different critical flux determination methods both generated critical flux values with large standard deviation. The average critical fluxes for the step up method is 8.3×10^{-6} m/s $\pm$ 30%, whereas the average of the critical fluxes for the step up down method is 9.7×10^{-6} m/s $\pm$ 11%. Thus, the two methods gave the same results within the experiment error, and because of the large standard deviation, the critical flux values are in itself useless as predictors for sustainable flux regimes. Furthermore, the theoretical possibility of determining the onset of irreversible fouling, using the step up down procedure, was not achievable in our case, and differentiation between irreversible critical flux form and weak critical flux was, therefore, not possible because of the large standard deviation in the obtained values. How to use the two flux-stepping procedures have been described in detail.

(ii) to show that step-by-step determined critical fluxes has to be verified against constant flux experiments.

Using the step-by-step determined critical fluxes as start guesses for constant flux verification experiments, a sub-critical and sustainable flux was actually identified. Distinctions in the fouling levels were observed at flux levels of 1.1×10^{-5} m/s, 8.3×10^{-6} m/s, and 5.6×10^{-6} m/s. Only the 5.6×10^{-6} m/s level was in the sub-critical flux region and sustainable. Thus, the lowest determined critical flux values turned out to be at a sustainable level.

(iii) to emphasize that when talking about critical fluxes and sustainable flux regimes, a time period for sustainability has to be assessed.

The duration of the constant flux verification experiments was 5 and 1/2 hours. Thus, in our case the sustainability time is 5 and 1/2 hours. Whether this flux level is sustainable after 5 and 1/2 hours cannot be assessed from these data.

Overall, one should be very cautious in talking about sustainable fluxes based on critical flux values determined from step-by-step determination procedures. One should at least consider the three conclusions of this article in the evaluation of critical flux results obtained from flux-stepping experiments.

Acknowledgments

The authors thank the help and support from Henning Koldbech, from the Workshop of the Department of Chemical and Biochemical Engineering, Technical University of Denmark, who rebuild our experimental equipment and proposed and implemented very useful ideas, thus, making the equipment to run smoothly.

Literature Cited

1. Beier SP, Jonsson G. Separation of enzymes and yeast cells with a vibrating hollow fiber membrane module. *Separ Purif Tech*. 2007; 53:111–118.
2. Bacchin P, Aimar P, Field RW. Review critical and sustainable fluxes: theory, experiments and applications. *J Membr Sci*. 2006; 281:42–69.

3. Cho BD, Fane AG. Fouling transients in nominally sub-critical flux operation of a membrane bioreactor. *J Membr Sci*. 2002;209:391–403.
4. Fane A, Chang S. Membrane bioreactors: design and operational options. *Filtr Separ*. 2002;39:26–29.
5. Fane AG, Chang S, Chardon E. Submerged hollow fibre membrane module–design options and operational considerations. *Desalination*. 2002;146:231–236.
6. Le Clech P, Jefferson B, Chang IS, Judd SJ. Critical flux determination by flux-step method in a submerged membrane bioreactor. *J Membr Sci*. 2003;227:81–93.
7. Kwon DY, Vigneswaran S. Influence of particle size and surface charge on critical flux of crossflow microfiltration. *Water Sci Technol*. 1998;38:481–488.
8. Guo WS, Vigneswaran S, Ngo HH. Effect of flucculation and/or adsorption as pretreatment on the critical flux of crossflow microfiltration. *Desalination*. 2005;172:53–62.
9. Choi KYJ, Dempsey BA. Bench-scale evaluation of critical flux and TMP in low-pressure membrane filtration. *J Am Water Works Asso*. 2005;97:134–143.
10. Beier SP, Jonsson G. A vibrating membrane bioreactor (VMBR): macromolecular transmission–influence of extracellular polymeric substances. *Chem Eng Sci*. 2009;64:1436–1444.
11. Espinasse B, Bacchin P, Aimar P. Filtration method characterizing the reversibility of colloidal fouling layers at a membrane surface: analysis through critical flux and osmotic pressure. *J Membr Sci*. 2008;320:483–490.
12. Beier SP, Guerra M, Garde A, Jonsson G. Dynamic microfiltration with a vibrating hollow fiber membrane module: Filtration of yeast suspensions. *J Membr Sci*. 2006;281:281–287.
13. Cho BD, Fane AG. Fouling phenomena in MBR: transmembrane pressure transients and the role of EPS (extracellular polymeric substances). *Water Sci Technol*. 2003;3:261–266.
14. Chen V, Fane AG, Madaeni S, Wenten IG. Particle deposition during membrane filtration of colloids: transition between concentration polarization and cake formation. *J Membr Sci*. 1997;125:109–122.
15. Bacchin P. A possible link between critical and limiting flux for colloidal systems: consideration of critical deposition formation along a membrane. *J Membr Sci*. 2004;228:237–241.
16. Field RW, Wu D, Howell JA, Gupta BB. Critical flux concept for microfiltration fouling. *J Membr Sci*. 1995;100:259–272.
17. Beier SP, Enevoldsen AD, Kontogeorgis GM, Hansen EB, Jonsson G. Adsorption of amylase enzyme on ultrafiltration membranes. *Langmuir*. 2007;23:9341–9351.

Manuscript received Apr. 24, 2009, and revision received Sept. 23, 2009.

Chemical Engineering Science 64 (2009) 1436 – 1444

Contents lists available at ScienceDirect

Chemical Engineering Science

journal homepage: www.elsevier.com/locate/ces

A vibrating membrane bioreactor (VMBR): Macromolecular transmission—influence of extracellular polymeric substances

Søren Prip Beier, Gunnar Jonsson*

CAPEC, Department of Chemical and Biochemical Engineering, Technical University of Denmark, DK-2800 Kgs. Lyngby, Denmark

ARTICLE INFO

Article history:
Received 9 July 2008
Received in revised form 27 November 2008
Accepted 8 December 2008
Available online 16 December 2008

Keywords:
Membranes
Vibrating filtration
Particle yeast cells
Adsorption
Critical flux
BSA transmission

ABSTRACT

The vibrating membrane bioreactor (VMBR) system facilitates the possibility of conducting a separation of macromolecules (BSA) from larger biological components (yeast cells) with a relatively high and stable macromolecular transmission at sub-critical flux. This is not possible to achieve for a static non-vibrating membrane module. A BSA transmission of 74% has been measured in the separation of 4 g/L BSA from 8 g/L dry weight yeast cells in suspension at sub-critical flux (20 L/(m^2 h)). However, this transmission is lower than the 85% BSA transmission measured for at pure 4 g/L BSA solution. This can be ascribed to the presence of extracellular polymeric substances (EPS) from the yeast cells. The initial fouling rate for constant sub-critical flux filtration of unwashed yeast cells is 3–4 times larger than for washed yeast cells (18 (mbar/h)/5 (mbar/h)). At sub-critical flux, an EPS transmission of around 32% is measured for a pure yeast cell suspension. Thus, EPS and BSA are "competing" in being transmitted which might explain the lowered BSA transmission in the presence of yeast cells. Additionally, EPS heavily foul the membranes, leading to a 86% permeability drop and a fouling resistance 6 times larger than the membrane resistance after 5 $\frac{1}{2}$ h of constant sub-critical flux filtration (20 L/(m^2 h)) of pure 8 g/L dry weight yeast cell suspensions. Thus, the addition of hydraulic resistance caused by EPS might also explain the lowered BSA transmission, in the presence of yeast cells, since the membrane pores might be narrowed or partly blocked. EPS is, furthermore, able to cause a relatively large permeability drop even on a membrane module pre-fouled by EPS.

1. Introduction

Submerged suction pressure driven membrane systems are of increasing interest and are often reported in relation to waste water treatment. However, applications in other areas are also seen. When connected to, or submerged into, a fermentation tank, waste water tank, or another tank or reactor, from which water or eventually a solute has to be continually removed, such a setup is called a submerged membrane bioreactor (SMBR) or simply just a membrane bioreactor (MBR). In contrast to more conventional membrane filtration systems, which are often operated at constant pressure, MBR's are often operated at constant flux, controlled by a suction pump. The pump creates a lowered pressure on the permeate side, thereby inducing a pressure driving force which often is relatively low. When operating at constant flux, the transport towards the membrane surface is kept constant which might be advantageous in order to handle and control fouling problems. MBR's in different configurations have been described widely in the literature in treatment of waste water (Defrance and Jaffrin, 1999; Le Clech et al., 2003; Ognier et al., 2004; Kimura et al., 2005; Yamato et al., 2006; Guglielmi et al., 2007; Jeison and van Lier, 2007; Guo et al., 2008; Matosic et al., 2008), yeast cell suspensions and biomass suspensions in general (Chang and Fane, 2001; Cho and Fane, 2002; Fane et al., 2002; Beier et al., 2006; Beier and Jonsson, 2007; Akram and Stucky, 2008), and different inorganic substances/particles (latex, bentonite) (Kim and DiGiano, 2006). The critical flux concept is widely used as a guideline flux, below which fouling in principle is avoided. Much have been said and stated about the strong and weak form of the critical flux hypothesis (Field et al., 1995), and in the later years there seem to be a general agreement that the term "normally sub-critical flux", "sub-critical flux", or "sustainable flux" is a term that can be used as a guideline level for the flux at which only an acceptable TMP increase in a given period of time is observed when the flux is kept constant (Cho and Fane, 2002; Ognier et al., 2004; Hughes and Field, 2006; Bacchin et al., 2006).

MBR operation performance and fouling is often related to the presence of extracellular polymeric substances (EPS)

* Corresponding author. Tel.: +45 4525 2946; fax: +45 4588 2258.
E-mail address: gj@kt.dtu.dk (G. Jonsson).

0009-2509/$ - see front matter © 2008 Elsevier Ltd. All rights reserved.
doi:10.1016/j.ces.2008.12.008

(Hernandez Rojas et al., 2005; Ye et al., 2005a,b; Chen et al., 2006; Al-Halbouni et al., 2008; Xiu-Fen et al., 2008; Li et al., 2008; Arabi and Nakhla, 2008) that cover a wide range of more or less defined components following in the wake of biological species, e.g. cells and bacteria. A widely used approach to avoid fouling in MBR's is the use of air bubbles (Fane et al., 2002; Psoch and Schiewer, 2005; Li et al., 2005; Kim and DiGiano, 2006), but membrane module vibrations, inducing shear at the membrane surface, can also be used in order to avoid or reduce fouling problems. Such a system have been described and tested by Genkin et al. (2006) in the filtration of yeast cell suspensions, and we have also earlier tested such a vibrating system, consisting of a vibrating hollow fiber membrane module, in the filtration of yeast cell suspensions (Beier et al., 2006) and in the separation of α-amylase enzymes from yeast cells (Beier and Jonsson, 2007). Our vibrating membrane bioreactor (VMBR) system is also often referred to as a *dynamic microfiltration system*. This system has the advantage of being able to operate at a very low feed flow velocity (< 1 cm/s in the module cylinder) and at very low trans-membrane pressures (TMP < 100 mbar). The advantage of our system is the possibility of separating macromolecules from cell and other particular material with a high macromolecular transmission. The transmission of macromolecules in microfiltration will often decrease with time as an eventual fouling layer is build up and consolidated. Therefore, it is a challenge to achieve constant and high macromolecular transmission in the separation from larger species like particles or cells. Not many papers have been published dealing with the macromolecular transmission and its change around the critical flux in MBR related systems. This, however, is very important when trying to control membrane fouling and macromolecular transmission.

The possibility of enhancing the macromolecular transmission by using a backshock technique during crossflow microfiltration has been reported by Jonsson and Wenten (1994) in combination with the introduction of the feed to the porous support layer inside asymmetric hollow fiber membranes. The backshock technique is a modification of backwash techniques in which the effective backshock time is less than 0.1 s and the intervals between the backshocks are 1–5 s. For microfiltration of beer, Jonsson and Wenten report 100% protein transmission with backshock compared to only 68% protein transmission without backshock. For rennet and cellulase solutions, 98% and 100% transmission is observed compared to a transmission without backshock of 55% and 50%, respectively. Guerra et al. (1997) also used the backshock technique to achieve 100% casein transmission, during crossflow microfiltration of skim milk, with a rather open membrane (0.87 μm) along with a high retention of spores. In all cases, the transmission is probably enhanced since the backshock technique effectively prevents the loose and open fouling layer inside the porous support of the hollow fiber membranes to consolidate and that way block the pores. In crossflow microfiltration of skim milk with a much smaller pore size (0.1 μm), Le Berre and Daufin (1996) report that when the ratio between flux and effective wall shear stress (J/τ_{weff}) is kept below a critical level, separation with almost complete casein retention and 70–80% whey protein transmission is possible. If the critical ratio is exceeded, the whey protein transmission decreases fast and the possible filtration time decreases. Also, Gésan-Guiziou et al. (1999, 2000) describe the decreasing flux and soluble protein transmission in skim milk microfiltration when the ratio of flux and effective wall shear stress is exceeded. Below the critical level, no marked fouling by colloidal particles is observed. Sadr Ghayeni et al. (1996) mention the "flux-retention dilemma"; below the critical flux the transmission of, for example, viruses and nutrients in wastewater microfiltration is high whereas it decreases because of pore fouling above the critical flux. Therefore, in some contexts the transmission is desirable whereas in other contexts it is not. Persson et al. (2001) reports that even though no filter cake is present (below the critical flux), protein retention could be detected because of protein adsorption on the membrane leading to narrowing of the pores in microfiltration of lactic acid-producing bacteria. This means that due to adsorption, one should not expect full protein transmission even though the flux is kept below the critical level. Metsämuuronen et al. (2002), however, did not detect a decrease in protein transmission when the critical flux is exceeded. In ultrafiltration of myoglobin solutions they report that the protein transmission is high and increasing with flux until the critical flux is reached. Beyond the critical flux, the transmission remains almost constant and is highest when the pH is closest to the isoelectric point (IEP) of the proteins. Altogether, it is important to be aware of the transmission performance and its behavior around the critical flux since it apparently influences the selectivity and, therefore, the separation performance of the system.

The aim of this paper is to evaluate the separation of macromolecules (BSA) from cells (yeast cells) and investigate the transmission of BSA at sub-critical constant flux using our VMBR system. The BSA transmission is affected by EPS from the yeast cells, and the influence on fouling and transmission performance is evaluated by comparing with transmission data from pure BSA filtration. In order to understand the nature and influence of EPS fouling on BSA transmission, pure yeast cell filtration are conducted and analyzed for (i) clean and pre-fouled membranes, (ii) for constant sub-critical flux filtration of washed and unwashed yeast cell suspensions, and (iii) for similar constant flux filtrations at supra-, sub- and at the critical flux.

2. Theory

The water permeability of clean and fouled membrane modules is used to evaluate the different operational conditions. The permeability of the membrane module is calculated according to Darcy's law (Bird et al., 2002):

$$J = l_p \cdot TMP \tag{1}$$

Thus, the permeability (l_p) is the proportionality factor between the volumetric flux (J), and the trans-membrane pressure (TMP). In order to evaluate the extent of membrane fouling and fouling resistance, Darcy's law can be rewritten into a resistance-in-series model (Mulder, 1996):

$$J = \frac{1}{R_{tot}} \cdot TMP = \left(\frac{1}{R_m + R_f}\right) \cdot TMP \tag{2}$$

The total resistance towards transport through the membrane (R_{tot}) can be divided into different sub-resistances. In this work, we are only dealing with the membrane resistance (R_m), a membrane constant, and the fouling resistance (R_f), an additional resistance caused by all kinds of membrane fouling. The membrane resistance is determined from pure water experiments in which no fouling of the membrane occurs. The permeability drop of the membrane is used to evaluate the filtration performance and fouling characteristics, as in our previous work (Beier et al., 2007):

$$Permeability\ drop = \frac{l_p(initial) - l_p(final)}{l_p(initial)} \cdot 100\% \tag{3}$$

The initial and final permeabilities are determined from water flux experiments and Darcy's law. The final permeability is measured after the experiment has been stopped and the system and membrane module has been rinsed with water. Transmission of EPS and BSA is determined from concentrations of bulk and permeate samples, respectively.

$$Transmission = \frac{c_p}{c_b} \cdot 100\% \tag{4}$$

The effects of vibrating the membrane module is the induction of an enhanced surface shear rate (γ_s). The main parameters affecting the surface shear rate are the vibration frequency (f) and the amplitude (amp) (Beier et al., 2006):

$$\gamma_s = v_0 \cdot \sqrt{\frac{\omega}{2v}}[\sin(\omega \cdot t) - \cos(\omega \cdot t)] \quad (5)$$

The oscillating surface shear rate is a function of time (t), angular frequency ($\omega = 2 \times \pi \times f$), velocity amplitude ($v_0 = amp \times \omega$), and finally the kinematic viscosity of the fluid (v). It is seen that, in theory, the dependency of the vibration amplitude and frequency on the average value of the surface shear rate is given as: $\gamma_s = \text{function}(amp^1, f^{3/2})$. Often, enhanced surface shear rate increases the flux or the critical flux. However, whether the flux-shear rate dependency is best described by empirical power law correlation, like $J = \text{function}(\gamma_s^n)$, or by more theoretical based back-transport mechanisms, like Brownian diffusion, interaction induced migration, shear-induced diffusivity, or lateral migration, is difficult to judge. For many dynamic membrane filtration systems, power law correlation is often reported suitable for describing flux-shear rate dependencies (Jaffrin et al., 2004). On the other side, for many more conventional crossflow based membrane filtration systems, shear-induced diffusivity back-transport is often suitable for prediction of critical fluxes for species like yeast cells (Li et al., 2000) which are being filtrated in this study.

3. Materials and methods

The VMBR system consists of a module with hollow fibers placed vertically in a bundle. The "old" version of the system (membrane area 488 cm^2, liquid level above module $\sim$ 1 cm) is described in details by Beier and Jonsson (2007) and a new/modified version (membrane area 84 cm^2, liquid level above module $\sim$ 15 cm) is described in a recent paper (Beier and Jonsson, 2008). Despite the different membrane areas, the old and new versions of the system are almost identical. However, the increased liquid level above the module in the new modified system eliminates the induction of air bubbles at the surface in the module cylinder during vibration so that the pure effect of module vibration is easier to evaluate. A sketch of the modified system is shown in Fig. 1.

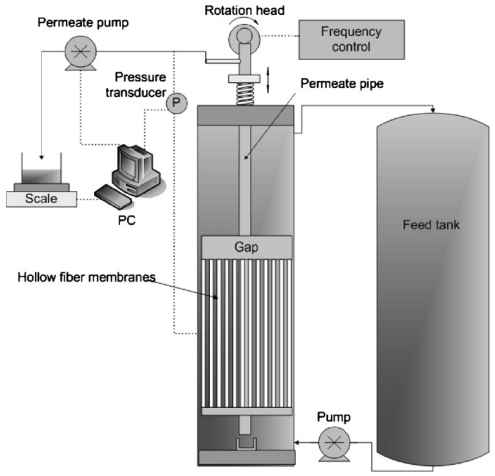

Fig. 1. Sketch of the experimental apparatus.

The fibers are made of a polyethersulphone (PES) and polyvinylpyrrolidone (PVP) blend in a 98%/2% ratio. PVP is added in order to make the fibers more hydrophilic. The pore sizes of the fibers vary from 0.36 to 0.50 μm. The skin layer is located on the outside of the fibers which are all closed in the bottom ends through the steel plate. The top ends of the fibers are, via a permeate gap and the hollow rod (permeate pipe), connected to a suction pump that sucks permeate through the fibers. Permeate is collected in a beaker on an electronic scale connected to a PC. Permeate is manually returned to the feed tank when the volume in the beaker is around 100 ml. The permeate pump is controlled by the PC, and the corresponding TMP is monitored and logged by the PC via a pressure transducer. The module is placed in a plastic cylinder connected to a feed tank. The feed fluid (3 L in total) is circulated between the feed tank and module cylinder by a feed pump at a very low pumping rate corresponding to a velocity in the module cylinder around 0.9 cm/s. The membrane module can be vibrated vertically in the module cylinder at variable frequency and amplitude by a "rotation head". Two different rotation heads were used with either 0.7 or 1.375 mm amplitude. With the old module, 25 Hz and 0.7 mm amplitude were chosen; corresponding to an average surface shear rate value of approximately 880 s^{-1} according to Eq. (5). With the new module, however, the frequency and amplitude were chosen to 20 Hz and 1.375 mm, respectively, corresponding to an average surface shear rate level of approximately 1230 s^{-1}. The vibrational levels were chosen rather arbitrarily with reduction of noise as a main factor. However, as described in our previous work (Beier et al., 2006), increasing surface shear rate increases the critical flux. This is the reason for the increase in vibrational mode from the experiments with old system to the experiments with the new system.

Feed solutions contained either 4 or 8 g/L dry weight bakers yeast. The suspensions were all buffered to a pH of 6.3 by adding 100 ml of 30 mM phosphate buffer ($KH_2PO_4/Na_2HPO_4 \cdot 7H_2O$) which yield a feed buffer concentration of 1 mM. In the experiments concerning BSA, a concentration of 4 g/L was used. The temperature in all experiments was kept at 29 °C using a thermostatic bath and controlled by a thermometer in the feed tank. This temperature was chosen since it is at the same level as the temperature during many primary separation steps (e.g. drum filtration or centrifugation) used in the industry in the recovery of macromolecules from fermentation broth. Higher temperatures also cause lower viscosity, and easier filterability. In theory, our VMBR system is thought to replace such primary separation.

Table 1 gives an overview of the conducted experiments. Five experiments have been carried out either at constant flux (J-constant), or at a flux-stepping mode (J-step). The flux and TMP data in Experiment 3 is adapted from our previous work (Beier and Jonsson, 2008). The effect of EPS from yeast cells is investigated in Experiment 4 by running identical filtrations on pre-washed and unwashed yeast suspensions.

- *Unwashed*: The dry yeast cells are suspended in water.
- *Washed*: The dry yeast cells are suspended in 1 L of water and centrifuged. After centrifugation, the supernatant is removed (and UV absorbance is measured) and the remaining bottom yeast slurry is resuspended in 1 L of water. The centrifugation procedure was repeated 6 times. The suspension was left in the refrigerator for 24 h between the 5th and 6th centrifugation in order to investigate the time effect of the EPS washing-out.

The bulk supernatant absorption maximum was detected at 260 nm for EPS from yeast cells which is used as a measurement for the EPS concentration. This is in agreement with the absorption maximum at 260–264 nm for yeast suspension supernatant reported by Hughes and Field (2006). Before and after each filtration, the

Table 1
Overview of experimental work.

Exp.	Module	Feed	Mode	Vibration	Description
1	New	4 g/L BSA	J-step + J-constant	20 Hz 1.375 mm	Measurement of BSA transmission at sub-critical flux
2	New	8 g/L yeast + 4 g/L BSA	J-step + J-constant	20 Hz 1.375 mm	Measurement of BSA transmission at sub-critical flux in separation from yeast cells
3	New	8 g/L yeast	J-constant	20 Hz 1.375 mm	Constant flux exp. below, at, and above J_c (Beier and Jonsson, 2008)
4	Old	4 g/L yeast	J-constant	25 Hz 0.7 mm	Exp. below J_c with washed and unwashed yeast cells.
5	Old	4 g/L yeast	J-step	25 Hz 0.7 mm	Flux step exp. with clean and pre-fouled membrane module

permeability of the membrane module is measured after rinsing with water. The concentration of BSA is determined by measuring the UV absorbance at 280 nm. The chemically cleaning in all experiments is conducted in 30 min using a solution of 2% P3 Ultrasil-141 (alkaline cleaner) at 50 °C. In Experiment 5, a pre-fouled module is used. The "pre-fouling state" is achieved after the filtration with the clean module only by rinsing the module with water and, therefore, no chemical cleaning.

A final minor batch experiments was conducted with a syringe on which a small housing containing a 0.45 μm membrane was mounted. The syringe has a volume of 50 ml and together with the membrane piece, the system comprises a batch microfiltration setup. 8 g/L yeast cell suspensions was filtrated on the system as well as supernatant of an 8 g/L yeast cell suspension. The supernatant was obtained by centrifugation at 3500 rpm for 5 min. UV absorbance was measured on both types of permeate samples.

4. Results and discussion

4.1. Experiment 1: transmission for a pure BSA solution

In order to evaluate the transmission performance of macromolecules through the membrane module, a pure BSA solution was filtrated and the transmission was determined. Initially, the critical flux was determined using a "*step up down*" procedure, described earlier (Beier et al., 2006; Beier and Jonsson, 2007, 2008) with a step length of 5 min, step height of 2 L/(m^2 h) and a flux start level of 6 L/(m^2 h). The critical flux experiment lasted $3\frac{1}{2}$ h, and the flux was increased to 50 L/(m^2 h). The fouling rate never exceeded 25 mbar/h, and by using our previous defined and used acceptable fouling rate limit of 40 mbar/h (Beier et al., 2006; Beier and Jonsson, 2007, 2008), we conclude that the critical flux of the pure BSA 4 g/L solution at the vibration degree of 20 Hz and 1.375 mm amplitude is above 50 L/(m^2 h). In order to evaluate the sub-critical transmission performance, a flux level of 20 L/(m^2 h) was chosen for the constant sub-critical flux experiment. For comparison, a similar experiment was conducted with a static membrane module (no vibrations).

As seen in Fig. 2, the vibrational mode facilitates a high and apparently stable BSA transmission around 85%. The corresponding TMP curve reveals that after the first 4 h, the pressure stabilizes at a constant level around 20 mbar. In the first 4 h, the pressure increases slightly from 10 to 20 mbar probably because of adsorption that increases the total hydraulic resistance of the membrane module. The benefit of vibrations of the module is also revealed in Fig. 2 since without vibrations, the TMP continually increases causing the transmission to decrease from around 68%, initially, to around 45% after 6 h of filtration. Finally, the vibrational mode vs. the non-vibrational mode reveals a significant difference in the initial transmission level; the initial transmission with vibrations is 85% whereas it is 68% without vibrations. Therefore, the vibrations not only facilitate the possibility of constant and stable transmission but also an enhanced initial transmission level. This might be due to the fouling build-up (even thought the BSA molecules are smaller than the membrane pores) that is much reduced at the vibrational mode. An adsorbed monolayer can be strongly irreversible attached to the membrane

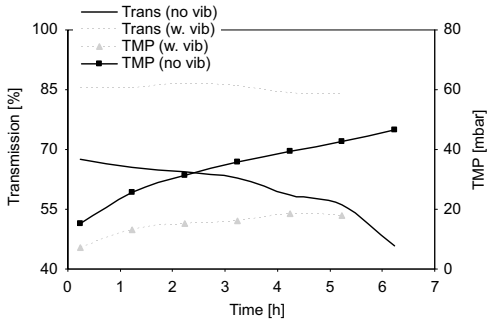

Fig. 2. Experiment 1. Transmission of BSA, and TMP for constant flux experiments (20 L/(m^2 h)) with BSA solutions (4 g/L) with vibrations (20 Hz, 1.375 mm amplitude, 1230 s^{-1} average surface shear rate), and without vibrations.

and might not be prevented by membrane vibrations and, therefore, the transmission is not 100% in the vibrational mode. However, an eventual initial adsorbed monolayer, probably present at both vibrational and non-vibrational mode, might very rapidly, in the non-vibrational mode, facilitate and act as a base for further fouling build-up. Such additional fouling is probably reversible and, thus, avoided in the vibrational mode. This might cause the difference in initial transmission level. We have earlier proved the existence of macromolecular monolayer adsorption on ultrafiltration polymeric membranes that is irreversible attached to the surface (Beier et al., 2007). Similar tendencies are described by Persson et al. (2001) who report that below the critical flux, protein retention is detected because of adsorption on the membrane leading to narrowing of the pores in microfiltration of lactic acid-producing bacteria. Jonsson et al. (1992) have described the shear around the pore entrances in microfiltration of BSA solutions in certain case to be quite high because of locally "high" hydrodynamic conditions. This might cause denaturation of BSA molecules possible leading to aggregation and eventually pore blocking. Therefore, complete protein transmission should not be expected.

4.2. Experiment 2: separation of BSA from yeast cells

The transmission of pure BSA solutions at sub-critical flux (20 L/(m^2 h)) from Experiment 1 is now used to compare with similar transmission data for at 4 g/L BSA solution containing 8 g/L dry weight yeast cells in suspension. Initially, the critical flux for the solution/suspension was measured in a similar manner as for the BSA solution in Experiment 1. The critical flux is measured to be above 20 L/(m^2 h). Thereafter, the constant sub-critical flux experiments were conducted as seen in Fig. 3.

Again, as in Experiment 1, the pressure stabilizes after around 4 h of sub-critical flux filtration. In the first 4 h, the TMP increases from

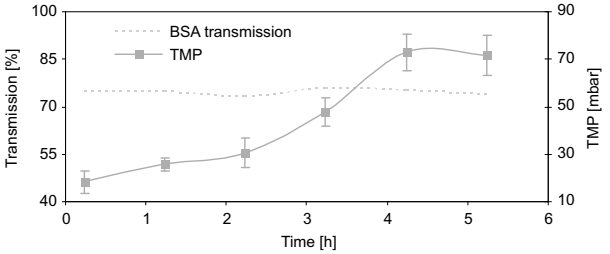

Fig. 3. Experiment 2. TMP, and BSA transmission for constant sub-critical flux experiment (20 L/(m^2 h)) with a 4 g/L BSA solution containing 8 g/L suspended dry weight bakers yeast cells. Module vibrations: 20 Hz, 1.375 mm amplitude, 1230 s^{-1} average surface shear rate. The experiment is repeated three times and the standard deviation is shown with error bars.

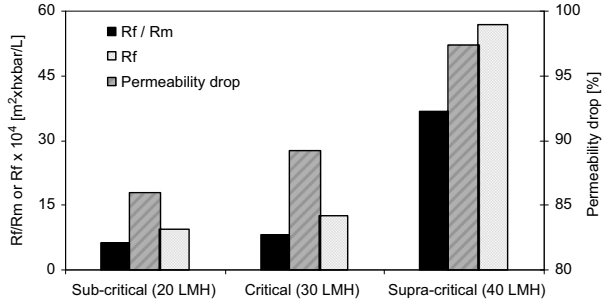

Fig. 4. Rf/Rm ratio, fouling resistance, and permeability drop after constant flux experiments at sub-critical flux, at critical flux, and at supra-critical flux. Feed: 8 g/L dry weight yeast cells. Module vibrations: 20 Hz, 1.375 mm amplitude, 1230 s^{-1} average surface shear rate. Each experiment is repeated three times. Flux and pressure data adapted from our previous work (Beier and Jonsson, 2008).

15 mbar to around 70 mbar probably because of adsorption and minor deposition on and inside the membrane of both BSA and EPS from the yeast cells. As for the pure BSA experiment (Experiment 1, Fig. 2), the BSA transmission at sub-critical flux is apparently stable. However, in the presence of yeast cells, the transmission is lower and around 74%, according to Fig. 3. Thus, the presence of yeast cells apparently influences the level of BSA transmission, and EPS from the yeast cells is probably the explanation. In order to investigate this, further experiments have been conducted with pure yeast cell suspensions to evaluate the impact of EPS fouling and EPS transmission (Experiment 3, 4 and 5).

4.3. Experiment 3: constant flux filtrations for yeast suspensions

We have earlier determined the overall average critical flux for a 8 g/L dry weight yeast cell to be 31 ± 7 L/(m^2 h) based on different types of flux stepping experiments using varied step length, step height, and flux start level (Beier and Jonsson, 2008). In that paper, we also presented $5\frac{1}{2}$ h constant suction filtrations at sub-critical flux (20 L/(m^2 h)), at critical flux (30 L/(m^2 h)), and at supra-critical flux (40 L/(m^2 h)) (Beier and Jonsson, 2008).

Analysis of these constant flux filtrations are shown in Fig. 4 where the fouling resistance (Eq. (2)) after the filtration test is shown together with the ratio between the fouling resistance and the membrane resistance. Permeability drop (Eq. (3)) during the filtrations are shown as well. First of all is worth noting that in all cases large permeability drop during the filtrations are observed; 86, 89 and 97% at sub-critical, at critical, and at supra-critical flux, respectively. Thus, even at sub-critical flux, a large permeability drop is observed probably caused by adsorption and irreversible deposition of EPS from the yeast cell that is washed out initially or during the filtration experiments. The permeability drop increases slightly when going from sub-critical flux to critical flux, and an additional permeability drop is observed when moving to supra-critical flux. Similarly, the fouling resistance increases from sub-critical flux to supra-critical flux. At sub-critical flux it is seen that after filtration the fouling resistance is around 6 times larger than the membrane resistance, whereas it is 8 times larger after constant critical flux filtration. However, after supra-critical flux filtration, the fouling resistance is 37 times larger than the membrane resistance. Altogether, it is seen that fouling caused by EPS during yeast cell filtration is very significant and mostly pronounced at supra-critical flux. However, even at sub-critical flux the effect of EPS from the yeast cells is large leading to a 86% drop in membrane permeability, and an irreversible fouling resistance 6 times larger than the membrane resistance.

The level of EPS during these constant flux filtrations were measured by UV absorbance measurements of permeate and bulk supernatant samples.

Fig. 5 reveals that the level of EPS increases continually and almost linear during the filtrations. From the data in Fig. 5, the transmission is calculated taking the absorbance values as the concentrations (Eq. (4)).

In Fig. 6 it is seen that the transmission of EPS is more or less the same for sub-critical flux and critical flux. The level is slightly decreasing during the experiment from around 35% to 31%. At supra-critical flux, however, the transmission is lower and around 26–27%. Thus, part of the EPS is transmitted through the membrane and, therefore, in Experiment 2 the transmission must be a "competition" between BSA and EPS. This might explain that the 74% BSA transmission in Experiment 2 for a mixture of BSA and yeast cells is lower than the 85% BSA transmission for pure BSA solutions (Experiment 1). In order to be able to propose that it is EPS (and not, e.g., yeast cell debris) that competes with BSA in being transmitted, a minor batch experiment was conducted. UV absorbance (260 nm) was measured on permeate from a microfiltration batch experiment on an 8 g/L yeast cell suspension (absorbance 1.125) and from supernatant from an 8 g/L yeast cell suspension (absorbance 1.122). Since the permeate absorbance is almost identical within experimental error in these two filtration trials, we believe that it is actually EPS that causes the decrease in BSA transmission in the presence of yeast cells.

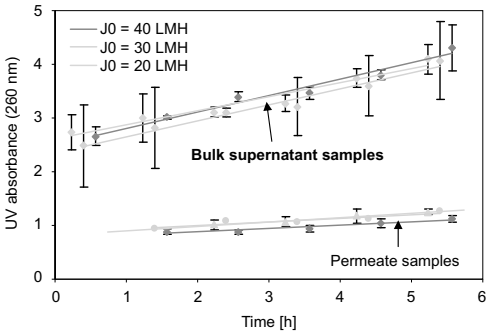

Fig. 5. Experiment 3. Bulk supernatant and permeate UV absorbance (260 nm) during constant sub-critical (20 LMH = 20 (L/(m^2 h)), critical (30 LMH), and supra-critical (40 LMH) filtration tests, respectively. Standard deviations of three repetitions are shown with error bars. Module vibrations: 20 Hz, 1.375 mm amplitude, 1230 s^{-1} average surface shear rate.

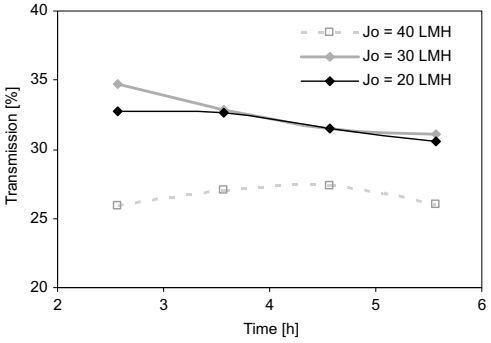

Fig. 6. Experiment 3. EPS transmission during constant sub-critical (20 LMH = 20 (L/(m^2 h)), critical (30 LMH), and supra-critical (40 LMH) constant flux experiments, respectively. Feed: 8 g/L dry weight yeast cells. Module vibrations: 20 Hz, 1.375 mm amplitude, 1230 s^{-1} average surface shear rate.

4.4. Experiment 4: washed vs. unwashed yeast suspensions

To further investigate the influence of EPS from the yeast cells during filtration, we have earlier conducted constant flux experiments with a 4 g/L dry weight yeast cell suspensions at sub-critical flux (30 L/(m^2 h)). With this feed concentration and a vibrational mode of 25 Hz and 0.7 mm amplitude, the critical flux has been determined to 36 L/(m^2 h) using the *step up down procedure* with a step length of 4 min, a step height of 2 L/(m^2 h), and a flux start level of 6 L/(m^2 h). Constant flux filtrations were carried out with both unwashed yeast cells and washed yeast cells. During the washing procedure, the supernatant UV absorbance was measured as seen in Fig. 7.

The amount of EPS decreases along with the suspension and centrifugation procedures. However, it is also revealed that some EPS is slowly washed out since the level of EPS is higher after the 6th centrifugation before which the suspension has been left for 24 h in a refrigerator. Thus, part of the EPS is easily removed and another part is apparently more slowly being washed out.

Fig. 8 shows that the level of the fouling resistance is higher and increases more for the unwashed yeast cells and after 2 h reaches a level equal to the membrane resistance. For the washed yeast cells, the fouling resistance reaches a level equal to the membrane resistance after around 7 h. It is seen that apparently not all EPS is washed out during the washing procedure (which was also seen in Fig. 7) since the fouling resistance also increases for the washed yeast cell suspension during filtration. Fig. 8 gives an impression of the impact of EPS on the evolution of the fouling resistance and that it can be reduced by a washing procedure and, therefore, has a high impact on hydraulic resistance when not washed. It might also explain the slightly decreasing EPS transmission which was seen in Fig. 6 since the fouling resistance is continually increasing which might be caused by partly blocking or pore narrowing.

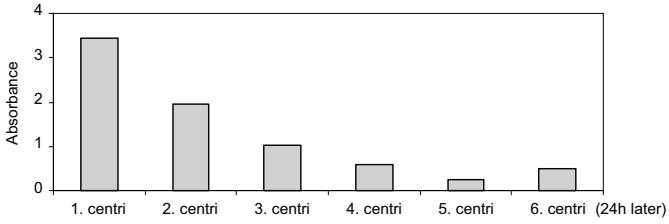

Fig. 7. Yeast cell washing procedure. Centrifugation of 4 g/L yeast cell suspension. UV absorbance of bulk supernatant at 260 nm. Between the 5th and 6th centrifugation the suspension was left for 24 h in a refrigerator.

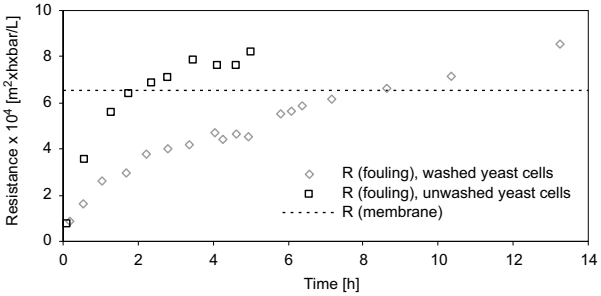

Fig. 8. Fouling resistance during constant sub-critical flux filtration (30 L/(m^2 h)) of washed yeast cells and unwashed yeast cells. Feed: 4 g/L dry weight yeast cells. Module vibrations: 25 Hz, 0.7 mm amplitude, 880 s^{-1} average surface shear rate.

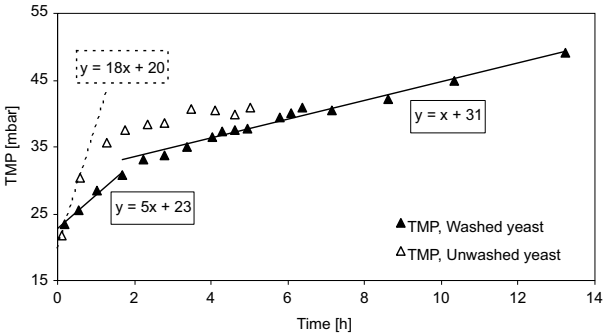

Fig. 9. TMP during constant sub-critical flux filtration (30 L/(m^2 h)) of washed yeast cells and unwashed yeast cells. Feed: 4 g/L dry weight yeast cells. Module vibrations: 25 Hz, 0.7 mm amplitude, 880 s^{-1} average surface shear rate. Linear regression lines show the fouling rates in "mbar/h" which equal the slopes.

It must be noted that even though the fouling resistances are increasing, the flux level is still characterized as sustainable and sub-critical since the fouling rates for both the washed and unwashed yeast cells never exceed our earlier defined acceptable fouling rate limit of 40 mbar/h (Beier et al., 2006; Beier and Jonsson, 2007, 2008). This limit is defined at being the transition to supra-critical flux level. In Fig. 9, however, it is seen that the initial fouling rate for the unwashed cells are 3–4 times larger than for the washed yeast cells (18 (mbar/h)/5 (mbar/h)).

4.5. Experiment 5: clean vs. pre-fouled membrane module

The effect of EPS fouling for two identical flux stepping experiments have been investigated with 4 g/L dry weight yeast cell suspensions. The flux was stepwise increased to 40 L/(m^2 h) on a clean and pre-fouled membrane module, respectively.

It is seen in Fig. 10 that the permeability drop for the pre-fouled membrane module is 24%, whereas it is 51% for the clean module. The clean module is being fouled completely leading to the given permeability drop, whereas a further addition of fouling, and therefore hydraulic resistance, is also possible for the pre-fouled module but not to the same extent as for the clean module, however. Also, the fouling resistance after the experiment with the pre-fouled module is around half of that with the clean module. Altogether, the effect of EPS fouling is seen again. Further deposition and fouling *is* possible onto the irreversible adsorbed layer that probably constitute the pre-fouled state which means that fouling of EPS continues even though the membrane is "already" covered by fouling.

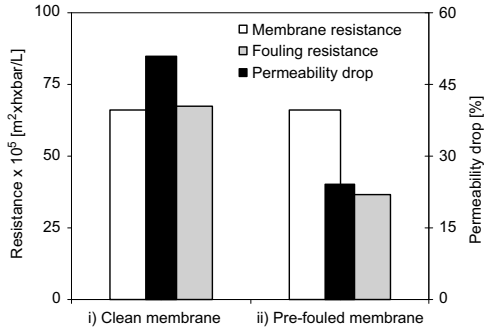

Fig. 10. Experiment 5. Permeability drop and fouling resistance after two identical flux stepping experiments on (i) a clean, and (ii) a pre-fouled membrane module. Feed: 4 g/L dry weight yeast cells. Module vibrations: 25 Hz, 0.7 mm amplitude, 880 s^{-1} average surface shear rate.

5. Conclusions

Five experiments have been conducted using the vibrating membrane bioreactor (VMBR) system using pure yeast cell suspensions, pure BSA solutions, and mixtures of these two. The aim was to evaluate the macromolecular transmissions of BSA and investigate how it is influenced by EPS in the separation from yeast cells.

- First of all, it has been shown that at a vibrational mode (20 Hz and 1.375 mm amplitude) of the VMBR, a constant 85% transmission of BSA can be achieved when filtering a pure 4 g/L solution. This was not possible for a static membrane module where the transmission decreased from 68% to 45% after 6 h of filtration (*Experiment* 1).
- The BSA transmission of 85% from Experiment 1 is higher than the 74% constant BSA transmission achieved in the separation from 8 g/L yeast cells in suspension (*Experiment* 2).
- In order to explain the BSA transmission decrease in the presence of yeast cells, it is important to account for the EPS fouling. Therefore, EPS fouling has been investigated through Experiment 3, 4 and 5. Large degree of EPS fouling is observed at supra-critical flux filtration of yeast cell suspensions, but also significant EPS fouling at sub-, and at critical flux is detected. After $5\frac{1}{2}$ h of sub-critical flux filtration at 20 L/(m^2 h), the fouling resistance is 6 times larger than the membrane resistance leading to a permeability drop of 86%. The transmission of EPS at supra-critical flux is measured to around 26–27% whereas it is slightly higher at sub-critical flux (around 32%). Thus, in Experiment 2 the BSA is "competing" with EPS in being transmitted. Additionally, the lowered BSA transmission in presence of yeast cells might also be explained by pore narrowing caused by EPS adsorption and deposition which is detected by the additional hydraulic resistance (permeability drop) observed in the presence of yeast cells (*Experiment* 3).
- The impact of EPS fouling is also seen in the difference of levels of fouling resistance for identical sub-critical experiments with both washed and unwashed yeast cells. Part of the EPS can be washed out using a suspension and centrifugation washing procedure. The initial fouling rate is 3–4 times larger for the unwashed yeast cells compared to the washed yeast cells. However, even for washed yeast cells, a slightly increasing fouling resistance can be observed showing that EPS, in a minor level, is also being released during filtration of washed yeast cells (*Experiment* 4).
- Membranes pre-fouled by EPS are able to adopt additional fouling since a permeability drop of 24% could be measured after the filtration of a pre-fouled membrane module. Therefore, EPS fouling continues even though the membrane has "already" been fouled (*Experiment* 5).

Altogether, EPS from yeast cells heavily causes membrane fouling even at sub-critical flux. This fouling influences both the permeability, and also the transmission, and therefore the macromolecular transmission of other species than EPS is lower in mixtures containing EPS than for pure solutions. This should be accounted for when such a separation is to be conducted using microfiltration. However, it has been shown that the VMBR still facilitate the possibility of actually conducting a separation with a relatively high and stable macromolecular transmission which is not possible to achieve for at static non-vibrating membrane module.

Notation

c_b	bulk concentration (9/1)
c_p	permeate concentration (9/1)
J	volumetric flux (L/(m^2 h))
J_c	critical flux (L/(m^2 h))
l_p	water permeability (L/(m^2 h bar))
R_f	fouling resistance (m^2 h bar/L)
R_m	membrane resistance (m^2 h bar/L)
R_{tot}	total resistance (m^2 h bar/L)
TMP	trans-membrane pressure (mbar)

Greek letters

γ_s	surface shear rate (s^{-1})
τ_{weff}	effective wall shear stress (Pa)

Acknowledgments

We acknowledge the help and support from Henning Koldbech from the Workshop of the Department of Chemical and Biochemical Engineering, Technical University of Denmark, who rebuild our experimental equipment and proposed and implemented very useful ideas and thoughts, thus, making the equipment run smoothly.

References

Akram, A., Stucky, D.C., 2008. Flux and performance improvement in a submerged anaerobic membrane bioreactor (SAMBR) using powdered activated carbon (PAC). Process Biochemistry 43, 93–102.

Al-Halbouni, D., Traber, J., Lyko, S., Wintgens, T., Melin, T., Tacke, D., Janot, A., Dott, W., Hollender, J., 2008. Correlation of EPS content in activated sludge at different sludge retention times with membrane fouling phenomena. Water Research 42, 1475–1488.

Arabi, S., Nakhla, G., 2008. Impact of calcium on the membrane fouling in membrane bioreactors. Journal of Membrane Science 314, 134–142.

Bacchin, P., Aimar, P., Field, R.W., 2006. Review critical and sustainable fluxes: theory, experiments and applications. Journal of Membrane Science 281, 42–69.

Beier, S.P., Jonsson, G., 2007. Separation of enzymes and yeast cells with a vibrating hollow fiber membrane module. Separation and Purification Technology 53, 111–118.

Beier, S.P., Jonsson, G., 2008. Critical flux determination by flux-stepping, Paper IV. In: Beier, S.P. (Ed.), Dynamic Microfiltration: Critical Flux and Macromolecular Transmission. PhD Thesis, ISBN: 978-87-91435-92-8.

Beier, S.P., Guerra, M., Garde, A., Jonsson, G., 2006. Dynamic microfiltration with a vibrating hollow fiber membrane module: filtration of yeast suspensions. Journal of Membrane Science 281, 281–287.

Beier, S.P., Enevoldsen, A.D., Kontogeorgis, G.M., Hansen, E.B., Jonsson, G., 2007. Adsorption of amylase enzyme on ultrafiltration membranes. Langmuir 23, 9341–9351.

Bird, R.B., Stewart, W.E., Lightfoot, E.N., 2002. Transport Phenomena. second ed. Wiley, New York.

Chang, S., Fane, A.G., 2001. The effect of fiber diameter on filtration and flux distribution–relevance to submerged hollow fibre modules. Journal of Membrane Science 184, 221–231.

Chen, M.Y., Lee, D.J., Tay, J.H., 2006. Extracellular polymeric substances in fouling layer. Separation Science and Technology 41, 1467–1474.

Cho, B.D., Fane, A.G., 2002. Fouling transients in nominally sub-critical flux operation of a membrane bioreactor. Journal of Membrane Science 209, 391–403.

Defrance, L., Jaffrin, M.Y., 1999. Comparison between filtrations at fixed transmembrane pressure and fixed permeate flux: application to a membrane bioreactor used for wastewater treatment. Journal of Membrane Science 152, 203–210.

Fane, A.G., Chang, S., Chardon, E., 2002. Submerged hollow fiber membrane module—design options and operational considerations. Desalination 146, 231–236.

Field, R.W., Wu, D., Howell, J.A., Gupta, B.B., 1995. Critical flux concept for microfiltration fouling. Journal of Membrane Science 100, 259–272.

Hernandez Rojas, M.E., Van Kaam, R., Schetrite, S., Albasi, C., 2005. Role and variations of supernatant compounds in submerged membrane bioreactor fouling. Desalination 179, 95–107.

Hughes, D., Field, R.W., 2006. Crossflow filtration of washed and unwashed yeast suspensions at constant shear under normally sub-critical conditions. Journal of Membrane Science 280, 89–98.

Genkin, G., Waite, T.D., Fane, A.G., Chang, S., 2006. The effect of vibration and coagulant addition on the filtration performance of submerged hollow fibre membranes. Journal of Membrane Science 281, 726–734.

Gésan-Guiziou, G., Boyaval, E., Daufin, G., 1999. Critical stability conditions in crossflow microfiltration of skimmed milk: transition to irreversible deposition. Journal of Membrane Science 158, 211–222.

Gésan-Guiziou, G., Daufin, G., Boyaval, E., 2000. Critical stability conditions in skimmed milk crossflow microfiltration: impact on operating mode. Lait 80, 129–140.

Guerra, A., Jonsson, G., Rasmussen, A., Nielsen, E.W., Edelsten, E., 1997. Low cross-flow velocity microfiltration of skim milk for removal of bacterial spores. International Dairy Journal 7, 849–861.

Guglielmi, G., Saroj, D.P., Chiarani, D., Andreottola, G., 2007. Sub-critical fouling in a membrane bioreactor for municipal wastewater treatment: experimental investigation and mathematical model. Water Research 41, 3903–3914.

Guo, W., Vigneswaran, S., Ngo, H.H., Xing, W., Goteti, P., 2008. Comparison of the performance of submerged membrane bioreactor (SMBR) and submerged membrane adsorption bioreactor (SMABR). Bioresource Technology 99, 1012–1017.

Jaffrin, M.Y., Ding, L., Akoum, O., Brou, A., 2004. A hydrodynamic comparison between rotating disk and vibratory dynamic filtration systems. Journal of Membrane Science 242, 155–167.

Jeison, D., van Lier, J.B., 2007. Cake formation and consolidation: main factors governing the applicable flux in anaerobic submerged membrane bioreactors (AnSMBR) treating acidified wastewater. Separation and Purification Technology 56, 71–78.

Jonsson, G., Johansen, P., Li, W., 1992. Influence of membrane fouling on ultrafiltration and microfiltration processes. In: Processes of The CEE–Brazil Workshop on Membrane Separation Processes, Rio de Janeiro, Brazil, May 3–8, pp. 265–276.

Jonsson, G., Wenten, I.G., 1994. Control of concentration polarization, fouling and protein transmission of microfiltration processes within the agro-based industry. In: Proceedings of the ASEAN-EC Workshop on Membrane Technology in Agro-based Industry, Kuala-Lumpur, Malaysia, July 26–29, pp. 157–166.

Kim, J., DiGiano, F.A., 2006. Defining critical flux in submerged membranes: influence of length-distribution. Journal of Membrane Science 280, 752–761.

Kimura, K., Yamato, N., Yamamura, H., Watanabe, Y., 2005. Membrane fouling in pilot-scale membrane bioreactors (MBRs) treating municipal wastewater. Environmental Science Technology 39, 6293–6299.

Le Berre, O., Daufin, G., 1996. Skim milk crossflow microfiltration performance versus permeation flux to wall shear stress ratio. Journal of Membrane Science 117, 261–270.

Le Clech, P., Jefferson, B., Chang, I.S., Judd, S.J., 2003. Critical flux determination by the flux-step method in a submerged membrane bioreactor. Journal of Membrane Science 227, 81–93.

Li, H., Fane, A.G., Coster, H.G.L., Vigneswaran, S., 2000. An assessment of depolarization models of crossflow microfiltration by direct observations through the membrane. Journal of Membrane Science 172, 135–147.

Li, J., Li, Y., Ohandja, D.G., Yang, F., Wong, F.S., Chua, H.C., 2008. Impact on filamentous bacteria on properties of activated sludge and membrane-fouling rate in a submerged MBR. Separation and Purification Technology 59, 238–243.

Li, Y.Z., He, Y.L., Liu, Y.H., Yang, S.C., Zhang, G.J., 2005. Comparison of the filtration characteristics between biological powdered activated carbon sludge and activated sludge in submerged membrane bioreactors. Desalination 174, 305–314.

Matosic, M., Vukovic, M., Curlin, M., Mijotovic, I., 2008. Fouling of hollow fibre submerged membranes during long-term filtration of activated sludge. Desalination 219, 57–65.

Metsämuuronen, S., Howell, J., Nyström, M., 2002. Critical flux in ultrafiltration of myoglobin and baker's yeast. Journal of Membrane Science 196, 13–25.

Mulder, M., 1996. Basic Principles of Membrane Technology. second ed. Kluwer Academic Publishers, Dordrecht.

Ognier, S., Wisniewski, C., Grasmick, A., 2004. Membrane bioreactor fouling in sub-critical filtration conditions: a local critical flux concept. Journal of Membrane Science 229, 171–177.

Persson, A., Jönsson, A.S., Zacchi, G., 2001. Separation of lactic acid-producing bacteria from fermentation broth using a ceramic microfiltration membrane with constant permeate flow. Biotechnology and Bioengineering 72 (3), 269–277.

Psoch, C., Schiewer, S., 2005. Critical flux aspect of air sparging and backflushing on membrane bioreactors. Desalination 175, 61–71.

Sadr Ghayeni, S.B., Madaeni, S.S., Fane, A.G., Schneider, R.P., 1996. Aspects of microfiltration and reverse osmosis in municipal wastewater reuse. Desalination 106, 25–29.

Xiu-Fen, L., Yan-Jun, L., He, L., Zhao-Zhe, H., Guo-Cheng, D., Jian, C., 2008. Correlation between extracellular polymeric substances and aerobic biogranulation in membrane bioreactor. Separation and Purification Technology 59, 26–33.

Yamato, N., Kimura, K., Miyoshi, T., Watanabe, Y., 2006. Difference in membrane fouling in membrane bioreactors (MBRs) caused by membrane polymeric material. Journal of Membrane Science 280, 911–919.

Ye, Y., Le Clech, P., Chen, V., Fane, A.G., Jefferson, B., 2005a. Fouling mechanisms of alginate solutions as model extracellular polymeric substances. Desalination 175, 7–20.

Ye, Y., Le Clech, P., Chen, V., Fane, A.G., 2005b. Evolution of fouling during crossflow filtration of model EPS solutions. Journal of Membrane Science 264, 190–199.

Department of Chemical
and Biochemical Engineering

DTU Building 229
Søltofts Plads
DK-2800 Kgs. Lyngby
www.kt.dtu.dk